NON-EQUILIBRIUM QUANTUM FIELD THEORY APPLIED TO TESTABLE SCENARIOS OF BARYOGENESIS

Diffusion Constants during the Electroweak Phase Transition, Leptogenesis with GeV-Scale Right-Handed Neutrinos

Dario Gueter

February, 2018

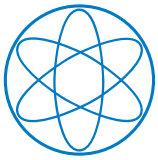

Technische Universität München
Physik Department
Institut für Theoretische Physik des frühen Universums
Prof. Dr. Björn Garbrecht

Non-Equilibrium Quantum Field Theory Applied to Testable Scenarios of Baryogenesis

Diffusion Constants during the Electroweak Phase Transition, Leptogenesis with GeV-Scale Right-Handed Neutrinos

Dario Gueter

Vollständiger Abdruck der von der Fakultät für Physik der Technischen Universität München zur Erlangung des akademischen Grades eines

Doktors der Naturwissenschaften (Dr. rer. nat.)

genehmigten Dissertation.

Vorsitzender:		Prof. Dr. Lothar Oberauer
Prüfer der Dissertation:	1.	Prof. Dr. Björn Garbrecht
	2.	Prof. Dr. Alejandro Ibarra
	3.	Prof. Laura Covi, Ph.D.

Die Dissertation wurde am 14.03.2018 bei der Technischen Universität München eingereicht und durch die Fakultät für Physik am 12.11.2018 angenommen.

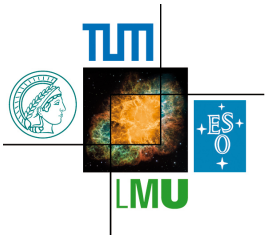

This work has been supported in part by the Max Planck Institute for Physics, the Excellence Cluster “Origin and Structure of the Universe” and the TUM Graduate School.

ZUSAMMENFASSUNG

Die Erzeugung der Baryonasymmetry des Universums durch CP-verletzende Oszillationen zweier nahezu massenentarteter schwerer Neutrinos wird in der Nichtgleichgewichtsquantenfeldtheorie untersucht. Für schnelle und überdämpfte Oszillationen werden analytische Näherungen hergeleitet. Es wird dann das Potenzial zukünftiger Experimente wie FCC-ee, ILC und CEPC für Tests des Parameterraums bestimmt. Ferner werden Diffusionskonstanten als essenzielle Parameter für die elektroschwache Baryogenese zur führenden Ordnung berechnet.

ABSTRACT

The generation of the baryon asymmetry of the universe via CP-violating oscillations of two almost mass degenerate heavy neutrinos is studied within non-equilibrium quantum field theory. Analytic approximations are found in the case of fast and overdamped oscillations. The perspective of future experiments such as FCC-ee, ILC and CEPC to probe the parameter space is determined. Further, diffusion constants as essential parameters for electroweak baryogenesis are computed to leading order.

PUBLICATIONS

This thesis is mainly based on the publications [1, 2] and the preprint [3] to which I significantly contributed during my research at the Technical University of Munich. Further, I provided a considerable input to a number of proceedings [4–7]. Additional work in progress will appear in [8, 9].

REFEREED PUBLICATIONS:

[1] M. Drewes, B. Garbrecht, D. Gueter and J. Klarić, "Testing the low scale seesaw and leptogenesis", JHEP **1708** (2017) 018, arXiv:1609.09069 [hep-ph],

[2] M. Drewes, B. Garbrecht, D. Gueter and J. Klarić, "Leptogenesis from Oscillations of Heavy Neutrinos with Large Mixing Angles", JHEP **1612** (2016) 150, arXiv:1606.06690 [hep-ph].

PREPRINTS:

[3] S. Antusch, E. Cazzato, M. Drewes, O. Fischer, B. Garbrecht, D. Gueter and J. Klarić, "Probing Leptogenesis at Future Colliders", arXiv:1710.03744 [hep-ph].

CONFERENCE PROCEEDINGS:

[4] S. Antusch, E. Cazzato, M. Drewes, O. Fischer, B. Garbrecht, D. Gueter and J. Klarić, "Probing the Seesaw Mechanism and Leptogenesis with the International Linear Collider", arXiv:1801.06534 [hep-ph],

[5] M. Drewes, B. Garbrecht, D. Gueter and J. Klarić, "Leptogenesis with GeV-Scale Right-Handed Neutrinos", J.Phys.Conf.Ser. 873 (2017) no.1, 012027,

[6] M. Drewes, B. Garbrecht, D. Gueter and J. Klarić, "Leptogenesis: Improving predictions for experimental searches", arXiv:1611.08504 [hep-ph],

[7] M. Drewes, B. Garbrecht, D. Gueter and J. Klarić, "On the relation between the CP phases in the PMNS matrix, CP-violation with sterile neutrinos and leptogenesis", arXiv:1611.04769 [hep-ph].

WORK IN PROGRESS:

[8] B. Garbrecht, D. Gueter, "Diffusion constants during the electroweak phase transition: leading order results",

[9] M. Drewes, D. Gueter, "Quasiparticles at finite temperature in the symmetric phase of the Standard Model".

ACKNOWLEDGEMENTS

I would like to take the opportunity to express my gratitude to different people who supported me during the past three years of my PhD.

First and foremost, I would like to acknowledge my supervisors, on the one hand, Prof. Dr. Björn Garbrecht, who has always taken the time to answer my questions and who has taught me the methods to conquer long analytic and very technical calculations in thermal field theory and on the other hand, Dr. Frank Steffen, who has always had an open ear and who has provided me the opportunity and especially encouraged me to attend a great variety of international conferences and schools where I was able to present my research outcomes in the international community. I am very thankful for their extraordinary support and their guidance, including all their valuable advices during this thesis process. Those conferences have not only helped me to connect with people, for whose discussions about physics I am very thankful, but also to visit interesting places in different countries. Thanks to Tanja Geib, Ignacio Izaguirre and Max Totzauer as my travel buddies in the majority of the journeys.

A very special thanks goes to Marco Drewes and to my office mate Juraj Klarić, not only as my collaborators on different projects throughout my PhD, out of which most of the outcomes of my thesis are based on, but especially as friends I could also meet in my free time. I am particularly thankful for Juraj's continuous support on IT questions and Marco's ability to come up with ideas for new projects, to push them towards publication and to embed our research topics in the physics community.

I am very grateful for various people at the Technical University of Munich who have provided me with a joyful and pleasant time during my PhD in Garching. Special thanks to Laura Darabas and Karin Ramm who have never hesitated to help me with anything I have asked them for.

Finally, I would like to extend my deepest gratitude to my family, my friends and particularly to Lisa, who have been keeping the life outside physics delightful. Most especially, this is for my family, who have always believed in me and supported me throughout my whole career. Without their encouragement I would not have been where I am now.

CONTENTS

LIST OF ABBREVIATIONS

$0\nu\beta\beta$	neutrinoless double beta (decay)
B	baryon number
C	charge
CP	charge and parity
CPT	charge, parity and time reversal
L	lepton number
P	parity
T	time reversal
$\mathcal{O}(1)$	order one (corrections)
νMSM	Neutrino Minimal Standard Model
s	entropy density
2PI	two-particle irreducible (action)
BAU	baryon asymmetry of the universe
BBN	Big Bang nucleosynthesis
BW	Breit-Wigner (approximation)
CEPC	Circular Electron Positron Collider
CKM	Cabibbo-Kobayashi-Maskawa (matrix)
CTP	closed-time-path (formalism)
DM	Dark Matter
EV	expectation value
EW	electroweak
FCC	Future Circular Collider (in the electron positron mode)
HTL	hard-thermal-loop (approximation)
ILC	International Linear Collider

IO . . . . . inverted (light neutrino mass) ordering

IR . . . . . infrared

KB . . . . . Kadanoff-Baym

KMS . . . . . Kubo–Martin–Schwinger (relation)

LFV . . . . . lepton flavour violation

LH . . . . . left-hand(ed)

LNC . . . . . lepton number conservation

LNV . . . . . lepton number violation

NO . . . . . normal (light neutrino mass) ordering

PF . . . . . purely flavoured

PMNS . . . . . Pontecorvo-Maki-Nakagawa-Sakata (matrix)

PT . . . . . (electroweak) phase transition

RH . . . . . right-hand(ed)

SB . . . . . (electroweak) symmetry breaking

SD . . . . . Schwinger-Dyson (equation)

SM . . . . . Standard Model of particle physics

VEV . . . . . vacuum expectation value (of the Higgs field)

LIST OF FIGURES

LIST OF TABLES

1

INTRODUCTION

1.1 MOTIVATION

Within the recent decades the Standard Model of particle physics (SM) has established itself as a powerful theory that is able to explain the majority of phenomena that can be observed in particle physics. With the detection of the Higgs boson in 2012 all of the SM particles have been finally discovered [10]. However, it is well-known the SM cannot be the full theory of nature.

On the one hand, the violation of charge and parity (CP) in the SM is too weak to explain the observed baryon asymmetry of the universe (BAU), that is conveniently quantified as the ratio of the baryon number (B) and the entropy density (s), i.e.

$$8.2 \times 10^{-11} \lesssim \frac{B}{s} \lesssim 9.4 \times 10^{-11} \,. \tag{1.1}$$

This value is accurately determined at a confidence level of 95% by comparing prediction of cosmic abundances of light elements that have been produced within the first three minutes of the universe via the theory of Big Bang nucleosynthesis (BBN) [11] to measurements of temperature fluctuations as anisotropies in the Cosmic Microwave Background by WMAP [12] and Planck [13].

On the other hand, the observed neutrino flavour oscillations require the existence of new degrees of freedom that generate the light neutrino masses, cf. [14–16] for reviews including many references. These can be either heavy fields that have been integrated out from non-renormalisable operators with mass dimension five or higher or right-handed (RH) neutrinos. The latter ones are well-motivated since neutrinos are the only fermions in the SM that only come with left-handed (LH) chirality. Further, these are not only able to explain the observed BAU via leptogenesis [17] in the early universe but can also account for the light neutrino masses via the seesaw mechanism [18–23]. Particularly the coupling to the SM particles via Yukawa interaction introduces new parameters including new CP-violating phases that are able to generate a sufficient amount of baryon charges in the primordial plasma.

Further, it is well-known [24] that only 4.9% of the universe is made out of ordinary matter. Since several attempts to explain the existence of the non-luminous matter or Dark Matter (DM), such as modifications of gravity, have failed, the most promising explanation is given by extending the SM by massive and electrically neutral particles, that only weakly interact with the visible sector.

In 1967, Andrei Sakharov stated that successful baryogenesis, i.e. any process that dynamically generates a non-zero BAU, requires three conditions to be fulfilled [25]. First, there have to be processes that lead to a non-conservation of B. Second, both charge (C) and CP have to be violated. And third, a departure from thermal equilibrium has

to be present. Given that the universe has started with zero amount of B, effects that end up in a violation of B are strictly necessary. If both C and CP were conserved, for any process that produces more matter than antimatter there would exists a symmetric counter process with the same rate. This prevents any generated net asymmetry from surviving over long periods of time. Due to the charge, parity and time reversal (CPT) invariance theorem a violation of CP is only possible when breaking the time reversal (T) invariance. Thermodynamically this is realised if the corresponding system is out-of-equilibrium. In comparison to parity (P), C and B violation in the SM, CP violation is too weak to explain the observed BAU. Any working baryogenesis scenario has to bring in new sources of CP violation and has to provide deviations from equilibrium. Due to the invariance of the SM Lagrangian under the global U(1) group, B and the total lepton number (L) are conserved at the perturbative level. However, as realised by Gerard 't Hooft in 1976 [26, 27], non-perturbative effects related to the chiral anomaly of the electroweak (EW) theory, so-called EW sphalerons [28], conserve the combination $B - L$ but violate $B + L$ by six units. These processes are fast enough to be in equilibrium for temperatures higher than the EW scale but are highly suppressed in the broken phase of the SM [29]. Therefore, any non-zero L is directly related to a non-zero amount of B before the EW phase transition (PT). In the broken phase, however, any B that has been generated in the symmetric phase can be prevented from a washout.

Amongst many promising scenarios of baryogenesis, the following two scenarios are discussed within this thesis. First, baryogenesis via leptogenesis [17], i.e. the dynamical generation of L, that is transferred into a net B through EW sphalerons, is studied. In particular, leptogenesis from oscillations of heavy RH neutrinos [30] with masses in the GeV-scale is investigated. A number of different scenarios is given in the review [31]. Second, EW baryogenesis where the B charge generation happens during the EWPT [28, 32, 33], cf. e.g. refs. [34, 35] for reviews, is studied. In particular, relevant diffusion constants are computed. Both scenarios have to happen at temperatures higher than the EW scale in order to allow for B violation via $B + L$ violation through EW sphaleron processes.

In a weakly coupled and dilute plasma quantum Boltzmann equations turn out to be a powerful tool to describe evolution processes of particle number densities. However, these are not suitable for the processes discussed in this thesis. In particular, these do not take account of the necessary screening for the different particles due to interactions with the surrounding plasma, a feature that is needed to regulate infrared (IR) divergences, that appear in certain tree-level scattering processes. Therefore, in order to correctly describe baryogenesis at temperatures above the EW scale, this thesis relies on non-equilibrium quantum field theory based on the closed-time-path (CTP) approach by Schwinger-Keldysh [36, 37], cf. e.g. refs. [38–41] for pedagogical reviews. Kinetic equations that determine the evolution of particle distribution functions are derived from the two-particle irreducible (2PI) action [42]. These implicitly provide the correct description of the physical screening.

As already mentioned above, heavy RH neutrinos can not only solve the neutrino mass problem [18–23] but can also generate the observed BAU via leptogenesis [17]. Due to their Yukawa interaction and their Majorana masses new sources of CP violation are present. The non-equilibrium condition can be realised in different ways depending on the parametric regime. Due to small Yukawa couplings, that are necessary in order to explain the light neutrino masses, it is reasonable to assume that there is zero initial abundance

of heavy neutrinos when the radiation dominated era starts [43]. Within this thesis we mainly focus on the scenario of two almost mass degenerate heavy neutrinos, while some of the outcomes are valid for three or more heavy neutrinos. In ref. [44] it has been shown for the first time that two heavy neutrinos are enough to explain the BAU via leptogenesis and the light neutrino masses via the seesaw mechanism. This requires the lightest SM neutrino to be massless. In the Neutrino Minimal Standard Model (νMSM) [44, 45], i.e. the minimal extension of the SM by three heavy neutrinos, the remaining heavy neutrino can be a DM candidate. This requires an extremely tiny coupling to the SM neutrinos such that the effect on the BAU and the light neutrino masses is negligible, cf. e.g. ref. [46].

The first proposed scenarios of leptogenesis [17] consider superheavy RH neutrinos, i.e. RH neutrinos with masses much above the EW scale. These are not only produced but decay long before the EW symmetry breaking (SB) as soon as their rate becomes Boltzmann suppressed at $T \lesssim M_i$, with M_i the masses of the heavy neutrinos. Interferences of different decay channels effectively lead to an asymmetry in the total lepton number L due to the CP-violating phases. Since EW sphalerons are active at these temperatures, any violation of L gets translated into a generation of B. The non-equilibrium condition is due to the expansion of the universe such the RH neutrinos cannot follow their equilibrium distribution. Even though flavour effects might be important [47–51], one finds that the dominant contribution to B generation in such leptogenesis scenarios is generically mainly due to lepton number violating (LNV) effects. Since these effects are suppressed for $T \lesssim M_i$, all L that has been produced via the decay is protected from a washout. Such leptogenesis scenarios including modified versions have been studied in refs. [52–54]. The disadvantage of such models is the inaccessibility in laboratory experiments since the mass of the lightest RH neutrino is required to be larger than 10^9 GeV [55, 56]. Studies of resonant leptogenesis [48, 57–62] with high degeneracies in the RH neutrino masses can push this lower bound further down to the TeV-scale.

In the case of heavy RH neutrino masses at the GeV-scale the asymmetry is not created in the decays but during the production of the heavy neutrinos via coherent oscillations amongst these due to CP-violating correlations between the different mass eigenstates. Such a scenario has first been discovered by Akhmedov, Rubakov and Smirnov [30], the reason why it is often referred to the ARS scenario. A further study has been provided in ref. [44]. In order to account for the small neutrino masses, the relative smallness of the heavy neutrino masses implies Yukawa couplings that are much smaller than those in leptogenesis scenarios from decays of heavy neutrinos. Consequently, the production of the heavy neutrinos happens rather late. The non-equilibrium condition is fulfilled when at least one of the heavy neutrinos has not equilibrated before the EW sphaleron freeze-out. The asymmetries which are produced during the oscillations are at first purely flavoured (PF), while the total lepton number is approximately conserved for $T \gg M_i$ in a substantial fraction of the parameter space. However, the asymmetries L_a in the different flavours can be converted into helicity asymmetries in the heavy neutrinos sector via washout processes. As the corresponding rates are different for the individual flavours, a total lepton asymmetry L is generated besides an equal amount of asymmetries in the heavy neutrino sector. If the washout is not completed before the EW sphaleron freeze-out a non-zero baryon number will be created due to fast EW sphalerons that convert L into B but are insensitive to heavy neutrino asymmetries. The heavy neutrino masses and their Yukawa couplings control both the time of the first oscillations as well as the relaxation to

equilibrium. This allows to differentiate between two regimes in which analytic solutions can be found [2]: The oscillatory regime and the overdamped regime.

When the oscillations of the heavy neutrinos happen much earlier than their equilibration, the baryon charge is created at very early times during the first few oscillations. In order to prevent the asymmetries to be washed out too early, this scenario requires small damping rates and consequently small Yukawa couplings, which is why it is often referred to the weak washout scenario. This allows to treat this scenario perturbatively in the Yukawa couplings, which gives rise to accurate analytic approximations.

The case of heavy neutrino oscillations that are so slow that not even one full oscillation has happened before the EWSB corresponds to the overdamped regime. One finds that the oscillation time scale is given by the mass difference of the heavy neutrinos. Thus, in such a regime a high mass degeneracy is required. Equilibration times that are small compared to the oscillation times allow for anomalously large Yukawa couplings. The requirement of having at least one heavy neutrino that must not equilibrate before the EW sphaleron freeze-out allows for analytic approximations in terms of quasi-static solutions, as applied in refs. [57, 63].

The fact that leptogenesis from oscillations of heavy RH neutrinos allows for heavy neutrino masses in the GeV-scale makes the low scale seesaw a testable theory [1]. Therefore, collecting information about their mixing to the SM particles, their CP properties and on their mass spectrum are essential to decide if the heavy neutrinos are the common origin of light neutrino masses and the BAU. Within this thesis it is thus assumed that heavy neutrinos will be detected in some future direct search experiments [64–66]. Further constraints can also come from a combination of indirect searches for signatures, such as lepton flavour violation (LFV) or neutrinoless double beta ($0\nu\beta\beta$) decay. Provided that heavy neutrinos are lighter than the W boson, direct searches can be performed at both lepton colliders [67–74] and hadron colliders [74–81], cf. ref. [74] for an overview of signatures at different collider types. For heavy neutrino masses smaller than the masses of the B mesons, B factories [82–86] and fixed target experiments [87] can be used as discovery machines. These include T2K [88], the NA62 experiment [88–90], as well as the SHiP experiment that is proposed at CERN [69, 91, 92] or also the DUNE beam at FNAL [93–95]. At the GeV-scale particularly future lepton colliders such as the Future Circular Collider (FCC) in the electron positron mode [3, 68, 70, 72, 96], i.e. the FCC-ee, the International Linear Collider (ILC) [3, 70, 71, 97–99] and the Circular Electron Positron Collider (CEPC) [3, 70, 100] are very capable of finding heavy neutrinos via displaced vertex searches. A huge number of displaced vertex events allows for a precision measurement of the coupling of the heavy neutrinos to all SM flavours [3]. Provided that the Dirac phase in the Pontecorvo-Maki-Nakagawa-Sakata (PMNS) matrix is measured to sufficient precision in neutrino oscillation experiments, which could be done at DUNE or NOνA [101], all the fundamental parameters of the type-I seesaw mechanism are in general determinable. As a consequence, the low scale seesaw is a fully testable theory of baryogenesis and the light neutrino masses [1].

The generation of the BAU can also happen during the EWPT locally at temperatures around 100 GeV, cf. the reviews [34, 35]. Above this temperature the universe is fully symmetric in the EW gauge groups and acts as a hot plasma of particles in which no initial amount of B is present. The universe expands and cools down until the EW gauge symmetry is broken via the Higgs mechanism. It is well-known that EW baryogenesis is only successful when this PT is first-order. In this case bubbles of broken symmetries

nucleate and expand until they fill out the whole space. As soon as the bubble wall hits the particles in the symmetric phase, they feel the coupling to the Higgs field, particularly because they receive their masses from the Higgs expectation value (EV) that builds up in the bubble wall. Provided that the underlying theory contains CP-violating parameters, this interaction implies reflection of particles at the wall that are in general different for different chiralities of the fermions and for antiparticles. This eventually does not only lead to an accumulation of CP asymmetries for one or more particle species at the wall, that diffuse into the symmetric phase, but also pushes the system out-of-equilibrium. During this diffusion process the different particles are interacting with the surrounding plasma. Due to scattering processes that are fast compared to the inverse diffusion length, equilibration processes redistribute charges in front of the wall. Particularly asymmetries of LH fermions are present. Since EW sphalerons are only sensitive to LH particles they provide the necessary C violation. Therefore, the asymmetry in the LH leptons is converted into a non-zero B via EW sphaleron transitions that are fast in the symmetric phase. The condition of non-equilibrium is met when the expanding bubbles soak up the baryon charge. In the broken phase the EW sphaleron transitions can be strongly suppressed what would prevent the baryon charge that has been created from a washout. This, however, is only the case if the PT is strongly first-order. As this puts an upper bound on the SM Higgs mass of $m_\phi \lesssim 70\,\text{GeV}$ [102, 103] which is far below the observed value of the Higgs mass, one needs to go beyond the SM. Further, the CP violation in the SM, which is due to the Dirac phase in the Cabibbo-Kobayashi-Maskawa (CKM), is too weak in order to produce sufficient amounts of charges during scatterings with the bubble wall [104–106]. Supersymmetric extensions of the SM and models with additional Higgs doublet, such as the two-Higgs-doublet model, can not only push this lower bound sufficiently high but also provide a necessary amount of CP sources, cf. e.g. [107–111]. The network of equations that describes the diffusion and scattering process in front of the bubble is particularly sensitive to the diffusion constants for the different particles in the plasma [107, 110, 111]. Therefore, an understanding of EW baryogenesis requires the determination of these diffusion constants.

1.2 OUTLINE

Chapter 2 reviews the SM and discusses its extension by two or more heavy RH neutrinos that can generate the light neutrino masses via the type-I seesaw mechanism. A distinction is made between normal neutrino mass ordering (NO) and inverted neutrino mass ordering (IO). Further, relevant Feynman rules that are necessary to evaluate different Feynman diagrams in this thesis are derived.

Properties of quasiparticles at finite temperatures in the symmetric phase of the SM are discussed in chapter 3. This requires a short introduction to the non-equilibrium CTP formalism, in which quantum kinetic equations, such as the Schwinger-Dyson (SD) and Kadanoff-Baym (KB) equations, for the different SM particles are derived from first principles. Fully one-loop resummed propagators are obtained when solving these equations. These are dressed by particle interactions with the plasma that provide a finite width and give rise to dispersion relations. Analytic expression for the relevant self-energies are provided. Particularly, a full analytic solution to the spectral part of the gauge boson self-energy is derived, while the thermal masses are given in the hard-thermal-loop (HTL) limit.

Diffusion constants for chiral fermions and the Higgs that describe the diffusion process of particles in front of the bubble wall are computed to leading order within the CTP formalism in chapter 4. These are derived from Boltzmann-like equations. The relevant collision terms receive contributions from one-loop self-energy type and two-loop vertex type diagrams. The first ones are logarithmically enhanced in the IR for soft momentum exchange and consequently require the use of resummed propagators. This gives a leading logarithmic contribution to the diffusion constants, while the vertex type diagrams only contribute to leading linear order and turn out to be subdominant. Numerical values for the different diffusion constants such as those of chiral fermion and the Higgs in the SM are compared to previous results.

In chapter 5 relativistic quantum kinetic equations describing leptogenesis from CP-violating oscillations of two almost mass degenerate heavy neutrino with masses in the GeV-range are derived within the CTP formalism. Spectator effects and backreaction are included in this study. Necessary transport coefficients, such as thermal masses and damping rates are computed to leading order in a momentum-averaged framework. By applying time-scale arguments the parameter space can be divided into two regimes. Approximate analytic solutions for both the oscillatory regime and the overdamped regime, that work well up to order one ($\mathcal{O}(1)$) corrections, are provided. Further, the importance of LNV processes, in contrast to the PF but lepton number conserving (LNC) processes, is highlighted.

Chapter 6 discusses how neutrino oscillation data and other constraints, such as direct and indirect constraints, can be used to test the low scale seesaw mechanism as the origin of the light neutrino masses. Provided that in addition heavy neutrinos can explain the observed baryon asymmetry via leptogenesis, new constraints arise on properties of the heavy neutrinos. In this case, the potential of future direct search experiments for discovering heavy neutrinos is studied. Particular attention is given to the future lepton colliders FCC-ee, ILC and CEPC and how these can constrain the low scale seesaw model parameters. Eventually, the testability of the low scale seesaw mechanism is elaborated.

Chapter 7 summarises the results obtained in this thesis and gives an outlook to future works.

Additional technicalities, such as the computation of spectral and Hermitian parts of self-energies, are given in appendix A. A few remarks regarding the test of the low scale seesaw and leptogenesis, such as expressions for active-sterile mixing angles, are discussed in appendix B.

2

MINIMAL EXTENSION OF THE STANDARD MODEL

Throughout this thesis different Feynman diagrams have to be evaluated, i.e. when describing dispersion relations and damping rates for quasiparticles at high temperatures in the symmetric phase of the SM. Therefore, it is essential to know the Feynman rules that are needed for the following computations within this thesis. Note that the Feynman rules in this chapter for the different vertices are given for zero temperature but can be applied to processes at finite temperatures. Since the BAU cannot be explained within the SM alone, one needs to consider physics beyond the SM. A minimal extension is given by introducing two or more heavy RH neutrinos that can explain the observed BAU and further account for the light neutrino masses via the seesaw mechanism, cf. e.g. refs. [17–23] and refs. [44, 45, 112].

In section 2.1 the SM, including neutrino flavour oscillations, is shortly discussed and a set of Feynman rules is derived from the SM Lagrangian, while RH neutrinos are introduced in section 2.2.

2.1 THE STANDARD MODEL OF PARTICLE PHYSICS

This section shortly introduces the SM for temperatures above the EW scale and provides a set of Feynman rules in subsection 2.2.1, while neutrinos and their oscillations that require the existence of non-zero neutrino masses are discussed in subsection 2.1.2. The discussion about the neutrino masses is based on ref. [16].

2.1.1 *Symmetries, Lagrangian and Feynman rules*

GAUGE GROUP OF THE SM: At high temperature, i.e. at temperatures above the EW scale $T \gtrsim T_{\mathrm{EW}} \simeq 140\,\mathrm{GeV}$, the SM Lagrangian exhibits the full gauge symmetry

$$\mathrm{U}(1)_Y \times \mathrm{SU}(2)_\mathrm{L} \times \mathrm{SU}(3)_\mathrm{c}\,. \tag{2.1}$$

The generators of the non-abelian gauge groups $\mathrm{SU}(2)_\mathrm{L}$ and $\mathrm{SU}(3)_\mathrm{c}$ are $\{I_a\}_{i=1}^3$ and $\{T_a\}_{a=1}^8$, respectively, while Y denotes the $\mathrm{U}(1)_Y$ hypercharge. From now on we stop explicitly indicating the gauge groups with the subindices Y, L and c. These generators are commonly expressed in terms of the Pauli matrices with $I_i = \sigma_i/2$ and in terms of the Gell-Mann matrices $T_a = \lambda_a/2$. In the symmetric phase no EWSB has happened yet, such that all gauge fields and all fermions remain massless. The fermions as well as the

	I	II	III	representation
q^i_{L}	$\begin{pmatrix} u_{\mathrm{L}} \\ d_{\mathrm{L}} \end{pmatrix}$	$\begin{pmatrix} c_{\mathrm{L}} \\ s_{\mathrm{L}} \end{pmatrix}$	$\begin{pmatrix} t_{\mathrm{L}} \\ b_{\mathrm{L}} \end{pmatrix}$	$(\mathbf{3},\mathbf{2})_{+\frac{1}{6}}$
u^i_{R}	u_{R}	c_{R}	t_{R}	$(\mathbf{3},\mathbf{1})_{+\frac{2}{3}}$
d^i_{R}	d_{R}	s_{R}	b_{R}	$(\mathbf{3},\mathbf{1})_{-\frac{1}{3}}$
ℓ^i_{L}	$\begin{pmatrix} \nu_{\mathrm{L}e} \\ e_{\mathrm{L}} \end{pmatrix}$	$\begin{pmatrix} \nu_{\mathrm{L}\mu} \\ \mu_{\mathrm{L}} \end{pmatrix}$	$\begin{pmatrix} \nu_{\mathrm{L}\tau} \\ \tau_{\mathrm{L}} \end{pmatrix}$	$(\mathbf{1},\mathbf{2})_{-\frac{1}{2}}$
e^i_{R}	e_{R}	μ_{R}	τ_{R}	$(\mathbf{1},\mathbf{1})_{-1}$
ϕ		$\begin{pmatrix} \phi^+ \\ \phi^0 \end{pmatrix}$		$(\mathbf{1},\mathbf{2})_{-\frac{1}{2}}$

TABLE 2.1: Fermions of the SM and the Higgs field with their representations.

Higgs field are displayed in table 2.1. The different gauge bosons are denoted as V^a_μ with B_μ, $\{W_\mu\}^3_{a=1}$ and $\{A_\mu\}^8_{a=1}$. The corresponding field strength tensors are given by

$$B_{\mu\nu} = \partial_\mu B_\nu - \partial_\nu B_\mu \,, \tag{2.2}$$

$$W^a_{\mu\nu} = \partial_\mu W^a_\nu - \partial_\nu W^a_\mu - g_2 f^a_{bc} W^b_\mu W^k_\nu \,, \tag{2.3}$$

$$A^a_{\mu\nu} = \partial_\mu A^a_\nu - \partial_\nu A^a_\mu - g_3 f^a_{bc} A^b_\mu A^c_\nu \,, \tag{2.4}$$

with the gauge couplings $g_{1,2,3}$. f_{abc} are the fully antisymmetric structure constants. Given a group SU(N) with generators t^a the structure constants are defined by the commutator relation

$$\left[t^a, t^b\right] = \mathrm{i} f^{abc} t_c \,. \tag{2.5}$$

For a general representation R the Casimir operator C^R and the quadratic Casimir operator C^R_2 are given by

$$\mathrm{tr}\left(t^a t^b\right) = C^R \delta^{ab} \,, \qquad t^a t_a = C^R_2 \mathbb{1}_{N\times N} \,. \tag{2.6}$$

In the fundamental (F) and adjoint (A) representation these take the following form

$$C^F = \frac{1}{2} \,, \quad C^F_2 = \frac{N^2-1}{2N} \,, \quad C^A = C^A_2 = N \,. \tag{2.7}$$

Other contractions such as

$$t^a t^b t_a = \left(C^R_2 - \frac{1}{2} C^A_2\right) t^b \,, \quad f^a_{cd} f^{bcd} = C^A_2 \delta^{ab} \,, \quad f^{abc} t_b t_c = \frac{\mathrm{i}}{2} C^A_2 t^a \,, \tag{2.8}$$

are particularly important when it comes to the evaluation of Feynman diagrams.

SM LAGRANGIAN: The SM Lagrangian in the symmetric phase can be decomposed as

$$\mathscr{L}_{\mathrm{SM}} \supset \mathscr{L}^{\mathrm{YM}}_{\mathrm{SM}} + \mathscr{L}^{\psi}_{\mathrm{SM}} + \mathscr{L}^{\phi}_{\mathrm{SM}} + \mathscr{L}^{t}_{\mathrm{SM}} \,, \tag{2.9}$$

with the following contributions

$$\mathscr{L}_{\mathrm{SM}}^{\mathrm{YM}} = -\frac{1}{4}B_{\mu\nu}B^{\mu\nu} - \frac{1}{4}\sum_{a=i}^{3} W_{\mu\nu}^{a}W_{a}^{\mu\nu} - \frac{1}{4}\sum_{i=a}^{8} A_{\mu\nu}^{a}A_{a}^{\mu\nu}\,, \tag{2.10}$$

$$\mathscr{L}_{\mathrm{SM}}^{\psi} = \sum_{\mathrm{i}=1}^{3}\left(\bar{q}_{\mathrm{L}}^{i}\mathrm{i}\not{D}q_{\mathrm{L}}^{i} + \bar{u}_{\mathrm{R}}^{i}\mathrm{i}\not{D}u_{\mathrm{R}}^{i} + \bar{d}_{\mathrm{R}}^{i}\mathrm{i}\not{D}d_{\mathrm{R}}^{i} + \bar{\ell}_{\mathrm{L}}^{i}\mathrm{i}\not{D}\ell_{\mathrm{L}}^{i} + \bar{e}_{\mathrm{R}}^{i}\mathrm{i}\not{D}e_{\mathrm{R}}^{i}\right)\,, \tag{2.11}$$

$$\mathscr{L}_{\mathrm{SM}}^{\phi} = (D_{\mu}\Phi)^{\dagger}(D^{\mu}\Phi) + \mu^{2}\Phi^{\dagger}\Phi - \lambda(\Phi^{\dagger}\Phi)^{2}\,, \tag{2.12}$$

$$\mathscr{L}_{\mathrm{SM}}^{t} = -h_{t}\bar{t}_{\mathrm{R}}\phi^{\dagger}t_{\mathrm{L}} + \mathrm{h.c.}\,, \tag{2.13}$$

where in $\mathscr{L}_{\mathrm{SM}}^{\psi}$ the sum over the three generations of the fermions is performed, while the Yang-Mills term $\mathscr{L}_{\mathrm{SM}}^{\mathrm{YM}}$ sums over all gauge bosons. Note that all Yukawa couplings are small compared to the top Yukawa coupling h_t. Hence, we only write down the coupling between the top quark and the Higgs field. Further note that gauge fixing terms are not explicitly written down. Moreover, unphysical degrees of freedom are removed from the theory when including the ghost fields c_2 and c_3 in the adjoint representations of the non-abelian groups $\mathrm{SU}(2)_{\mathrm{L}}$ and $\mathrm{SU}(3)_c$, respectively. This modifies the Lagrangian as follows

$$\mathscr{L}_{\mathrm{SM}} \to \mathscr{L}_{\mathrm{SM}} + \sum_{a,b=1}^{3}\partial_{\mu}\bar{c}_{2}^{a}D^{\mu}c_{2}^{b}\delta_{ab} + \sum_{a,b=1}^{8}\partial_{\mu}\bar{c}_{3}^{a}D^{\mu}c_{3}^{b}\delta_{ab}\,. \tag{2.14}$$

The different covariant derivatives acting on the individual SM are essential in order to keep the Lagrangian terms $\mathscr{L}_{\mathrm{SM}}^{\psi}$ and $\mathscr{L}_{\mathrm{SM}}^{\phi}$ invariant under gauge transformations

$$D_{\mu}q_{\mathrm{L}}^{i} = \left(\partial_{\mu} + \mathrm{i}g_{1}B_{\mu}Y_{q_{\mathrm{L}}} + \mathrm{i}g_{2}W_{\mu}^{a}I_{a} + \mathrm{i}g_{3}A_{\mu}^{a}T_{a}\right)q_{\mathrm{L}}^{i}\,, \tag{2.15}$$

$$D_{\mu}u_{\mathrm{R}}^{i} = \left(\partial_{\mu} + \mathrm{i}g_{1}B_{\mu}Y_{u_{\mathrm{R}}} + \mathrm{i}g_{3}A_{\mu}^{a}T_{a}\right)u_{\mathrm{R}}^{i}\,, \tag{2.16}$$

$$D_{\mu}d_{\mathrm{R}}^{i} = \left(\partial_{\mu} + \mathrm{i}g_{1}B_{\mu}Y_{d_{\mathrm{R}}} + \mathrm{i}g_{3}A_{\mu}^{a}T_{a}\right)d_{\mathrm{R}}^{i}\,, \tag{2.17}$$

$$D_{\mu}\ell_{\mathrm{L}}^{i} = \left(\partial_{\mu} + \mathrm{i}g_{1}B_{\mu}Y_{\ell_{\mathrm{L}}} + \mathrm{i}g_{2}W_{\mu}^{a}I_{a}\right)\ell_{\mathrm{L}}^{i}\,, \tag{2.18}$$

$$D_{\mu}e_{\mathrm{R}}^{i} = \left(\partial_{\mu} + \mathrm{i}g_{1}B_{\mu}Y_{e_{\mathrm{R}}}\right)e_{\mathrm{R}}^{i}\,, \tag{2.19}$$

$$D_{\mu}\phi = \left(\partial_{\mu} + \mathrm{i}g_{1}B_{\mu}Y_{\phi} + \mathrm{i}g_{2}W_{\mu}^{a}I_{a}\right)\phi\,, \tag{2.20}$$

with the individual weak hypercharges Y_i that are given as subindices of the representations in table 2.1.

FEYNMAN RULES: With the Lagrangian terms (2.9) and (2.14) we can derive Feynman rules for the different vertices of the SM particles in the symmetric phase. These are given in figure 2.1.

2.1.2 *Neutrinos in the Standard Model*

Several experiments from the last decades have observed flavour changing processes in the neutrino sector, cf. refs. [14, 15] for instructive reviews. This requires the neutrinos to have non-zero masses such that they can undergo flavour oscillations as will be discussed quickly in the following.

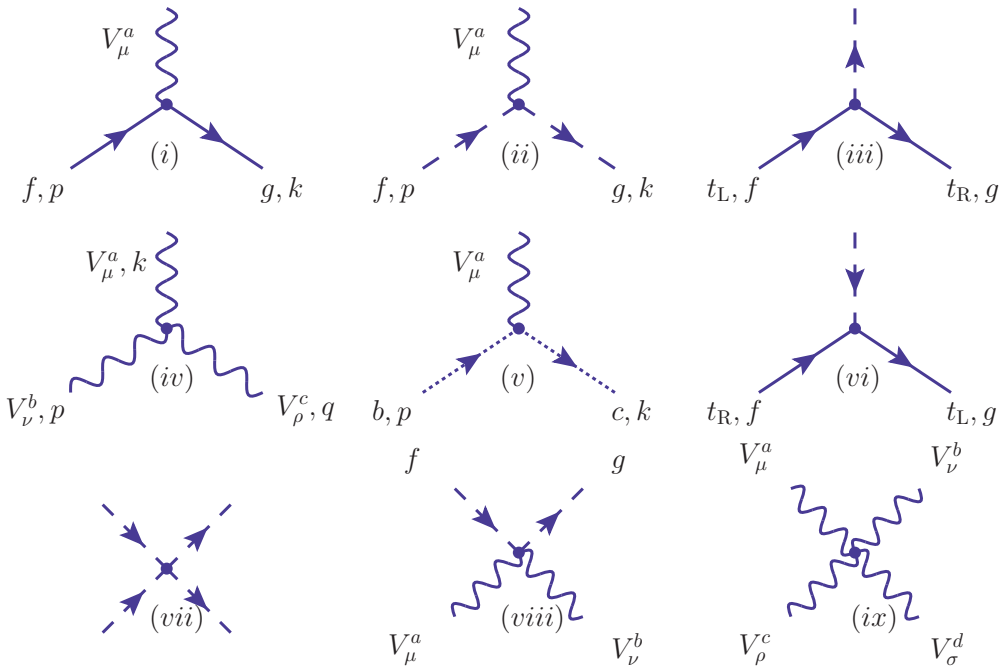

(i)	$= \begin{cases} -\mathrm{i}g_1\gamma_\mu(Y_\mathrm{L}P_\mathrm{L} + Y_\mathrm{R}P_\mathrm{R})\delta_{fg} \\ -\mathrm{i}g_{2,3}\gamma_\mu P_\mathrm{L} t^a_{fg} \end{cases}$
(ii)	$= \begin{cases} -\mathrm{i}g_1(p+k)_\mu Y_\phi \delta_{fg} \\ -\mathrm{i}g_2(p+k)_\mu I^a_{fg} \end{cases}$
(iii)	$= -\mathrm{i}h_t P_\mathrm{L}\delta_{fg}$
(iv)	$= -g_{2,3}f^{abc}[g_{\mu\nu}(k-p)_\rho$ $+g_{\nu\rho}(p-q)_\mu + g_{\rho\mu}(q-k)_\nu]$
(v)	$= -g_{2,3}f^{abc}k_\mu$
(vi)	$= -\mathrm{i}h_t P_\mathrm{R}\delta_{fg}$
(vii)	$= -6\mathrm{i}\lambda$
$(viii)$	$= \begin{cases} 2\mathrm{i}g_1^2 Y_\phi^2 g_{\mu\nu}\delta_{fg} \\ \mathrm{i}g_2^2 g_{\mu\nu}\{I^a, I^b\}_{fg} \end{cases}$
(ix)	$= -\mathrm{i}g_{2,3}^2[f^{abe}f^{cde}(g_{\mu\rho}g_{\nu\sigma} - g_{\mu\sigma}g_{\nu\rho})$ $+f^{ace}f^{bde}(g_{\mu\nu}g_{\rho\sigma} - g_{\mu\sigma}g_{\nu\rho})$ $+f^{ade}f^{bce}(g_{\mu\nu}g_{\rho\sigma} - g_{\mu\rho}g_{\nu\sigma})]$

FIGURE 2.1: Collection of Feynman rules for SM particles in Feynman gauge. f, g are SU(N) flavour indices, μ, ν, ρ, σ are Lorentz indices and a, b, c, d are indices in the adjoint representation. p, k and q are momenta that point in arrow direction for fermions and the Higgs fields. In diagram (iv) momenta are chosen such that they point towards the vertex. I^a_{fg} and T^a_{fg} are the generators of the $\mathrm{SU}(2)_\mathrm{L}$ and $\mathrm{SU}(3)_c$, respectively, while $t^a_{fg} \in \{I^a_{fg}, T^a_{fg}\}$. Only top Yukawa vertices are shown. However, diagrams (iii) and (vi) can be generalised to the other quarks as well.

STANDARD SCENARIO OF MASSIVE NEUTRINOS: Neutrino masses can arise in two ways. On the one hand, these can be expressed as Majorana spinors ν_{L} with definite Majorana mass m_ν, such that the mass term is given by

$$\overline{\nu_{\mathrm{L}}} m_\nu \nu_{\mathrm{L}}^c + \mathrm{h.c.}\,. \tag{2.21}$$

Such a mass terms comes without the need of adding new degrees of freedom to the SM. Note, however, that this term violates gauge invariance and it is a priori not allowed. Nevertheless, it can only be the low energy limit of a higher dimensional operator in an effective field theory, when integrating out the heavy degrees of freedom. One example is the dimension-five Weinberg operator [113]

$$\frac{1}{2}\bar{\ell}_{\mathrm{L}}\tilde{\phi} f \tilde{\phi}^T \ell_{\mathrm{L}}^c + \mathrm{h.c.}\,, \tag{2.22}$$

that constructs the tern (2.21) after a spontaneous SB of the field ϕ and violates total L by two units. f, as a remnant of the heavy fields that have been integrated out, is a flavour matrix with mass dimension of (-1). A well-motivated example for such heavy fields are the RH neutrinos, which are introduced and discussed in subsection 2.2.2.

NEUTRINO FLAVOUR OSCILLATIONS: The Lagrangian which represents the EW interactions after the EWSB is given by

$$\mathscr{L}_{\mathrm{EW}} = -\frac{g_2}{\sqrt{2}}\overline{\nu_{\mathrm{L}}}\gamma^\mu e_{\mathrm{L}} W_\mu^+ - \frac{g_2}{\sqrt{2}}\overline{e_{\mathrm{L}}}\gamma^\mu \nu_{\mathrm{L}} W_\mu^- - \frac{g_2}{2\cos\theta_W}\overline{\nu_{\mathrm{L}}}\gamma^\mu \nu_{\mathrm{L}} Z_\mu + \mathrm{h.c.}\,, \tag{2.23}$$

where g_2 is the SU(2) coupling constant and θ_{W} is the Weinberg angle with $\sin^2\theta_{\mathrm{W}} \simeq 0.22$. The Lagrangian (2.23) is given in the basis of the EW interaction eigenstates ν_e, ν_μ, ν_τ. When allowing for massive neutrinos, the mass term is not necessarily diagonal in the same basis. Rather, the EW interaction states are superpositions of the three mass eigenstates, i.e. the eigenstates of the vacuum Hamiltonian. In analogy to the quark sector, this is achieved by a unitary transformation

$$\begin{pmatrix}\nu_e\\ \nu_\mu\\ \nu_\tau\end{pmatrix} = U_\nu \begin{pmatrix}\nu_1\\ \nu_2\\ \nu_3\end{pmatrix}\,, \tag{2.24}$$

where U_ν is the PMNS neutrino matrix [114, 115]. U_ν depends on three real mixing angles θ_{12}, θ_{23}, θ_{13} and on one Dirac phase δ. When allowing for the Majorana nature of the neutrinos U_ν additionally needs the existence of two Majorana phases $\alpha_{1,2}$. Consequently, the most general form describing the relation between the flavour and mass eigenstates in the neutrino sector is given by [114, 115]

$$U_\nu = V^{(23)} U_\delta V^{(13)} U_{-\delta} V^{(12)} \mathrm{diag}(\mathrm{e}^{\mathrm{i}\alpha_1/2}, \mathrm{e}^{\mathrm{i}\alpha_2/2}, 1)\,, \tag{2.25}$$

with $U_{\pm\delta} = \mathrm{diag}(\mathrm{e}^{\mp \mathrm{i}\delta/2}, 1, \mathrm{e}^{\pm \mathrm{i}\delta/2})$, as well as with the matrices $V^{(ab)}$, i.e.

$$V^{(23)} = \begin{pmatrix}1 & 0 & 0\\ 0 & c_{23} & s_{23}\\ 0 & -s_{23} & c_{23}\end{pmatrix}, V^{(13)} = \begin{pmatrix}c_{13} & 0 & s_{13}\\ 0 & 1 & 0\\ -s_{13} & 0 & c_{13}\end{pmatrix}, V^{(12)} = \begin{pmatrix}c_{12} & s_{12} & 0\\ -s_{12} & c_{12} & 0\\ 0 & 0 & 1\end{pmatrix}. \tag{2.26}$$

	NO	IO
$\sin^2\theta_{12}$	0.307	0.307
$\sin^2\theta_{13}$	0.002195	0.002212
$\sin^2\theta_{23}$	0.565	0.572
$\frac{\Delta m^2_{21}}{10^{-5}\,\mathrm{eV}^2}$	7.40	7.40
$\frac{\Delta m^2_{3k}}{10^{-3}\,\mathrm{eV}^2}$	2.515	-2.483

TABLE 2.2: Best fit values for the neutrino mixing angles and the two mass differences from November 2017 (NuFIT v3.1) [116]. $\Delta m^2_\odot \equiv \Delta m^2_2 - \Delta m^2_1 > 0$ corresponds to the solar mass difference. $\Delta m^2_{3k} \equiv \Delta m^2_3 - \Delta m^2_1 > 0$ for NO and $\Delta m^2_{3k} \equiv \Delta m^2_3 - \Delta m^2_2 < 0$ for IO are referred to as the atmospheric mass difference.

s_{ab} and c_{ab} as shorthand notations for $\sin\theta_{ab}$ and $\cos\theta_{ab}$, respectively. In vacuum, i.e. not in matter, the probability of detecting a neutrino that has been produced with flavour a via the EW interactions with a flavour b at some later time is given by

$$P(\nu_a \to \nu_b) = \delta_{ab} - 4\sum_{i>j} \mathrm{Re}\left(U^*_{ai}U_{bi}U_{aj}U^*_{bj}\right)\sin^2\left(\frac{\Delta m^2_{ij}L_\nu}{4E_\nu}\right) + 2\sum_{i>j}\mathrm{Im}\left(U^*_{ai}U_{bi}U_{aj}U^*_{bj}\right)\sin\left(\frac{\Delta m^2_{ij}L_\nu}{2E_\nu}\right), \tag{2.27}$$

with the mass difference $\Delta m^2_{ij} = m^2_i - m^2_j$, the neutrino energy E_ν and the oscillation distance L_ν.

CURRENT EXPERIMENTAL STATUS OF NEUTRINO MASSES AND MIXINGS: Due to accumulation of neutrino oscillation data in the past, it is possible to determine the three neutrino mixing angles and the two mass differences. Results from November 2017 (NuFIT v3.1) [116] from a global fit analysis, collecting data from solar, atmospheric, reactor and accelerator experiments, are shown in table 2.2. Even though, the following puzzles need to be resolved:

- *Neutrino mass ordering:* While the sign of the solar mass difference $\Delta m^2_\odot \equiv m^2_2 - m^2_1$ is known, only the absolute value of the atmospheric mass difference $|m^2_{\mathrm{atm}}| \equiv |m_3 - m_{1,2}| \gg m^2_\odot$ is accessible. Consequently, there is an ambiguity in the neutrino mass ordering. NO describes the setup $m^2_1 < m^2_2 < m^2_3$, while IO corresponds to $m^2_3 < m^2_2 < m^2_1$.

- *Determination of CP-violating phases:* The CP-violating phases such as the Dirac phase δ and the Majorana phases $\alpha_{1,2}$ have not been determined so far. Ref. [116] prefers $\delta = (228^{+51}_{-33})^\circ$ for NO and $\delta = (281^{+30}_{-33})^\circ$ for IO. Due to these rather large error bars δ is kept as a free unconstrained parameter throughout this thesis. Constraints on the Majorana phases $\alpha_{1,2}$ might be available when detecting heavy neutrinos in future experiments [1].

- *Absolute mass scale:* As only two mass differences have been measured, the absolute mass scale still remains undetermined. It is convenient to use, besides the solar and atmospheric mass difference, the mass of the lightest neutrino m_0 to quantify

	NO	IO
m_1^2	m_0^2	$m_0^2 - \Delta m^2_\odot + \Delta m^2_{\text{atm}}$
m_2^2	$m_0^2 + \Delta m^2_\odot$	$m_0^2 + \Delta m^2_{\text{atm}}$
m_3^2	$m_0^2 + \Delta m^2_{\text{atm}}$	m_0^2

TABLE 2.3: Neutrino masses expressed in terms of the undetermined mass of the lightest neutrino m_0, the solar mass difference $\Delta m^2_\odot$ and the atmospheric mass difference Δm^2_{atm}, cf. table 2.2.

the neutrino masses, cf. table 2.3. It is $m_0 = m_1$ for NO and $m_0 = m_3$ for IO. Note that $m_0 = 0$ is required when the neutrino masses are generated within the seesaw mechanism with only two RH neutrinos. Although the absolute mass scale is unknown, the sum of the three neutrinos is limited [24]:

$$m_{\text{lower}} < \sum_{a=e,\mu,\tau} m_a < m_{\text{upper}} \,. \tag{2.28}$$

On the one hand the lower bounds $m_{\text{lower}} \simeq 0.06\,\text{eV}$ for NO and $m_{\text{lower}} \simeq 0.1\,\text{eV}$ for IO are due to the measured mass differences, when setting the mass of the lightest neutrino to $m_0 = 0$. On the other hand, cosmology can imply an upper bound. Ref. [24] e.g. suggests $m_{\text{upper}} \simeq 0.23\,\text{eV}$. Stronger bounds are e.g. given in ref. [117].

2.2 INTRODUCING RIGHT-HANDED NEUTRINOS

The section describes how the SM can be extended minimally be two or more RH neutrinos. The coupling to the SM particles via the Yukawa coupling is accounted for by the Lagrangian in subsection 2.2.1. This extension allows for a generation of the observed SM neutrino masses via the seesaw mechanism, as shown in subsection 2.2.2. A useful parametrisation of the Yukawa couplings, that depend on new parameters, is given in subsection 2.2.3. The symmetry protected scenario as well as the physical mass splitting are shortly introduced in subsections 2.2.4 and 2.2.5. This section is based on the review [16].

2.2.1 *Lagrangian*

Since the neutrinos are the only chiral fermions in the SM that only appear with LH chirality, it sounds reasonable to add RH neutrino fields ν_R to the SM in analogy to the quark sector, see figure 2.2. These new fields are required to be SM gauge singlets and their communication with the SM fields should be only via Yukawa interactions with the LH leptons and the Higgs field, analogously as the RH quarks couple to the LH quarks. Under suppression of flavour indices this minimal extension of the SM is given by the following Lagrangian

$$\mathscr{L} = \mathscr{L}_{\text{SM}} + \mathrm{i}\overline{\nu_\text{R}}\partial\!\!\!/\nu_\text{R} - \mathrm{i}\overline{\ell_\text{L}}Y^\dagger\nu_\text{R}\tilde{\phi} - \mathrm{i}\tilde{\phi}^\dagger\overline{\nu_\text{R}}Y\ell_\text{L} - \frac{1}{2}\left(\overline{\nu_\text{R}^c}M\nu_\text{R} + \overline{\nu_\text{R}}M^\dagger\nu_\text{R}^c\right) . \tag{2.29}$$

Here $\ell_\text{L} = (\nu_\text{L}, e_\text{L})^T$ is the LH SM SU(2)-doublet and ϕ is the Higgs field with $\tilde{\phi} = \varepsilon\phi^*$, where ε is the totally antisymmetric rank two tensor with $\varepsilon_{12} = 1$. Y is the Yukawa matrix that describes the sole coupling of the RH neutrinos to the SM. RH neutrinos are Majorana particles with the Majorana mass matrix M that fulfils $\nu_\text{R}^c = C\overline{\nu_\text{R}}^T$, where

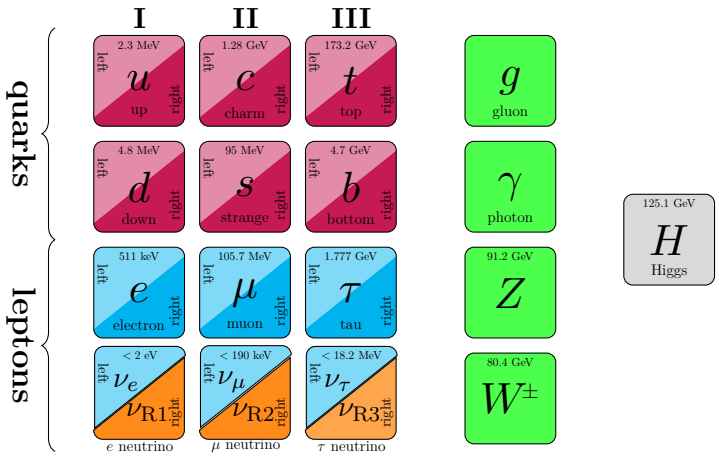

FIGURE 2.2: Minimal extension of the SM by two or three RH neutrinos (orange). The third RH neutrino is displayed in light orange since two RH neutrinos are already sufficient to generate the light neutrino masses and to account for the BAU.

$C = \mathrm{i}\gamma_2\gamma_0$ the charge conjugation matrix in the Weyl representation. This induces a new scale that is not necessarily connected to the EW scale. Nevertheless, RH neutrino masses in the GeV-scale are well motivated when it comes to an experimental discovery, cf. chapters 5 and 6. Within this thesis, when not mentioned explicitly, calculations are done in the EW interaction basis for the SM neutrinos and in addition in the basis where the Majorana matrix M is real and diagonal.

For $T < T_{\mathrm{EW}}$ the Higgs acquires a non-vanishing vacuum expectation value (VEV) due to the spontaneous EWSB of the SM, $\phi \to \langle\phi\rangle = (0, v)^T$, with $v = 174\,\mathrm{GeV}$. In analogy to the quarks a Dirac mass term for the neutrinos

$$\overline{\nu_{\mathrm{R}}} m_D \nu_{\mathrm{L}} + \mathrm{h.c.}\,, \tag{2.30}$$

is constructed from the Yukawa terms in eq. (2.29) with the Dirac mass matrix

$$m_D = v Y^\dagger\,. \tag{2.31}$$

If the neutrinos are Dirac particles, i.e. for $M = 0$, the LH and RH neutrino fields can be grouped into spinors $\Psi_\nu = U_\nu^\dagger \nu_{\mathrm{L}} + \hat{U}_\nu^\dagger \nu_{\mathrm{R}}$ with definite mass. U_ν and $\hat{U}_\nu$ are 3×3 unitary matrices that diagonalise the mass term $m_\nu^{\mathrm{diag}} = U_\nu^\dagger m_D \hat{U} \nu = \mathrm{diag}(m_1, m_2, m_3)$, such that $\overline{\Psi_\nu}(\mathrm{i}\partial\!\!\!/ - m_\nu^{\mathrm{diag}})\Psi_\nu$. In this case U_ν is the PMNS matrix (2.25) for $\alpha_{1,2} = 0$ when using the EW interaction basis. Note that $\hat{U}_\nu$ is unphysical and can be absorbed into field redefinitions of ν_{R}, while U_ν appears in the Yukawa terms in eq. (2.29). Such Dirac neutrinos would be ruled out as soon as $0\nu\beta\beta$-decays are observed. In order to be consistent with the observation of small neutrino masses, see table 2.2, eq. (2.31) implies that the Yukawa couplings need to be very tiny, i.e. $Y \sim 10^{-12}$.

In contrast to that, neutrino masses can not only be explained for $M = 0$, but also when ν_{R} have masses far above the EW scale ($M \gg v$). As discussed within eqs. (2.21) and (2.22) these can be integrated out and yield $f = Y^\dagger M^{-1} Y^*$.

2.2.2 *Type-I seesaw mechanism*

As discussed above, both for $M = 0$ and for $M \gg v$, the RH neutrinos do not appear as new particles in experimental searches. If, however, M has eigenvalues that are both non-zero and not too large, it would be possible to detect RH neutrinos as new particles in near future experiments. This motivates to combine both the Majorana mass term and the Yukawa term after EWSB into the general form

$$\frac{1}{2}\left(\overline{\nu_{\mathrm{L}}}\,\overline{\nu_{\mathrm{R}}^{c}}\right)\mathfrak{M}\begin{pmatrix}\nu_{\mathrm{L}}^{c}\\ \nu_{\mathrm{R}}\end{pmatrix}+\mathrm{h.c.}=\frac{1}{2}\left(\overline{\nu_{\mathrm{L}}}\,\overline{\nu_{\mathrm{R}}^{c}}\right)\begin{pmatrix}0 & m_D\\ m_D^T & M\end{pmatrix}\begin{pmatrix}\nu_{\mathrm{L}}^{c}\\ \nu_{\mathrm{R}}\end{pmatrix}+\mathrm{h.c.}\,, \tag{2.32}$$

where $\overline{\nu_{\mathrm{R}}^{c}}M\nu_{\mathrm{R}} = \overline{\nu_{\mathrm{R}}^{c}}M^T\nu_{\mathrm{R}}$ is used due to the Majorana nature of the RH neutrinos. Note that the upper left block matrix of $\mathfrak{M}$ is vanishing at tree level and receives its first contribution $\delta m_\nu^{1\mathrm{loop}}$ at one-loop order [118, 119]. For the purpose of this thesis, i.e. for parameters where leptogenesis works, it is sufficient to neglect this contribution.

The type-I seesaw mechanism is realised when the eigenvalues of M are much larger than those of m_D from eq. (2.30). Hence, a useful expansion parameter (matrix) is

$$\theta \equiv m_D M^{-1}\,, \tag{2.33}$$

which is often referred to as the active-sterile mixing, which will become clear in the following. The mass matrix $\mathfrak{M}$ from eq. (2.32) can then block-diagonalised

$$\tilde{U}^T\mathfrak{M}\tilde{U} = \mathfrak{M}^{\mathrm{diag}} = \mathrm{diag}(m_\nu, M)\,, \tag{2.34}$$

with the matrices

$$m_\nu = \theta M\theta^T = v^2 Y^\dagger M^{-1} Y^*\,, \tag{2.35}$$

$$M_N = M + \frac{1}{2}\left(\theta^\dagger\theta M + M^T\theta^T\theta^*\right)\,, \tag{2.36}$$

when using the unitary matrix

$$\tilde{U} = \begin{pmatrix}1-\frac{1}{2}\theta\theta^\dagger & \theta\\ -\theta^\dagger & 1-\frac{1}{2}\theta^\dagger\theta\end{pmatrix} + \mathcal{O}(\theta^3)\,. \tag{2.37}$$

Eq. (2.35) implies that larger masses M end up in smaller masses of m_ν. Consequently, one can achieve smaller neutrino masses by increasing the Majorana masses - justifying the name seesaw mechanism. In order to diagonalise these two mass matrices, $\mathfrak{M}$ has to be effectively rotated via the matrix

$$\tilde{U}\,\mathrm{diag}(U_\nu, U_N^*)\,, \tag{2.38}$$

with the unitary matrices U_ν and U_N^*. Therefore, two sets of mass eigenstates appear:

$$\upsilon_{\mathrm{L}} \equiv U_\nu^\dagger\left((\mathbb{1}-\frac{1}{2}\theta\theta^\dagger)\nu_{\mathrm{L}} - \theta\nu_{\mathrm{R}}\right) \simeq U_\nu^\dagger\nu_{\mathrm{L}}\,, \tag{2.39}$$

$$m_\nu^{\mathrm{diag}} = U_\nu^\dagger m_\nu U_\nu^* = \mathrm{diag}(m_1, m_2, m_3)\,, \tag{2.40}$$

and

$$\upsilon_{\mathrm{R}} \equiv U_N^\dagger\left((\mathbb{1}-\frac{1}{2}\theta^T\theta^*)\nu_{\mathrm{R}} - \theta^T\nu_{\mathrm{L}}^{c}\right) \simeq U_N^\dagger\nu_{\mathrm{R}}\,, \tag{2.41}$$

$$M_N^{\mathrm{diag}} = U_N^T M_N U_N = \mathrm{diag}(M_{N1}, \cdots, M_{Nn_s})\,. \tag{2.42}$$

Provided that the light neutrino masses are generated by the type-I seesaw mechanism, the LH neutrinos which have measured in experiments are the υ_{L}. These are mainly SU(2) charged doublets ν_{L} and their masses are given by the eigenvalues of m_ν, while having a contribution from ν_{R} that is suppressed by θ. Although the light neutrino mixing matrix

$$V_\nu = \left(\mathbb{1} - \frac{1}{2}\theta\theta^\dagger + \mathcal{O}(\theta^4)\right) U_\nu \,, \tag{2.43}$$

from eq. (2.39) is close to the unitary PMNS matrix U_ν, it theoretically implies a change of the EW currents at $\mathcal{O}(\theta^2)$, cf. eq. (2.23), that can be measured. Due to the active participation in the EW interactions, υ_{L} are often called active neutrinos. On the other hand υ_{R} are mainly SM gauge singlets and do only interact with the SM via the ν_{L} doublet contribution. Since this is suppressed by the small matrix $\theta \ll 1$, their interaction with the SM is feeble. This is why the υ_{R} are often called sterile neutrinos. U_ν is the PMNS matrix (2.25), while U_N is the corresponding unitary matrix in the RH neutrino sector. Usually, due to the smallness of θ, eq. (2.36) simplifies to $M_N \simeq M$, such that $U_N \simeq \mathbb{1}$. However, when having mass splittings that go below the scale of the atmospheric mass difference, this argument fails [1] for the corresponding mass splittings, cf. eq. (2.64) and the discussion in subsection 2.2.4.

It is convenient to introduce the Majorana fields

$$\mathrm{N} \equiv \upsilon_{\mathrm{R}} + \upsilon_{\mathrm{R}}^c \,, \qquad \boldsymbol{\nu} \equiv \upsilon_{\mathrm{L}} + \upsilon_{\mathrm{L}}^c \,, \tag{2.44}$$

that fulfil $\mathrm{N}_i^c = \mathrm{N}_i$ and $\boldsymbol{\nu}_a^c = \boldsymbol{\nu}_a$ as well as $\upsilon_{\mathrm{R}i} = P_{\mathrm{R}}\mathrm{N}_i$ and $\upsilon_{\mathrm{L}a} = P_{\mathrm{L}}\boldsymbol{\nu}_a$ with i the RH neutrino flavour and a the flavour of the LH leptons. This allows to obtain the kinetic and mass terms of the Lagrangian (2.29) after the EWSB in the basis where the mass matrices M_N and m_ν are diagonal:

$$\frac{1}{2}\bar{\boldsymbol{\nu}}\left(\mathrm{i}\partial\!\!\!/ - m_\nu^{\mathrm{diag}}\right)\boldsymbol{\nu} + \frac{1}{2}\bar{\mathrm{N}}\left(\mathrm{i}\partial\!\!\!/ - M_N^{\mathrm{diag}}\right)\mathrm{N} \,. \tag{2.45}$$

Note that one can analogously use eq. (2.44) for the RH SM singlet neutrinos ν_{R} instead of the sterile neutrinos υ_{R} and also ν_{L} instead of υ_{L} in order to rewrite the Lagrangian (2.29):

$$\mathscr{L} = \mathscr{L}_{\mathrm{SM}} + \frac{1}{2}\bar{N}_i\left(\mathrm{i}\partial\!\!\!/ - M\right)_{ij} N_j - Y_{ia}^* \bar{\ell}_{\mathrm{L}a}\varepsilon\phi P_{\mathrm{R}} N_i - Y_{ia}\bar{N}_i P_{\mathrm{L}}\phi^\dagger\varepsilon^\dagger\ell_{\mathrm{L}a} \,. \tag{2.46}$$

where the spinor N_i is such that observes the Majorana condition $N_i^c = N_i$. With this choice of basis the Yukawa couplings Y_{ia} are non-diagonal. Feynman rules are given in the top row of figure 5.1. Further, we use the nomenclature that both υ_{R} and ν_{R} as well as the N are referred to as heavy neutrinos, while υ_{L}, ν_{L} and $\boldsymbol{\nu}_{\mathrm{L}}$ are denoted as light neutrinos from now on.

Eq. (2.41) suggests that after the EWSB the heavy neutrinos take part in the EW interaction via the mixing with ν_{L}. The coupling of the heavy neutrinos in the basis where M is diagonal to the SM via the EW couplings is then obtained from eq. (2.23), such that

$$\begin{aligned}
\mathscr{L}_{\mathrm{EW}} \simeq & -\frac{g_2}{\sqrt{2}}\bar{N}_i\Theta_{ia}^\dagger\gamma^\mu e_{\mathrm{L}a}W_\mu^+ - \frac{g_2}{\sqrt{2}}\bar{e}_{\mathrm{L}a}\gamma^\mu\Theta_{ai}N_i W_\mu^- \\
& - \frac{g_2}{2\cos\theta_W}\bar{N}_i\Theta_{ia}^\dagger\gamma^\mu\nu_{\mathrm{L}a}Z_\mu - \frac{g_2}{2\cos\theta_W}\bar{\nu}_{\mathrm{L}a}\gamma^\mu\Theta_{ai}N_i Z_\mu \\
& - \frac{g_2}{\sqrt{2}}\frac{M_i}{m_W}\bar{N}_i\Theta_{ia}^\dagger h\bar{N}_i\nu_{\mathrm{L}a} - \frac{g_2}{\sqrt{2}}\frac{M_i}{m_W}\bar{\nu}_{\mathrm{L}a}\Theta_{ai}hN_i \,,
\end{aligned} \tag{2.47}$$

up to higher orders in Θ. h is the physical Higgs field after EWSB. Therefore, the interaction with the EW gauge bosons $W^{\pm}, Z$ and the coupling to h are suppressed by the mixing angle

$$\Theta_{ai} \equiv (\theta U_N^*)_{ai} \simeq \theta_{ai} \,, \tag{2.48}$$

with θ from eq. (2.33) together with eq. (2.31). This defines the active-sterile mixing angles

$$U_{ai}^2 \equiv |\Theta_{ai}|^2 \simeq |\theta_{ai}|^2 \,, \tag{2.49}$$

often just referred to mixing angles or even mixings, which future experiments can constrain. Provided that the mass resolution is too low to distinguish the heavy neutrinos, constraints from experiments should be applied to

$$U_a^2 = \sum_i U_{ai}^2 = \sum_i |\theta_{ai}|^2 \,. \tag{2.50}$$

Within this thesis the ratios U_a^2/U^2 will be denoted as flavour mixing ratios or just flavour ratios. When summing over the heavy neutrino flavours i, U_a^2 looses its dependence on U_N. Thus, it is not possible to probe U_N in such experiments. If the experiment is insensitive the SM neutrino flavour as well, only the total mixing can be measured

$$U^2 = \sum_a U_a^2 \,. \tag{2.51}$$

2.2.3 *Parametrisation of Yukawa couplings*

By extending the SM by n_s heavy neutrinos, $7n_s - 3$ new parameters are generated including the light neutrino masses: These are the n_s masses M_i of the heavy neutrinos. When considering the basis, where the mass matrix for the heavy neutrino is real and diagonal, the Yukawa matrix Y from eq. (2.29) is non-diagonal and has $3 \times n_s$ complex entries, out of which three can by absorbed via phase rotations of the SM leptons ℓ_{L}. Note that the Majorana mass term (2.36) is not invariant under such a rephasing due to the charge conjugated field. A connection between the low energy neutrino oscillation data, cf. table 2.2, and the Lagrangian (2.29) is established by the Casas-Ibarra parametrisation [120]

$$Y^\dagger = \frac{1}{v} U_\nu \sqrt{m_\nu^{\mathrm{diag}}} \mathcal{R} \sqrt{M^{\mathrm{diag}}} \,. \tag{2.52}$$

$v = 174\,\mathrm{GeV}$ is the VEV of the Higgs field after EWSB, $\sqrt{m_\nu^{\mathrm{diag}}}$ is the diagonalised mass matrix for the light neutrinos, see eq. (2.40), and $\sqrt{M^{\mathrm{diag}}}$ is the diagonal heavy neutrino mass matrix (2.42). The remaining n_s complex angles are contained in the orthogonal matrix $\mathcal{R}$ with $\mathcal{R}^T\mathcal{R} = \mathbb{1}$. Eq. (2.35) implies that within the type-I seesaw mechanism there have to be at least two or more heavy neutrinos in order to explain the light neutrino mass differences. Therefore, we limit our discussion to two and three heavy neutrinos.

TWO HEAVY NEUTRINOS: This scenario is highly motivated as it is the minimal extension of the SM in terms of heavy neutrinos that is able to explain the neutrino masses, in which case the lightest neutrino is massless, and which can also account for the

BAU. This was first shown ref. [44]. In this case the SM receives 11 new parameters: two masses for both the RH and the SM neutrinos. The three mixing angles in the SM lepton sector θ_{ab}, two phases α and δ, as well as one complex angle ω. Note that for NO only α_2, while for IO only the combination $\alpha_2 - \alpha_1$ is physical. For that reason it is possible to set $\alpha_1 = 0$ and to define $\alpha \equiv \alpha_2$. The most general form of the orthogonal matrix for the two mass orderings is given by

$$\mathcal{R}^{\rm NO} = \begin{pmatrix} 0 & 0 \\ \cos\omega & \sin\omega \\ -\xi\sin\omega & \xi\cos\omega \end{pmatrix}, \qquad \mathcal{R}^{\rm IO} = \begin{pmatrix} \cos\omega & \sin\omega \\ -\xi\sin\omega & \xi\cos\omega \\ 0 & 0 \end{pmatrix}, \tag{2.53}$$

with $\xi = \pm 1$.

THREE HEAVY NEUTRINOS: The scenario of three heavy neutrinos can motivated by the νMSM [44, 45], where the third heavy neutrino can be a DM candidate, while the other two can account for the BAU and the light neutrino masses as discussed above. This comes along with 18 new parameters. The six masses of the neutrinos, the three mixing angles θ_{ab}, three phases $\alpha_{1,2}$ and δ, as well as three complex angles ω_{ij}. $\mathcal{R}$ in its most general form is given by

$$\mathcal{R} = \mathcal{R}^{(23)}\mathcal{R}^{(13)}\mathcal{R}^{(12)}, \tag{2.54}$$

where the non-vanishing entries read

$$\mathcal{R}^{(ij)}_{ii} = \mathcal{R}^{(ij)}_{jj} = \cos\omega_{ij}, \tag{2.55}$$

$$\mathcal{R}^{(ij)}_{ij} = -\mathcal{R}^{(ij)}_{ji} = \sin\omega_{ij}, \tag{2.56}$$

$$\mathcal{R}^{(ij)}_{kk} = 1 \quad \text{for } k \neq i, j. \tag{2.57}$$

The parameters that need to be determined in the future are the masses M_i of the heavy neutrinos, the Majorana phases $\alpha_{1,2}$, as well as Reω_{ij} and Imω_{ij}. Further, δ requires a more accurate determination in order to be quantitatively meaningful. Scenarios with more than three heavy neutrinos are possible. However, these introduce even more new unknown parameters to the SM, making the model even harder to test and to constrain.

2.2.4 *Symmetry protected scenario*

Eq. (2.35) naively implies that Yukawa couplings, and so the active-sterile mixing angles, for heavy neutrino masses in the GeV-range need to be small in order to account for the light neutrino masses. In this case the active-sterile mixing can be related to the heavy neutrino mass via the naive seesaw relation

$$U_0^2 \sim \sqrt{m_{\rm atm}^2 + m_0^2}/\bar{M}. \tag{2.58}$$

When introducing the SB parameters

$$\mu = \frac{\Delta M}{\bar{M}}, \qquad \epsilon = \mathrm{e}^{-2{\rm Im}\omega}, \tag{2.59}$$

where

$$\bar{M} \equiv \frac{M_1 + M_2}{2}, \qquad \Delta M = \frac{M_2 - M_1}{2}, \tag{2.60}$$

for two heavy neutrinos, one can express the total mixing angle as

$$U^2 \simeq \frac{\mu}{1-\mu^2}\frac{m_2-m_3}{\bar{M}}\cos(2\mathrm{Re}\omega) + \frac{1}{1-\mu^2}\frac{m_2+m_3}{\bar{M}}\left(\epsilon+\frac{1}{\epsilon}\right), \tag{2.61}$$

for NO and analogously for IO

$$U^2 \simeq \frac{\mu}{1-\mu^2}\frac{m_1-m_2}{\bar{M}}\cos(2\mathrm{Re}\omega) + \frac{1}{1-\mu^2}\frac{m_1+m_2}{\bar{M}}\left(\epsilon+\frac{1}{\epsilon}\right). \tag{2.62}$$

Expressions for the different U_{ai}^2 are given in appendix B.1. U_{ai}^2 that are much larger than what eq. (2.58) suggests, which is particularly interesting in terms of an experimental discovery of heavy neutrinos, can be achieved in the limit, $\mu \to 0$ and $\epsilon \to 0$. One finds that in this limit the Lagrangian (2.45) features a global U(1) symmetry, where the heavy neutrinos form so-called pseudo-Dirac spinors, that conserve $B-L$, cf. e.g. ref. [70, 112]. As a consequence, one can conclude that small μ, that are needed for successful leptogenesis with two heavy neutrinos [2] with mixing angles large enough for an experimental discovery in the near future, naturally arise in the symmetric limit. Such a scenario is called the symmetry protected scenario. Note, however, that ϵ needs to remain finite in order to explain the non-zero SM neutrino masses. Within this thesis we often refer this symmetry protected scenario to as the approximate $B-L$ conserving limit. Further, $\mu, \epsilon \ll 1$ implies that $Y_{1a} = \mathrm{i}Y_{2a} = Y_a/\sqrt{2}$ holds in the mass basis, and thus

$$U_{a1}^2 = U_{a2}^2 = \frac{1}{2}U_a^2\,. \tag{2.63}$$

2.2.5 *Physical mass splitting*

It is worth mentioning that even though $M_N \simeq M$ up to $\mathcal{O}(\theta^2)$, cf. eq. (2.36), the corresponding mass differences ΔM can differ sizeably. In fact, the argument from eq. (2.50) only holds for the physical mass splitting, i.e. the mass splitting from M_N after the EWSB. In refs. [3, 121] it is shown that it can be related to ΔM, the Majorana mass difference, via

$$\Delta M_{\mathrm{phys}} = \sqrt{\Delta M^2 + \Delta M_{\theta\theta}^2 - 2\Delta M \Delta M_{\theta\theta}\cos(2\mathrm{Re}\omega)}\,, \tag{2.64}$$

where $\Delta M_{\theta\theta} = m_2 - m_3$ for NO and $\Delta M_{\theta\theta} = m_1 - m_2$ for IO. Therefore, experiments are only sensitive to U_{ai}^2 if they can resolve the physical mass splitting ΔM_{phys}.

Note that for any choice of μ the limit $\epsilon \to 0$ implies that ratios U_a^2/U^2 do neither depend on $\mathrm{Re}\omega$ nor on the seesaw scale $\bar{M}$, while the dependence on $\mathrm{Im}\omega$ vanishes. Therefore, these ratios can be expressed solely by the low energy parameters contained in the PMNS matrix U_ν from eq. (2.25). On the one hand, neutrino oscillation data can predict the range of U_a^2/U^2. On the other hand, a detection of heavy neutrinos in experiments can be used to determine the Majorana phase α. This will be discussed in detail in chapter 6.

3

QUASIPARTICLES AT FINITE TEMPERATURE

In contrast to the in-out formalism, that describes scattering processes by computing S-matrix elements for asymptotically free particles, a powerful framework that allows for a quantum field theory at finite temperatures and for non-equilibrium effects was developed by Schwinger and Keldysh [36, 37] and is based on a 2PI effective action approach on a closed-time-path, the so-called CTP formalism or in-in formalism.

This does not only allow for kinetic equations that account for finite density effects but also to derive full propagators that exhibit the necessary information from the plasma as poles in the complex plane. These can be interpreted as particles excitations propagating through the medium. On the one hand, the real part of these poles gives rise to the dispersion relation, which in general has non-trivial momentum structure. These can be expressed in terms of thermal masses of the particle excitations, that are of order gT, with the corresponding coupling constant g. In the symmetric phase of the SM the Higgs field is unbroken. Therefore, the masses of the different SM particles are simply given by the thermal masses. On the other hand, it is the imaginary part of the complex poles that determines the damping rate of these excitations, which are of order g^2T. Thus, the medium makes the excitations decay, resulting in a finite lifetime and consequently provides a finite width. Provided that the medium is weakly coupled, these excitations can be interpreted as quasiparticles with a well defined (thermal) mass. In such a case one finds that the width of the particles is only important for momenta near the quasiparticle pole, otherwise it is negligible. For this reason, when the damping term behaves smoothly at the pole, one can evaluate it directly at the pole. This corresponds to the Breit-Wigner (BW) approximation. Since properties of quasiparticles in a medium can be read off from the fully resummed propagators, it is necessary to have explicit expressions for these including the relevant self-energies that account for the screening and the dispersion.

Section 3.1 sketches the derivation of quantum kinetic equations for quasiparticle states in a medium at finite temperature within the 2PI CTP approach. In section 3.2 one-loop resummed propagators that account for the surrounding plasma are derived for the different SM particles. Properties of gauge bosons at finite temperature are discussed in appendix A.1. The dispersion relations and the damping behaviour, respectively, for quasiparticles are discussed in section 3.3, while analytic expressions for the necessary one-loop self-energies are computed in appendix A.2 and appendix A.3, respectively.

3.1 QUANTUM KINETIC EQUATIONS AT HIGH TEMPERATURE

In this section the CTP formalism introduced by Schwinger and Keldysh, that is particularly suitable to describe out-of-equilibrium dynamics of quantum fields, is shortly described based on more detailed studies [40, 41].

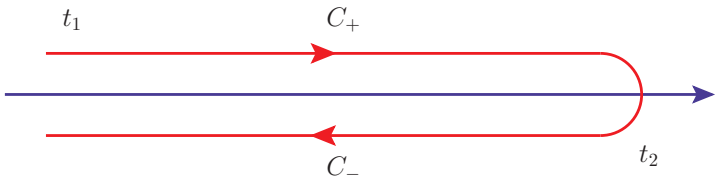

FIGURE 3.1: Time contour in the CTP formalism that runs from a time t_1 on a closed branch $\mathcal{C}_+$ to t_2 and backwards to t_1 on a branch $\mathcal{C}_-$.

For the purpose of this thesis subsection 3.1.1 defines two-point correlation functions as well as self-energy expressions in a hot medium. Kinetic and constraint equations that describe the behaviour of quasiparticles in the plasma are deduced from SD equations for gauge bosons, chiral fermions and the scalar fields in subsection 3.1.2.

3.1.1 *Short introduction to the Schwinger-Keldysh formalism*

The well-known formalism of using S-matrix elements to describe scattering processes fails to describe out-of-equilibrium systems. This is because it is not possible to use well-defined asymptotic states. Further, the properties of quasiparticles in a medium are in general different from those in vacuum. Therefore, it is useful to express the relevant observables in terms of correlation functions that are constructed out of quantum fields.

CORRELATION FUNCTIONS IN A MEDIUM ON A CTP: Two-point functions are defined on the closed-time branch $\mathcal{C}$, as shown in figure 3.1, via

$$\mathrm{i}\Delta(u,v) \equiv \langle \mathcal{T}_{\mathcal{C}} \phi(u)\phi(v)\rangle\,, \qquad \mathrm{i}S_{\alpha\beta}(u,v) \equiv \langle \mathcal{T}_{\mathcal{C}} \psi_\alpha(u)\bar{\psi}_\beta(v)\rangle\,, \tag{3.1}$$

where α,β are spinor indices and $\mathcal{T}_{\mathcal{C}}$ denotes time-ordering on the path $\mathcal{C}$. Further, the EV $\langle\dots\rangle$ should be understood as the quantum statistical average. On the branch $\mathcal{C}$ one can construct in total four different two-point functions for each field, i.e. $\mathrm{i}\Delta^{ab}(u,v)$ and $\mathrm{i}S^{ab}_{\alpha\beta}(u,v)$,

$$= \mathrm{i}\Delta^{ab}(u,v)\,, \tag{3.2}$$

$$= \mathrm{i}S^{ab}(u,v)\,, \tag{3.3}$$

for the CTP indices $a,b=\pm$, out of which only two are linearly independent: The Wightman two-point functions switch path and consequently do not follow any time-ordering. These are given by

$$\mathrm{i}\Delta^{>}(u,v) \equiv \mathrm{i}\Delta^{-+}(u,v) = \langle \phi(u)\phi^\dagger(v)\rangle\,, \tag{3.4}$$
$$\mathrm{i}\Delta^{<}(u,v) \equiv \mathrm{i}\Delta^{+-}(u,v) = \langle \phi^\dagger(v)\phi(u)\rangle\,, \tag{3.5}$$

for scalars fields. For chiral fermion field one analogously has

$$\mathrm{i}S^{>}_{\alpha\beta}(u,v) \equiv \mathrm{i}S^{-+}_{\alpha\beta}(u,v) = \langle \psi_\alpha(u)\bar{\psi}_\beta(v)\rangle\,, \tag{3.6}$$
$$\mathrm{i}S^{<}_{\alpha\beta}(u,v) \equiv \mathrm{i}S^{+-}_{\alpha\beta}(u,v) = -\langle \bar{\psi}_\beta(v)\psi_\alpha(u)\rangle\,. \tag{3.7}$$

In contrast to that, time-ordered and anti-time-ordered two-point functions, accomplished by the time- and anti-time-ordering operator $\mathcal{T}$ and $\bar{\mathcal{T}}$, stay on a given branch and are defined via

$$\mathrm{i}\Delta^{t}(u,v) \equiv \mathrm{i}\Delta^{++}(u,v) = \langle \mathcal{T}\phi(u)\phi^{\dagger}(v)\rangle\,, \tag{3.8}$$

$$\mathrm{i}\Delta^{\bar{t}}(u,v) \equiv \mathrm{i}\Delta^{--}(u,v) = \langle \bar{\mathcal{T}}\phi(u)\phi^{\dagger}(v)\rangle\,, \tag{3.9}$$

for the scalars fields, while for fermion fields these read

$$\mathrm{i}S^{t}_{\alpha\beta}(u,v) \equiv \mathrm{i}S^{++}_{\alpha\beta}(u,v) = \langle \mathcal{T}\psi_{\alpha}(u)\bar{\psi}_{\beta}(v)\rangle\,, \tag{3.10}$$

$$\mathrm{i}S^{\bar{t}}_{\alpha\beta}(u,v) \equiv \mathrm{i}S^{--}_{\alpha\beta}(u,v) = \langle \bar{\mathcal{T}}\psi_{\alpha}(u)\bar{\psi}_{\beta}(v)\rangle\,. \tag{3.11}$$

These can be obtained via linear combination of the Wightman two-point functions

$$G^{t}(u,v) = \vartheta(u^0-v^0)G^{>}(u,v) + \vartheta(v^0-u^0)G^{<}(u,v)\,, \tag{3.12}$$

$$G^{\bar{t}}(u,v) = \vartheta(u^0-v^0)G^{<}(u,v) + \vartheta(v^0-u^0)G^{>}(u,v)\,, \tag{3.13}$$

where G can be either Δ or S.

OTHER USEFUL RELATIONS: When it comes to the derivation of the full propagators it is useful to define the retarded and advanced propagator via

$$G^{r,a} \equiv G^{t} - G^{<,>} = G^{>,<} - G^{\bar{t}}\,. \tag{3.14}$$

Additionally, the linear combinations

$$G^{\mathcal{A}} \equiv \frac{\mathrm{i}}{2}\left(G^{>} - G^{<}\right) = \frac{\mathrm{i}}{2}\left(G^{r} - G^{a}\right)\,, \tag{3.15}$$

$$G^{H} \equiv \frac{1}{2}\left(G^{t} - G^{\bar{t}}\right) = \frac{1}{2}\left(G^{r} + G^{a}\right)\,, \tag{3.16}$$

contain intuitive physical interpretations. The spectral function $G^{\mathcal{A}}$, in particular the spectral part of the self-energy, describes the quasiparticle spectrum and provides a finite width around the quasiparticle pole. The corresponding dispersion relation is given by the Hermitian part G^{H}. Further, it is useful to denote the hermiticity properties of the two-point function

$$\left(\mathrm{i}\Delta^{<,>}(u,v)\right)^{\dagger} = \mathrm{i}\Delta^{<,>}(v,u)\,, \qquad \left(\mathrm{i}\gamma^0 S^{<,>}(u,v)\right)^{\dagger} = \mathrm{i}\gamma^0 S^{<,>}(v,u)\,, \tag{3.17}$$

such that

$$\left(\Delta^{\mathcal{A},H}(u,v)\right)^{\dagger} = \Delta^{\mathcal{A},H}(v,u)\,, \qquad \left(\gamma^0 S^{\mathcal{A},H}(u,v)\right)^{\dagger} = \gamma^0 S^{\mathcal{A},H}(v,u)\,. \tag{3.18}$$

SELF-ENERGIES IN A MEDIUM: In coordinate space the self-energies are obtained through a functional derivative

$$\mathrm{i}\Pi^{ab}(u,v) = \mathrm{i}ab\frac{\partial\Gamma_2[\mathrm{i}\Delta,\mathrm{i}S]}{\partial\mathrm{i}\Delta^{ba}(v,u)}\,, \tag{3.19}$$

$$\mathrm{i}\Sigma^{ab}(u,v) = -\mathrm{i}ab\frac{\partial\Gamma_2[\mathrm{i}\Delta,\mathrm{i}S]}{\partial\mathrm{i}S^{ba}(v,u)}\,, \tag{3.20}$$

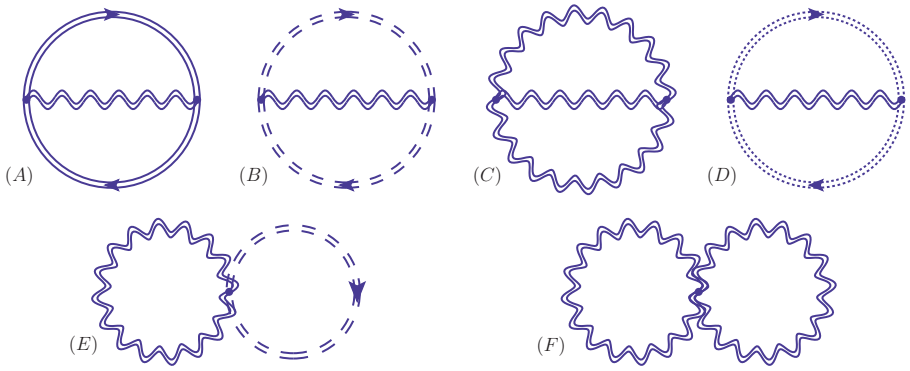

FIGURE 3.2: Collection of 2PI vacuum graphs that are relevant for this thesis. Functional derivatives of the graphs in the upper row produce sunset diagrams, while the bottom row are used to obtain tadpole and seagull diagrams.

of Γ_2, which, as a subset of the 2PI effective action [39, 42, 122], corresponds to $(-\mathrm{i})$ times the sum of all 2PI vacuum graphs. Up to two-loops these are shown in figure 3.2 and are functionals of the full propagators Δ and S. Note that these self-energies are also acting on the CTP and consequently fulfil all the relations given by eqs. (3.12)-(3.18) in analogy to the two-point functions.

Note that we refer not only the (anti-)time-ordered but also the Wightman two-point functions, as well as their Hermitian and spectral parts, to as propagators.

3.1.2 *Schwinger-Dyson equations*

The dynamical behaviour of quasiparticles in a medium can be described by SD equations. Within the 2PI formalism these are obtained via functional derivatives of the 2PI effective action with respect to the two-point functions Δ and S, cf. ref. [40]. For scalar fields, chiral fermions and gauge bosons in Feynman gauge these are given by

$$-\partial^2 \Delta_\phi^{ab}(u,v) = a\delta^{ab}\delta^4(u-v) + \sum_{c=\pm} c \int \mathrm{d}^4 w\, \Pi_\phi^{ac}(u,w)\Delta_\phi^{cb}(w,v)\,, \tag{3.21}$$

$$\mathrm{i}\not{\partial} S_{\mathrm{R,L}}^{ab} = a\delta^{ab}\delta^4(u-v)P_{\mathrm{R,L}} + \sum_{c=\pm} c \int \mathrm{d}^4 w\, \not{\Sigma}_{\mathrm{R,L}}^{ac}(u,w) S_{\mathrm{R,L}}^{cb}(w,v)\,, \tag{3.22}$$

$$\partial^2 \Delta_{\mu\nu}^{ab}(u,v) = a\delta^{ab}\delta^4(u-v)g_{\mu\nu} + \sum_{c=\pm} c \int \mathrm{d}^4 w\, \Pi_{\mu\rho}^{ac}(u,w)\Delta_\nu^{\rho\, cb}(w,v)\,, \tag{3.23}$$

with a, b CTP indices and $\not{\Sigma} = \Sigma^0\gamma_0 - \Sigma^i\gamma_i$. When using the relations (3.14)-(3.16) the SD equations can decomposed into the KB equations

$$-\partial^2 \Delta_\phi^{<,>} - \Pi_\phi^H \odot \Delta_\phi^{<,>} - \Pi_\phi^{<,>} \odot \Delta_\phi^H = \frac{1}{2}\left(\Pi_\phi^> \odot \Delta_\phi^< - \Pi_\phi^< \odot \Delta_\phi^>\right)\,, \tag{3.24}$$

$$\mathrm{i}\not{\partial} S_{\mathrm{R,L}}^{<,>} - \not{\Sigma}_{\mathrm{R,L}}^H \odot S_{\mathrm{R,L}}^{<,>} - \not{\Sigma}_{\mathrm{R,L}}^{<,>} \odot S_{\mathrm{R,L}}^H = \frac{1}{2}\left(\not{\Sigma}_{\mathrm{R,L}}^> \odot S_{\mathrm{R,L}}^< - \not{\Sigma}_{\mathrm{R,L}}^< \odot S_{\mathrm{R,L}}^>\right)\,, \tag{3.25}$$

$$\partial^2 g_{\mu\rho}\Delta_\nu^{\rho\,<,>} - \Pi_{\mu\rho}^H \odot \Delta_\nu^{\rho\,<,>} - \Pi_{\mu\rho}^{<,>} \odot \Delta_\nu^{\rho\, H} = \frac{1}{2}\left(\Pi_{\mu\rho}^> \odot \Delta_\nu^{\rho\,<} - \Pi_{\mu\rho}^> \odot \Delta_\nu^{\rho\,>}\right)\,, \tag{3.26}$$

which only depend on the Hermitian parts and the Wightman functions of the self-energies and two-point functions, as well as into equations that determine the retarded and advanced propagators

$$-\partial^2 \Delta_\phi^{r,a} - \Pi_\phi^{r,a} \odot \Delta_\phi^{r,a} = \delta\,, \tag{3.27}$$

$$\mathrm{i}\not{\partial} S_{\mathrm{R,L}}^{r,a} - \not{\Sigma}_{\mathrm{R,L}}^{r,a} \odot S_{\mathrm{R,L}}^{r,a} = \delta P_{\mathrm{R,L}}\,, \tag{3.28}$$

$$\partial^2 \Delta_{\mu\nu}^{r,a} - \Pi_{\mu\rho}^{r,a} \odot \Delta_\nu^{\rho\, r,a} = \delta g_{\mu\nu}\,. \tag{3.29}$$

The operator $\odot$ is used to define the convolution over $w = (t', \mathbf{w})$:

$$A \odot B \equiv \int_{t_1}^{t_2} \mathrm{d}t' \int \mathrm{d}^3\mathrm{w}\, A(u,w) B(w,v)\,. \tag{3.30}$$

In the following it is useful to send the integration limits to $\pm\infty$, i.e. $t_1 \to -\infty$ and $t_2 \to \infty$ [2, 40].

WIGNER TRANSFORMATION: Although one could compute the dynamics of particles in the high temperature plasma in position space, it is more useful to transform the relevant quantities into Wigner space [40, 123] by performing the Fourier transformation

$$G(k,x) = \int \mathrm{d}^4 r\, \mathrm{e}^{\mathrm{i}k\cdot r}\, G(u,v)\,, \qquad \text{with } x = \frac{u+v}{2} \text{ and } r = u - v\,, \tag{3.31}$$

after introducing the average space-time coordinate $x = (t, \mathbf{x}) = (u+v)/2$ and the relative coordinate $r = u - v$. While in equilibrium Δ and S only depend on r, out-of-equilibrium processes are able to affect the dependence of Δ and S on x. Hence, particularly in baryogenesis scenarios, the Wigner transformation turns out to be useful as it separates the small fluctuations, that happen on microscopic scales, from the macroscopic behaviour of the plasma as the background field, given by x. Moreover, quantities such as self-energies and two-point functions are functions of the momentum k, which is the typical energy scale of the quasiparticles in the plasma. In Wigner space the convolution

$$\int \mathrm{d}^4 r\, e^{ikr} \int \mathrm{d}^4 w\, A(u,w) B(w,v) = e^{-\mathrm{i}\diamond} \{A(k,x)\}\{B(k,x)\}\,, \tag{3.32}$$

can be simplified when making use of the Moyal star product that is defined via the diamond operator

$$\diamond\{\cdot\}\{\cdot\} \equiv \frac{1}{2}(\partial_x^{(1)}\partial_k^{(2)} - \partial_k^{(1)}\partial_x^{(2)})\{\cdot\}\{\cdot\}\,, \tag{3.33}$$

where the superscripts (1) and (2) describe the derivative acting on the first and second argument, respectively. Note that the symmetry relations (3.17) and (3.18) remain unchanged when being transformed to Wigner space:

$$(\mathrm{i}\Delta^{<,>}(k,x))^\dagger = \mathrm{i}\Delta^{<,>}(k,x)\,, \qquad \left(\mathrm{i}\gamma^0 S^{<,>}(k,x)\right)^\dagger = \mathrm{i}\gamma^0 S^{<,>,x}(k,x)\,, \tag{3.34}$$

and

$$\left(\Delta^{\mathcal{A},H}(k,x)\right)^\dagger = \Delta^{\mathcal{A},H}(k,x)\,, \qquad \left(\gamma^0 S^{\mathcal{A},H}(k,x)\right)^\dagger = \gamma^0 S^{\mathcal{A},H}(k,x)\,, \tag{3.35}$$

and analogously for the self-energies Π and Σ.

Solving the SD equations (3.21)-(3.29) with this diamond operator (3.33) is highly challenging as these are complicated integro-differential equations. However, it is possible to find solutions at a certain level of approximation. Both leptogenesis from oscillations from heavy neutrinos and EW baryogenesis happen at early times. Before the EWSB the condition of homogeneity and isotropy allows to neglect the dependence on the spatial component $\mathbf{x}$, i.e. one can get rid of $\mathbf{x}$, such that $G(k,x) \to G(k,t)$. Even during the first-order PT the bubble wall can be treated as a slowly evolving background field when being compared to the typical energy scale $|\mathbf{k}| \sim T$ of quasiparticles in the plasma [40]. Therefore, one can make use of the gradient expansion that allows to expand in small gradients

$$\partial_{\mathbf{x}} \ll k\,. \tag{3.36}$$

To zeroth order in gradients the diamond operator (3.33) vanishes and one obtains the simple relation for the convolutions

$$e^{-\mathrm{i}\diamond}\{A(k,x)\}\{B(k,x)\} = A(k,x)B(k,x) + \mathcal{O}(\partial_{x,k})\,. \tag{3.37}$$

Therefore, the KB equations (3.24)-(3.26) to zeroth order in the gradients (3.36) read

$$\left(k^2 + \mathrm{i}k^0\partial_t - \frac{1}{4}\partial_t^2 - \Pi_\phi^H\right)\Delta_\phi^{<,>} - \Pi_\phi^{<,>}\Delta_\phi^H = \frac{1}{2}\left(\Pi_\phi^>\Delta_\phi^< - \Pi_\phi^<\Delta_\phi^>\right)\,, \tag{3.38}$$

$$\left(\not{k} + \frac{\mathrm{i}}{2}\gamma^0\partial_t - \not{\Sigma}_{\mathrm{R,L}}^H\right)S_{\mathrm{R,L}}^{<,>} - \not{\Sigma}_{\mathrm{R,L}}^{<,>}S_{\mathrm{R,L}}^H = \frac{1}{2}\left(\not{\Sigma}_{\mathrm{R,L}}^>S_{\mathrm{R,L}}^< - \not{\Sigma}_{\mathrm{R,L}}^<S_{\mathrm{R,L}}^>\right)\,, \tag{3.39}$$

$$\left(-\left(k^2 + \mathrm{i}k^0\partial_t - \frac{1}{4}\partial_t^2\right)g_{\mu\rho} - \Pi_{\mu\rho}^H\right)\Delta_\nu^{\rho\,<,>} - \Pi_{\mu\rho}^{<,>}\Delta_\nu^{\rho\,H} = \frac{1}{2}\left(\Pi_{\mu\rho}^>\Delta_\nu^{\rho\,<} - \Pi_{\mu\rho}^>\Delta_\nu^{\rho\,>}\right)\,, \tag{3.40}$$

where the dependence on $\mathbf{x}$ is neglected due to homogeneity of the universe.

Note that since $H \simeq \sqrt{8\pi^3 g_\star/90}T^2/m_{\mathrm{Pl}} \ll T$, with the Planck mass m_{Pl} and $g_\star$ the number of relativistic degrees of freedom, the change of the temperature due to the Hubble expansion is small compared to the typical time scale $1/T$ of microscopical processes. This includes LFV Yukawa processes as well as heavy neutrino production. Consequently, terms of $\mathcal{O}(\partial_t^2)$ in eqs. (3.38)-(3.40) can be neglected, while terms of $\mathcal{O}(\partial_t)$ need to be kept as these describe the time evolution of particle distribution functions.

The equations for the retarded and advanced propagators (3.27)-(3.29) are analogously transformed into Wigner space

$$\left(q^2 - \Pi_\phi^H \pm \mathrm{i}\Pi_\phi^{\mathcal{A}}\right)\Delta_\phi^{r,a} = 1\,, \tag{3.41}$$

$$\left(\not{q} - \not{\Sigma}_{\mathrm{R,L}}^H \pm \mathrm{i}\not{\Sigma}_{\mathrm{R,L}}^{\mathcal{A}}\right)S_{\mathrm{R,L}}^{r,a} = P_{\mathrm{R,L}}\,, \tag{3.42}$$

$$\left(-q^2 g_{\mu\rho} - \Pi_{\mu\rho}^H \pm \mathrm{i}\Pi_{\mu\rho}^{\mathcal{A}}\right)\Delta_\nu^{r,a\,\rho} = g_{\mu\nu}\,. \tag{3.43}$$

KINETIC AND CONSTRAINT EQUATIONS: The Hermitian and anti-Hermitian parts of the KB equations (3.38)-(3.40) correspond to the constraint and kinetic equations, respectively. For the Higgs and the gauge bosons these read

$$\left(k^2 - \Pi_\phi^H\right)\mathrm{i}\Delta_\phi^{<,>} - \mathrm{i}\Pi_\phi^{<,>}\Delta_\phi^H = 0\,, \tag{3.44}$$

$$k^0\partial_t\mathrm{i}\Delta_\phi^{<,>} = -\frac{1}{2}\left(\mathrm{i}\Pi_\phi^>\mathrm{i}\Delta_\phi^< - \mathrm{i}\Pi_\phi^<\mathrm{i}\Delta_\phi^>\right)\,, \tag{3.45}$$

and

$$\left(-k^2 g_{\mu\rho} - \Pi^H_{\mu\rho}\right) \mathrm{i}\Delta^{\rho\,<,>}_{\nu} - \mathrm{i}\Pi^{<,>}_{\mu\rho}\Delta^{\rho\,H}_{\nu} = 0\,, \tag{3.46}$$

$$-\mathrm{i}\partial_t \Delta^{<,>}_{\mu\nu} = -\frac{1}{2}\left(\mathrm{i}\Pi^{>}_{\mu\rho}\mathrm{i}\Delta^{\rho\,<}_{\nu} - \mathrm{i}\Pi^{>}_{\mu\rho}\mathrm{i}\Delta^{\rho\,>}_{\nu}\right)\,, \tag{3.47}$$

while for the fermions they are given by

$$\{\Omega, \mathrm{i}\mathcal{S}^{<,>}\} - \left\{\mathrm{i}\mathcal{G}^{<,>}, \mathcal{S}^H\right\} = -\frac{\mathrm{i}}{2}\left([\mathrm{i}\mathcal{G}^{>}, \mathrm{i}\mathcal{S}^{<}] - [\mathrm{i}\mathcal{G}^{<}, \mathrm{i}\mathcal{S}^{>}]\right)\,, \tag{3.48}$$

$$\mathrm{i}\partial_t \mathrm{i}\mathcal{S}^{<,>} + [\Omega, \mathrm{i}\mathcal{S}^{<,>}] - \left[\mathrm{i}\mathcal{G}^{<,>}, \mathcal{S}^H\right] = -\frac{\mathrm{i}}{2}\left(\{\mathrm{i}\mathcal{G}^{>}, \mathrm{i}\mathcal{S}^{<}\} - \{\mathrm{i}\mathcal{G}^{<}, \mathrm{i}\mathcal{S}^{>}\}\right)\,, \tag{3.49}$$

with

$$\Omega \equiv \left(\not{k} - \not{\Sigma}^H\right)\gamma^0\,, \quad \mathcal{S} \equiv \gamma^0 S\,, \quad \mathcal{G} \equiv \gamma^0 \not{\Sigma}\,. \tag{3.50}$$

3.2 ONE-LOOP RESUMMED PROPAGATORS

The properties of quasiparticles in a hot medium can be read off from full propagators. Particularly the dispersion relations and the damping behaviour are given by the Hermitian and spectral parts of the self-energies that appear in the propagators. These propagators are given as solutions to eqs. (3.41)-(3.43). Note that in general it is not easy to solve such systems since the self-energies exhibit a functional dependence on the propagators. However, as a useful approximation, one can neglect this dependence. This allows to obtain analytic expressions for the retarded and advanced propagators. The corresponding spectral and Hermitian propagators are obtained by taking the imaginary and real part of the advanced propagator, respectively, cf. eqs. (3.15) and (3.16).

The spectral and Hermitian parts of the full propagators for the different SM particles are derived in subsection 3.2.1. In subsection 3.2.2 Wightman propagators are expressed in terms of the spectral propagators and particle distribution functions. Tree-level expressions for the different correlation functions are provided in subsection 3.2.3.

3.2.1 *Spectral and Hermitian contributions*

Fully resummed propagators are most conveniently decomposed into their spectral and Hermitian parts. Particularly when solving the KB equations in Wigner space (3.38)-(3.40), the Hermitian parts of propagators need to be inserted. Solution to the constraint equations (3.44), (3.46) and (3.49) allow to express the Wightman propagators in terms of the spectral propagators, that accounts for the finite width and the dispersion, as well as a particle distribution function.

HIGGS FIELD: For the Higgs the full propagator is simply obtained by inverting eq. (3.41), such that

$$\Delta^{r,a}_{\phi}(q) = \frac{1}{q^2 - \Pi^H_\phi \pm \mathrm{i}\Pi^{\mathcal{A}}_\phi}\,, \tag{3.51}$$

with the spectral and Hermitian propagators

$$\Delta^{\mathcal{A}}_{\phi}(q) = \frac{\Pi^{\mathcal{A}}_\phi}{\left(q^2 - \Pi^H_\phi\right)^2 + \Pi^{\mathcal{A}\,2}_\phi}\,, \qquad \Delta^{H}_{\phi}(q) = \frac{q^2 - \Pi^H_\phi}{\left(q^2 - \Pi^H_\phi\right)^2 + \Pi^{\mathcal{A}\,2}_\phi}\,. \tag{3.52}$$

FERMIONS: In case of the fermions one needs to get rid of the Dirac structure. This can be done in two ways. The approach which seems to be more straightforward is to multiply the LH side of eq. (3.42) with $(\not{q} - \not{\Sigma}^H \mp \mathrm{i}\not{\Sigma}^{\mathcal{A}})$. This yields

$$S^{r,a}_{\mathrm{R,L}}(q) = \frac{\not{q} - \not{\Sigma}^H \mp \mathrm{i}\not{\Sigma}^{\mathcal{A}}}{(q^2 - \Sigma^H)^2 - \Sigma^{\mathcal{A}\,2} \mp [q - \Sigma^H, \mathrm{i}\Sigma^{\mathcal{A}}]}\,, \tag{3.53}$$

and recovers the known result from ref. [124–126]

$$S^{\mathcal{A}}_{\mathrm{R,L}}(q) = P_{\mathrm{R,L}} \frac{2\left(\not{q} - \not{\Sigma}^H\right)\Sigma^{\mathcal{A}}(q - \Sigma^H) - \left[\left(q - \Sigma^H\right)^2 - \Sigma^{\mathcal{A}\,2}\right]\not{\Sigma}^{\mathcal{A}}}{\left[\left(q - \Sigma^H\right)^2 - \Sigma^{\mathcal{A}\,2}\right]^2 + \left[2\Sigma^{\mathcal{A}}(q - \Sigma^H)\right]^2}\,. \tag{3.54}$$

This approach, however, hides some crucial physical information, namely the fact that, besides the electron poles, there are so-called holes or plasminos [127]. In order to account for these one can decompose the fermion propagator into the two contributions

$$S^{ab}_{\mathrm{R,L}}(q) = \frac{1}{2} P_{\mathrm{R,L}} \sum_{\pm} (\gamma^0 \mp \gamma^i \hat{q}_i) S^{ab}_{\pm}(q)\,, \tag{3.55}$$

where S_+ is the electron contribution and S_- refers to the holes, given as the positive and negative helicity eigenstates. With the notation $\Sigma^i(q) \equiv |\mathbf{\Sigma}(q)|\hat{q}^i$ the different contributions read

$$S^{r,a}_{\pm}(q) = \frac{1}{q^0 - \Sigma^{H0} - \mathrm{i}\Sigma^{\mathcal{A}0} \mp (|\mathbf{q}| - |\mathbf{\Sigma}^H| - \mathrm{i}|\mathbf{\Sigma}^{\mathcal{A}}|)}\,, \tag{3.56}$$

$$S^{\mathcal{A}}_{\pm}(q) = \frac{\Sigma^{\mathcal{A}0} \mp |\mathbf{\Sigma}^{\mathcal{A}}|}{\left[q^0 \mp |\mathbf{q}| - (\Sigma^{H0} \mp |\mathbf{\Sigma}^H|)\right]^2 + \left[\Sigma^{\mathcal{A}0} \mp |\mathbf{\Sigma}^{\mathcal{A}}|\right]^2}\,, \tag{3.57}$$

$$S^{H}_{\pm}(q) = \frac{q^0 \mp |\mathbf{q}| - (\Sigma^{H0} \mp |\mathbf{\Sigma}^H|)}{\left[q^0 \mp |\mathbf{q}| - (\Sigma^{H0} \mp |\mathbf{\Sigma}^H|)\right]^2 + \left[\Sigma^{\mathcal{A}0} \mp |\mathbf{\Sigma}^{\mathcal{A}}|\right]^2}\,. \tag{3.58}$$

GAUGE BOSONS: In order to obtain the retarded and advanced gauge boson propagators one needs to get rid of the Minkowski tensor structure in eq. (3.43). Therefore, the propagator

$$\Delta^{ab}_{\mu\nu}(q) = \Delta^{ab}_{\mathrm{T}} P^{\mathrm{T}}_{\mu\nu} + \Delta^{ab}_{\mathrm{L}} P^{\mathrm{L}}_{\mu\nu} + \Delta^{ab}_{\mathrm{q}} \frac{q_\mu q_\nu}{q^2}\,, \tag{3.59}$$

is decomposed into three orthonormal contributions, with the projectors $P^{\mathrm{T,L}}_{\mu\nu}$ describing transverse and a longitudinal projections [128]. A more detailed study is provided in appendix A.1, where explicit expression for the projectors are given in eqs. (A.3) and (A.4). The decomposition for the propagator (3.59) as well as the one for the self-energy, see eq. (3.59), can be inserted into eq. (3.43) to obtain the retarded and advanced propagators

$$\Delta^{r,a}_{\mu\nu}(q) = -\frac{P^{\mathrm{T}}_{\mu\nu}}{q^2 + \Pi^{r,a}_{\mathrm{T}}} - \frac{P^{\mathrm{L}}_{\mu\nu}}{q^2 + \Pi^{r,a}_{\mathrm{L}}} - \frac{q_\mu q_\nu}{q^2} \frac{1}{q^2 \pm \mathrm{i}\,\mathrm{sign}(q^0)\epsilon}\,. \tag{3.60}$$

The spectral and Hermitian contributions are simply given by using eq. (3.15) and (3.16), such that

$$\Delta^{\mathcal{A}}_{\mu\nu}(q) = -P^{\mathrm{T}}_{\mu\nu}\Delta^{\mathcal{A}}_{\mathrm{T}}(q) - P^{\mathrm{L}}_{\mu\nu}\Delta^{\mathcal{A}}_{\mathrm{L}}(q) - \frac{q_\mu q_\nu}{q^2}\pi\delta(q^2)\mathrm{sign}(q^0)\,, \tag{3.61}$$

$$\Delta^{H}_{\mu\nu}(q) = -P^{\mathrm{T}}_{\mu\nu}\Delta^{H}_{\mathrm{T}}(q) - P^{\mathrm{L}}_{\mu\nu}\Delta^{H}_{\mathrm{L}}(q) - \frac{q_\mu q_\nu}{q^4}\,, \tag{3.62}$$

where the scalar parts of the propagator read

$$\Delta^{\mathcal{A}}_{\mathrm{T,L}}(q) = \frac{(-\Pi^{\mathcal{A}}_{\mathrm{T,L}})}{\left(q^2 + \Pi^{H}_{\mathrm{T,L}}\right)^2 + \Pi^{\mathcal{A}\,2}_{\mathrm{T,L}}}\,, \qquad \Delta^{H}_{\mathrm{T,L}}(q) = \frac{q^2 + \Pi^{H}_{\mathrm{T,L}}}{\left(q^2 + \Pi^{H}_{\mathrm{T,L}}\right)^2 + \Pi^{\mathcal{A}\,2}_{\mathrm{T,L}}}\,. \tag{3.63}$$

Note that, as an expansion in the coupling constants, all self-energies appearing in the fully resummed propagators $\Sigma^{\mathcal{A},H}$, $\Pi^{\mathcal{A},H}$ and $\Pi^{\mathcal{A},H}_{\mathrm{T,L}}$ are one-loop self-energies throughout this thesis. One-loop analytic solutions in an equilibrium situation with zero chemical potentials are derived in appendix A.2, while the HTL expressions are given in the next sections. Further, we find that particularly the diffusion constants, which are computed in chapter 4, are unaffected by the on-shell term in eq. (3.61), i.e. the contribution of this terms vanishes. Therefore, we neglect this term from now on. Obtaining a deeper understand of this gauge dependent term might be interesting for future works.

3.2.2 *Wightman propagators*

Wightman propagators are derived by inserting the Hermitian propagators, cf. eqs. (3.52), (3.58) and (3.63), into the constraint equations (3.44), (3.46) and (3.49). This procedure is analogously applied for fermions, scalar fields as well as for gauge bosons and allows to express the Wightman propagators in terms of the spectral propagators when using eqs. (3.52), (3.57) and (3.63). The equilibrium solutions of the Wightman functions, i.e. time-independent solutions that are obtained by neglecting the time-derivative in the constraint equations (3.44),(3.48) and (3.46), then read:

$$\mathrm{i}\Delta^{<,>}_{\phi,\mathrm{T,L}}(k) = 2\Delta^{\mathcal{A}}_{\phi,\mathrm{T,L}}(k)\frac{\Pi^{<,>}_{\phi,\mathrm{T,L}}}{\Pi^{>}_{\phi,\mathrm{T,L}} - \Pi^{<}_{\phi,\mathrm{T,L}}}\,, \tag{3.64}$$

$$\mathrm{i}S^{<,>}_{\pm}(k) = 2S^{\mathcal{A}}_{\pm}(k)\frac{\Sigma^{<,>0} \mp |\boldsymbol{\Sigma}^{<,>}|}{(\Sigma^{>0} \mp |\boldsymbol{\Sigma}^{>}|) - (\Sigma^{<0} \mp |\boldsymbol{\Sigma}^{<}|)}\,. \tag{3.65}$$

In equilibrium the Kubo-Martin-Schwinger (KMS) relations for the self-energies for zero chemical potential $\mu = 0$ can be used,

$$\mathrm{i}\not{\Sigma}^{>}_{\mathrm{eq}}(k) = -\mathrm{i}\mathrm{e}^{\beta k^0}\not{\Sigma}^{<}_{\mathrm{eq}}(k)\,, \qquad \mathrm{i}\Pi^{>}_{\mathrm{eq}}(k) = \mathrm{i}\mathrm{e}^{\beta k^0}\Pi^{<}_{\mathrm{eq}}(k)\,, \tag{3.66}$$

which analogously hold for equilibrium propagators

$$\mathrm{i}S^{>}_{\mathrm{eq}}(k) = -\mathrm{i}\mathrm{e}^{\beta k^0}S^{<}_{\mathrm{eq}}(k)\,, \qquad \mathrm{i}\Delta^{>}_{\mathrm{eq}}(k) = \mathrm{i}\mathrm{e}^{\beta k^0}\Delta^{<}_{\mathrm{eq}}(k)\,, \tag{3.67}$$

where Π and Δ can be representing both scalars as well as gauge bosons. This justifies the quasiparticle approximations for bosons

$$\mathrm{i}\Delta^{<}_{\phi,\mathrm{T,L}}(k) = 2\Delta^{\mathcal{A}}_{\phi,\mathrm{T,L}}(k)f_{\phi,\mathrm{T,L}}(k)\,, \qquad \mathrm{i}\Delta^{>}_{\phi,\mathrm{T,L}}(k) = 2\Delta^{\mathcal{A}}_{\phi,\mathrm{T,L}}(k)\left[1 + f_{\phi,\mathrm{T,L}}(k)\right]\,, \tag{3.68}$$

and for the fermions

$$\mathrm{i}S^{<}_{\pm}(k) = -2S^{\mathcal{A}}_{\pm}(k)f_{\pm}(k)\,, \qquad \mathrm{i}S^{>}_{\pm}(k) = 2S^{\mathcal{A}}_{\pm}(k)\left[1 - f_{\pm}(k)\right]\,, \tag{3.69}$$

with

$$f_{\phi,\mathrm{T,L}}(k) = \vartheta(k^0)f_{\phi,\mathrm{T,L}}(\mathbf{k}) - \vartheta(-k^0)\left[1 + \bar{f}_{\phi,\mathrm{T,L}}(-\mathbf{k})\right]\,, \tag{3.70}$$

$$f_{\pm}(k) = \vartheta(k^0)f_{\pm}(\mathbf{k}) + \vartheta(-k^0)\left[1 - \bar{f}_{\pm}(-\mathbf{k})\right]\,, \tag{3.71}$$

where $f(\mathbf{k})$ are the corresponding distribution functions, while $\bar{f}(\mathbf{k})$ account for their antiparticles. These do not necessarily need to be in equilibrium as will be shortly shown in the following. For non-vanishing spectral self-energies the Wightman propagators acquire a finite with in equilibrium. In contrast to that, out-of-equilibrium solutions are derived when allowing for the first non-vanishing solutions to the constraint equations (3.44),(3.48) and (3.46), cf. ref. [129] for a detailed study. It is shown that such solutions are described by an additional contributions that decays towards the equilibrium solutions (3.64). When expanding in gradients the decaying solutions does not feature a finite width. Intuitively one should expect that one cannot distinguish between propagators that are in or out-of-equilibrium by just measuring their width. It has been shown that the finite width of the out-of-equilibrium solution arises when summing to all order in gradients [129]. This eventually allows to use the quasiparticle approximation, cf. eqs. (3.68) and (3.69) not only for equilibrium states but also in out-of-equations situations. Therefore, it is possible to use eqs. (3.68) and (3.69) in order to describe baryogenesis scenarios, such as leptogenesis from oscillations of heavy neutrinos as well as EW baryogenesis, that require the existence of non-equilibrium effects. In kinetic equilibrium the distribution functions are of the Fermi-Dirac (F) and Bose-Einstein (B) form

$$f_{\mathrm{F,B}}(k) = \frac{1}{\mathrm{e}^{\beta(k^0-\mu)} \pm 1}\,, \tag{3.72}$$

with the inverse temperature $\beta = 1/T$.

3.2.3 *Tree-level propagators*

The free solutions, denoted by superscripts (0), for the spectral part of the propagator are obtained when neglecting thermal effects. Therefore, neither holes nor longitudinal excitations of the gauge bosons should contribute. The tree-level solutions are then obtained in the limit of vanishing spectral and Hermitian self-energies. In this case the spectral propagators (3.52), (3.57) and (3.63) converge to Dirac delta functions:

$$\Delta_\phi^{(0)\mathcal{A}}(k) = \pi\delta(k^2)\mathrm{sign}(k^0)\,, \tag{3.73}$$

$$S_{\mathrm{R,L}}^{(0)\mathcal{A}}(k) = \pi P_{\mathrm{R,L}}\not{k} P_{\mathrm{L,R}}\delta(k^2)\mathrm{sign}(k^0)\,. \tag{3.74}$$

Consequently, in the absence of thermal effects, the particles are put on their mass shell, i.e. $k^2 = 0$, such that the tree-level Wightman function are given by

$$\Delta_\phi^{(0)<}(k) = 2\pi\delta(k^2)\mathrm{sign}(k^0) f_\phi(k)\,, \tag{3.75}$$

$$\Delta_\phi^{(0)>}(k) = 2\pi\delta(k^2)\mathrm{sign}(k^0)\left[1 + f_\phi(k)\right]\,, \tag{3.76}$$

$$S_{\mathrm{R,L}}^{(0)<}(k) = -2\pi P_{\mathrm{R,L}}\not{k} P_{\mathrm{L,R}}\delta(k^2)\mathrm{sign}(k^0) f_\psi(k)\,, \tag{3.77}$$

$$S_{\mathrm{R,L}}^{(0)>}(k) = 2\pi P_{\mathrm{R,L}}\not{k} P_{\mathrm{L,R}}\delta(k^2)\mathrm{sign}(k^0)\left[1 - f_\psi(k)\right]\,, \tag{3.78}$$

with the distribution functions from eq. (3.72). Note that these tree-level results can also be obtained by inserting the mode sum of the scalar and fermion fields into eqs. (3.4)-

(3.6) and solving the EVs in Wigner space. Analogously, the time and anti-time-ordered propagators

$$\mathrm{i}\Delta_{\phi}^{(0)t,\bar{t}}(k) = \pm\frac{\mathrm{i}}{k^2 \pm \mathrm{i}\epsilon} + 2\pi\delta(k^2)\left[\vartheta(k^0)f_{\phi}(\mathbf{k}) + \vartheta(-k^0)\bar{f}_{\phi}(-\mathbf{k})\right], \tag{3.79}$$

$$\mathrm{i}S_{\mathrm{R,L}}^{(0)t,\bar{t}}(k) = \pm P_{\mathrm{R,L}}\frac{\mathrm{i}\not{k}}{k^2 \pm \mathrm{i}\epsilon}P_{\mathrm{L,R}} - 2\pi\delta(k^2)P_{\mathrm{R,L}}\not{k}P_{\mathrm{L,R}}\left[\vartheta(k^0)f_{\phi}(\mathbf{k}) + \vartheta(-k^0)\bar{f}_{\phi}(-\mathbf{k})\right], \tag{3.80}$$

are obtained by solving (3.8)-(3.11) in Wigner space. In Feynman gauge the tree-level gauge boson propagators are simply reduced to the scalar functions, see also ref. [125, 130], via

$$\mathrm{i}\Delta_{\mu\nu}^{(0)ab} = -g_{\mu\nu}\mathrm{i}\Delta_{V}^{(0)ab}\,. \tag{3.81}$$

Note that throughout this thesis the index V is used to distinguish the gauge bosons, or vector bosons, from the scalar fields. It is useful to decompose the tree-level fermion propagator into a scalar contribution and into a term that accounts for the Dirac structure, such that

$$\mathrm{i}S_{\mathrm{R,L}}^{(0)ab}(k) = P_{\mathrm{R,L}}\not{k}P_{\mathrm{L,R}}\mathrm{i}\tilde{S}_{\mathrm{R,L}}^{(0)ab}(k)\,. \tag{3.82}$$

Note that in a weakly coupled plasma, such as the SM at high temperatures due to small gauge couplings, the effective width of the quasiparticles can be small enough to use free solutions. However, it is not always justified to also neglect the Hermitian self-energies as they put the particles on the correct, non-zero, mass shell.

3.3 PARTICLE INTERACTION WITH THE PLASMA

In order to describe the finite width and the dispersion relations for quasiparticle states in the plasma, one needs to compute both spectral and Hermitian parts of the corresponding self-energies. Note that for our purposes it is sufficient to calculate the self-energies that enter the resummed propagators at one-loop order and in equilibrium. This is justified because one can expand in small couplings and because the distribution function, rather than the spectral part of the propagator, accounts for deviations from equilibrium, cf. eqs. (3.68) and (3.69). Two-dimensional plots for the spectral parts of the resummed propagators at one-loop are shown in figure 3.3 for the Higgs field, for fermions and for both transverse and longitudinal gauge boson modes, cf. eqs. (3.52), (3.57) and (3.63).

With the Feynman rules shown in figure 2.1, analytic one-loop self-energy expressions for the different SM particles are provided in subsection 3.3.1. Dispersion relations and the finite width of quasiparticles are discussed in subsection 3.3.2 and 3.3.3, while the Hermitian and spectral self-energies are computed analytically in appendix A.2 and A.3. The BW approximation and the zero width limit of the propagators are given in subsection 3.3.4.

3.3.1 *Derivation of self-energy expressions*

In the CTP formalism self-energies G^{ab} can be deduced from a functional derivative of the 2PI effective action, cf. eqs. (3.19) and (3.20). This effective action is given by $(-\mathrm{i})$ times the vacuum graphs. One can show that in Wigner space this translates to:

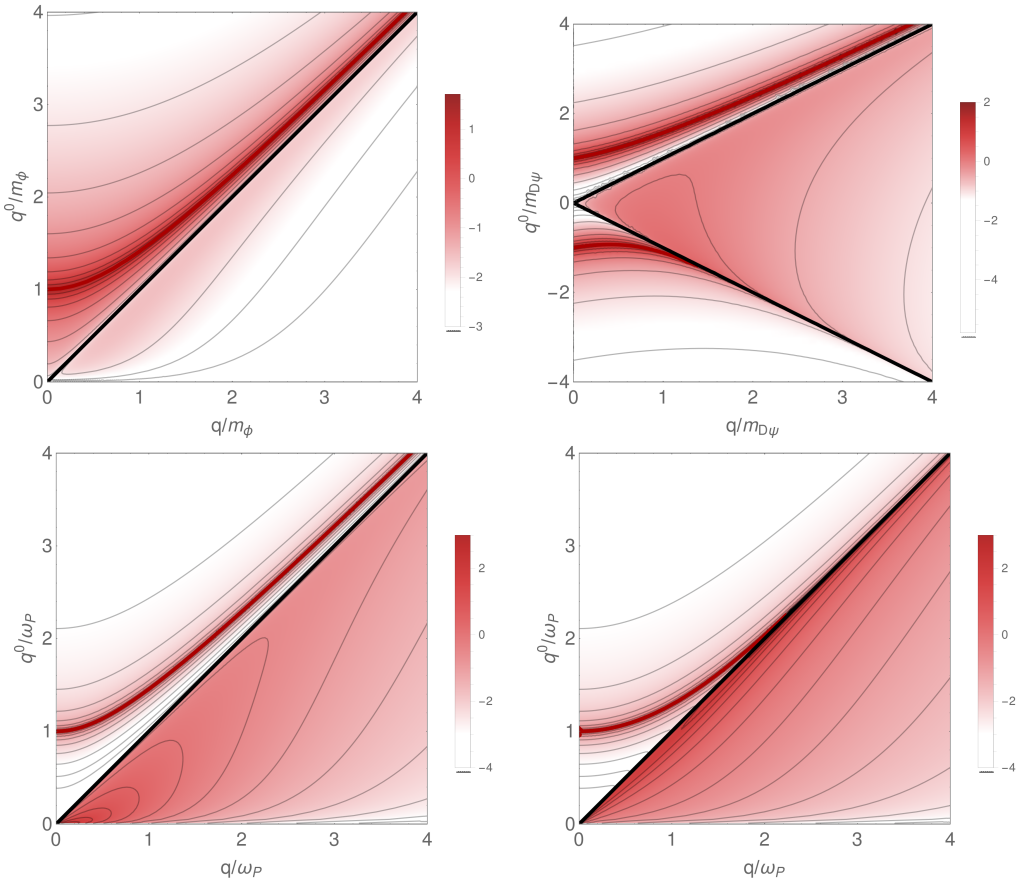

FIGURE 3.3: Spectral part of the propagator with the full one-loop solution to the spectral self-energies. The light cone $q^0 = \pm|\mathbf{q}|$ is displayed with a thick black line, while the half-integer logarithmic contour lines are given by thin black lines. On the top left panel the spectral density of the Higgs $\log_{10}|\Delta_\phi^{\mathcal{A}}(q)|$ from eq. (3.52) is shown for $G_\phi = 0.6$, cf. eq. (3.89), $h_t = 1$ and $\lambda = 0.28$, while on the right panel the density of fermions and holes $\log_{10}|S_+^{\mathcal{A}}(q)|$ from eq. (3.57) are shown for $G_\psi = 0.6$, cf. eq. (3.93). Accordingly, the lower panel shows the spectral density of the transverse and longitudinal modes of the gauge bosons $\log_{10}|\Delta_{\mathrm{T,L}}^{\mathcal{A}}(q)|$ from eq. (3.63). Note that $\Delta_\phi^{\mathcal{A}} > 0$ for $q^2 < 0$ and $\Delta_\phi^{\mathcal{A}} < 0$ for $q^2 \geq 0$, while $S_+^{\mathcal{A}} > 0$ for all q. Further, $\Delta_{\mathrm{T}}^{\mathcal{A}} < 0$ for all q, while $\Delta_{\mathrm{L}}^{\mathcal{A}} < 0$ for $q^2 \geq 0$ and $\Delta_{\mathrm{L}}^{\mathcal{A}} > 0$ for $q^2 < 0$. The dispersion relations for the corresponding quasiparticles are clearly visible by the dark red lines and converge to the momentum independent Higgs mass, to the Debye mass $m_{D\psi}$ and to the plasma frequency ω_p for both transverse and longitudinal modes for a U(1) gauge boson with $g_1 = 0.3$. While in the HTL approximation these would simply be red lines without any smearing, because the self-energies do not feature any HTL contribution for $q^2 \geq 0$, the finite width effect around the quasiparticle poles is obvious here.

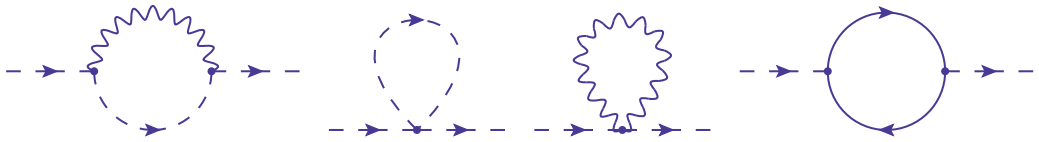

FIGURE 3.4: One-loop contributions to the Higgs self-energy $\mathrm{i}\Pi^{ab} = \mathrm{i}\Pi_\phi^{(V)} + \mathrm{i}\Pi_\phi^{(\mathrm{tp})} + \mathrm{i}\Pi_\phi^{(\mathrm{sg})} + \mathrm{i}\Pi_\phi^{(t)}$.

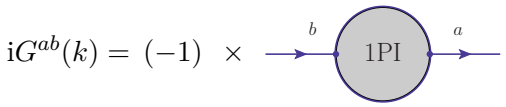

In Wigner space two point function for the Higgs field, fermions and for gauge bosons are given by

$$= \mathrm{i}\Delta^{ab}(k)\,, \tag{3.83}$$

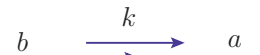

$$= \mathrm{i}S^{ab}(k)\,, \tag{3.84}$$

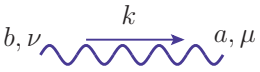

$$= \mathrm{i}\Delta^{ab}_{\mu\nu}(k)\,. \tag{3.85}$$

The vacuum bubbles that are relevant are displayed in figure 3.2. It will be shown in the following that at one-loop order only sunset diagrams, i.e. diagrams that are obtained by functional derivatives of diagrams (A)-(D) in figure 3.2, contribute to the spectral part of self-energies. In contrast to that not only these sunset but also seagull and tadpole diagrams, obtained from (E)-(F), contribute to the Hermitian parts of self-energies. In the following discussion we consider the particles running in the loop to be massless.

HIGGS FIELD: At one-loop order the Higgs field receives contributions from the exchange of gauge bosons $\Pi_\phi^{(V)} + \Pi_\phi^{(\mathrm{sg})}$ and the Higgs self-interaction $\Pi_\phi^{(\mathrm{tp})}$. Another contributions arises from the exchange of the top quark Π_ϕ^t, as its Yukawa coupling is not small compared to the gauge coupling. The corresponding diagrams are illustrated in figure 3.4. In total the Higgs self-energy can be decomposed as

$$\mathrm{i}\Pi_\phi = \mathrm{i}\Pi_\phi^{(t)} + \mathrm{i}\Pi_\phi^{(V)} + \mathrm{i}\Pi_\phi^{(\mathrm{tp})} + \mathrm{i}\Pi_\phi^{(\mathrm{sg})}\,, \tag{3.86}$$

where the individual contributions from the sunset diagrams read

$$\mathrm{i}\Pi_\phi^{(t)\,ab}(k) = -N_c h_t^2 \int \frac{\mathrm{d}^4p}{(2\pi)^4}\frac{\mathrm{d}^4q}{(2\pi)^4}(2\pi)^4\delta^4(q-p-k)\mathrm{i}\tilde{S}^{ab}(q)\mathrm{i}\tilde{S}^{ba}(p)\mathrm{tr}[P_{\mathrm{R,L}}p\cdot q]\,, \tag{3.87}$$

$$\mathrm{i}\Pi_\phi^{(V)\,ab}(k) = -G_\phi \int \frac{\mathrm{d}^4p}{(2\pi)^4}\frac{\mathrm{d}^4q}{(2\pi)^4}(2\pi)^4\delta^4(q-p-k)\mathrm{i}\Delta_\phi^{ab}(q)\mathrm{i}\Delta_V^{ba}(p)(k+q)^2\,, \tag{3.88}$$

with $N_c = 3$ the number of SU(3)-colours and the effective coupling of the Higgs to the U(1) and SU(2) gauge bosons

$$G_\phi \equiv g_1^2 Y_\phi^2 + g_2 C_2^F = \frac{1}{4}g_1^2 + \frac{3}{4}g_2\,. \tag{3.89}$$

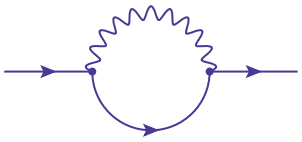

FIGURE 3.5: One-loop contribution to the fermion self-energy $\mathrm{i}\not{\Sigma}^{ab}$.

	U(1)	SU(2)	SU(3)
N_ψ	10	12	12
N_ϕ	1/2	1	0

TABLE 3.1: Effective number of fermions N_ψ and Higgs fields N_ϕ in the different subgroups of the SM as the total number of fermions and Higgs fields in one-loop gauge boson diagrams. In the U(1) the gauge couplings get additionally multiplied with the square of the weak hypercharges. Note that $N_\phi^{\mathrm{SU}(3)} = 0$ since the Higgs is a SU(3) singlet.

Further, the tadpole and seagull contributions are given by

$$\mathrm{i}\Pi_\phi^{(\mathrm{tp})\,ab}(k) = 6\mathrm{i}\lambda\delta^{ab}\int\frac{\mathrm{d}^4p}{(2\pi)^4}\mathrm{i}\Delta_\phi^{aa}(p)\,, \tag{3.90}$$

$$\mathrm{i}\Pi_\phi^{(\mathrm{sg})\,ab}(k) = 4\mathrm{i}G_\phi\delta^{ab}\int\frac{\mathrm{d}^4p}{(2\pi)^4}\mathrm{i}\Delta_\phi^{aa}(p)\,. \tag{3.91}$$

and do only contribute to Π^H but not to $\Pi^{\mathcal{A}}$, as mentioned before, due to the fact that these are diagonal in CTP space.

FERMIONS: In the absence of Yukawa interactions, the only contribution to the fermionic self-energies at one-loop order is due to the exchange of gauge bosons, as displayed in figure 3.5, and reads

$$\mathrm{i}\not{\Sigma}_\psi^{ab}(k) = 2G_\psi P_{\mathrm{R,L}}\int\frac{\mathrm{d}^4p}{(2\pi)^4}\frac{\mathrm{d}^4q}{(2\pi)^4}(2\pi)^4\delta^4(q-p-k)\mathrm{i}\tilde{S}^{ab}(q)\mathrm{i}\Delta_V^{ba}(p)\not{q}\,. \tag{3.92}$$

For any chosen fermion the self-energy depends on the possible gauge coupling, that is in general written as

$$G_\psi \equiv g_1^2Y_\psi^2 + \frac{3}{4}g_2^2 + \frac{4}{3}g_3^2\,, \tag{3.93}$$

with Y_ψ the weak hypercharge of the corresponding fermion. Note that $g_2, g_3 = 0$ for $\mathrm{SU}(2), \mathrm{SU}(3)$ singlets. For later calculations it is convenient to make use of the decomposition

$$\not{\Sigma} = \Sigma^0\gamma_0 + \Sigma^i\gamma_i\,, \tag{3.94}$$

such that computations of the slashed quantity $\not{\Sigma}$ is fully determined by the components Σ^0 and Σ^i. Note that the projectors $P_{\mathrm{R,L}}$ are included in $\Sigma^{0,i}$. However, they effectively contribute with a factor of 1/2 to the components $\Sigma^{0,i}$. This can be seen when taking Dirac traces, where the γ_5 part of the projectors usually vanishes.

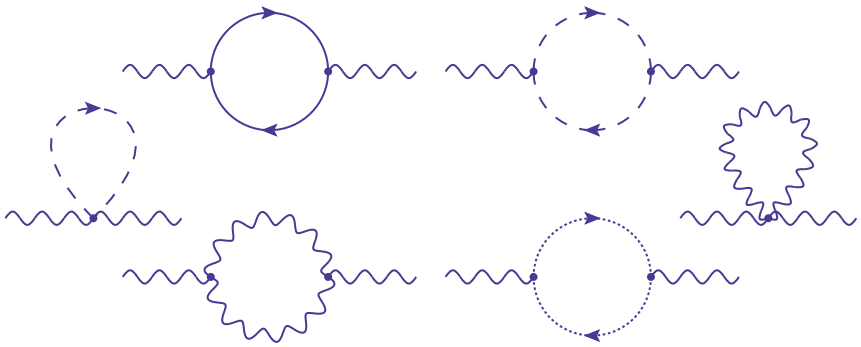

FIGURE 3.6: One-loop contribution to the gauge boson self-energy $\mathrm{i}\Pi_{\mu\nu} = N_\psi\,\mathrm{i}\Pi^{(\psi)}_{\mu\nu} + N_\phi\,\mathrm{i}\Pi^{(\phi)}_{\mu\nu} + \mathrm{i}\Pi^{(V)}_{\mu\nu} + \mathrm{i}\Pi^{(\mathrm{tp})}_{\mu\nu} + \mathrm{i}\Pi^{(\mathrm{sg})}_{\mu\nu}$.

GAUGE BOSONS: Gauge bosons of a certain gauge group receive contributions from the exchange of N_ψ fermions $\Pi^{(\psi)}_{\mu\nu}$ and N_ϕ Higgses $\Pi^{(\phi)}_{\mu\nu}$, as well as the seagull contribution $\Pi^{(\mathrm{sg})}_{\mu\nu}$ at one-loop order. The effective number of fermions and Higgs fields are given in table 3.1. In addition to that the self-interaction due to the sunset diagram $\Pi^{(V)}_{\mu\nu}$ and the tadpole $\Pi^{(\mathrm{tp})}_{\mu\nu}$ have to be taken into account as well. Note that $\Pi^{(V)}_{\mu\nu}$ does not only consider gauge bosons but also the ghost fields. The decomposition of the self-energy then reads

$$\mathrm{i}\Pi_{\mu\nu} = N_\psi\,\mathrm{i}\Pi^{(\psi)}_{\mu\nu} + N_\phi\,\mathrm{i}\Pi^{(\phi)}_{\mu\nu} + \mathrm{i}\Pi^{(V)}_{\mu\nu} + \mathrm{i}\Pi^{(\mathrm{tp})}_{\mu\nu} + \mathrm{i}\Pi^{(\mathrm{sg})}_{\mu\nu}\,, \tag{3.95}$$

which is graphically illustrated in figure 3.6. The individual components are given by

$$\mathrm{i}\Pi^{(\phi)\,ab}_{\mu\nu}(k) = g^2 C^F \int \frac{\mathrm{d}^4p}{(2\pi)^4}\frac{\mathrm{d}^4q}{(2\pi)^4}(2\pi)^4\delta^4(q-p-k)\mathrm{i}\Delta^{ab}_\phi(q)\mathrm{i}\Delta^{ba}_\phi(p)U_{\mu\nu}(p,q)\,, \tag{3.96}$$

$$\mathrm{i}\Pi^{(\psi)\,ab}_{\mu\nu}(k) = -g^2 C^F \int \frac{\mathrm{d}^4p}{(2\pi)^4}\frac{\mathrm{d}^4q}{(2\pi)^4}(2\pi)^4\delta^4(q-p-k)\mathrm{i}\tilde{S}^{ab}(q)\mathrm{i}\tilde{S}^{ba}(p)T_{\mu\nu}(p,q)\,, \tag{3.97}$$

$$\mathrm{i}\Pi^{(V)\,ab}_{\mu\nu}(k) = \frac{1}{2}g^2 C_2^A \int \frac{\mathrm{d}^4p}{(2\pi)^4}\frac{\mathrm{d}^4q}{(2\pi)^4}(2\pi)^4\delta^4(q-p-k)\mathrm{i}\Delta^{ab}_V(q)\mathrm{i}\Delta^{ba}_V(p)G_{\mu\nu}(p,q)\,, \tag{3.98}$$

with the tensorial functions

$$U_{\mu\nu}(p,q) = (p+q)_\mu(p+q)_\nu\,, \tag{3.99}$$

$$T_{\mu\nu}(p,q) = \mathrm{tr}[P_{\mathrm{R,L}}\not{p}\gamma_\nu\not{q}\gamma_\mu]\,, \tag{3.100}$$

$$G_{\mu\nu}(p,q) = (4k^2+p^2+q^2)g_{\mu\nu} - 2p_\mu p_\nu - 2q_\mu q_\nu + 6(p_\mu q_\nu + q_\mu p_\nu)\,. \tag{3.101}$$

The tadpole and the seagull contribution are written as

$$\mathrm{i}\Pi^{(\mathrm{tp})\,ab}_{\mu\nu}(k) = -3\mathrm{i}g^2 C_2^A g_{\mu\nu}a\delta^{ab}\int\frac{\mathrm{d}^4p}{(2\pi)^4}\mathrm{i}\Delta^{aa}_V(p)\,, \tag{3.102}$$

$$\mathrm{i}\Pi^{(\mathrm{sg})\,ab}_{\mu\nu}(k) = -2\mathrm{i}g^2 C^F g_{\mu\nu}a\delta^{ab}\int\frac{\mathrm{d}^4p}{(2\pi)^4}\mathrm{i}\Delta^{aa}_V(p)\,. \tag{3.103}$$

Note that for a U(1) gauge boson one has $g^2C^F = g_1^2$, while $C_2^A = 0$, such that $\Pi^{(V)}_{\mu\nu}$ and $\Pi^{(\mathrm{tp})}_{\mu\nu}$ are only present for the non-abelian groups SU(2) and SU(3). In this case one has $g^2C^F = \frac{1}{2}g_2^2$ and $g^2C^F = \frac{1}{2}g_3^2$ or $g^2C_2^A = 2g_2^2$ and $g^2C_2^A = 3g_3^2$, respectively.

3.3.2 *Dispersion of quasiparticles*

Provided that the theory is weakly coupled, quasiparticle states can be inferred from the use of full propagators. These are given in the form of Wightman function, that can be expressed in terms of the spectral parts (3.52), (3.57) and (3.63) via eqs. (3.68) and (3.69). The dispersion laws $\omega_{|\mathbf{q}|}$ for these quasiparticles as a function of the three-momentum $|\mathbf{q}|$ are defined as the real parts of the poles of the retarded and advanced propagators. In terms of the spectral propagators these poles for positive energies q^0 can be obtained by solving the following equations

$$\omega^2_{\phi|\mathbf{q}|} = |\mathbf{q}|^2 - \Pi^H_\phi(q)|_{q^0=\omega_{\phi|\mathbf{q}|}}\,, \tag{3.104}$$

$$\omega_{\pm|\mathbf{q}|} = \pm|\mathbf{q}| + (\Sigma^{H0}(q) \mp |\mathbf{\Sigma}^H(q)|)|_{q^0=\omega_{\pm|\mathbf{q}|}}\,, \tag{3.105}$$

$$\omega^2_{\mathrm{T,L}|\mathbf{q}|} = |\mathbf{q}|^2 + \Pi^H_{\mathrm{T,L}}(q)|_{q^0=\omega_{\mathrm{T,L}|\mathbf{q}|}}\,. \tag{3.106}$$

These are shown by the red lines in figure 3.3 for $q^2 \geq 0$. In general the Hermitian self-energies are not only complicated functions of the momentum q but it is also difficult to derive analytic expressions. Full expressions up to one remaining momentum integral are given by solving for

$$G^H = \frac{1}{2}\left(G^t - G^{\bar{t}}\right)\,, \tag{3.107}$$

and are derived in appendix A.2. A high temperature approximation allows to solve this integral analytically. These approximate solutions correspond to HTL expressions for the Hermitian self-energies. Throughout this thesis it is sufficient to use these HTL expressions, that are discussed in appendix A.2. In the following the Hermitian self-energies are expressed in terms of momentum independent thermal masses and into a momentum-dependent remainder.

HERMITIAN SELF-ENERGIES AND THERMAL MASSES: The HTL expression of the Hermitian self-energy for scalar particles is momentum independent and can be expressed in terms of the thermal Higgs mass

$$\Pi^H_\phi(q) = m^2_\phi\,. \tag{3.108}$$

The zeroth and spatial component of the Hermitian fermionic self-energy in the HTL limit depend non-trivially on the momentum

$$\Sigma^{H0}_\psi(q) = \frac{m^2_\psi}{4|\mathbf{q}|}\log\left|\frac{q^0+|\mathbf{q}|}{q^0-|\mathbf{q}|}\right|, \qquad \Sigma^{Hi}_\psi(q) = \left(\frac{q^0}{|\mathbf{q}|}\Sigma^{H0}_\psi(q) - \frac{m^2_\psi}{2|\mathbf{q}|}\right)\frac{q^i}{|\mathbf{q}|}\,, \tag{3.109}$$

and can be expressed in terms of thermal masses m_Ψ for a given fermion. The HTL part for the longitudinal and transverse Hermitian self-energies of the gauge boson are written in terms of the thermal gauge boson mass m_V and also exhibits a non-trivial momentum structure

$$\Pi^H_{\mathrm{L}}(q) = -2m^2_V\left(1-\frac{(q^0)^2}{|\mathbf{q}|^2}\right)\left(1-\frac{q^0}{2|\mathbf{q}|}\log\left|\frac{q^0+|\mathbf{q}|}{q^0-|\mathbf{q}|}\right|\right)\,, \tag{3.110}$$

$$\Pi^H_{\mathrm{T}}(q) = -m^2_V - \frac{1}{2}\Pi^H_{\mathrm{L}}(q^0,|\mathbf{q}|)\,. \tag{3.111}$$

Full expressions are derived in appendix A.2 and define the different thermal masses

$$m_\phi^2 = \left(\frac{G_\phi}{4} + \frac{h_t^2}{4} + \frac{\lambda}{2}\right) T^2 \,, \tag{3.112}$$

$$m_\psi^2 = \frac{G_\psi T^2}{4} \,, \tag{3.113}$$

$$m_V^2 = \frac{1}{6}\left(\frac{1}{2} C^F N_\psi + C^F N_\phi + C_2^A\right) g^2 T^2 \,. \tag{3.114}$$

G_ϕ is the effective coupling of the Higgs field to the U(1) and SU(2) gauge fields, see eq. (3.89), while G_ψ accounts for the allowed couplings of a given fermion to the gauge bosons, see eq. (3.93). The individual thermal masses for the three SM gauge bosons $V \in \{B, W, g\}$ are

$$m_B^2 = \frac{11}{12} g_1^2 T^2 \,, \qquad m_W^2 = \frac{11}{12} g_2^2 T^2 \,, \qquad m_g^2 = g_3^2 T^2 \,. \tag{3.115}$$

DISPERSION LAWS FOR SOFT AND HARD MOMENTA: According to eqs. (3.104), (3.105) and (3.106) the dispersion relations are determined by the Hermitian self-energies. With the HTL expressions one can derive dispersion relations in the limit of soft and hard momenta $|\mathbf{q}|$, see e.g. ref. [131] for a more detailed study.

Since the Hermitian self-energy of the Higgs is momentum independent, the thermal Higgs mass is chosen in such a way that it fulfils the relativistic dispersion relation

$$\omega_{\phi|\mathbf{q}|}^2 = |\mathbf{q}|^2 + m_\phi^2 \,. \tag{3.116}$$

The dispersion of the fermions and the holes and analogously the transverse and longitudinal modes of the gauge bosons can be approximated in the soft $|\mathbf{q}| \ll m_\psi, m_V$ limit

$$\omega_{\pm|\mathbf{q}|} \simeq m_{\mathrm{D}\psi} \pm \frac{|\mathbf{q}|}{3} \,, \tag{3.117}$$

$$\omega_{\mathrm{T}|\mathbf{q}|}^2 \simeq \omega_\mathrm{p}^2 + \frac{6}{5}|\mathbf{q}|^2 \,, \tag{3.118}$$

$$\omega_{\mathrm{L}|\mathbf{q}|}^2 \simeq \omega_\mathrm{p}^2 + \frac{3}{5}|\mathbf{q}|^2 \,, \tag{3.119}$$

with the plasma frequency $\omega_\mathrm{p} = \sqrt{\frac{2}{3}} m_V$ and the zero momentum fermion mass, often referred to as the Debye mass $m_{\mathrm{D}\psi} = \frac{m_\psi}{\sqrt{2}}$. These are defined as the energy of the particles at rest and are obvious in figure 3.3. It is interesting to note that for very soft $|\mathbf{q}| \to 0$ one cannot distinguish fermion excitations from hole excitations nor transverse from longitudinal gauge boson modes. For hard $|\mathbf{q}| \gg m_\psi, m_V$ momenta one can approximate

$$\omega_{+,\mathrm{T}|\mathbf{q}|}^2 \simeq |\mathbf{q}|^2 + m_{\psi,V}^2 \,, \tag{3.120}$$

$$\omega_{-,\mathrm{L}|\mathbf{q}|} \simeq |\mathbf{q}| \left(1 + 2\exp\left(-1 - \frac{|\mathbf{q}|^2}{m_{\psi,V}^2}\right)\right) \,. \tag{3.121}$$

As the Hermitian self-energies for the fermions and the gauge bosons are not momentum independent, we have to stick to a certain convention for the thermal masses. The approximations above indicate that we are using the so-called asymptotic thermal masses. These are defined as the solutions to $\omega_{+,\mathrm{T}|\mathbf{q}|}^2 = |\mathbf{q}|^2 + m_{+,\mathrm{T}}^2$ for hard $|\mathbf{q}| \gg m$ for both the fermions and the transverse modes of the gauge bosons. At hard momenta, as will be shown later, the hole and longitudinal excitations will decouple from the plasma, while for soft momenta they are equally important to the fermions and transverse gauge bosons.

3.3.3 *Finite width of quasiparticles*

We have pointed out that the distribution of quasiparticles acquires a finite width around the quasiparticle mass pole in the s-channel, i.e. for $q^2 = (q^0)^2 - |\mathbf{q}|^2 \geq 0$. While those pole equations are described by the Hermitian parts of the self-energies, the width is given by the spectral parts. At one-loop order only the sunset diagrams shown in figures 3.4, 3.5 and 3.6 contribute the spectral self-energy. Details and full expressions are given in appendix A.3. Since computations within this thesis are mostly dominated by hard momenta, it is sufficient to use HTL expressions for the spectral self-energies that appear in the resummed propagators. As shown in appendix A.3 these only appear in the t-channel, i.e. for $q^2 = (q^0)^2 - |\mathbf{q}|^2 < 0$, and are only present for the gauge bosons and the fermions. Hence, for $q^2 < 0$, the spectral parts of the self-energies in the HTL approximation for the fermions are given by

$$\Sigma_\psi^{\mathcal{A}0}(q) = \frac{\pi}{4|\mathbf{q}|} m_\psi^2 \,, \qquad \Sigma_\psi^{\mathcal{A}i}(q) = \frac{\pi q^0 q^i}{4|\mathbf{q}|^3} m_\psi^2 \,, \tag{3.122}$$

while the spectral parts of the self-energies of the transverse and longitudinal gauge bosons read

$$\Pi_{\mathrm{T}}^{\mathcal{A}}(q) = \frac{\pi}{4} \frac{q^2 q^0}{|\mathbf{q}|^3} m_V^2 \,, \qquad \Pi_{\mathrm{L}}^{\mathcal{A}}(q) = -\frac{\pi}{2} \frac{q^2 q^0}{|\mathbf{q}|^3} m_V^2 \,. \tag{3.123}$$

3.3.4 *Breit-Wigner approximation and zero-width limit*

For weak couplings the main contribution of the spectral propagator in the s-channel comes from the quasiparticle pole at $q^0 = \pm\omega_{|\mathbf{q}|}$. In that case one can evaluating the spectral propagators directly at the pole. The BW approximation decomposes the propagator into such a BW distribution plus a continuous part, which is basically given by the remainder of the propagator after the pole part has been subtracted, namely the propagator in the t-channel:

$$\Delta_\phi^{\mathcal{A}}(q)|_{\mathrm{BW}} = \mathcal{Z}_{\phi|\mathbf{q}|} \frac{q^0 \Gamma_{\phi|\mathbf{q}|}}{\left((q^0)^2 - \omega_{\phi|\mathbf{q}|}^2\right)^2 + (q^0 \Gamma_{\phi|\mathbf{q}|})^2} + \Delta_\phi^{\mathcal{A}}(q)|_{\mathrm{cont}} \,, \tag{3.124}$$

$$S_\pm^{\mathcal{A}}(q)|_{\mathrm{BW}} = \mathcal{Z}_{|\mathbf{q}|}^{\pm} \frac{\Gamma_{\pm|\mathbf{q}|}}{\left(q^0 - \omega_{\pm|\mathbf{q}|}\right)^2 + \Gamma_{\pm|\mathbf{q}|}^2} + \mathcal{Z}_{|\mathbf{q}|}^{\mp} \frac{\Gamma_{\mp|\mathbf{q}|}}{\left(q^0 + \omega_{\mp|\mathbf{q}|}\right)^2 + \Gamma_{\mp|\mathbf{q}|}^2} + S_\pm^{\mathcal{A}}(q)|_{\mathrm{cont}} \,, \tag{3.125}$$

$$\Delta_{\mathrm{T,L}}^{\mathcal{A}}(q)|_{\mathrm{BW}} = \mathcal{Z}_{|\mathbf{q}|}^{\mathrm{T,L}} \frac{\Gamma_{\mathrm{T,L}|\mathbf{q}|}}{\left((q^0)^2 - \omega_{\mathrm{T,L}|\mathbf{q}|}^2\right)^2 + \Gamma_{\mathrm{T,L}|\mathbf{q}|}^2} + \Delta_{\mathrm{T,L}}^{\mathcal{A}}(q)|_{\mathrm{cont}} \,. \tag{3.126}$$

The damping rates evaluated at the pole read

$$\Gamma_{\phi,\mathrm{T,L}|\mathbf{q}|} = \mathcal{Z}_{|\mathbf{q}|}^{\phi,\mathrm{T,L}} \frac{\Pi_\phi^{\mathcal{A}}(q)}{q^0}\bigg|_{q^0=\omega_{\phi,\mathrm{T,L}|\mathbf{q}|}} \,, \qquad \Gamma_{\mp|\mathbf{q}|} = \mathcal{Z}_{|\mathbf{q}|}^{\pm} (\Sigma^{\mathcal{A}0} \mp |\mathbf{\Sigma}^{\mathcal{A}}|)\Big|_{q^0=\omega_{\pm|\mathbf{q}|}} \,, \tag{3.127}$$

and depend on the residues, which are given by

$$\mathcal{Z}_{|\mathbf{q}|}^{\pm} = \frac{\omega_{\pm|\mathbf{q}|}^2 - |\mathbf{q}|^2}{m_\psi^2} \,, \tag{3.128}$$

and

$$\mathcal{Z}^{\mathrm{T}}_{|\mathbf{q}|} = \frac{\omega_{\mathrm{T}|\mathbf{q}|}(\omega^2_{\mathrm{T}|\mathbf{q}|} - |\mathbf{q}|^2)}{2m_V^2\omega^2_{\mathrm{T}|\mathbf{q}|} - (\omega^2_{\mathrm{T}|\mathbf{q}|} - |\mathbf{q}|^2)}\,, \quad \mathcal{Z}^{\mathrm{L}}_{|\mathbf{q}|} = \frac{\omega_{\mathrm{L}|\mathbf{q}|}(\omega^2_{\mathrm{L}|\mathbf{q}|} - |\mathbf{q}|^2)}{|\mathbf{q}|^2(|\mathbf{q}|^2 + 2m_V^2 - \omega^2_{\mathrm{L}|\mathbf{q}|})}\,. \tag{3.129}$$

Note that $Z^{\phi}_{|\mathbf{q}|} = 1$ is momentum independent as Π^H_ϕ does not depend on q^0 in the HTL limit. The residues for the fermion and holes as well as the transverse and longitudinal excitations depend non-trivially on the momentum $|\mathbf{q}|$, as $\omega_{|\mathbf{q}|}$ is a function on the momentum. For soft momenta ($|\mathbf{q}| \ll m_\psi, m_V$) they read

$$\mathcal{Z}^{\pm}_{|\mathbf{q}|} \simeq \frac{1}{2} \pm \frac{|\mathbf{q}|}{3m_{\mathrm{D}\psi}}\,, \quad \mathcal{Z}^{\mathrm{T}}_{|\mathbf{q}|} \simeq \frac{1}{2\omega_{\mathrm{p}}}\left(1 - \frac{4}{5}\frac{|\mathbf{q}|^2}{\omega_{\mathrm{p}}^2}\right), \quad \mathcal{Z}^{\mathrm{L}}_{|\mathbf{q}|} \simeq \frac{\omega_{\mathrm{p}}}{2|\mathbf{q}|^2}\left(1 - \frac{3}{10}\frac{|\mathbf{q}|^2}{\omega_{\mathrm{p}}^2}\right), \tag{3.130}$$

where all the excitations are of equal importance. However, in the limit of large $|\mathbf{q}| \gg m_\psi, m_V$ the holes and the longitudinal excitations decouple from the plasma

$$\mathcal{Z}^{-}_{|\mathbf{q}|} \simeq \frac{|\mathbf{q}|^2}{m_\psi^2}\exp\left(-1 - \frac{|\mathbf{q}|^2}{m_\psi^2}\right) \to 0\,, \qquad \mathcal{Z}^{\mathrm{L}}_{|\mathbf{q}|} \simeq \frac{2|\mathbf{q}|}{m_V^2}\exp\left(-1 - \frac{|\mathbf{q}|^2}{m_V^2}\right) \to 0\,, \tag{3.131}$$

while the plasma is dominated by the fermion and transverse modes of the gauge bosons

$$\mathcal{Z}^{+}_{|\mathbf{q}|} \simeq 1 + \frac{m_\psi^2}{|\mathbf{q}|^2}\left(1 - \log\left(\frac{|\mathbf{q}|^2}{m_\psi^2}\right)\right) \simeq 1\,, \qquad \mathcal{Z}^{\mathrm{T}}_{|\mathbf{q}|} \simeq \frac{1}{2|\mathbf{q}|}\,. \tag{3.132}$$

ZERO-WIDTH LIMIT: Provided that the plasma is sufficiently weakly coupled, one can take the zero-width limit, which basically corresponds to $\Gamma \to 0$. In the SM this is allowed due to the smallness of the relevant couplings. Therefore, the BW distribution converges to the Dirac delta function

$$\Delta^{\mathcal{A}}_\phi(q)|_{\mathrm{ZW}} = \pi\delta(q^2 - \omega^2_{\phi|\mathbf{q}|})\mathrm{sign}(q^0) + \Delta^{\mathcal{A}}_\phi(q)|_{\mathrm{cont}}\,, \tag{3.133}$$

$$S^{\mathcal{A}}_{\pm}(q)|_{\mathrm{ZW}} = \pi\left[\mathcal{Z}^{\pm}_{|\mathbf{q}|}\delta\left(q^0 - \omega_{\mp|\mathbf{q}|}\right) + \mathcal{Z}^{\mp}_{|\mathbf{q}|}\delta\left(q^0 + \omega_{\mp|\mathbf{q}|}\right)\right] + S^{\mathcal{A}}_{\pm}(q)|_{\mathrm{cont}}\,, \tag{3.134}$$

$$\Delta^{\mathcal{A}}_{\mathrm{T,L}}(q)|_{\mathrm{ZW}} = \pi\left[\mathcal{Z}^{\mathrm{T,L}}_{|\mathbf{q}|}\delta\left(q^0 - \omega_{\mathrm{T,L}|\mathbf{q}|}\right) - \mathcal{Z}^{\mathrm{T,L}}_{|\mathbf{q}|}\delta\left(q^0 + \omega_{\mathrm{T,L}|\mathbf{q}|}\right)\right] + \Delta^{\mathcal{A}}_{\mathrm{T,L}}(q)|_{\mathrm{cont}}\,, \tag{3.135}$$

when making use of the Dirac delta representation

$$\delta(x) = \frac{1}{\pi}\lim_{\epsilon\to 0}\frac{\epsilon}{x^2 + \epsilon^2}\,. \tag{3.136}$$

Note that S_+ describes the propagation of fermions with positive energy $q^0 = \omega_{+|\mathbf{q}|}$, while S_- refers to fermions with negative energies $q^0 = -\omega_{+|\mathbf{q}|}$. For hard momenta $|\mathbf{q}| \gg m_{\psi,\phi,V}$ the pole part of the spectral propagator, i.e. the spectral propagator in the s-channel, simplifies further

$$\Delta^{\mathcal{A}}_\phi(q) \to \pi\delta(q^2 - m^2_\phi)\mathrm{sign}(q^0)\,, \tag{3.137}$$

$$S^{\mathcal{A}}_{\mathrm{R,L}}(q) \to \pi P_{\mathrm{R,L}}\not{q}\delta(q^2 - m^2_\psi)\mathrm{sign}(q^0)\,, \tag{3.138}$$

$$\Delta^{\mathcal{A}}_{\mathrm{T}}(q) \to \pi\delta(q^2 - m^2_V)\mathrm{sign}(q^0)\,, \tag{3.139}$$

and puts the particles on their mass shell, that is given by the thermal masses (3.112), (3.113) and (3.114). When neglecting the thermal masses one directly recovers the free tree-level solutions (3.75)-(3.78) with eq. (3.81).

4

DIFFUSION CONSTANTS DURING THE ELECTROWEAK PHASE TRANSITION

The BAU can be generated during the EWPT via EW baryogenesis provided that the PT is strongly first-order, cf. the reviews [34, 35]. This is required to quench the EW sphalerons in the broken phase such that any baryon asymmetry, that has been produced in front of the bubble wall via CP-violating reflections, is prevented from a washout. The set of equation that describes the EW baryogenesis is sensitive to the diffusion constants of SM particles such as chiral fermions and the Higgs field. In order to account for non-equilibrium and thermal effects calculations, the CTP formalism [36, 37] is used. This allows to write down Boltzmann-like equations for distribution functions with a collision term that contains all the necessary scattering information about the surrounding plasma. A variational approach based on refs. [132, 133] is used to extract the diffusion constants. On the one hand, these receive contributions from one-loop self-energy type diagrams that would be IR divergent in the absence of thermal effects in the t-channel. However, as an implicit feature of the CTP formalism, particularly the exchanged particles are dressed by the plasma and obtain a finite width which is why the divergences are regulated by the thermal masses. Thus, these diagrams contribute to the diffusion constants at leading logarithmic order in the relevant couplings. On the other hand, there are two-loop vertex type diagrams. These seem to be IR divergent. However, when summing up all the relevant diagrams, certain symmetry properties of the collision term can be applied to get rid of the divergences. Therefore, it is sufficient to use free propagators rather than resummed propagators at leading order. In contrast to the self-energy type diagrams, the vertex type diagrams only contribute at leading linear order in the couplings and are subdominant.

Section 4.1 is devoted to the derivation of the diffusion network and relates the generated baryon asymmetry to the diffusion constants. Further, it is described how to extract diffusion constants from a linearised Boltzmann equation. Contributions from self-energy type and vertex type diagrams are computed in sections 4.2 and 4.3, respectively, before the results are discussed in section 4.4.

4.1 DIFFUSION TRANSPORT EQUATIONS

Boltzmann equations that describe the diffusion of particles around the bubble wall into the symmetric are derived and solved based on refs. [110, 111] in subsection 4.1.1, such that an analytic expression is found that expresses the baryon asymmetry in the broken phase in terms of the diffusion constants. In subsection 4.1.2 the variational approach by refs. [132, 133] is applied to extract diffusion constants from Boltzmann-like equations that are derived from first principles in the CTP formalism and take account of the relevant

thermal effects of the plasma. Both, one-loop self-energy type and two-loop vertex type contributions to the collision term are introduced in subsection 4.1.3.

4.1.1 *Solving Boltzmann equations*

During the EWPT, transport dynamics, such as the diffusion process, can be described by Boltzmann equations. Within the non-equilibrium CTP formalism by Schwinger and Keldysh the charge current density of a particle of species i can be determined by solving [110, 111]

$$\partial_\mu j_i^\mu = -\frac{T^2}{6}\sum_X \Gamma_X \left(\mu_i + \mu_j + \cdots - \mu_k - \mu_l - \dots\right) + S_i^{\mathrm{CPV}} \,. \tag{4.1}$$

The production of a non-zero charge happens due to the presence of some CP-violating source S_i^{CPV}, while equilibration happens with the rate Γ_X for a process X that describes the interaction $i + j \cdots \leftrightarrow k + l \dots$. In case of large Γ_X, i.e. for fast rates, chemical equilibrium can be reached and implies

$$\mu_i + \mu_j + \cdots = \mu_k + \mu_l + \dots \,. \tag{4.2}$$

The diffusion constant D_i as the mean free path a particle i in the medium comes into play when using Fick's law for the charge number density $n_i = j_i^0$,

$$\mathbf{j}_i = -D_i \boldsymbol{\nabla} n_i \,. \tag{4.3}$$

Note that we have expressed the diffusion equation (4.1) in terms of chemical potentials. In the limit of small $\mu_i \ll T$, which is a justified assumption for temperatures relevant for EW baryogenesis, these can be related to the charge densities via

$$n_i = \frac{T^2}{6} k_i \mu_i + \mathcal{O}(\mu_i^3/T^3) \,. \tag{4.4}$$

The factor k_i counts the effective degrees of freedom of a particle i with mass m_i in the plasma

$$k_i = g_i \frac{6}{\pi^2} \int_{m_i/T}^{\infty} \mathrm{d}x \, x \frac{\mathrm{e}^x}{\left(\mathrm{e}^x \pm 1\right)^2} \sqrt{x^2 - m_i^2/T^2} \,, \tag{4.5}$$

where $\pm$ corresponds to fermions and bosons, respectively, and g_i is the number of internal degrees of freedom. Note hat k_i incorporates Boltzmann suppression, which becomes important for masses close to the EW scale. Successful EW baryogenesis requires the PT to be strongly first-order. Further, the diffusion process happens mainly in the symmetric phase of the SM. This allows to compute the diffusion constants by relying on the fully symmetric SM Lagrangian. Due to a zero Higgs EV in this phase of the SM, the vacuum masses of the SM particle are vanishing. Since thermal masses are small compared to the EW scale, it is sufficient to neglect the masses of the SM particles in k_i. This leads to the simple relation $k_i = \pi^2/6\lambda_i$, where $\lambda_i = 1$ for fermions and $\lambda_i = 2$ for bosons. Note, however, the SM alone is not able to account for first-order PT and further CP-violating sources are too weak to generate sufficient asymmetries around the bubble wall. These issues can be solved by introducing extra degrees of freedom that couple to the SM, such as scalars in supersymmetric extension of the SM. This justifies the general form of eq. (4.5).

The baryon charge n_B is determined by the sum of LH number densities over all flavours $a = e, \mu, \tau$

$$n_{\mathrm{L}} = \sum_{a=1}^{3} \left(n_{q_{\mathrm{L}}^a} + n_{\ell_{\mathrm{L}}^a} \right) , \tag{4.6}$$

due to EW sphaleron processes that are only sensitive to LH particles, with the LH quark $n_{q_{\mathrm{L}}^a} = n_{u_{\mathrm{L}}^a} + n_{d_{\mathrm{L}}^a}$ and LH lepton $n_{\ell_{\mathrm{L}}^a} = n_{\nu_{\mathrm{L}}^a} + n_{\ell_{\mathrm{L}}^a}$ densities.

For simplicity, we neglect the curvature of the bubble wall. Thus, we can assume the bubble to move into z-direction with bubble wall velocity v_{w}. In the following we work in wall-frame coordinates $z = |\mathbf{r} + v_{\mathrm{w}} \mathbf{e}_z t|$. Note that for typical scenarios of baryogenesis one has $v_{\mathrm{w}} \simeq 0.05$ [134, 135], which allows for a non-relativistic treatment of the wall motion. Further, CP-violating interaction appear through scatterings with the wall, within which CP-violating sources are present. The thickness of the wall is denoted by L_{w}. Eventually, using eq. (4.3), the LH side of eq. (4.1) is given by

$$\partial_\mu = v_{\mathrm{w}} \partial_z n_i - D_i \partial_z^2 n_i \, . \tag{4.7}$$

DIFFUSION SCALE: For the following discussion we define the diffusion time scale $\tau_{\mathrm{diff}} = \bar{D}/v_{\mathrm{w}}^2$ with the average diffusion constant $\bar{D}$. This is given when comparing the distance that a particle diffuses on average $d_{\mathrm{diff}} = \sqrt{\bar{D} t}$ to the distance the bubble wall advances $d_{\mathrm{w}} = v_{\mathrm{w}} t$ within a time t. τ_{diff} describes how long it takes for the LH charge to diffuse into the symmetric phase after it has been produced at the bubble wall and to be collected by the expanding bubble wall where the charge is eventually frozen in due the quenching of the EW sphalerons in the bubble wall. With $\bar{D} = \mathcal{O}(10^2)$, as will be shown in section 4.4, the diffusion time scale is approximately given by $\tau_{\mathrm{diff}} T = \mathcal{O}(10^4)$. This needs to be compared to the interaction time scale $\tau_X = \Gamma_X^{-1}$ for a given process X.

On the one hand, $\tau_X \ll \tau_{\mathrm{diff}}$ implies quick equilibration of the charges since the particles are diffusing ahead of the relatively slow moving bubble wall. Γ_X cannot be neglected in this case. In particular, EW interactions being fast force particles within the same isodoublet to have equal chemical potential.

On the other hand, when $\tau_X \gg \tau_{\mathrm{diff}}$, the charges are captured by the bubble wall before EW sphalerons are able to transform these into baryon charges. In this case Γ_X can be neglected within the Boltzmann equations. With $\tau_{\mathrm{ws}} = 10^5/T \gg \tau_{\mathrm{diff}}$, EW sphaleron interactions are too slow to be included into the set of diffusion equations. This implies that the baryon and the lepton number, which in the SM can be only violated by these EW sphalerons, are approximately globally conserved, i.e. the integral of the baryon and lepton densities over all z vanishes. Note that lepton number is not locally conserved since the diffusion constant for RH leptons is much larger than the one for the LH leptons. This is because RH leptons do only interact with U(1) gauge bosons. Therefore, they can travel longer distances on average before being scattered. In contrast to that, diffusion constants for baryons are dominated by the strong interaction. Therefore, RH and LH baryons exhibit a similar diffusion behaviour such that baryon number is approximately locally conserved:

$$\sum_{a=1}^{3} \left(n_{q_{\mathrm{L}}^a} + n_{u_{\mathrm{R}}^a} + n_{d_{\mathrm{R}}^a} \right) = 0 \, . \tag{4.8}$$

Further, first and second generation Yukawa interactions for both leptons and quarks are slow enough to be neglected. Consequently, there is no production of leptons of the first

and second generation, while quarks of first and second generation are only produced by strong sphalerons, that are fast enough to be in equilibrium, in equal numbers. This implies the relations

$$n_{q_{\mathrm{L}}^1} = n_{q_{\mathrm{L}}^2} = -2n_{u_{\mathrm{R}}^1} = -2n_{u_{\mathrm{R}}^2} = -2n_{d_{\mathrm{R}}^1} = -2n_{d_{\mathrm{R}}^2} \,. \tag{4.9}$$

With eq. (4.8) it follows

$$n_{d_{\mathrm{R}}^3} = -n_{u_{\mathrm{R}}^3} - n_{q_{\mathrm{L}}^3} \,. \tag{4.10}$$

Before we write down the set of Boltzmann equations, we introduce some heavy fields, indicated by a tilde, that are in equilibrium with the SM particles, which can be the case for heavy superpartners due to fast gaugino interactions [110, 111]. Therefore, we make use of the following notation for the quarks

$$U_i = n_{u_{\mathrm{R}}^i} + n_{\tilde{u}_{\mathrm{R}}^i} \,, \quad D_i = n_{d_{\mathrm{R}}^i} + n_{\tilde{d}_{\mathrm{R}}^i} \,, \quad Q_i = n_{q_{\mathrm{L}}^i} + n_{\tilde{q}_{\mathrm{L}}^i} \,, \tag{4.11}$$

and for the leptons

$$R_i = n_{e_{\mathrm{R}}^i} + n_{\tilde{e}_{\mathrm{R}}^i} \,, \quad L_i = n_{\ell_{\mathrm{L}}^i} + n_{\tilde{\ell}_{\mathrm{L}}^i} \,, \tag{4.12}$$

while density of the Higgs is given by the sum of all components of the Higgs doublets

$$H = \sum_i n_{H^i} \,. \tag{4.13}$$

Further, we use $T \equiv U_3$, $B \equiv D_3$, $Q \equiv Q_3$ for the quarks and $R \equiv R_3$ and $L = L_3$ for the leptons. This motivates the notation for more general k-factors from eq. (4.5): $k_R = k_{\tau_{\mathrm{R}}} + k_{\tilde{\tau}_{\mathrm{R}}}$, $k_Q = k_{q_{\mathrm{L}}} + k_{\tilde{q}_{\mathrm{L}}}$, etc.

SET OF BOLTZMANN EQUATIONS: With the considerations above the set of Boltzmann equation is given by only considering interactions that are fast compared to the diffusion time scale. One finds that, while in general top Yukawa interaction are fast compared to the diffusion time scale, bottom and tau Yukawa interaction are too slow in the SM to be considered. However, as reported in refs. [109], these other two third generation Yukawa interaction can be large enough not to be neglected. This happens e.g. in supersymmetric EW baryogenesis, when the ratio of the VEVs of the Higgs doublets $v_u/v_d \equiv \tan\beta$ is enhanced, i.e. when $\tan\beta \gg 1$. Refs. [110, 111] state that for $\tan\beta \gtrsim 5$ bottom Yukawa interactions become important for the generation of LH densities, while $\tan\beta \gtrsim 20$ also tau Yukawa interaction have to be taken into account.

Therefore, we use the general approach and include $\Gamma_{t,b,\tau}$ that describe third generation Yukawa interaction rates from top, bottom and tau Yukawa couplings $h_{t,b,\tau}$ and $\Gamma_{\mathrm{ss}} = 16\kappa'\alpha_s^4 T$ as the strong sphaleron rate with the strong coupling $\alpha_s = g_3^2/(4\pi)$ and $\kappa' \sim \mathcal{O}(1)$ [136]. Note that it is sufficient to write down Boltzmann equations for the number densities Q, T, Q_1, L, R and H only, while all the other charges are obtained via eqs. (4.9) and (4.10). For the Higgs boson, the diffusion equation reads

$$\begin{aligned} v_{\mathrm{w}} H' - D_H H'' = &-\Gamma_t \left(\frac{Q}{k_Q} - \frac{T}{k_T} + \frac{H}{k_H} \right) + \Gamma_b \left(\frac{Q}{k_Q} + \frac{Q+T}{k_B} - \frac{H}{k_H} \right) - \Gamma_h \frac{H}{k_H} \\ &- \Gamma_\tau \left(\frac{L}{k_L} - \frac{R}{k_R} - \frac{H}{k_H} \right) + S_H^{\mathrm{CPV}} \,, \end{aligned} \tag{4.14}$$

while for the leptons we have

$$v_w L' - D_L L'' = -\Gamma_\tau \left(\frac{L}{k_L} - \frac{R}{k_R} - \frac{H}{k_H} \right) - \Gamma_{m\tau} \left(\frac{L}{k_L} - \frac{R}{k_R} \right) - S_\tau^{\mathrm{CPV}} , \tag{4.15}$$

$$v_w R' - D_R'' = \Gamma_\tau \left(\frac{L}{k_L} - \frac{R}{k_R} - \frac{H}{k_H} \right) + \Gamma_{m\tau} \left(\frac{L}{k_L} - \frac{R}{k_R} \right) + S_\tau^{\mathrm{CPV}} , \tag{4.16}$$

and eventually for the quarks

$$\begin{aligned} v_w Q' - D_Q Q'' = &-\Gamma_t \left(\frac{Q}{k_Q} - \frac{T}{k_T} + \frac{H}{k_H} \right) - \Gamma_b \left(\frac{Q}{k_Q} + \frac{Q+T}{k_B} - \frac{H}{k_H} \right) \\ &- \Gamma_{mt} \left(\frac{Q}{k_Q} - \frac{T}{k_T} \right) - \Gamma_{mb} \left(\frac{Q}{k_Q} + \frac{T+Q}{k_B} \right) - S_t^{\mathrm{CPV}} - S_b^{\mathrm{CPV}} \\ &- 2\Gamma_{\mathrm{ss}} \left(2\frac{Q}{k_Q} - \frac{T}{k_T} + \frac{Q+T}{k_B} + \frac{1}{2} \sum_{a=1}^{2} \left[4\frac{1}{k_{Q_a}} + \frac{1}{k_{U_a}} + \frac{1}{k_{D_a}} \right] Q_1 \right) , \end{aligned} \tag{4.17}$$

$$\begin{aligned} v_w T' - D_Q T'' = &\Gamma_t \left(\frac{Q}{k_Q} - \frac{T}{k_T} + \frac{H}{k_H} \right) + \Gamma_{mt} \left(\frac{Q}{k_Q} - \frac{T}{k_T} \right) + S_t^{\mathrm{CPV}} \\ &+ \Gamma_{\mathrm{ss}} \left(2\frac{Q}{k_Q} - \frac{T}{k_T} + \frac{Q+T}{k_B} + \frac{1}{2} \sum_{a=1}^{2} \left[4\frac{1}{k_{Q_a}} + \frac{1}{k_{U_a}} + \frac{1}{k_{D_a}} \right] Q_1 \right) , \end{aligned} \tag{4.18}$$

$$v_w Q_1' - D_Q Q_1'' = -2\Gamma_{\mathrm{ss}} \left(2\frac{Q}{k_Q} - \frac{T}{k_T} + \frac{Q+T}{k_B} + \frac{1}{2} \sum_{a=1}^{2} \left[4\frac{1}{k_{Q_a}} + \frac{1}{k_{U_a}} + \frac{1}{k_{D_a}} \right] Q_1 \right) . \tag{4.19}$$

In addition to the Yukawa and strong sphaleron interactions, $\Gamma_{h,mi}$ describe CP-conserving scattering rates within the bubble with the background Higgs field [137]. Further, the different S_i^{CPV} account for CP-violating sources, cf. e.g. refs. [110, 111].

SOLVING THE BOLTZMANN EQUATIONS: When solving the system of Boltzmann equations (4.14)-(4.19) and further assuming top and bottom Yukawa couplings to be in equilibrium, we can express the quark densities in terms of the Higgs density

$$T \equiv \kappa_T H = \frac{k_T}{k_H} \frac{2k_B + k_Q}{k_B + k_Q + k_T} H , \tag{4.20}$$

$$Q \equiv \kappa_Q H = \frac{k_Q}{k_H} \frac{k_B - k_T}{k_B + k_Q + k_T} H , \tag{4.21}$$

$$B \equiv \kappa_B H = -\frac{k_B}{k_H} \frac{2k_T + k_Q}{k_B + k_Q + k_T} H . \tag{4.22}$$

Furthermore, the term in eq. (4.19) that is not proportional to Q_1 vanishes due to equilibrated top and bottom Yukawa interactions. When applying the boundary condition $Q_1(z \to \pm\infty) \to 0$, it can be shown that both Q_1 and also $U_{1,2}$, $D_{1,2}$ and Q_2 vanish, which is due to the approximate baryon number conservation (4.8). Therefore, fast top and bottom Yukawa interactions lead to vanishing first and second generation quarks densities.

When further assuming the τ Yukawa couplings to be in equilibrium it is possible to approximately relate n_{L} to the Higgs charge density H, where non-local terms are neglected [111]:

$$\begin{aligned} n_{\mathrm{L}} &\simeq \left(\frac{k_q}{k_H} \frac{k_B - k_T}{k_B + k_Q + k_T} + \frac{k_\ell}{k_H} \frac{k_{\mathrm{R}} D_{\mathrm{R}}}{k_{\mathrm{L}} D_{\mathrm{L}} + k_{\mathrm{R}} D_{\mathrm{R}}} \right) H \\ &\simeq \frac{k_\ell}{k_H} \frac{k_{\mathrm{R}} D_{\mathrm{R}}}{k_{\mathrm{L}} D_{\mathrm{L}} + k_{\mathrm{R}} D_{\mathrm{R}}} H \,. \end{aligned} \tag{4.23}$$

For illustrative purposes we have used that the masses of the new degrees of freedom fulfil $m_{\tilde{b}} = m_{\tilde{t}}$ and thus $k_B \simeq k_T$. Thus, the first term in eq. (4.23), that is due to fast top and bottom Yukawa interactions, vanishes. Therefore, this case is referred to as lepton-mediated EW baryogenesis [111].

Note that the discussion of the diffusion process is quite general, in the sense that it can be applied to theories where both Yukawa interactions of the third generations are fast compared to the diffusion time scale and where CP violation affects the first and second generations of quarks only through strong sphaleron processes.

We have seen that all the relevant densities can be expressed in terms of H. Since the baryon number is determined by n_{L} alone, it is sufficient to solve the system for H only. Eventually, the set of Boltzmann equation gives rise to a differential equation for H

$$\frac{\mathrm{d}^2}{\mathrm{d}z^2} H(z) - \frac{v_{\mathrm{w}}}{\bar{D}} \frac{\mathrm{d}}{\mathrm{d}z} H(z) - \frac{\bar{\Gamma}}{\bar{D}} H(z) = -\frac{S(z)}{\bar{D}} \,, \tag{4.24}$$

with

$$\bar{D} = \frac{D_H + D_Q(\kappa_T - \kappa_B) + D_{\mathrm{L}} \kappa_{\mathrm{L}}}{1 + \kappa_T - \kappa_B + \kappa_{\mathrm{L}}} \,, \tag{4.25}$$

$$\bar{\Gamma} = \frac{\Gamma_h + \Gamma_{mt} + \Gamma_{mb} + \Gamma_{m\tau}}{\kappa_H (1 + \kappa_T - \kappa_B + \kappa_{\mathrm{L}})} \,, \tag{4.26}$$

$$\bar{S} = \frac{S_H^{\mathrm{CPV}} + S_t^{\mathrm{CPV}} - S_b^{\mathrm{CPV}} - S_\tau^{\mathrm{CPV}}}{1 + \kappa_T - \kappa_B + \kappa_{\mathrm{L}}} \,. \tag{4.27}$$

In this case the effective decay rate $\bar{\Gamma}$ is given by the scattering rates with the Higgs background field. These are only present in the broken phase, i.e. for $z > 0$. Therefore, we can use $\bar{\Gamma}(z) = \vartheta(z)\bar{\Gamma}$ with a spatially constant $\bar{\Gamma}$. Further, we assume $\bar{S}$ to be an effective CP-violating source term that is only vanishing for $z < -L_{\mathrm{w}}/2$. Consequently, H can be solved in the three regimes: regime I is given by $z < -L_{\mathrm{w}}/2$, where neither the source $\bar{S}$ nor the relaxation term $\bar{\Gamma}$ is present. Regime II corresponds to $-L_{\mathrm{w}}/2 < z < 0$ for $\bar{\Gamma} = 0$, while regime III is given by $z > 0$ with $\bar{S} \neq 0$ and $\bar{\Gamma} \neq 0$. Given that $H(z \to \pm\infty) \to 0$, solutions to H in the symmetric phase are given by

$$H_{\mathrm{I}}(z) = A \mathrm{e}^{\frac{v_{\mathrm{w}}}{\bar{D}} z} \,, \tag{4.28}$$

where the integration constant A is obtained by the use of the continuity conditions $H_{\mathrm{I}}(-L_{\mathrm{w}}/2) = H_{\mathrm{II}}(-L_{\mathrm{w}}/2)$, $H'_{\mathrm{I}}(-L_{\mathrm{w}}/2) = H'_{\mathrm{II}}(-L_{\mathrm{w}}/2)$ and $H_{\mathrm{II}}(0) = H_{\mathrm{III}}(0)$, $H'_{\mathrm{II}}(0) = H'_{\mathrm{III}}(0)$, such that

$$A = \int_0^\infty \mathrm{d}y \bar{S}(y) \frac{\mathrm{e}^{-\gamma_+ y}}{\bar{D}\gamma_+} + \int_{-L_{\mathrm{w}}/2}^0 \mathrm{d}y \bar{S}(y) \left[\frac{\gamma_-}{v_{\mathrm{w}}\gamma_+} + \frac{\mathrm{e}^{-v_{\mathrm{w}} y/\bar{D}}}{v_{\mathrm{w}}} \right] , \tag{4.29}$$

with

$$\gamma_\pm \equiv \frac{1}{2\bar{D}}\left(v_\mathrm{w} \pm \sqrt{v_\mathrm{w}^2 + 4\bar{\Gamma}\bar{D}}\right) . \tag{4.30}$$

With $v_\mathrm{w} \simeq 0.05$ and $\bar{D} \sim \mathcal{O}(10^2)$ we can expand in small $v_\mathrm{w}/\bar{D}$, such that $\gamma_\pm = \pm\sqrt{\bar{\Gamma}/\bar{D}} + \mathcal{O}(v_\mathrm{w})$. This implies a relaxation of the charge densities in the broken phase, given by the rate $\sqrt{\bar{\Gamma}/\bar{D}}$, that is much stronger than the equilibration of the charges, given by the rate $\sqrt{v_\mathrm{w}/\bar{D}}$, in front of the wall.

Note that eq. (4.29) can be solved for an arbitrary dependence of the source $\bar{S}$ on z. However, for illustrative purposes, it is beneficial to assume a source $\bar{S}$ that is only non-vanishing for $-L_\mathrm{w}/2 < z < 0$ and also spatially constant. This allows to get rid of the first integral in eq. (4.29) and further allows to evaluate the second term analytically. In the limit of $v_\mathrm{w}/\bar{D} \ll 1$, A can then be approximated by

$$A = \bar{S}\left(\frac{\bar{D}}{v_\mathrm{w}}\left(\mathrm{e}^{\frac{L_\mathrm{w}}{2}\frac{v_\mathrm{w}}{\bar{D}}} - 1\right) + \frac{L_\mathrm{w}}{2}\frac{\gamma_-}{\gamma_+}\right)\frac{1}{v_\mathrm{w}} . \tag{4.31}$$

Thus, eq. (4.23) can be used to determine the LH lepton density in the symmetric phase

$$n_\mathrm{L}(z) \simeq \frac{k_\ell}{k_H}\frac{k_\mathrm{R} D_\mathrm{R}}{k_\mathrm{L} D_\mathrm{L} + k_\mathrm{R} D_\mathrm{R}}\bar{S}\left(\left(\frac{L_\mathrm{w}}{2}\right)^2\frac{1}{2\bar{D}} + \frac{L_\mathrm{w}}{2}\frac{1}{\sqrt{\bar{D}\bar{\Gamma}}}\right)\mathrm{e}^{\frac{v_\mathrm{w}}{\bar{D}}z} , \tag{4.32}$$

that allows to compute the baryon asymmetry in the broken phase.

BARYON ASYMMETRY: The baryon charge n_B is then obtained by solving [107]

$$D_q\frac{\mathrm{d}^2 n_B(z)}{\mathrm{d}z^2} - v_\mathrm{w}\frac{\mathrm{d}n_B(z)}{\mathrm{d}z} - \vartheta\left(-\frac{L_\mathrm{w}}{2} - z\right)\Gamma_b n_B(z) = 3\vartheta\left(-\frac{L_\mathrm{w}}{2} - z\right)\Gamma_\mathrm{ws} n_\mathrm{L}(z) , \tag{4.33}$$

where the Heaviside step function accounts for the fact that EW sphalerons are only active in the symmetric phase, i.e. for $z < -L_\mathrm{w}/2$. Further, we account for the relaxation of the baryon charge in the symmetric phase with rate $\Gamma_b \simeq 15/4\Gamma_\mathrm{ws}$ [138]. Solutions are given by

$$\begin{aligned} n_B(z) = &-\frac{3\Gamma_\mathrm{ws}}{D_q(\lambda_+ - \lambda_-)}\int_{-\infty}^{-L_\mathrm{w}/2}\mathrm{d}y\, n_\mathrm{L}(y)\mathrm{e}^{-\lambda_- y} \\ &+ \frac{3\Gamma_\mathrm{ws}}{D_q(\lambda_+ - \lambda_-)}\sum_\pm \mathrm{e}^{\gamma_- y}(\pm 1)\int_{-L_\mathrm{w}/2}^{z}\mathrm{d}y\,\vartheta\left(-\frac{L_\mathrm{w}}{2} - y\right) n_\mathrm{L}(y)\mathrm{e}^{-\lambda_\pm y} , \end{aligned} \tag{4.34}$$

with

$$\lambda_\pm = \frac{v_\mathrm{w}^2 \pm \sqrt{v_\mathrm{w}^2 + 4\Gamma_b D_q}}{2D_q} , \tag{4.35}$$

where the integration constant is chosen such that $n_B(z \to -\infty) \to 0$. Therefore, the baryon charge density inside the bubble (for $z > L_\mathrm{w}/2$) is a constant that is given by the first integral of eq. (4.34). For $v_\mathrm{w}^2 \gg 4\Gamma_b D_q$, which is a justified assumption [137, 138], we have $\lambda_- \simeq 0$ and $\lambda_+ \simeq v_\mathrm{w}/D_q$. With the approximate solution (4.32) that integral can be solved analytically, such that

$$n_B(z > L_\mathrm{w}/2) = -\bar{S}\left(\frac{3\Gamma_\mathrm{ws}}{v_\mathrm{w}^2}\right)\frac{k_\ell}{k_H}\frac{k_\mathrm{R} D_\mathrm{R}}{k_\mathrm{L} D_\mathrm{L} + k_\mathrm{R} D_\mathrm{R}}\left[\frac{1}{2}\left(\frac{L_\mathrm{w}}{2}\right)^2 + \frac{L_\mathrm{w}}{2}\sqrt{\frac{\bar{D}}{\Gamma}}\right] . \tag{4.36}$$

4.1.2 *Linearised transport equation*

Diffusion constants $D_{\psi,\phi}$ are defined by Fick's law (4.3). We describe particles participating in the diffusion process by local equilibrium distribution functions $f_0^{\psi,\phi}(|\mathbf{k}|,\mathbf{x})$, that are slowly evolving in space since $\mu_{\psi,\phi}(\mathbf{x})$ varies slowly, and a departure from equilibrium $\delta f^{\psi,\phi}(k,\mathbf{x})$. Thus, we can write

$$f_0^{\psi,\phi}(k,\mathbf{x}) = \left[\mathrm{e}^{\beta(k^0-\mu_{\psi,\phi}(\mathbf{x}))} \pm 1\right]^{-1}, \tag{4.37}$$

$$\delta f^{\psi,\phi}(k,\mathbf{x}) = f_0^{\psi,\phi}(k,\mathbf{x})\left(1 \mp f_0^{\psi,\phi}(k,\mathbf{x})\right) f_1^{\psi,\phi}(k,\mathbf{x}), \tag{4.38}$$

where the deviations are written in such a way that $f_1^{\psi,\phi}(k,\mathbf{x})$ is driven by chemical potentials and is first order in gradients. Note that gauge interactions are fast enough to keep the gauge bosons in equilibrium. When writing the current as

$$\mathbf{j}_{\psi,\phi} = \int \frac{\mathrm{d}^3\mathbf{k}}{(2\pi)^3}\hat{\mathbf{k}}\,\delta f^{\psi,\phi}(k,\mathbf{x}), \tag{4.39}$$

one can obtain the different diffusion constants by solving transport equations for the function $f_1^{\psi,\phi}(k,\mathbf{x})$. In the following we will work in the local rest frame and consequently drop the notation on $\mathbf{x}$. Further we will work up to first order in the deviations from equilibrium or in gradients.

In this limit and without flavour effects, the leading order transport equation is deduced from the kinetic equations (3.49) in absence of the commutator term. Further, since the bubble wall breaks the homogeneity of the universe, the dependence on the spatial $\mathbf{x}$ must not be neglected. Therefore, eq. (3.49) requires the replacement $\partial_t \to \partial_t + \hat{\mathbf{k}}\cdot\boldsymbol{\nabla}$. Note that the time derivative is already second order in gradients [132]. Consequently, the relevant transport equation is given by

$$\frac{\mathbf{k}\cdot\boldsymbol{\nabla}}{|\mathbf{k}|} f_0^{\psi,\phi}(\mathbf{k}) = \pm\int_0^\infty \frac{\mathrm{d}k^0}{2\pi}\mathcal{C}_{\psi,\phi}(k), \tag{4.40}$$

for a given fermion ψ or the Higgs field. Note that throughout this thesis we compute diffusion constants for particles. This is realised by putting the putting the particle on-shell and further assume positive energy $k^0 = |\mathbf{k}|$. Diffusion constants for antiparticles, i.e. for $k^0 = -|\mathbf{k}|$, can be obtained analogously but do not differ from diffusion constants for particles. This is because the procedure in the following is insensitive to $\mathrm{sign}(k^0)$. The transport equation (4.40) describes the phase space behaviour of the distribution. This is basically determined by the collision terms

$$\mathcal{C}_\phi(k) = \mathrm{i}\Pi_\phi^>(k)\mathrm{i}\Delta_\phi^<(k) - \mathrm{i}\Pi_\phi^<(k)\mathrm{i}\Delta_\phi^>(k), \tag{4.41}$$

$$\mathcal{C}_\psi(k) = \mathrm{tr}\left[\mathrm{i}\not{\Sigma}_\psi^>(k)\mathrm{i}S_\psi^<(k) - \mathrm{i}\not{\Sigma}_\psi^<(k)\mathrm{i}S_\psi^>(k)\right], \tag{4.42}$$

that contain all the necessary scattering informations, cf. eq. (3.49), of the surrounding plasma. It can be shown that $\mathcal{C}_{\psi,\phi}$ vanishes in equilibrium. Therefore, these can be written as functions that are linear in the deviations f_1, i.e.

$$\mathcal{C}_{\psi,\phi}[f] = (\mathcal{C}f_1)_{\psi,\phi} + \mathcal{O}(f_1^2), \tag{4.43}$$

where higher order terms in f_1 are neglected. The LH side of the transport equations (4.40) is given by

$$\frac{\mathbf{k}\cdot\boldsymbol{\nabla}}{|\mathbf{k}|} f_0^{\psi,\phi}(\mathbf{k}) = \beta f_0^{\psi,\phi}(k)(1 \mp f_0^{\psi,\phi}(k))\hat{k}_i(\nabla_i\mu) + \mathcal{O}(\mu^2)\,, \tag{4.44}$$

and requires the deviations to be of the following form [132]

$$f_1^{\psi,\phi}(k) = \beta^2(\nabla_i\mu)\,\chi_i^{\psi,\phi}(k)\,, \tag{4.45}$$

with $\chi^{\psi,\phi}(k) \propto \hat{\mathbf{k}}$ a function that is chosen such that it solves the transport equation. With the definition

$$S_i^{\psi,\phi}(k) = -T f_0^{\psi,\phi}(k)(1 \mp f_0^{\psi,\phi}(k))\hat{k}_i\,, \tag{4.46}$$

we are able to write down a linearised transport equation

$$S_i^{\psi,\phi}(k) = (\mathcal{C}_{\psi,\phi}\chi_i^{\psi,\phi})(k)\,. \tag{4.47}$$

When solving this equation for χ, we can determine the current $\mathbf{j}$ from eq. (4.39) by making use of the definition (4.45). In the limit of small chemical potential, i.e. for $\mu_{\psi,\phi} \ll T$, the number density appearing eq. (4.3) can be expressed in terms of the $\mu_{\psi,\phi}$ via

$$n_{\psi,\phi} = \mu_{\psi,\phi}\,\Xi_{\psi,\phi}\,, \tag{4.48}$$

with the charge susceptibility

$$\Xi_{\psi,\phi} = \frac{\partial n_{\psi,\phi}}{\partial\mu_{\psi,\phi}} = \int \frac{\mathrm{d}^3\mathbf{k}}{(2\pi)^3}\beta f^{\psi,\phi}(\mathbf{k})(1 \mp f^{\psi,\phi}(\mathbf{k})) = \begin{cases} \frac{T^2}{6} & \text{for bosons} \\ \frac{T^2}{12} & \text{for fermions} \end{cases}. \tag{4.49}$$

Consequently, both expressions of the current (4.3) and (4.39) depend on the gradient of the chemical potentials. This allows to extract the diffusion constant when having solved the system (4.47) for χ.

VARIATIONAL APPROACH: In the following we use the approach from ref. [132, 133] by solving the system by extremalisation. With the inner product

$$(a,b)_3 \equiv \beta^3 \int \frac{\mathrm{d}^3k}{(2\pi)^3} a(k)b(k)\,, \tag{4.50}$$

$$(a,b)_4 \equiv \beta \int_0^\infty \frac{\mathrm{d}k^0}{2\pi}(a,b)_3 = \beta^4 \int \frac{\mathrm{d}^4k}{(2\pi)^4}\vartheta(k^0)a(k)b(k)\,, \tag{4.51}$$

the functional

$$Q^{\psi,\phi}[\chi] \equiv \left(\chi_i, S_i^{\psi,\phi}\right)_3 - \frac{1}{2}\left(\chi_i^{\psi,\phi}, \mathcal{C}_{\psi,\phi}\chi_i^{\psi,\phi}\right)_4\,, \tag{4.52}$$

is defined such that it is maximal when χ is a solution to eq. (4.47). Therefore, diffusion constants are given by

$$D_{\psi,\phi} = \mp\frac{2}{3} Q_{\max}^{\psi,\phi}\Xi_{\psi,\phi}^{-1}\,. \tag{4.53}$$

In order to maximise $Q[\chi]$ we express χ_i in terms of a N-dimensional set of basis functions $\phi^{(m)}$ with coefficients a_m

$$\chi_i(k) = \sum_{m=1}^{N} a_m \phi_i^{(m)}(k)\,. \tag{4.54}$$

This allows to write

$$Q_{\max}^{\psi,\phi} = \mp\frac{1}{2}\tilde{S}^{\dagger}_{\psi,\phi}\tilde{C}^{-1}_{\psi,\phi}\tilde{S}_{\psi,\phi}\,, \tag{4.55}$$

where $\tilde{S}$ is the vector with components $\tilde{S}_m = (S_i, \phi_i^{(m)})_3$, while $\tilde{C}$ corresponds to the matrix with entries $\tilde{\mathcal{C}}_{mn} = (\phi_i^{(m)}, \mathcal{C}\phi_i^{(n)})_4$. It is known [132, 133] that a convenient choice of basis functions is given by

$$\phi_i^{(m)}(k) = \mathrm{sign}(k^0)\hat{k}_i \frac{(|\mathbf{k}/T)^m}{(1+|\mathbf{k}|/T)^{N-1}}\,, \qquad \text{for } m < N\,. \tag{4.56}$$

Eventually, diffusion constants for fermions and Higgs are given by

$$D_{\psi,\phi} = \tilde{S}^{\dagger}_{\psi,\phi}\tilde{C}^{-1}_{\psi,\phi}\tilde{S}_{\psi,\phi}\left(\frac{T^2}{4}\lambda_{\psi,\phi}\right)^{-1}\,, \tag{4.57}$$

where $\lambda_\psi = 1$ and $\lambda_\phi = 2$. Note that when computing $\tilde{C}_{\psi,\phi}$ we have to divide it by symmetry factor $\mathcal{N}_{\mathrm{sym}}$, that corresponds to the number of equivalent processes, in order to avoid overcounting.

4.1.3 *Contributions to the collision term*

Throughout this thesis we calculate diffusion constants to leading order in the relevant couplings. Within this approximation, thermal effects on the particles that are on-shell can be neglected, i.e. the zero-width approximation is used and thermal masses are neglected. This allows to use eqs. (3.75)-(3.78) with eq. (3.81). As a consequence, $1 \leftrightarrow 2$ (inverse) decays are kinematically forbidden and do not contribute to the diffusion process. Therefore, it is sufficient to only consider $2 \leftrightarrow 2$ scattering processes. There are two types of self-energies in the collision terms (4.41) and (4.42) that contain such processes, which allows for the decomposition [125]

$$\mathcal{C}_{\psi,\phi} = \mathcal{C}^{\mathrm{self}}_{\psi,\phi} + \mathcal{C}^{\mathrm{vert}}_{\psi,\phi}\,. \tag{4.58}$$

On the one hand, the self-energy type contributions are given by one-loop diagrams, see figure 4.1, that are obtained from functional derivatives of the 2PI vacuum bubbles, cf. figure 3.2. These are discussed in section 4.2. With CTP indices a, b these are written as

$$\mathrm{i}\not{\Sigma}^{\mathrm{self}\,ab}_{\psi}(k) = g^2 C_2^F \int \frac{\mathrm{d}^4p}{(2\pi)^4}\frac{\mathrm{d}^4q}{(2\pi)^4}(2\pi)^4\delta^4(q-k+p)\gamma^\mu \mathrm{i}S^{ab}(p)\gamma^\nu \mathrm{i}\Delta^{ab}_{\mu\nu}(q)\,, \tag{4.59}$$

$$\mathrm{i}\Pi^{\mathrm{self}\,ab}_{\phi}(k) = g^2 C_2^F \int \frac{\mathrm{d}^4p}{(2\pi)^4}\frac{\mathrm{d}^4q}{(2\pi)^4}(2\pi)^4\delta^4(q-k+p)\mathrm{i}\Delta^{ab}(p)\mathrm{i}\Delta^{ab}_{\mu\nu}(q)(k+p)^\mu(k+p)^\nu\,. \tag{4.60}$$

FIGURE 4.1: Self-energy type contribution to the collision term $\mathcal{C}^{\text{self}}_{\phi,\psi}$ for chiral fermions and the Higgs boson, respectively. Double lines indicate exact propagators, while single lines correspond to tree-level propagators.

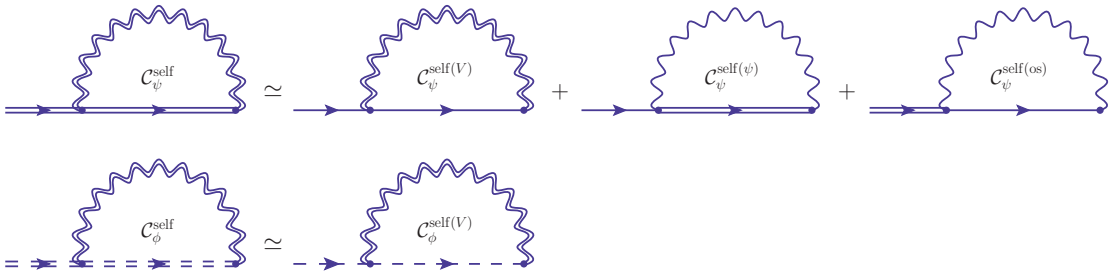

FIGURE 4.2: Leading order decomposition of the self-energy type contribution to the collision term $\mathcal{C}^{\text{self}}_{\phi,\psi}$ for the Higgs bosons and fermions. Double lines indicate full propagators.

While all propagators are fully resummed in this case, a leading order expansion that corresponds to $2 \leftrightarrow 2$ scattering processes is presented in figure 4.2. Due to the use of the resummed propagators, as an implicit feature of the CTP formalism, the exchanged particles are provided with a finite with and a thermal mass. Analytic expression for the resummed propagators are given in section 3.2. Therefore, IR divergences, that would appear for soft momentum exchange $|\mathbf{q}| \lesssim gT$ in the zero width limit, are cured automatically. This requires to compute Hermitian self-energies that work well in this soft scale. This justifies the use of the HTL approximation within the derivation of the Hermitian self-energies, cf. appendix A.2 for a detailed discussion. One finds that the enhancement in the IR gets converted into logarithmic contribution in the couplings, the so-called leading logarithmic contribution.

On the other hand, vertex type diagrams are given by two-loop diagrams, as shown in figures 4.3 and 4.6, and are discussed in section 4.3. $2 \leftrightarrow 2$ scattering processes are recovered by cuts through on-shell particles, see figures 4.4, 4.5 and 4.7. We find that these types of diagrams do not exhibit divergences in the IR when summing up all the individual contributions and further making use of symmetry properties of the collision terms. This allows to neglect thermal effects, such that all the particles, including the exchanged off-shell particles, have zero width and zero thermal masses. Therefore, the vertex type diagrams only contribute to leading linear order and are suppressed to the leading logarithmic contributions from the self-energy type diagrams.

4.2 SELF-ENERGY TYPE CONTRIBUTIONS

By construction of the 2PI effective action, the collision term is given by fully resummed propagators. A useful leading order expansion in the couplings is given when decomposing the collision term

$$\mathcal{C}_\psi^{\text{self}}(k) \simeq \mathcal{C}_\psi^{\text{self}(V)}(k) + \mathcal{C}_\psi^{\text{self}(\psi)}(k) + \mathcal{C}_\psi^{\text{self(os)}}(k)\,, \tag{4.61}$$

into the three contributions

$$\begin{aligned}
\mathcal{C}_\psi^{\text{self}(\psi)}(k) &= G_\psi \int \frac{\mathrm{d}^4p}{(2\pi)^4}\frac{\mathrm{d}^4q}{(2\pi)^4}(2\pi)^4\delta^4(q-k+p) \\
&\quad \times \mathrm{tr}[\gamma_\nu \mathrm{i}S^{>}(p)\gamma_\mu \mathrm{i}\Delta_{\mu\nu}^{(0)>}(q)\mathrm{i}S^{(0)<}(k) - (<\leftrightarrow>)]\,, \qquad (4.62)\\
\mathcal{C}_\psi^{\text{self(os)}}(k) &= G_\psi \int \frac{\mathrm{d}^4p}{(2\pi)^4}\frac{\mathrm{d}^4q}{(2\pi)^4}(2\pi)^4\delta^4(q-k+p) \\
&\quad \times \mathrm{tr}[\gamma_\nu \mathrm{i}S^{(0)>}(p)\gamma_\mu \mathrm{i}\Delta_{\mu\nu}^{(0)>}(q)\mathrm{i}S^{<}(k) - (<\leftrightarrow>)]\,, \qquad (4.63)\\
\mathcal{C}_\psi^{\text{self}(V)}(k) &= G_\psi \int \frac{\mathrm{d}^4p}{(2\pi)^4}\frac{\mathrm{d}^4q}{(2\pi)^4}(2\pi)^4\delta^4(q-k+p) \\
&\quad \times \mathrm{tr}[\gamma_\nu \mathrm{i}S^{(0)>}(p)\gamma_\mu \mathrm{i}\Delta_{\mu\nu}^{>}(q)\mathrm{i}S^{(0)<}(k) - (<\leftrightarrow>)]\,. \qquad (4.64)
\end{aligned}$$

In this way only one propagator per contribution is resummed as shown in figure 4.2, while the remaining propagators are evaluated at tree-level. In the latter case, these particles not only have zero width but also their thermal masses are neglected. Tree-level propagators are given in eqs. (3.75)-(3.78) with eq. (3.81), while resummed propagators are provided in section 3.2. For a leading order analysis it is sufficient to use one-loop resummed propagators. These depend on the Hermitian and spectral self-energies, that are derived in appendix A.2 and A.3, and account for the dispersion relation and finite width of the exchanged particle, respectively. Note that these are the contributions that effectively lead to $2 \leftrightarrow 2$ scatterings. This fact is more obvious when recalling that the particles in those loops are on-shell. When applying on-shell cuts those $2 \leftrightarrow 2$ processes arise. Note that both the resummed gauge boson and the fermion propagators are necessary to cure IR divergences via their finite width that appear in t-channel exchanges due to enhanced HTL contributions, cf. figure 3.3. In contrast to that no such divergences appear for processes where scalars are exchanged. Therefore, there is no need to resum the Higgs propagator. The equivalent diagram with a zero-width exchanged Higgs is given by diagram (F) in figure 4.3. Consequently, the self-energy type collision term for the Higgs is solely given by using a resummed gauge boson propagator

$$\begin{aligned}
\mathcal{C}_\phi^{\text{self}}(k) = \mathcal{C}_\phi^{\text{self}(V)}(k) &= G_\phi \int \frac{\mathrm{d}^4p}{(2\pi)^4}\frac{\mathrm{d}^4q}{(2\pi)^4}(2\pi)^4\delta^4(q-k+p)(k+p)^\mu(k+p)^\nu \\
&\quad \times [\mathrm{i}\Delta_\phi^{(0)>}(p)\mathrm{i}\Delta_{\mu\nu}^{>}(q)\mathrm{i}\Delta_\phi^{(0)<}(k) - (<\leftrightarrow>)]\,. \qquad (4.65)
\end{aligned}$$

In the following we use the freedom to choose momenta such that $p_{1,3}$ indicate the on-shell particles, while the momentum $q = p_1 - p_3$ is assigned to the off-shell exchanged particle. Further, we calculate the diffusion constant for the particle with momentum p_1 and limit the discussion on diffusion constants for particles and not antiparticles, i.e. we choose $p_1^0 = |\mathbf{p}_1|$. This opens up two channels:

S-CHANNEL: This channel is defined for $q^2 \geq 0$, where q is the momentum of the exchanged particle, and implies $p_3^0 = -|\mathbf{p}_3|$. Consequently, the spectral one-loop self-energies in the resummed propagator vanish in the HTL limit, cf. appendix A.3, since HTL contributions are only non-vanishing for $q^2 < 0$. The mass pole is present in the s-channel that can be seen as the line of dispersion in figure 3.3. This pole only has an analytic expression in case of soft and very hard momentum exchange, which makes the numerical integration suffer from uncertainties. Nevertheless, the contribution to the diffusion constant can be computed approximately when neglecting all the self-energies in the denominator of the resummed propagators (3.54) and (3.63), such that

$$S^{\mathcal{A}}(q) \simeq P_X \frac{2q\!\!\!/\Sigma_\psi^{\mathcal{A}} \cdot q - \not{\Sigma}_\psi^{\mathcal{A}} q^2}{q^4}\,, \tag{4.66}$$

with the chiral projection operator $P_X = P_{\mathrm{R,L}}$. The resummed gauge boson propagator for a given mode $\eta = \mathrm{T}, \mathrm{L}$ is analogously obtained from eq. (3.63) and reads

$$\Delta_\eta^{\mathcal{A}}(q) = \frac{\Pi_\eta^{\mathcal{A}}}{(q^2 + \Pi_\eta^H)^2 + (\Pi_\eta^{\mathcal{A}})^2} \simeq \frac{\Pi_\eta^{\mathcal{A}}}{q^4} = \frac{1}{q^4}\left(N_\psi \Pi_\eta^{(\psi)\mathcal{A}} + N_\phi \Pi_\eta^{(\phi)\mathcal{A}} + \Pi_\eta^{(V)\mathcal{A}}\right). \tag{4.67}$$

This implies the decomposition of the gauge boson propagator into the contributions from fermions, from the Higgs and also from self-interactions, cf. figure 3.6. Such a procedure is motivated by ref. [125] and is valid in a leading order discussion since it can be shown that the numerator of these resummed propagators are first order in q^2 for $q^2 \to 0$. Consequently, the integrands of the collision terms (4.62)-(4.64) and (4.65) are finite in the limit of zero four-momentum q exchange and thus do not suffer from IR divergences. Note that within this assumption, the collision terms are simply proportional to g^4 for a given gauge coupling g.

T-CHANNEL: This channel is given for $q^2 < 0$, where q is the momentum of the exchanged particles, and implies $p_3^0 = |\mathbf{p}_3|$ for the momentum convention we choose. It is not possible to neglect the self-energies in the denominator in this channel as in eqs. (4.66) and (4.67) because these are required to cure logarithmic enhancements that appear for $q^0, |\mathbf{q}| \to 0$ due to the presence of HTL terms of the self-energies appearing in the resummed propagators (3.54) and (3.63). Analytic expressions for the spectral one-loop self-energies with their HTL terms are provided in appendix A.3, while the necessary Hermitian self-energies are given in appendix A.2.

Particularly the inclusion of these HTL terms themselves prevent the contribution from such an IR divergence and become important for soft momentum exchanges, i.e. for $|\mathbf{q}| \lesssim gT$, because these are non vanishing for $q^0, |\mathbf{q}| \to 0$ and provide the finite width that is needed to cure the IR divergence. For larger momentum exchanges, i.e. for $|\mathbf{q}| \gg gT$, the self-energies in the denominator of the resummed propagators (4.66) and (4.67) are subdominant compared to the exchanged momentum q. This justifies the usage of the HTL approximation in the derivation of the Hermitian self-energies, cf. appendix A.2. In this case the integrals that have to be solved to determine the diffusion constants get regulated by the thermal masses, i.e. the HTL part of the Hermitian self-energies for small $|\mathbf{q}| \lesssim gT$. This leads to a logarithmic contribution to the diffusion constants in the thermal masses of the given exchanged particle.

An approximate procedure to compute diffusion constants in the t-channel is given by dividing the collision terms into two parts: First, a finite (fin) contribution arises when

subtracting the HTL parts from the spectral self-energies by dropping the parts of the Heaviside step functions in appendix A.3 that are proportional to T^2, i.e. eq. (A.61). This, in analogy to the s-channel, allows to neglect the self-energies in the denominator of the resummed propagators (3.54) and (3.63) such that eqs. (4.66) and (4.67) can be used. The second contribution is given by only using HTL parts of the self-energies, namely by only using eq. (A.61), and completely neglecting the finite contributions. The corresponding expressions are given by eqs. (3.122) and (3.123). This is allowed since only the HTL parts of the self-energies appearing in the denominator of the resummed propagators are needed to soften the IR divergences for $q^0, |\mathbf{q}| \to 0$, while the finite parts of the self-energies are first order in q^2 for $q^2 \to 0$ and are consequently subdominant for $|\mathbf{q}| \lesssim gT$. For $|\mathbf{q}| \gg gT$ both the finite and the HTL parts of the self-energies are negligible compared to the exchanged momentum q. We could in general neglect these for $|\mathbf{q}| \gg gT$ within a leading order approximation in the couplings. However, as mentioned above, we consider HTL parts of the self-energies only and just neglect the finite contributions for all q.

Note that diffusion constants are computed via the variational approach introduced in subsection 4.1.2. A precision better than the percent level is already reached by using a three-dimensional basis set (4.54).

Eventually, the inverse diffusion constants from self-energy type contributions can be decomposed as follows

$$D^{-1} = D_{\text{fin}}^{-1} + D_{\text{HTL}}^{-1} \,. \tag{4.68}$$

D_{fin}^{-1} is from s-channel and t-channel exchanges without HTL terms and is proportional to g^4 for a given gauge coupling g. In contrast, D_{HTL}^{-1} is solely due to HTL approximated self-energies and thus only appears in the t-channel. These lead to a contribution that is proportional to the logarithm of the thermal mass of the exchanged particles since these regulate the IR divergence. Therefore, D_{HTL}^{-1} is logarithmically enhanced compared to D_{fin}^{-1}.

In subsection 4.2.1 diffusion constants are calculated to leading order for contributions where gauge bosons are exchanged, while 4.2.2 discusses the contribution from the exchange of fermions.

4.2.1 *Contribution from gauge boson exchange*

Within the collision terms $\mathcal{C}_{\psi,\phi}^{\text{self}(V)}$, see eq. (4.64), only the gauge boson propagator is resummed at one-loop level, while the other particles are on-shell with vanishing thermal mass. As already mentioned these are the diagrams that contribute to $2 \leftrightarrow 2$ scattering processes of scalars and fermions, where gauge bosons are the exchanged particles. With the quasiparticle approximation (3.68) we obtain the collision term

$$\begin{aligned}\mathcal{C}_{\phi,\psi}^{\text{self}(V)}(p_1) = \pm 2g^2 C_2^F \int \frac{\mathrm{d}^4 p_3}{(2\pi)^4} (2\pi)^2 \text{sign}(p_1^0)\text{sign}(p_3^0)\delta(p_1^2)\delta(p_3^2) \\ \times \sum_{\eta=\text{T,L}} P_{\mu\nu}^{\eta}(p_1 - p_3) X^{\mu\nu}(p_1, p_3) \Delta_{\eta}^{\mathcal{A}}(p_1 - p_3) \\ \times f_0^{\phi}(p_1)[1 \pm f_0^{\phi,\psi}(p_3)][1 + f_0^{V}(p_1 - p_3)][f_1^{\phi,\psi}(p_1) - f_1^{\phi,\psi}(p_3)] \,,\end{aligned} \tag{4.69}$$

that is linear in the deviations f_1, where $\eta = \text{T}, \text{L}$ distinguishes between the exchange of transverse and longitudinal gauge bosons, cf. eqs. (A.3) and (A.4). Further $X_{\mu\nu}$ is

$U_{\mu\nu}$ for scalars while it corresponds to $T_{\mu\nu}$ for fermions, cf. eqs. (3.99) and (3.100). The contraction of the Lorentz indices is given by

$$P^{\mathrm{T}}_{\mu\nu}(q)U^{\mu\nu}(p_1,p_3) = -\frac{q^2}{|\mathbf{q}|^2}\left(|\mathbf{q}|^2-(p_1^0+p_3^0)^2\right), \tag{4.70}$$

$$P^{\mathrm{L}}_{\mu\nu}(q)U^{\mu\nu}(p_1,p_3) = -\frac{q^2}{|\mathbf{q}|^2}(p_1^0+p_3^0)^2, \tag{4.71}$$

$$P^{\mathrm{T}}_{\mu\nu}(q)T^{\mu\nu}(p_1,p_3) = \frac{q^2}{|\mathbf{q}|^2}\left(|\mathbf{q}|^2+(p_1^0+p_3^0)^2\right), \tag{4.72}$$

$$P^{\mathrm{L}}_{\mu\nu}(q)T^{\mu\nu}(p_1,p_3) = \frac{q^2}{|\mathbf{q}|^2}\left(|\mathbf{q}|^2-(p_1^0+p_3^0)^2\right), \tag{4.73}$$

when using relations from appendix A.1. The contraction that is needed for computing the diffusion constants within the variational approach from subsection 4.1.2 is given by

$$\begin{aligned}\left(\chi_i^{\phi,\psi},(\mathcal{C}\chi_i^{\phi,\psi})^{\mathrm{self}(V)}_{\phi,\psi}\right) = \pm g^2C_2^F\int\frac{\mathrm{d}^4p_1}{(2\pi)^4}\int\frac{\mathrm{d}^4p_3}{(2\pi)^4}(2\pi)^2\mathrm{sign}(p_1^0)\mathrm{sign}(p_3^0)\delta(p_1^2)\delta(p_3^2)\\ \times\sum_{\eta=\mathrm{T,L}}P^{\eta}_{\mu\nu}(p_1-p_3)X^{\mu\nu}(p_1,p_3)\Delta^{\mathcal{A}}_{\eta}(p_1-p_3)\\ \times f_0^{\phi}(p_1)[1\pm f_0^{\phi,\psi}(p_3)][1+f_0^{V}(p_1-p_3)][\chi_i^{\phi,\psi}(p_1)-\chi_i^{\phi,\psi}(p_3)]^2,\end{aligned} \tag{4.74}$$

where we accounted for a symmetry factor of 1/2 due to two particles of the same species in each case. This integral can be simplified when choosing $\mathbf{p}_1=|\mathbf{p}_1|\mathbf{e}_z$, such that $p_1\cdot p_3 = |\mathbf{p}_1||\mathbf{p}_3|(\mathrm{sign}(p_1^0)\mathrm{sign}(p_3^0)-\cos\theta)$. Thus,

$$\begin{aligned}\left(\chi_i^{\phi,\psi},(\mathcal{C}\chi_i^{\phi,\psi})^{\mathrm{self}(V)}_{\phi,\psi}\right) = \pm\frac{g^2C_2^F}{32\pi^4}\int_0^\infty\mathrm{d}|\mathbf{p}_1||\mathbf{p}_1|\int_0^\infty\mathrm{d}|\mathbf{p}_3||\mathbf{p}_3|\int_{-1}^{1}\mathrm{d}\cos\theta\,\mathrm{sign}(p_3^0)\\ \times\sum_{\eta=\mathrm{T,L}}P^{\eta}_{\mu\nu}(p_1-p_3)X^{\mu\nu}(p_1,p_3)\Delta^{\mathcal{A}}_{\eta}(p_1-p_3)\\ \times f_0^{\phi}(p_1)[1\pm f_0^{\phi,\psi}(p_3)][1+f_0^{V}(p_1-p_3)][\chi_i^{\phi,\psi}(p_1)-\chi_i^{\phi,\psi}(p_3)]^2,\end{aligned} \tag{4.75}$$

where we choose $\mathrm{sign}(p_1^0)=1$. $\mathrm{sign}(p_3^0)=\pm1$ then determines if the process takes place in the t-channel or in the s-channel.

The computation of the inverse diffusion constants for the non-HTL contributions is simply performed by a numerical integration for both the s-channel and the t-channel, where all the dependence on the couplings can be factored out.

$$\left(D_{\phi}^{\mathrm{self}(V)}\right)^{-1}_{\mathrm{fin}} = g^2TC_2^F(-8.7\times10^{-3}C_FN_{\phi}g^2-1.4\times10^{-3}C_FN_{\psi}g^2-1.7\times10^{-3}C_2^Ag^2), \tag{4.76}$$

$$\left(D_{\psi}^{\mathrm{self}(V)}\right)^{-1}_{\mathrm{fin}} = g^2TC_2^F(3.0\times10^{-5}C_FN_{\psi}g^2-6.3\times10^{-3}C_FN_{\phi}g^2-5.8\times10^{-3}C_2^Ag^2). \tag{4.77}$$

Since the main contribution happens for soft $|\mathbf{q}|\lesssim gT$, longitudinal and transverse modes of the gauge bosons are equally important, cf. chapter 3.

The inverse diffusion constants due to the HTL contributions, that are only present in the t-channel, can be obtained when performing numerical integrations for different couplings

$$G_V \equiv \frac{1}{6}\left(\frac{1}{2}C^FN_{\psi}+C^FN_{\phi}+C_2^A\right), \tag{4.78}$$

cf. eq. (3.114). With the help of a numerical fitting procedure we obtain

$$\left(D_{\phi}^{\text{self}(V)}\right)^{-1}_{\text{HTL}} \simeq g^2 C_2^F G_V T \times (9.1\times10^{-2} + 6.5\times10^{-3}\log G_V^{-1} + 1.1\times10^{-2} G_V)\,, \quad (4.79)$$

$$\left(D_{\psi}^{\text{self}(V)}\right)^{-1}_{\text{HTL}} \simeq g^2 C_2^F G_V T \times (5.8\times10^{-2} + 2.9\times10^{-3}\log G_V^{-1} + 4.1\times10^{-3} G_V)\,, \quad (4.80)$$

where higher orders in G_V are used to ensure a stable fit.

4.2.2 *Contribution from fermion exchange*

Within the collision terms $\mathcal{C}_{\psi}^{\text{self}(\psi)}$ and $\mathcal{C}_{\psi}^{\text{self(os)}}$, see eqs. (4.62) and (4.63), only one of the fermion propagator is resummed at one-loop level, while the remaining particles are on the zero thermal mass shell. These two diagrams contribute to $2 \leftrightarrow 2$ scattering processes of fermions, where fermions are exchanged. In analogy to the contributions from gauge boson exchange we end up at the contraction

$$\left(\chi_i^{\psi}, (\mathcal{C}\chi_i^{\psi})_{\psi}^{\text{self}(\psi+\text{os})}\right)_4 = -8G_{\psi}\int \frac{\mathrm{d}^4p_1}{(2\pi)^4}\frac{\mathrm{d}^4p_3}{(2\pi)^4}(2\pi)^2 \text{sign}(p_1^0)\text{sign}(p_3^0)\delta(p_1^2)\delta(p_3^2) \quad (4.81)$$
$$p_1^{\mu} S_{\mu}^{\mathcal{A}}(p_1-p_3) \times f_0^{\psi}(p_1)[1+f_0^V(p_3)][1-f^{\psi}(p_1-p_3)][\chi_i^{\psi}(p_1)]^2\,,$$

with G_{ψ} from eq. (3.93) when using the quasiparticle approximation (3.69). Note that the outer integral over p_1 implies that $\mathcal{C}_{\psi}^{\text{self}(\psi)}$ and $\mathcal{C}_{\psi}^{\text{self(os)}}$ contribute with the same magnitude to the diffusion process. This gets compensated by using a symmetry factor of 1/2. It is possible to reduce this integral to a three-dimensional integral. Inverse diffusion constants are computed by numerical integration while the couplings can be factored out. In contrast to that, the HTL contribution is obtained by numerically integrating over different couplings. Inverse diffusion constants are then given by performing a numerical fitting procedure. Eventually, we have

$$\left(D_{\psi}^{\psi+\text{os}}\right)^{-1}_{\text{fin}} = -\frac{1}{4}\left(8.2\times10^{-3}\times G_{\psi}^2 T\right)\,, \quad (4.82)$$

$$\left(D_{\psi}^{\psi+\text{os}}\right)^{-1}_{\text{HTL}} = \frac{1}{4}\left(8.3\times10^{-2}\times G_{\psi}^2 T + 1.9\times10^{-2}\times G_{\psi}^2 T\log G_{\psi}^{-1} + 4.6\times10^{-3}\times G_{\psi}^3 T\right)\,. \quad (4.83)$$

4.3 VERTEX TYPE CONTRIBUTIONS

Besides the self-energy type contributions, two-loop vertex type diagrams contribute to the diffusion of the Higgs and fermions. A collection of diagrams is given in figure 4.3 for the Higgs field and in figure 4.6 for fermions. In contrast to the self-energy type diagrams it is sufficient to leading order in the couplings to use zero-width propagators, i.e. we neglect the width of the particles, since all IR divergences vanish when summing up all the necessary diagrams, as we will show in the following. Thermal masses are neglected as a higher order effect, too. When summing over the CTP indices in the loop, several contributions arise out of which we only consider $2 \leftrightarrow 2$ processes. All other processes, such as $1 \leftrightarrow 2$ (inverse) decays are kinematically suppressed in the limit of zero masses. These $2 \leftrightarrow 2$ processes are shown in figures 4.4 and 4.5 for the Higgs field and in figure 4.7 for fermions as on-shell cuts through the vertex type diagrams. Depending on the sign of

	$\text{sign}(p_1^0)$	$\text{sign}(p_2^0)$	$\text{sign}(p_3^0)$	$\text{sign}(p_4^0)$	process	$\mathcal{N}_{\text{sym}}$
Ia	+	+	+	+	$\phi\phi \to \phi\phi$ & $\psi\psi \to \psi\psi$	4
Ib	+	-	+	-	$\phi\bar{\phi} \to \phi\bar{\phi}$ & $\psi\bar{\psi} \to \psi\bar{\psi}$	2
Ic	+	-	-	+	$\phi\bar{\phi} \to \phi\bar{\phi}$ & $\psi\bar{\psi} \to \psi\bar{\psi}$	2
IIa	+	+	+	+	$\phi V \to \phi V$ & $\psi V \to \psi V$	2
IIb	+	-	+	-	$\phi V \to \phi V$ & $\psi V \to \psi V$	2
IIc	+	-	-	+	$\phi\bar{\phi} \to VV$ & $\psi\bar{\psi} \to VV$	2

TABLE 4.1: Different $2 \leftrightarrow 2$ scattering processes that contribute to the diffusion process for the Higgs field and the fermions. Scenarios Ia-Ic describe processes of identical particles and antiparticles as external particles, while IIa-IIc account for processes including gauge bosons as external particles. Symmetry factors for the different processes are given in the last row.

the zeroth component of the four-momentum for the given particles, different processes are recovered. Without loss of generality we compute diffusion functions for particles only. This allows to use $p_1^0 = |\mathbf{p}_1|$. Further, for both scalars and fermions two type of scenarios appear, see table 4.1:

Scenario I describes processes where only scalars or fermions are present as external particles. In this case the Wightman functions, i.e. the propagators which are on-shell and indicate the external particles of the different scattering processes, that appear in $\mathrm{i}\Pi_\phi^>(p_1)\mathrm{i}\Delta_\phi^<(p_1)$, cf. eq. (4.41), are of the form

$$\mathrm{i}\Delta_\phi^<(p_1)^<\mathrm{i}\Delta_\phi^<(p_2)^<\mathrm{i}\Delta_\phi^>(p_3)^>\mathrm{i}\Delta_\phi^>(p_4)\,, \tag{4.84}$$

and are chosen such that $p_{1,2}$ are incoming, given by $\mathrm{i}\Delta_\phi^<$, while $p_{3,4}$ are outgoing, given by $\mathrm{i}\Delta_\phi^>$. This is valid analogously for fermions, cf. eq. (4.42), and will be clear within the following discussion. Depending on the sign of p_i^0, two redundant physical processes are recovered, see table 4.1. Contractions that are needed for the calculation of the diffusion constants are then of the form

$$\begin{aligned}\left(\chi_i^{\phi,\psi}, (\mathcal{C}\chi_i^{\phi,\psi})_{\phi,\psi}^{\text{vert,I}}\right)_4 = \mathcal{N}_{\text{sym}}^{-1}|\mathcal{M}|^2 \int \frac{\mathrm{d}^4p_1}{(2\pi)^4}\frac{\mathrm{d}^4p_2}{(2\pi)^4}\frac{\mathrm{d}^4p_3}{(2\pi)^4}\frac{\mathrm{d}^4p_4}{(2\pi)^4}(2\pi)^4\delta^4(p_1+p_2-p_3-p_4)\\ \times (2\pi)^4\delta(p_1^2)\delta(p_2^2)\delta(p_3^2)\delta(p_4^2)\text{sign}(p_1^0)\text{sign}(p_2^0)\text{sign}(p_3^0)\text{sign}(p_4^0)\\ \times f_0^{\phi,\psi}(p_1)f_0^{\phi,\psi}(p_2)[1+f_0^{\phi,\psi}(p_3)][1+f_0^{\phi,\psi}(p_4)]\\ \times \left(\chi_i^{\phi,\psi}(p_1)+\chi_i^{\phi,\psi}(p_2)-\chi_i^{\phi,\psi}(p_3)-\chi_i^{\phi,\psi}(p_4)\right)^2\,.\end{aligned} \tag{4.85}$$

The matrix element $|\mathcal{M}|^2$ is expressed in terms of Mandelstam variables: $s = (p_1+p_2)^2 = (p_3+p_4)^4$, $t = (p_1-p_3)^2 = (p_2-p_4)^2$ and $u = (p_1-p_4)^2 = (p_2-p_3)^2$. In the case of massless particles these fulfil $s+t+u = 0$. Note that for small chemical potentials $\mu \ll T$ we can always use the relation

$$\mathrm{i}\Delta^<(-p_i) = \mathrm{i}\Delta^>(p_i)\,, \qquad \mathrm{i}\tilde{S}^<(-p_i) = \mathrm{i}\tilde{S}^>(p_i)\,. \tag{4.86}$$

Therefore, the contraction (4.85) is invariant under the exchange of $p_1 \leftrightarrow p_3$, $p_1 \leftrightarrow p_4$ and $p_2 \leftrightarrow p_3$ or $p_2 \leftrightarrow p_4$ op to an error of $\mathcal{O}(\mu/T)$. This allows to exchange $s \leftrightarrow t$, $s \leftrightarrow u$ and $t \leftrightarrow u$ in scenario I.

In contrast, scenario II from table 4.1 describes $2 \leftrightarrow 2$ scattering processes of two scalars or fermions and two gauge bosons as external particles. The Wightman functions that are contained in $\mathrm{i}\Pi_\phi^{>}\mathrm{i}\Delta_\phi^{<}$ are chosen such that they are of the form

$$\mathrm{i}\Delta_\phi^{<}(p_1)^{<}\mathrm{i}\Delta_V^{<}(p_2)^{<}\mathrm{i}\Delta_\phi^{>}(p_3)^{>}\mathrm{i}\Delta_V^{>}(p_4)\,. \tag{4.87}$$

Thus, $p_{1,2}$ are incoming and $p_{3,4}$ are outgoing particles, while gauge bosons are labelled with momenta $p_{2,4}$. This implies that the contractions are written as

$$\begin{aligned}\left(\chi_i^{\phi,\psi},(\mathcal{C}\chi_i^{\phi,\psi})_{\phi,\psi}^{\mathrm{vert,II}}\right)_4 = \mathcal{N}_{\mathrm{sym}}^{-1}|\mathcal{M}|^2 \int \frac{\mathrm{d}^4p_1}{(2\pi)^4}\frac{\mathrm{d}^4p_2}{(2\pi)^4}\frac{\mathrm{d}^4p_3}{(2\pi)^4}\frac{\mathrm{d}^4p_4}{(2\pi)^4}(2\pi)^4\delta^4(p_1+p_2-p_3-p_4)\\ \times (2\pi)^4\delta(p_1^2)\delta(p_2^2)\delta(p_3^2)\delta(p_4^2)\mathrm{sign}(p_1^0)\mathrm{sign}(p_2^0)\mathrm{sign}(p_3^0)\mathrm{sign}(p_4^0)\\ \times f_0^{\phi,\psi}(p_1)f_0^V(p_2)[1+f_0^{\phi,\psi}(p_3)][1+f_0^V(p_4)]\\ \times\left(\chi_i^{\phi,\psi}(p_1)-\chi_i^{\phi,\psi}(p_3)\right)^2\,.\end{aligned} \tag{4.88}$$

This can be done by simply renaming momenta in the self-energy expressions. The contraction (4.88) is invariant under exchanging momenta of particles of the same species, i.e. $p_1 \leftrightarrow p_3$ and $p_2 \leftrightarrow p_4$. Due to fast gauge interactions we can assume vanishing chemical potentials for the gauge bosons. Therefore, we have $\chi_i^V \simeq 0$ and can consequently use the replacement $s \leftrightarrow u$ within scenario II.

With these symmetry arguments we show in the following that the sum over the given matrix elements for each of the two scenarios is momentum independent. This allows to use the procedure from subsection 4.1.2 to compute the diffusion constants when using the variational approach for the contractions (4.85) and (4.88). A complete list for the matrix elements for the different processes is given in table 4.2 for the Higgs and in in table 4.3 for fermions.

In subsection 4.3.1 leading order diffusion constants for the Higgs field are computed for both scenario I and scenario II after analytic Feynman expressions are derived. Analogously diffusion constants for fermions are given in subsection 4.3.2. Results are presented in subsection 4.3.3.

4.3.1 *Contribution to the diffusion of the Higgs field*

In the following Feynman expressions in Wigner space are derived for the different diagrams in figure 4.3. The procedure is performed in a general SU(N) theory with gauge coupling g, while U(1) contributions can be deduced from those. A complete list of matrix elements for the different processes is given in table 4.2.

FEYNMAN EXPRESSIONS: Diagram (A) results in the following analytic expression

$$\begin{aligned}\mathrm{i}\Pi_\phi^{(\mathrm{A})ab}(p_1) = -g^4C_2^F\left(C_2^F-\frac{C_2^A}{2}\right)\int\frac{\mathrm{d}^4p_2}{(2\pi)^4}\frac{\mathrm{d}^4p_3}{(2\pi)^4}\frac{\mathrm{d}^4p_4}{(2\pi)^4}(2\pi)^4\delta^4(p_1+p_2-p_3-p_4)\\ \times\sum_{c,d=\pm}cd\,\mathrm{i}\Delta_\phi^{dc}(p_2)\mathrm{i}\Delta_\phi^{cb}(p_3)\mathrm{i}\Delta_\phi^{ad}(p_4)\mathrm{i}\Delta_V^{db}(p_1-p_3)\mathrm{i}\Delta_V^{ac}(p_1-p_4)\\ \times[(p_1+p_3)\cdot(p_2+p_4)][(p_2+p_3)\cdot(p_1+p_4)]\,.\end{aligned} \tag{4.89}$$

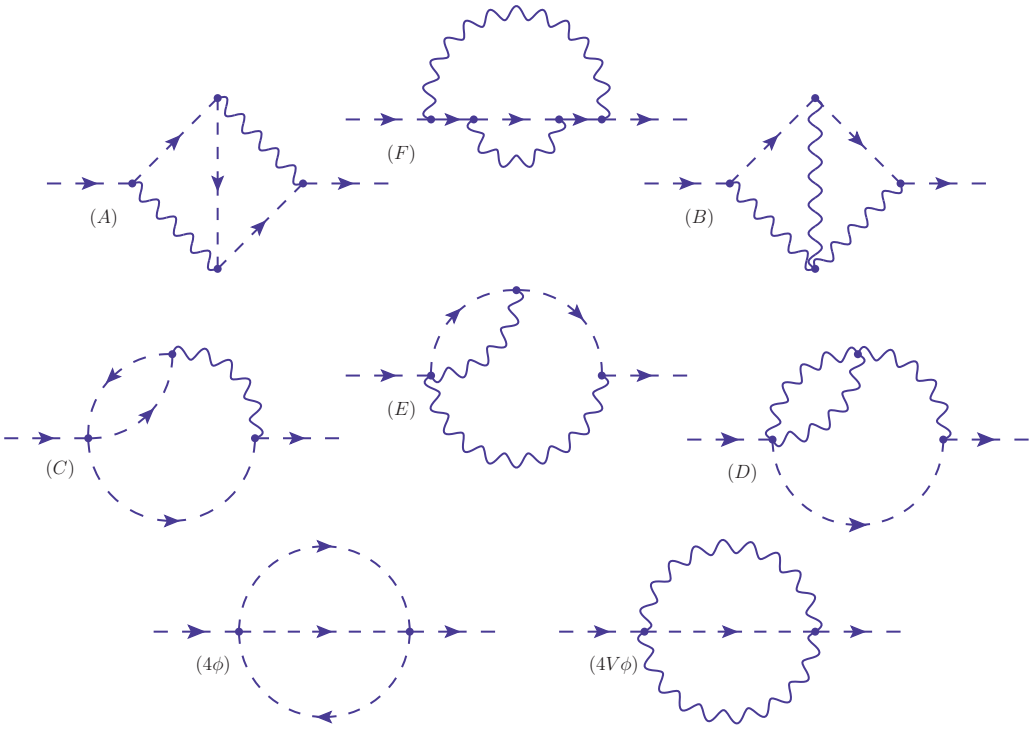

FIGURE 4.3: Collection of two-loop vertex type diagrams that contribute to the Higgs diffusion constant and give rise to $2 \leftrightarrow 2$ scattering processes. Diagrams (B) and (D) are only present in the non-abelian group SU(2), whereas the remaining diagrams receive contributions from U(1) and SU(2) gauge bosons. Note that diagrams (C), (E) and (D) with reversed arrows also contribute to the Higgs diffusion constant. However, it can be shown that they contribute with the same magnitude as diagrams (C), (E) and (D).

Higgs	$\lvert\mathcal{M}\rvert^2$	$\sum \lvert\mathcal{M}\rvert^2$
$(A1)$	$g^4 C_2^F \left(C_2^F - \frac{C_2^A}{2}\right)\left(\frac{2s^2}{tu}+1\right)$	
(C)	$2\mathrm{i}\lambda g^2 C_2^F \left(\frac{t-s}{u}\right)$	$\Rightarrow 3C_2^F\left(C_2^F - \frac{C_2^A}{2}\right) g^4 + \frac{1}{2}\lambda^2$
(4ϕ)	$\frac{1}{2}\lambda^2$	
$(A2)$	$g^4 C_2^F \left(C_2^F - \frac{C_2^A}{2}\right)\frac{t^2}{su}$	
(F)	$4g^4 (C_2^F)^2$	
(B)	$-g^4 C_2^F C_2^A \left(\frac{t}{2u} + 2\frac{u}{t}\right)$	
(D)	$6C_2^F C_2^A g^4 \frac{s-u}{t}$	$\Rightarrow 4C_2^F\left(C_2^F - \frac{C_2^A}{4}\right) g^4$
$(4V\phi)$	$8C_2^F\left(C_2^F - \frac{C_2^A}{4}\right) g^4$	
(E)	$-2C_2^F\left(C_2^F - \frac{C_2^A}{4}\right) g^4 \left(5 + \frac{s}{u}\right)$	

TABLE 4.2: List of matrix elements for the different diagrams that contribute to the diffusion constant of the Higgs, see figure 4.3. The upper block corresponds to scenario I from table 4.1, while the lower block describes processes in scenario II. The total matrix element for each scenario, after symmetry relations of the collision term have been used, is given in the last row.

The collision term appearing in the contractions (4.85) and (4.88) is only sensitive to the quantities $\mathrm{i}\Pi^{<,>}$. Therefore, we need to evaluate

$$\begin{aligned}\mathrm{i}\Pi_\phi^{(\mathrm{A})>}(p_1) = -g^4 C_2^F \left(C_2^F - \frac{C_2^A}{2}\right) \int \frac{\mathrm{d}^4p_2}{(2\pi)^4}\frac{\mathrm{d}^4p_3}{(2\pi)^4}\frac{\mathrm{d}^4p_4}{(2\pi)^4}(2\pi)^4\delta^4(p_1+p_2-p_3-p_4)\\ \times\Big[\mathrm{i}\Delta_\phi^t(p_2)\mathrm{i}\Delta_\phi^t(p_3)\mathrm{i}\Delta_\phi^>(p_4)\mathrm{i}\Delta_V^t(p_1-p_3)\mathrm{i}\Delta_V^>(p_1-p_4)\\ +\mathrm{i}\Delta_\phi^{\bar t}(p_2)\mathrm{i}\Delta_\phi^>(p_3)\mathrm{i}\Delta_\phi^{\bar t}(p_4)\mathrm{i}\Delta_V^>(p_1-p_3)\mathrm{i}\Delta_V^{\bar t}(p_1-p_4)\\ -\mathrm{i}\Delta_\phi^<(p_2)\mathrm{i}\Delta_\phi^>(p_3)\mathrm{i}\Delta_\phi^>(p_4)\mathrm{i}\Delta_V^t(p_1-p_3)\mathrm{i}\Delta_V^{\bar t}(p_1-p_4)\\ -\mathrm{i}\Delta_\phi^>(p_2)\mathrm{i}\Delta_\phi^t(p_3)\mathrm{i}\Delta_\phi^{\bar t}(p_4)\mathrm{i}\Delta_V^>(p_1-p_3)\mathrm{i}\Delta_V^>(p_1-p_4)\Big]\\ \times[(p_1+p_3)\cdot(p_2+p_4)][(p_2+p_3)\cdot(p_1+p_4)]\,.\end{aligned} \tag{4.90}$$

Being solely interested in $2\leftrightarrow 2$ scattering processes, we only consider terms where exactly two propagators are off-shell, i.e. when these propagators are time- and anti-time-ordered Green functions, cf. eqs. (3.79) and (3.80) with eq. (3.81). In contrast Wightman functions are purely on-shell. Therefore, we only consider the last two terms that lead to the decomposition $\mathrm{i}\Pi_\phi^{(\mathrm{A})>} = \mathrm{i}\Pi_\phi^{(\mathrm{A1})>} + \mathrm{i}\Pi_\phi^{(\mathrm{A2})>}$. When inserting the parts of the time- and anti-time-ordered propagators that are not on-shell and simplifying the numerator algebra we obtain

$$\begin{aligned}\mathrm{i}\Pi_\phi^{(\mathrm{A1})>}(p_1) = g^4 C_2^F \left(C_2^F - \frac{C_2^A}{2}\right) \int \frac{\mathrm{d}^4p_2}{(2\pi)^4}\frac{\mathrm{d}^4p_3}{(2\pi)^4}\frac{\mathrm{d}^4p_4}{(2\pi)^4}(2\pi)^4\delta^4(p_1+p_2-p_3-p_4)\\ \times\mathrm{i}\Delta_\phi^<(p_2)\mathrm{i}\Delta_\phi^>(p_3)\mathrm{i}\Delta_\phi^>(p_4)\left(\frac{2s^2}{tu}+1\right),\end{aligned} \tag{4.91}$$

$$\begin{aligned}\mathrm{i}\Pi_\phi^{(\mathrm{A2})>}(p_1) = g^4 C_2^F \left(C_2^F - \frac{C_2^A}{2}\right) \int \frac{\mathrm{d}^4p_2}{(2\pi)^4}\frac{\mathrm{d}^4p_3}{(2\pi)^4}\frac{\mathrm{d}^4p_4}{(2\pi)^4}(2\pi)^4\delta^4(p_1+p_2-p_3-p_4)\\ \times\mathrm{i}\Delta_V^<(p_2)\mathrm{i}\Delta_\phi^>(p_3)\mathrm{i}\Delta_V^>(p_4)\frac{t^2}{su}\,.\end{aligned} \tag{4.92}$$

In order to arrive at $\mathrm{i}\Pi_\phi^{(\mathrm{A2})>}$, we have switched momenta according to $p_2\to -p_2$, $p_3\to p_1-p_3$ as well as $p_4\to p_1-p_4$ and have made use of the relation $\mathrm{i}\Delta_V^{<,>}(-p) = \mathrm{i}\Delta_V^{>,<}(p)$ which is true for zero chemical potential. Afterwards, we have renamed $p_2\leftrightarrow -p_3$. This allows to use assign the momenta p_2 and p_4 to the gauge bosons as mentioned in table 4.1.

An analytic expression for diagram (B) is analogously obtained. In this case both cuts contribute with the same magnitude such that we are left with

$$\begin{aligned}\mathrm{i}\Pi_\phi^{(\mathrm{B})>}(p_1) = g^4 C_2^F C_2^A \int \frac{\mathrm{d}^4p_2}{(2\pi)^4}\frac{\mathrm{d}^4p_3}{(2\pi)^4}\frac{\mathrm{d}^4p_4}{(2\pi)^4}(2\pi)^4\delta^4(p_1+p_2-p_3-p_4)\\ \times\mathrm{i}\Delta_V^<(p_2)\mathrm{i}\Delta_\phi^>(p_3)\mathrm{i}\Delta_V^>(p_4)\left(-\frac{t}{2u}-2\frac{u}{t}\right).\end{aligned} \tag{4.93}$$

The expression for the self-energy of diagram (F) is given by

$$\begin{aligned}
\mathrm{i}\Pi_\phi^{(\mathrm{F})>}(p_1) = -g^4\left(C_2^F\right)^2 \int \frac{\mathrm{d}^4p_2}{(2\pi)^4}\frac{\mathrm{d}^4p_3}{(2\pi)^4}\frac{\mathrm{d}^4p_4}{(2\pi)^4}(2\pi)^4\delta^4(p_1+p_2-p_3-p_4) \\
\times\Big[\mathrm{i}\Delta_V^t(p_2)\mathrm{i}\Delta_V^>(p_3)\mathrm{i}\Delta_\phi^t(p_4)\mathrm{i}\Delta_\phi^t(p_1-p_3)\mathrm{i}\Delta_\phi^>(p_1-p_3) \\
+\mathrm{i}\Delta_V^{\bar{t}}(p_2)\mathrm{i}\Delta_V^>(p_3)\mathrm{i}\Delta_\phi^{\bar{t}}(p_4)\mathrm{i}\Delta_\phi^>(p_1-p_3)\mathrm{i}\Delta_\phi^{\bar{t}}(p_1-p_3) \\
-\mathrm{i}\Delta_V^<(p_2)\mathrm{i}\Delta_V^>(p_3)\mathrm{i}\Delta_\phi^>(p_4)\mathrm{i}\Delta_\phi^t(p_1-p_3)\mathrm{i}\Delta_\phi^{\bar{t}}(p_1-p_3) \\
-\mathrm{i}\Delta_V^>(p_2)\mathrm{i}\Delta_V^>(p_3)\mathrm{i}\Delta_\phi^<(p_4)\mathrm{i}\Delta_\phi^>(p_1-p_3)\mathrm{i}\Delta_\phi^>(p_1-p_3)\Big] \\
\times(2p_1-p_3)^2(p_1+p_4-p_3)^2\,. \qquad (4.94)
\end{aligned}$$

In our case only term three is of physically relevant. When renaming $p_3 \leftrightarrow p_4$ we obtain

$$\begin{aligned}
\mathrm{i}\Pi_\phi^{(\mathrm{F})>}(p_1) = 4g^4\left(C_2^F\right)^2 \int \frac{\mathrm{d}^4p_2}{(2\pi)^4}\frac{\mathrm{d}^4p_3}{(2\pi)^4}\frac{\mathrm{d}^4p_4}{(2\pi)^4}(2\pi)^4\delta^4(p_1+p_2-p_3-p_4) \\
\times\mathrm{i}\Delta_V^<(p_2)\mathrm{i}\Delta_\phi^>(p_3)\mathrm{i}\Delta_V^>(p_4)\,. \qquad (4.95)
\end{aligned}$$

after the numerator algebra has been evaluated to $(2p_1-p_3)^2(p_1+p_4-p_3)^2/t^2 = 4$. The diagrams (C)-(E) do not only appear as the ones from figure 4.3 but also as mirrored diagrams, i.e. where arrows of the scalar propagators are reversed. It can be shown that these contribute with the same strength to the diffusion constant. Therefore, we multiply these by a factor of two. Diagram (C) then reads

$$\begin{aligned}
\mathrm{i}\Pi_\phi^{(\mathrm{C})>}(p_1) = 2\mathrm{i}\lambda g^2 C_2^F \int \frac{\mathrm{d}^4p_2}{(2\pi)^4}\frac{\mathrm{d}^4p_3}{(2\pi)^4}\frac{\mathrm{d}^4p_4}{(2\pi)^4}(2\pi)^4\delta^4(p_1+p_2-p_3-p_4) \\
\times(p_1+p_4)(p_2+p_3)\Big[\mathrm{i}\Delta_\phi^t(p_2)\mathrm{i}\Delta_\phi^t(p_3)\mathrm{i}\Delta_\phi^>(p_4)\mathrm{i}\Delta_V^>(p_1-p_4) \\
-\mathrm{i}\Delta_\phi^<(p_2)\mathrm{i}\Delta_\phi^>(p_3)\mathrm{i}\Delta_\phi^>(p_4)\mathrm{i}\Delta_V^{\bar{t}}(p_1-p_3)\Big] \\
\to 2\lambda g^2 C_2^F \int \frac{\mathrm{d}^4p_2}{(2\pi)^4}\frac{\mathrm{d}^4p_3}{(2\pi)^4}\frac{\mathrm{d}^4p_4}{(2\pi)^4}(2\pi)^4\delta^4(p_1+p_2-p_3-p_4) \\
\times\mathrm{i}\Delta_\phi^<(p_2)\mathrm{i}\Delta_\phi^>(p_3)\mathrm{i}\Delta_\phi^>(p_4)\left(\frac{t-s}{u}\right)\,. \qquad (4.96)
\end{aligned}$$

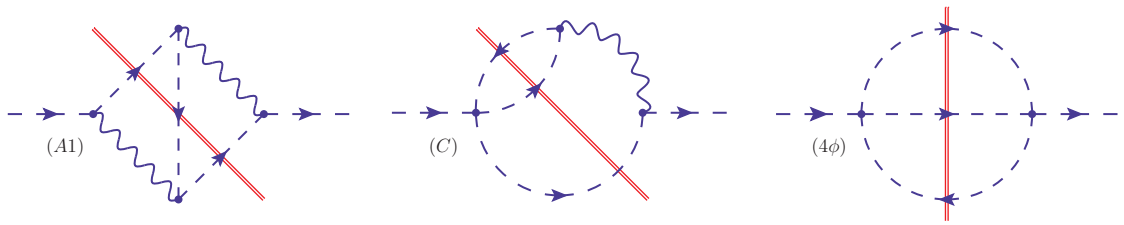

FIGURE 4.4: $\phi\phi \to \phi\phi$ and $\phi\bar{\phi} \to \phi\bar{\phi}$ elastic scattering processes that are obtained by on-shell cuts (red double lines) of the Higgs vertex type diagrams.

All the remaining diagrams are given by

$$\begin{aligned}
\mathrm{i}\Pi_\phi^{(\mathrm{D})>}(p_1) &= 6C_2^F C_2^A g^4 \int \frac{\mathrm{d}^4p_2}{(2\pi)^4}\frac{\mathrm{d}^4p_3}{(2\pi)^4}\frac{\mathrm{d}^4p_4}{(2\pi)^4}(2\pi)^4\delta^4(p_1+p_2-p_3-p_4) \\
&\quad \times \mathrm{i}\Delta_V^<(p_2)\mathrm{i}\Delta_\phi^>(p_3)\mathrm{i}\Delta_V^>(p_4)\left(\frac{s-u}{t}\right), \qquad (4.97)\\
\mathrm{i}\Pi_\phi^{(\mathrm{E})>}(p_1) &= -2C_2^F\left(C_2^F-\frac{C_2^A}{4}\right)g^4\int \frac{\mathrm{d}^4p_2}{(2\pi)^4}\frac{\mathrm{d}^4p_3}{(2\pi)^4}\frac{\mathrm{d}^4p_4}{(2\pi)^4}(2\pi)^4\delta^4(p_1+p_2-p_3-p_4) \\
&\quad \times \mathrm{i}\Delta_V^<(p_2)\mathrm{i}\Delta_\phi^>(p_3)\mathrm{i}\Delta_V^>(p_4)\left(5+\frac{s}{u}\right), \qquad (4.98)\\
\mathrm{i}\Pi_\phi^{(4\phi)>}(p_1) &= \frac{1}{2}\lambda^2\int \frac{\mathrm{d}^4p_2}{(2\pi)^4}\frac{\mathrm{d}^4p_3}{(2\pi)^4}\frac{\mathrm{d}^4p_4}{(2\pi)^4}(2\pi)^4\delta^4(p_1+p_2-p_3-p_4) \\
&\quad \times \mathrm{i}\Delta_\phi^<(p_2)\mathrm{i}\Delta_\phi^>(p_3)\mathrm{i}\Delta_\phi^>(p_4), \qquad (4.99)\\
\mathrm{i}\Pi_\phi^{(4\mathrm{V}\phi)>}(p_1) &= 8C_2^F\left(C_2^F-\frac{C_2^A}{4}\right)g^4\int \frac{\mathrm{d}^4p_2}{(2\pi)^4}\frac{\mathrm{d}^4p_3}{(2\pi)^4}\frac{\mathrm{d}^4p_4}{(2\pi)^4}(2\pi)^4\delta^4(p_1+p_2-p_3-p_4) \\
&\quad \times \mathrm{i}\Delta_V^<(p_2)\mathrm{i}\Delta_\phi^>(p_3)\mathrm{i}\Delta_V^>(p_4). \qquad (4.100)
\end{aligned}$$

SCENARIO I: Diagrams $(A1)$, (C) and (4ϕ) correspond to the processes $\phi\phi \to \phi\phi$ and $\phi\bar{\phi} \to \phi\bar{\phi}$ depending on the sign of the zeroth momentum, see scenario I of table 4.1. These can be visualised as on-shell cuts of the vertex type diagrams, as shown in figure 4.4.

The individual expressions have a non-trivial momentum structure and are not IR divergence-free. However, we can get rid of these divergences when making use of symmetry properties of the integrand. For small chemical potentials the relation $\mathrm{i}\Delta_\phi^{<,>}(-p_i) = \mathrm{i}\Delta_\phi^{>,<}(p_i)$. Therefore, the three integrands are invariant under renaming $p_2 \leftrightarrow -p_3$, $p_2 \leftrightarrow -p_4$ and $p_3 \leftrightarrow p_4$. This effectively allows to exchange $s \leftrightarrow t$, $s \leftrightarrow u$ and $t \leftrightarrow u$:

$$\begin{aligned}
\frac{s^2}{tu} &= \frac{-s(t+u)}{tu} = -\frac{s}{u}-\frac{s}{t} \to -\frac{u}{s}-\frac{t}{s} = 1, \qquad (4.101)\\
\frac{t}{u} &= \frac{1}{2}\left(\frac{t}{u}+\frac{t}{u}\right) \to \frac{1}{2}\left(\frac{t}{u}+\frac{s}{u}\right) = -\frac{1}{2}, \qquad (4.102)\\
\frac{s}{u} &= \frac{1}{2}\left(\frac{s}{u}+\frac{s}{u}\right) \to \frac{1}{2}\left(\frac{s}{u}+\frac{t}{u}\right) = -\frac{1}{2}. \qquad (4.103)
\end{aligned}$$

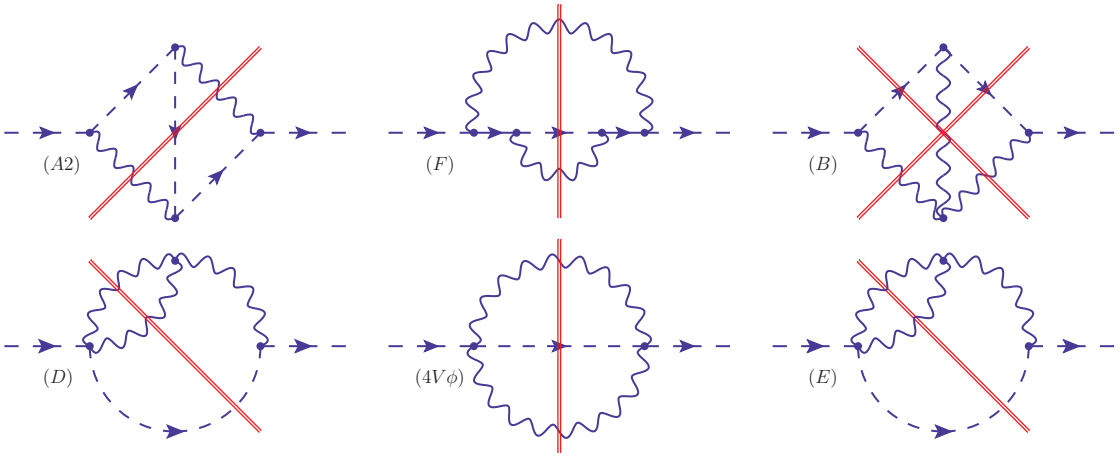

FIGURE 4.5: $\phi V \to \phi V$ elastic scattering, as well as $\phi\bar{\phi} \to VV$ Higgs-anti-Higgs annihilation that are obtained by on-shell cuts (red double lines) of the Higgs vertex type diagrams.

As a consequence, the total self-energy for scenario I from table 4.1 is given by

$$\left(\mathrm{i}\Pi^{>}_{\phi}(p_1)\mathrm{i}\Delta^{<}_{\phi}(p_1)\right)_{\mathrm{I}} = \int \frac{\mathrm{d}^4p_2}{(2\pi)^4}\frac{\mathrm{d}^4p_3}{(2\pi)^4}\frac{\mathrm{d}^4p_4}{(2\pi)^4}(2\pi)^4\delta^4(p_1+p_2-p_3-p_4) \tag{4.104}$$
$$\times\, \mathrm{i}\Delta^{<}_{\phi}(p_1)\mathrm{i}\Delta^{<}_{\phi}(p_2)\mathrm{i}\Delta^{>}_{\phi}(p_3)\mathrm{i}\Delta^{>}_{\phi}(p_4)\left[3C_2^F\left(C_2^F-\frac{C_2^A}{2}\right)g^4+\frac{1}{2}\lambda^2\right],$$

and determines the total matrix element in the last column of table 4.2.

SCENARIO II: Diagrams $(A2)$, (B), (D), (E) , (F) and (4ϕ) correspond to the processes $\phi V \to \phi V$ and $\phi\bar{\phi} \to VV$ depending on the sign of the zeroth momentum, see scenario II of table 4.1. These can be visualised as on-shell cuts of the vertex type diagrams, as shown in figure 4.5.

The individual diagrams are IR divergent. However, we can use the symmetry relation $\mathrm{i}\Delta_V^{<,>}(-p_{2,4}) = \mathrm{i}\Delta_V^{>,<}(p_{2,4})$. This allows us to exchange s with u such that

$$\frac{u}{t} \to \frac{1}{2}\left(\frac{u}{t}+\frac{s}{t}\right) = -\frac{1}{2}, \tag{4.105}$$
$$\frac{t^2}{su} = \frac{s}{u}+\frac{u}{s}+2 \to 2\frac{s}{u}+2\,. \tag{4.106}$$

When summing over all contributions, we eventually obtain an IR free self-energy expression

$$\left(\mathrm{i}\Pi^{>}_{\phi}(p_1)\mathrm{i}\Delta^{<}_{\phi}(p_1)\right)_{\mathrm{II}} = \int \frac{\mathrm{d}^4p_2}{(2\pi)^4}\frac{\mathrm{d}^4p_3}{(2\pi)^4}\frac{\mathrm{d}^4p_4}{(2\pi)^4}(2\pi)^4\delta^4(p_1+p_2-p_3-p_4) \tag{4.107}$$
$$\times\, \mathrm{i}\Delta^{<}_{\phi}(p_1)\mathrm{i}\Delta^{<}_{V}(p_2)\mathrm{i}\Delta^{>}_{\phi}(p_3)\mathrm{i}\Delta^{>}_{V}(p_4)\,4C_2^F\left(C_2^F-\frac{C_2^A}{4}\right)g^4\,.$$

for scenario II from table 4.1. This determines the total matrix element in the last column of table 4.2.

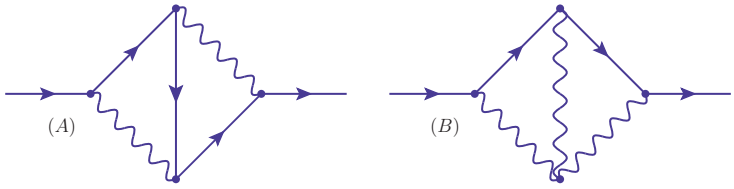

FIGURE 4.6: Collection of two-loop vertex type diagrams that contribute to the diffusion constants for fermions. While diagram (A) receives contributions from U(1) as well as from SU(2) and SU(3) gauge bosons, diagram (B) is only present in the non-abelian gauge group SU(2) and SU(3).

Fermions	$\lvert\mathcal{M}\rvert^2$	$\sum\lvert\mathcal{M}\rvert^2$
$(A1)$	$4g^4C_2^F\left(C_2^F-\frac{C_2^A}{2}\right)\frac{s^2}{tu}$	$\Rightarrow 4g^4C_2^F\left(C_2^F-\frac{C_2^A}{2}\right)$
(B)	$4g^4C_2^FC_2^A\frac{u}{t}$	$\Rightarrow -2g^4C_2^FC_2^A$

TABLE 4.3: List of matrix elements for the different diagrams that contribute to the diffusion constant of fermions, see figure 4.6. The upper block corresponds to scenario I from table 4.1, while the lower block describes processes in scenario II. The total matrix element for each scenario, after symmetry relations of the collision term have been used, is given in the last row.

4.3.2 *Contribution to the diffusion of chiral fermions*

In analogy to the Higgs case, we derive Feynman expressions in Wigner space for the diagrams in figure 4.6. In the following we limit ourselves to a general SU(N) theory with gauge coupling g, while U(1) contributions can be derived from those. The different matrix elements are given in table 4.3.

FEYNMAN EXPRESSIONS: Diagram (A) can be written as follows

$$\begin{aligned}\mathrm{i}\not{\Sigma}_\psi^{(\mathrm{A})ab}(p_1) = &-g^4C_2^F\left(C_2^F-\frac{C_2^A}{2}\right)\int\frac{\mathrm{d}^4p_2}{(2\pi)^4}\frac{\mathrm{d}^4p_3}{(2\pi)^4}\frac{\mathrm{d}^4p_4}{(2\pi)^4}(2\pi)^4\delta^4(p_1+p_2-p_3-p_4)\\ &\times\sum_{c,d=\pm}cd\,\gamma_\sigma\mathrm{i}S^{ad}(p_4)\gamma^\mu\mathrm{i}S^{dc}(p_2)\gamma^\sigma\mathrm{i}S^{cb}(p_3)\gamma_\mu\mathrm{i}\Delta_V^{db}(p_1-p_3)\mathrm{i}\Delta_V^{ac}(p_1-p_4)\,.\end{aligned} \tag{4.108}$$

The collision term in the contractions (4.85) and (4.88) depends on $\mathrm{tr}[\mathrm{i}\not{\Sigma}_\psi^{<,>}\mathrm{i}S^{>,<}]$. Therefore,

$$\begin{aligned}\mathrm{tr}\left[\mathrm{i}\not{\Sigma}_\psi^{(\mathrm{A})>}(p_1)\mathrm{i}S^<(p_1)\right] = &\\ -g^4C_2^F\left(C_2^F-\frac{C_2^A}{2}\right)&\int\frac{\mathrm{d}^4p_2}{(2\pi)^4}\frac{\mathrm{d}^4p_3}{(2\pi)^4}\frac{\mathrm{d}^4p_4}{(2\pi)^4}(2\pi)^4\delta^4(p_1+p_2-p_3-p_4)\\ \times\,\mathrm{tr}\Big[\mathrm{i}S^<(p_1)\Big\{&\gamma_\sigma\mathrm{i}S^>(p_4)\gamma^\mu\mathrm{i}S^t(p_2)\gamma^\sigma\mathrm{i}S^t(p_3)\gamma_\mu\mathrm{i}\Delta_V^t(p_1-p_3)\mathrm{i}\Delta_V^>(p_1-p_4)\\ &+\gamma_\sigma\mathrm{i}S^{\bar t}(p_4)\gamma^\mu\mathrm{i}S^{\bar t}(p_2)\gamma^\sigma\mathrm{i}S^>(p_3)\gamma_\mu\mathrm{i}\Delta_V^>(p_1-p_3)\mathrm{i}\Delta_V^{\bar t}(p_1-p_4)\\ &-\gamma_\sigma\mathrm{i}S^{\bar t}(p_4)\gamma^\mu\mathrm{i}S^>(p_2)\gamma^\sigma\mathrm{i}S^t(p_3)\gamma_\mu\mathrm{i}\Delta_V^>(p_1-p_3)\mathrm{i}\Delta_V^>(p_1-p_4)\\ &-\gamma_\sigma\mathrm{i}S^>(p_4)\gamma^\mu\mathrm{i}S^<(p_2)\gamma^\sigma\mathrm{i}S^>(p_3)\gamma_\mu\mathrm{i}\Delta_V^t(p_1-p_3)\mathrm{i}\Delta_V^{\bar t}(p_1-p_4)\Big\}\Big]\,.\end{aligned} \tag{4.109}$$

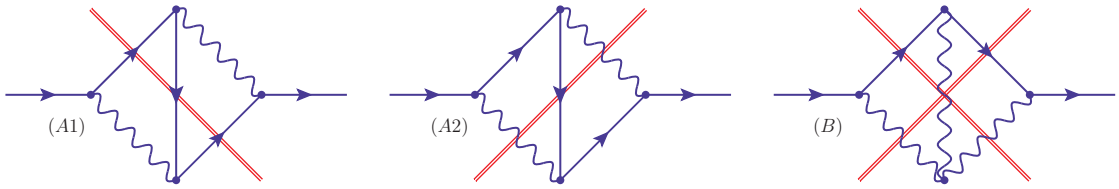

FIGURE 4.7: Scattering processes of fermions that are obtained by on-shell cuts (red double lines) of the fermionic vertex type diagrams. The processes $\psi\psi \to \psi\psi$ and $\psi\bar{\psi} \to \psi\bar{\psi}$ are given by diagram $(A1)$, while $\psi V \to \psi V$ elastic scattering and $\psi\bar{\psi} \to VV$ pair annihilation are given by diagrams $(A2)$ and (B).

Here, we can drop the first two terms as they do not contribute to $2 \leftrightarrow 2$ scattering processes. Further, it can be shown that term three, i.e. diagram $(A2)$ in figure 4.7, has a negligible contribution. This can be seen when looking at the numerator algebra

$$\mathrm{tr}\left[P_{\mathrm{R,L}}\not{p}_1\gamma_\sigma\not{p}_4\gamma^\mu\not{p}_2\gamma^\sigma\not{p}_3\gamma_\mu\right] = -16(p_1\cdot p_2)(p_3\cdot p_4)\,. \tag{4.110}$$

In this case, particles with momenta p_1, p_2, p_1-p_3 and p_1-p_4 are on-shell. This implies that $p_3\cdot p_4 = 0$ which makes the trace (4.110) vanish. Note that this is only true for massless particles. Therefore, only term four, i.e. diagram $(A1)$ in figure 4.7, is physically relevant:

$$\begin{aligned}\mathrm{tr}[\mathrm{i}\not{\Sigma}_\psi^{(\mathrm{A1})>}(p_1)\mathrm{i}S^<(p_1)] = -\int \frac{\mathrm{d}^4p_2}{(2\pi)^4}\frac{\mathrm{d}^4p_3}{(2\pi)^4}\frac{\mathrm{d}^4p_4}{(2\pi)^4}(2\pi)^4\delta^4(p_1+p_2-p_3-p_4)\\ \times 4g^4C_2^F\left(C_2^F-\frac{C_2^A}{2}\right)\mathrm{i}\tilde{S}^<(p_1)\mathrm{i}\tilde{S}^<(p_2)\mathrm{i}\tilde{S}^>(p_3)\mathrm{i}\tilde{S}^>(p_4)\frac{s^2}{tu}\,.\end{aligned} \tag{4.111}$$

Analogously, diagram (B) can be obtained, where two cuts contribute with the same magnitude, such that the expression is given by

$$\begin{aligned}\mathrm{tr}[\mathrm{i}\not{\Sigma}_\psi^{(\mathrm{B})>}(p_1)\mathrm{i}S^<(p_1)] = 4g^4C_2^FC_2^A\int \frac{\mathrm{d}^4p_2}{(2\pi)^4}\frac{\mathrm{d}^4p_3}{(2\pi)^4}\frac{\mathrm{d}^4p_4}{(2\pi)^4}(2\pi)^4\delta^4(p_1+p_2-p_3-p_4)\\ \times \mathrm{i}\tilde{S}^<(p_1)\mathrm{i}\Delta_V^<(p_2)\mathrm{i}\tilde{S}^>(p_3)\mathrm{i}\Delta_V^>(p_4)\frac{u}{t}\,.\end{aligned} \tag{4.112}$$

SCENARIO I: Diagrams $(A1)$ corresponds to the processes $\psi\psi \to \psi\psi$ and $\psi\bar{\psi} \to \psi\bar{\psi}$ depending on the sign of the zeroth momentum, see scenario I of table 4.1. It is shown as the on-shell cut in figure 4.7.

Diagram $(A1)$ is not IR divergence-free. However, when using the symmetry relations $\mathrm{i}S^{<,>}(-p_i) = \mathrm{i}S^{>,<}(p_i)$, the integrand is invariant under renaming $p_2 \leftrightarrow -p_3$, $p_2 \leftrightarrow -p_4$ and $p_3 \leftrightarrow p_4$. Thus, we are allowed to exchange $s \leftrightarrow t$, $s \leftrightarrow u$ and $t \leftrightarrow u$, such that

$$\frac{s^2}{tu} = \frac{-s(t+u)}{tu} = -\frac{s}{u}-\frac{s}{t} \to -\frac{u}{s}-\frac{t}{s} = 1\,. \tag{4.113}$$

Consequently,

$$\begin{aligned}\mathrm{tr}[\mathrm{i}\not{\Sigma}_\psi^{(\mathrm{A1})>}(p_1)\mathrm{i}S^<(p_1)] = -\int \frac{\mathrm{d}^4p_2}{(2\pi)^4}\frac{\mathrm{d}^4p_3}{(2\pi)^4}\frac{\mathrm{d}^4p_4}{(2\pi)^4}(2\pi)^4\delta^4(p_1+p_2-p_3-p_4)\\ \times 4g^4C_2^F\left(C_2^F-\frac{C_2^A}{2}\right)\mathrm{i}\tilde{S}^<(p_1)\mathrm{i}\tilde{S}^<(p_2)\mathrm{i}\tilde{S}^>(p_3)\mathrm{i}\tilde{S}^>(p_4)\,,\end{aligned} \tag{4.114}$$

determines the total matrix element in the last column of table 4.3.

SCENARIO II: Diagrams (B) corresponds to the processes $\psi V \to \psi V$ and $\psi\bar{\psi} \to VV$ depending on the sign of the zeroth momentum, see scenario II of table 4.1. It is shown as the two on-shell cut in figure 4.7. This diagram is also not IR divergence-free due to its momentum structure. Nevertheless, when can make use the relations $\mathrm{i}\Delta_V^{<,>}(-p_{2,4}) = \mathrm{i}\Delta_V^{>,<}(p_{2,4})$, which is true for vanishing chemical potentials. Consequently, the integrand is invariant under renaming $p_2 \leftrightarrow -p_4$. This allows to use $s \leftrightarrow u$, such that

$$\frac{u}{t} \to \frac{1}{2}\left(\frac{u}{t} + \frac{s}{t}\right) = -\frac{1}{2}\,. \tag{4.115}$$

The self-energy expression that determines the total matrix element in the last column of table 4.3 is given by

$$\begin{aligned}\mathrm{tr}[\mathrm{i}\not{\Sigma}_\psi^{(\mathrm{B})>}(p_1)\mathrm{i}S^<(p_1)] = -2g^4 C_2^F C_2^A \int \frac{\mathrm{d}^4p_2}{(2\pi)^4}\frac{\mathrm{d}^4p_3}{(2\pi)^4}\frac{\mathrm{d}^4p_4}{(2\pi)^4}(2\pi)^4\delta^4(p_1+p_2-p_3-p_4)\\ \times \mathrm{i}\tilde{S}^<(p_1)\mathrm{i}\Delta_V^<(p_2)\mathrm{i}\tilde{S}^>(p_3)\mathrm{i}\Delta_V^>(p_4)\,.\end{aligned} \tag{4.116}$$

4.3.3 *Diffusion constants*

When inserting tree-level expressions for the Wightman function, cf. eqs. (3.75)-(3.78) with eq. (3.81), we can expand the different collision terms in terms of the deviations from equilibrium. Therefore, the contraction (4.85) and (4.88) with the matrix elements given in tables 4.2 and 4.3 are valid for all the vertex type contributions. These contractions are of the form of eq. (A.62) and can be solved with the procedure presented in appendix A.4. When applying the variational approach from subsection 4.1.2 inverse diffusion constants to leading linear order are given for the different processes from tables 4.2 and 4.3. A precision much better than the percent level is reached by using a six-dimensional basis set (4.54). Note that we have to take symmetry factors $\mathcal{N}_{\mathrm{sym}}$ into account, which are given in table 4.1 for the different scenarios.

We find that the process of scattering of four identical particles, i.e. when all the external particles of the scattering processes belong to the same species, does not contribute to the diffusion constant:

$$\left(D_\phi^{\mathrm{vert}}\right)^{-1}_{\mathrm{Ia}} = \left(D_\psi^{\mathrm{vert}}\right)^{-1}_{\mathrm{Ia}} = 0\,. \tag{4.117}$$

Diffusion constants for the Higgs for the remaining scenarios are given by

$$\left(D_\phi^{\mathrm{vert}}\right)^{-1}_{\mathrm{Ib}} = \left(D_\phi^{\mathrm{vert}}\right)^{-1}_{\mathrm{Ic}} = \frac{1}{4}\left[\frac{1}{2}\lambda^2 + 3\sum_{\mathrm{SU}(N)} C_2^F\left(C_2^F - \frac{C_2^A}{2}\right)g^4\right] T \times 8.08 \times 10^{-3}\,, \tag{4.118}$$

$$\left(D_\phi^{\mathrm{vert}}\right)^{-1}_{\mathrm{IIa}} = \left(D_\phi^{\mathrm{vert}}\right)^{-1}_{\mathrm{IIb}} = \frac{1}{2}\times 4\sum_{\mathrm{SU}(N)} C_2^F\left(C_2^F - \frac{C_2^A}{4}\right)g^4 T \times 2.03 \times 10^{-3}\,, \tag{4.119}$$

$$\left(D_\phi^{\mathrm{vert}}\right)^{-1}_{\mathrm{IIc}} = \frac{1}{2}\times 4\sum_{\mathrm{SU}(N)} C_2^F\left(C_2^F - \frac{C_2^A}{4}\right)g^4 T \times 4.04 \times 10^{-3}\,, \tag{4.120}$$

	q_{L}	u_{R}	d_{R}	ℓ_{L}	e_{R}	ϕ
$D \times T$	5.8	6.7	6.8	112.7	701.1	91.4
$D_{\mathrm{comp}} \times T$	6	6	6	100	380	–

TABLE 4.4: Our estimates $D \times T$ of leading order diffusion constants for SM particles in the symmetric phase at the EW scale compared to previous outcomes $D_{\mathrm{comp}} \times T$ from ref. [139].

while diffusion constants for fermions read

$$\left(D_{\psi}^{\mathrm{vert}}\right)^{-1}_{\mathrm{Ib}} = \left(D_{\psi}^{\mathrm{vert}}\right)^{-1}_{\mathrm{Ic}} = \frac{1}{4} \times 4 \sum_{\mathrm{SU}(N)} C_2^F \left(C_2^F - \frac{C_2^A}{2}\right) g^4 T \times 1.30 \times 10^{-3}\,, \tag{4.121}$$

$$\left(D_{\psi}^{\mathrm{vert}}\right)^{-1}_{\mathrm{IIa}} = \left(D_{\psi}^{\mathrm{vert}}\right)^{-1}_{\mathrm{IIb}} = \frac{1}{2} \times 2 \sum_{\mathrm{SU}(N)} C_2^F C_2^A g^4 T \times 6.58 \times 10^{-4}\,, \tag{4.122}$$

$$\left(D_{\psi}^{\mathrm{vert}}\right)^{-1}_{\mathrm{IIc}} = -\frac{1}{2} \times 2 \sum_{\mathrm{SU}(N)} C_2^F C_2^A g^4 T \times 1.13 \times 10^{-3}\,. \tag{4.123}$$

4.4 RESULTS

Within this section diffusion constants have been calculated in parametrical dependence of the gauge couplings $g_{1,2,3}$ and the Higgs self-coupling λ. Results for the inverse diffusion constants from self-energy type diagrams are given by eqs. (4.76)-(4.77), (4.79)-(4.80) and (4.82)-(4.83), while the results from vertex type diagrams are shown in eqs. (4.118)-(4.123). Note that the results are general in the sense that these can be applied to any SU(N) gauge theory of interests with N_ψ fermions and N_ϕ scalars as well with the hypercharges Y_ψ and Y_ϕ, respectively. In the SM these are given by the values presented in tables 3.1 and 2.1, respectively.

Due to running couplings, the diffusion constants depend non-trivially on the temperature and the renormalisation group equations have to be taken into account. For the purpose of EW baryogenesis, however, we evaluate the diffusion constants at the EW scale: $g_1 = 0.357$, $g_2 = 0.651$, $g_3 = 1.121$ and $\lambda = 0.280$. Renormalisation group equations that are needed to obtain these numerical values are e.g. given in ref. [125]. Eventually, the diffusion constants for the different SM particles are given in table 4.4.

We find that both the LH quarks q_{L} and the RH quarks u_{R}, d_{R} have diffusion constants with roughly equal magnitude since the strong interactions are the dominant contributions. Further, both the LH leptons ℓ_{L} and the Higgs field ϕ receive contributions from the SU(2) and U(1) interactions. This explains that their diffusion constants are almost equal in size. The RH leptons e_{R} do only interact with U(1) gauge bosons. Therefore, their diffusion length is the largest and, hence, e_{R} have the largest diffusion constants of all the SM particles.

Diffusion constants for SM particles have already been estimated in ref. [139], with the numerical values given in the bottom row of table 4.4. However, only the case where gauge bosons are exchanged has been taken into account. This corresponds to the neglect of the contribution from fermion exchange, cf. eqs. (4.82)-(4.83). Furthermore, that calculation has been based on a leading logarithmic approximation of the t-channel, which is supposed to be the dominant channel. Therefore, the contributions from vertex type

diagrams, cf. eqs. (4.118)-(4.123), and the finite contributions from self-energy type diagrams, cf. eqs. (4.76)-(4.77), are not taken into account. Hence, our computation is more advanced in the sense that we consider both s-channel and t-channel exchanges as well as the leading linear contributions from vertex type diagrams. While the diffusion constants for the quarks and the LH leptons coincide very well with the ones from ref. [139], the diffusion constant for the RH leptons e_{R} is by almost a factor of two larger than their estimates. This deviation slightly enhances the baryon charge generation in EW baryogenesis, as can be seen from eq. (4.36).

Note that the discussion of this section is not complete in the sense that the calculation of the diffusion constant does not take flavour changing Yukawa interactions into account. This effect seems to affect the current estimates at $\mathcal{O}(1)$ and needs to be included in future works. Further, close-to-collinear effects that are due to an arbitrary number of soft scatterings during the emission are neglected. This so-called Landau-Pomeranchuk-Migdal (LPM) effect, cf. e.g. ref. [140], might affect the diffusion constants at leading linear order. However, we expect that this effect is subdominant because the diffusion constants receive their main contribution at leading logarithmic order.

5

LEPTOGENESIS WITH GEV-SCALE RIGHT-HANDED NEUTRINOS

This chapter is mainly based on own publications [1–3] but also extended in some points. In particular LNV effects are included and discussed, which have been neglected in ref. [2]. Throughout this chapter the generation of BAU through CP-violating oscillations [30] of two GeV-scale heavy RH neutrinos is studied from first principles by relying on the CTP formalism, that was first proposed by Schwinger [36] and Keldysh [37]. This formalism including the relevant definitions is discussed in chapter 3. Such a minimal extension of the SM is not only able to account for the light neutrino masses via the seesaw mechanism [18–23] but can also explain the observed BAU via leptogenesis [17]. Certain parameter regions are identified where the evolution of the baryon asymmetry can be computed analytically up to corrections of $\mathcal{O}(1)$.

In section 5.1 quantum kinetic equations for heavy neutrinos are derived, while in section 5.2 the evolution of the SM charges are discussed. In contrast to most of the previous studies spectator effects are included, as well as feedback effects, which are referred to as backreaction effects within this thesis. Further, the importance of LNV effects is highlighted and corresponding leading order damping rates, as well as the modification to the thermal masses of the heavy neutrinos, are derived within a momentum-averaged treatment in section 5.3, where also all the necessary transport coefficients are discussed. Eventually, this derivation implies a coupled system of the differential equations for the heavy neutrinos and the SM leptons, as given in section 5.4. By applying time scale arguments, two different parameter scenarios are discussed for which approximate analytic solutions are found. On the one hand, there is the oscillatory regime, as discussed in section 5.5, which corresponds to an early oscillation compared to the time of their equilibration. This separation of scales allows for a descriptive perturbative treatment, which is divided into three key steps. First, the heavy neutrinos oscillate. Second, these act as the source for the generation of flavoured SM asymmetries. Third, even without LNV effects, a lepton asymmetry is produced indirectly through an incomplete cancellations of the flavoured charges when the produced SM leptons react back into the heavy neutrino sector. On the other hand, particularly for large mixing angles, a certain flavour structure is favoured which causes one of heavy neutrinos to equilibrate quickly, while the other one only couples feebly to the SM. Due to this early equilibration, the heavy neutrinos do not manage to perform a single oscillation before the EW sphalerons freeze out. This overdamped scenario is discussed in section 5.6. In both cases the produced L is converted into B via EW sphaleron transitions in the symmetric phase of the SM. Any B that remains non-zero after the EWSB is frozen in since the rate of these transitions are suppressed in the broken phase of the SM. Note that, in contrast to EW baryogenesis, that is discussed

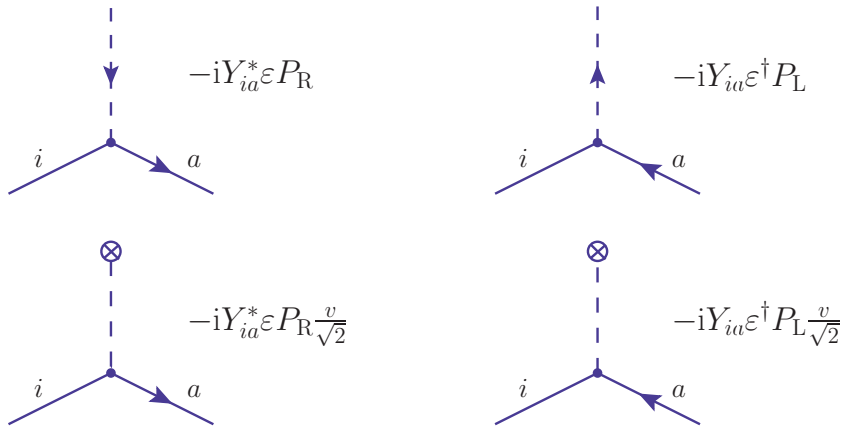

FIGURE 5.1: Vertex rules for heavy neutrinos of flavour i, where the upper diagrams show the exchange of the Higgs field and the lepton doublet of SM flavour a, while the lower diagrams demonstrate the background due to the EV v of the Higgs field (indicated by crossed circle) together with an exchanged lepton doublet.

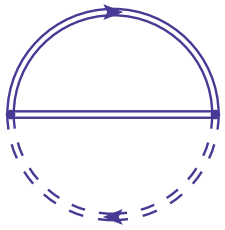

FIGURE 5.2: Vacuum graph including the heavy neutrinos interacting with the SM leptons and the Higgs field.

in chapter 4, leptogenesis from oscillations of heavy neutrinos does not require the PT to be strongly first-order. Within this chapter EWSB via a crossover is assumed.

Note that sections 5.1-5.3 are for the readers that are interested in a detailed derivation of kinetic equations driving leptogenesis from oscillations of GeV-scale heavy neutrinos. Since sections 5.5 and 5.6 provide special parameter regions, section 5.4 might be interesting for the readers that are solely interested in a rather pragmatic understanding of leptogenesis from oscillations heavy neutrinos.

5.1 DERIVATION OF QUANTUM KINETIC EQUATIONS FOR RIGHT-HANDED NEUTRINOS

In order to describe the evolution for heavy neutrinos, both the kinetic and the constraint equations in the non-equilibrium CTP framework from chapter 3 are generalised to massive Majorana particles. The necessary self-energy expressions are listed in subsection 5.1.1, while a detailed derivation of the evolution for the deviation of the heavy neutrino number densities from their equilibrium value is provided in subsection 5.1.2.

5.1.1 *One-loop self-energies*

Feynman rules for vertices where heavy neutrinos are exchanged in the symmetric phase of the SM can simply be read of from the Lagrangian (2.46) and are shown in the top row of figure 5.1. In the 2PI formalism self-energies are obtained via functional derivatives of vacuum graphs, cf. eqs. (3.19) and (3.20). The corresponding vacuum graph that includes heavy neutrinos is given by

$$\Gamma_2 = -g_w (Y^* Y^T)_{ij} \sum_{cd=\pm} cd \int \mathrm{d}^4x \, \mathrm{d}^4y \, \mathrm{tr}\left[P_\mathrm{R} (S_N)^{cd}_{ij}(x,y) P_\mathrm{L} S^{dc}_\ell(y,x)\right] \Delta^{dc}_\phi(y,x)\,, \tag{5.1}$$

and shown in figure 5.2. c, d are CTP indices and should not be confused with the SM lepton flavour indices a, b and the heavy neutrino flavour indices i, j. Due to the SM doublet running in the loop we need to introduce a factor $g_w = 2$ that accounts for the SU(2) multiplicity. Further, we use that the lepton propagator S_ℓ is diagonal in SU(2) flavour space, such that $Y^*_{ia} Y_{jb} \to Y^*_{ia} Y_{ja} = Y^*_{ia} Y^T_{aj} = (Y^* Y^T)_{ij}$. When performing the functional derivative we have to keep in mind that the heavy neutrino propagators S^{cd}_N and S^{dc}_N are not independent but are related to each other via the Majorana condition

$$(S_N)^{cd}_{ij}(x,y) = C (S_N)^{dc}_{ji}(y,x) C^\dagger\,, \tag{5.2}$$

with the charge operator $C = \mathrm{i}\gamma_2\gamma_0$. In coordinate space the self-energy of the heavy neutrino is then given by two individual contributions

$$\begin{aligned}
\mathrm{i}\Sigma^{cd}_{Nij}(x,y) &= cd \frac{\partial \Gamma_2}{\partial (S_N)^{dc}_{ji}(y,x)} \\
&= g_w \Big((Y Y^\dagger)_{ij} P_\mathrm{L} \mathrm{i} S^{cd}_\ell(x,y) P_\mathrm{R} \mathrm{i}\Delta^{cd}_\phi(x,y) \\
&\quad + (Y^* Y^T)_{ij} C P_\mathrm{R} \mathrm{i} S^{dct}_\ell(y,x) P_\mathrm{L} C^\dagger P_\mathrm{L} \mathrm{i}\Delta^{dc}_\phi(y,x) \Big)\,.
\end{aligned} \tag{5.3}$$

The corresponding self-energies in momentum space are obtained by Wigner-transforming the expressions in coordinate space, cf. eq. (3.31), such that

$$\begin{aligned}
\mathrm{i}\not{\Sigma}^{cd}_{Nij}(k) &= g_w \int \frac{\mathrm{d}^4k'}{(2\pi)^4} \frac{\mathrm{d}^4k''}{(2\pi)^4} (2\pi)^4 \delta(k - k' - k'') \\
&\quad \times \left((Y Y^\dagger)_{ij} P_\mathrm{L} \mathrm{i} S^{cd}_\ell(k') P_\mathrm{R} \mathrm{i}\Delta^{cd}_\phi(k'') + (Y^* Y^T)_{ij} C \left[P_\mathrm{L} \mathrm{i} S^{dc}_\ell(-k') P_\mathrm{R} \right]^T C^\dagger \mathrm{i}\Delta^{dc}_\phi(-k'') \right).
\end{aligned} \tag{5.4}$$

These are shown in the top row of figure 5.3. Note that if CTP indices are not written explicitly, the corresponding expressions are valid for any combination of CTP indices. We can now decompose

$$\begin{aligned}
(\mathrm{i}\not{\Sigma}_N)_{ij} &= (\not{\Sigma}_{N\mathrm{R}})_{ij} P_\mathrm{R} + (\not{\Sigma}_{N\mathrm{L}})_{ij} P_\mathrm{L} \\
&= g_w \gamma_\mu \sum_{a=e,\mu,\tau} \left(\hat{\Sigma}^\mu_{N\mathrm{R}a} Y_{ia} Y^\dagger_{aj} P_\mathrm{R} + \hat{\Sigma}^\mu_{N\mathrm{L}a} Y^*_{ia} Y^T_{aj} P_\mathrm{L} \right),
\end{aligned} \tag{5.5}$$

with the reduced self-energies $\hat{\Sigma}_{\mathrm{R,L}a}$ that depend on the chemical potentials μ_ϕ of the Higgs field and $\mu_{\ell a}$ of the SM lepton doublets ℓ^a_L of flavour a, while the dependence on the Yukawa couplings is factored out. It is convenient to refer the part which is given for vanishing chemical potential to the equilibrium solution $\bar{\Sigma}$, while $\delta\Sigma$ is driven by non-zero

chemical potentials of the SM particles and corresponds to the deviation of equilibrium. This allows to decompose the heavy neutrino self-energy as follows:

$$\Sigma = \bar{\Sigma} + \delta\Sigma\,, \tag{5.6}$$

which should be understood as matrix valued quantities in the heavy neutrino flavour space. Since the equilibrium solution neither contains any chiral information nor depends on the SM flavours a,

$$\bar{\Sigma}^{\mu}_{N} = \bar{\Sigma}^{\mu}_{N\mathrm{R}a} = \bar{\Sigma}^{\mu}_{N\mathrm{L}a}\,, \tag{5.7}$$

it makes sense to define the equilibrium quantity

$$\bar{\not{\Sigma}}_{N} = g_w \hat{\not{\Sigma}}_{N}(Y^* Y^T P_{\mathrm{R}} + Y Y^\dagger P_{\mathrm{L}})\,, \tag{5.8}$$

where the flavour dependence is now solely contained in the Yukawa couplings. Note that even though we omit the bar in $\hat{\not{\Sigma}}_N$ for notational purposes, it always refers to the equilibrium solution and is expressed as

$$\mathrm{i}\hat{\not{\Sigma}}^{cd}_{N}(k) = \int \frac{\mathrm{d}^4k'}{(2\pi)^4}\frac{\mathrm{d}^4k''}{(2\pi)^4}(2\pi)^4\delta(k-k'-k'')\mathrm{i}S^{cd}_{\ell}(k')\mathrm{i}\Delta^{cd}_{\phi}(k'')\,. \tag{5.9}$$

Due to the crossover nature of the SM the background Higgs field starts to continuously follow a temperature dependent Higgs field EV $v(T)$, such that

$$\langle\phi\rangle = \begin{pmatrix} 0 \\ v(T) \end{pmatrix}\,, \tag{5.10}$$

with the zero temperature limit $v(T\to 0) = 174\,\mathrm{GeV}$. The corresponding Feynman rules for the heavy neutrino to SM lepton conversion due to the background field of the Higgs EV during the crossover is shown in the bottom row of figure 5.1. The evaluation of the diagram with two insertions of the background field can thus be described by the following self-energy

$$\hat{\not{\Sigma}}^{cd}_{N}|_{\mathrm{EV}} = \frac{v^2(T)}{2}\int\frac{\mathrm{d}^4k}{(2\pi)^4}\mathrm{i}S^{cd}_{\ell}(k)\,, \tag{5.11}$$

which is shown in the bottom row of figure 5.3. Note that at tree-level the spectral part has a vanishing contribution $k\cdot\hat{\Sigma}^{\mathcal{A}}_{N}|_{\mathrm{EV}} = 0$, while $k\cdot\hat{\Sigma}^{H}_{N}|_{\mathrm{EV}}$ is non-vanishing and shall contribute to the effective (thermal) mass of the heavy neutrino.

The deviations from equilibrium are most conveniently expressed in terms of the chemical potentials when assuming a generalised KMS relation

$$\hat{\not{\Sigma}}^{>}_{N\mathrm{R,L}a} = -\mathrm{e}^{\beta(k^0\pm\mu_{\ell a}\pm\mu_{\phi})}\hat{\not{\Sigma}}^{<}_{N\mathrm{R,L}a}\,, \tag{5.12}$$

that only holds for gauge interaction that are fast enough to keep all SM degrees of freedom in equilibrium. Due to the feebly strength of the small Yukawa couplings, compared to the gauge couplings, gauge interactions make the SM always equilibrate quicker. In this case we can assign chemical potentials μ_ϕ to the Higgs field and $\mu_{\ell a}$ to the SM leptons of flavour a. These are supposed to be small at all times that are relevant for the leptogenesis scenario presented in this thesis, which allows for a system of equation that can already

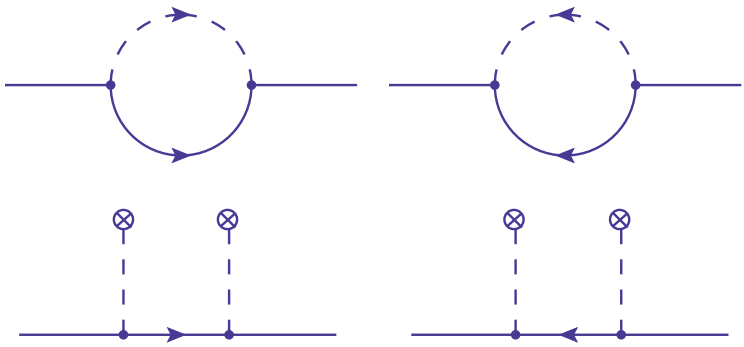

FIGURE 5.3: Effective one-loop contributions to the heavy neutrino self-energy Σ_N. the upper diagrams show the exchange of the Higgs field and the lepton doublet, while the lower diagrams demonstrate the background due to the EV of the Higgs field (indicated by crossed circle) together with an exchanged lepton doublet. Although these are not indicated with double lines, these can in general be resummmed.

be sufficiently described at linear order in $\beta\mu_{\ell a}, \beta\mu_\phi$. Therefore, the deviations $\delta\hat{\not{\Sigma}}_N$ can be related to each other via a linearised KMS relation

$$\begin{aligned}\delta\hat{\not{\Sigma}}^{>}_{N\mathrm{R,L}a} &\simeq -\mathrm{e}^{\beta k^0}\left[\delta\hat{\not{\Sigma}}^{<}_{N\mathrm{R,L}a} \pm \beta(\mu_{\ell a}+\mu_\phi)\left(\hat{\not{\Sigma}}^{<}_N P_{\mathrm{R,L}} + \delta\hat{\not{\Sigma}}^{<}_{N\mathrm{R,L}a}\right)\right] \\ &\simeq -\mathrm{e}^{\beta k^0}\left[\delta\hat{\not{\Sigma}}^{<}_{N\mathrm{R,L}a} \pm \beta(\mu_{\ell a}+\mu_\phi)\hat{\not{\Sigma}}^{<}_N P_{\mathrm{R,L}}\right], \end{aligned} \tag{5.13}$$

an approximation that is valid to linear order in $\beta\mu$ and $\delta\hat{\not{\Sigma}}_N$ as well as in the combination of these. Note that the KMS relation for the equilibrium solution is simply given by

$$\bar{\not{\Sigma}}^{>}_N = -\mathrm{e}^{\beta k^0}\bar{\not{\Sigma}}^{<}_N . \tag{5.14}$$

5.1.2 *Quantum kinetic equations*

The kinetic equations for heavy neutrinos can be easily deduced from the fermionic kinetic equations (3.49), such that

$$\mathrm{i}\partial_t \mathrm{i}\mathcal{S}^{+}_N + \left[\Omega, \mathrm{i}\mathcal{S}^{+}_N\right] - \left[\mathrm{i}\mathcal{G}^{+}_N, \mathcal{S}^{H}_N\right] = -\frac{\mathrm{i}}{2}\left(\{\mathrm{i}\mathcal{G}^{>}_N, \mathrm{i}\mathcal{S}^{<}_N\} - \{\mathrm{i}\mathcal{G}^{<}_N, \mathrm{i}\mathcal{S}^{>}_N\}\right), \tag{5.15}$$

with

$$\Omega_N \equiv \left(\not{k} - \not{\Sigma}^{H}_{N\mathrm{R,L}} - M\right)\gamma^0, \quad \mathcal{S}_N \equiv \gamma^0 S_{N\mathrm{R,L}}, \quad \mathcal{G}_N \equiv \gamma^0 \not{\Sigma}_{N\mathrm{R,L}}, \tag{5.16}$$

where Ω_N does not only depend on the thermal mass, given by $\not{\Sigma}^{H}_{N\mathrm{R,L}}$, but also on the non-thermal Majorana mass M of the heavy neutrino. Here, we stick to the notation from ref. [2], where the statistical propagator

$$S^{+}_N = \frac{1}{2}\left(S^{>}_N + S^{<}_N\right), \tag{5.17}$$

is used instead of $S^{<,>}_N$. As its name implies S^{+}_N measures the occupation numbers. Analogously to the decomposition of Σ_N, we decompose

$$\Omega_N = \bar{\Omega}_N + \delta\Omega_N, \qquad \mathcal{G} = \bar{\mathcal{G}}_N + \delta\mathcal{G}_N, \tag{5.18}$$

into an equilibrium solution and some deviation from equilibrium. The solution for the algebraic equations

$$\left[\bar{\Omega}_N, \mathrm{i}\bar{\mathcal{S}}_N^+\right] - \left[\mathrm{i}\bar{\mathcal{G}}_N^+, \bar{\mathcal{S}}_N^H\right] = -\frac{1}{2}\left(\left\{\mathrm{i}\bar{\mathcal{G}}_N^>, \mathrm{i}\bar{\mathcal{S}}_N^<\right\} - \left\{\mathrm{i}\bar{\mathcal{G}}_N^<, \mathrm{i}\bar{\mathcal{S}}_N^>\right\}\right), \tag{5.19}$$

defines the static solution $\bar{\mathcal{S}}_N$. To leading order in gradients and small couplings the decomposition

$$\mathcal{S}_N^{<,>} = \bar{\mathcal{S}}_N^{<,>} + \delta\mathcal{S}_N\,, \qquad \mathcal{S}_N^+ = \bar{\mathcal{S}}_N^+ + \delta\mathcal{S}_N\,, \tag{5.20}$$

holds, provided that the self-energies are described by particles that are approximately in equilibrium. Therefore, the spectral and Hermitian parts of the heavy neutrino propagator are also in equilibrium

$$S^H = \bar{S}^H\,, \qquad S^{\mathcal{A}} = \bar{S}^{\mathcal{A}}\,. \tag{5.21}$$

Eventually, the static solution, cf. eq. (5.19), allows to write down the kinetic evolution for the deviation $\delta\mathcal{S}_N$

$$\begin{aligned}\partial_t\delta\mathcal{S}_N = {}& -\partial_t\bar{\mathcal{S}}_N^+ + \mathrm{i}\left[\bar{\Omega}_N, \delta\mathcal{S}_N\right] + \mathrm{i}\left[\delta\Omega_N, \bar{\mathcal{S}}_N^+\right] - \mathrm{i}\left[\delta\mathcal{G}_N^+, \bar{\mathcal{S}}_N^H\right] - \left\{\bar{\mathcal{G}}_N^{\mathcal{A}}, \delta\mathcal{S}_N\right\} \\ & - \frac{1}{2}\left(\left\{\delta\mathcal{G}_N^>, \bar{\mathcal{S}}_N^<\right\} - \left\{\delta\mathcal{G}_N^<, \bar{\mathcal{S}}_N^>\right\}\right).\end{aligned} \tag{5.22}$$

DECOMPOSITION FOR NON-ZERO CHEMICAL POTENTIAL: Particularly the term in the lower line of the RH side of eq. (5.22) is only present for non-vanishing chemical potential of the SM particles. It can be simplified and expressed in terms of the chemical potentials $\beta\mu_{\ell a}, \beta\mu_\phi$ by the use of the linearised KMS relation (5.13). From now on we will neglect the term with $\delta\mathcal{G}_N^+$ in eq. (5.22) as it can be shown that it is quadratic in the chemical potentials. It also makes sense to drop the term with $\delta\Omega_N$ in eq. (5.22). The reason for that is that it only appears in the commutator together with $\bar{\mathcal{S}}_N$ that is close to unity since $\delta\mathcal{S}_N$ is and initially $\delta\mathcal{S}_N = -\bar{\mathcal{S}}_N$ for $T \gg M_i$ and $Y_{ia} \ll 1$. With these considerations the kinetic equation for the deviation $\delta\mathcal{S}_N$ can be expressed in terms of equilibrium quantities and the chemical potentials at linear order:

$$\partial_t\delta\mathcal{S}_N = 2\frac{\partial_t f_{\mathrm{F}}}{1-2f_{\mathrm{F}}}\bar{\mathcal{S}}_N^+ + \mathrm{i}\left[\bar{\Omega}_N, \delta\mathcal{S}_N\right] - \left\{\bar{\mathcal{G}}_N^{\mathcal{A}}, \delta\mathcal{S}_N\right\} - \frac{2}{1-2f_{\mathrm{F}}}\sum_{a=e,\mu,\tau}\frac{\mu_{\ell a}+\mu_\phi}{T}\{\tilde{\mathcal{G}}_N^a, \bar{\mathcal{S}}_N^+\}\,. \tag{5.23}$$

Here, the Leibniz rule for the term $\partial_t\bar{\mathcal{S}}_N^+$ in eq. (5.22) has been used after it has been related to the static quantities $\bar{\mathcal{S}}_N^{<,>}$ via the KMS relation (5.14). This is why the Fermi-Dirac distribution $f_{\mathrm{F}} = f_{\mathrm{F}}(k^0) = 1/(\mathrm{e}^{\beta k^0}+1)$ appears. Accordingly, the linearised KMS relation (5.13) for the terms $\delta\mathcal{G}_N^{<,>}$ has been inserted, such that

$$\tilde{\mathcal{G}}_N^a = -g_w f_{\mathrm{F}}(1-f_{\mathrm{F}})\hat{\not{Y}}_N^{\mathcal{A}}\left(Y_{ia}^* Y_{aj}^T P_{\mathrm{R}} - Y_{ia}Y_{aj}^\dagger P_{\mathrm{L}}\right)\gamma^0\,. \tag{5.24}$$

LORENTZ DECOMPOSITION: In case of an isotropic and homogeneous universe it makes sense to employ the following decomposition [141, 142]

$$-\mathrm{i}\gamma^0\delta S_N = \frac{1}{2}\sum_h P_h\left(g_{0h} + \gamma^0 g_{1h} - \mathrm{i}\gamma^0\gamma^5 g_{2h} - \gamma^5 g_{3h}\right), \tag{5.25}$$

with g_{ah} Hermitian matrices in the heavy neutrino flavour space that are determined in the following. The helicity projector of a certain helicity $h = \pm$ is defined via

$$P_h = \frac{1}{2}\left(1 + h\hat{k}_i\gamma^0\gamma^i\gamma^5\right) . \tag{5.26}$$

Throughout this chapter we are using the chiral (Weyl) representation of the Dirac matrices. Note the useful relation of the helicity operator acting on the momentum

$$P_h \not{k} = \frac{1}{2}\left(\not{k} - h\not{\tilde{k}}\gamma^5\right) , \tag{5.27}$$

which is given by introducing the quantity

$$\tilde{k} = (|\mathbf{k}|, k^0\hat{\mathbf{k}}) , \tag{5.28}$$

that fulfils the orthogonality relation in Minkowski space $k \cdot \tilde{k} = 0$, as well as $\tilde{k}^2 = -k^2$. Note that the decomposition (5.25) is analogously usable for $\bar{S}_N^+$ when replacing the Hermitian matrices g_{ah} by $\bar{g}_{ah}$.

CONSTRAINT EQUATIONS: In contrast to the kinetic equation, the constraint equation does not determine the kinetic behaviour of the heavy neutrinos but further constrains g_{ah}. To zeroth order in the Yukawa couplings the constraint equation for the heavy neutrino can be deduced from eq. (3.48) and is given by

$$\{(\not{k} - M)\gamma^0, \mathrm{i}\delta\mathcal{S}_N\} = 0 , \tag{5.29}$$

where we make use of the static equation $\{(\not{k} - M)\gamma^0, \mathrm{i}\bar{\mathcal{S}}_N^+\} = 0$. With this equation we can relate all g_{ah} from the Lorentz decomposition (5.25) to g_{0h}. In order to do so we insert the decomposition (5.25) of $\delta\mathcal{S}_N$ into the constraint equation (5.29) and multiply it either with the unit matrix, γ^0, γ^5 or $\gamma^0\gamma^5$. In the most general case of allowing for a complex mass matrix M we obtain the constraint equations to zeroth order in the Yukawas by taking Dirac traces

$$g_{1h} = \frac{1}{2k^0}\left(\{\mathrm{Re}M, g_{0h}\} + [\mathrm{iIm}M, g_{3h}]\right) , \tag{5.30}$$

$$g_{2h} = \frac{1}{2\mathrm{i}k^0}\left([\mathrm{Re}M, g_{3h}] + \{\mathrm{iIm}M, g_{0h}\}\right) , \tag{5.31}$$

$$g_{3h} = h\frac{|\mathbf{k}|}{k^0}g_{0h} , \tag{5.32}$$

and analogously for $\bar{g}_{ah}$. Next order results are provided in ref. [141]. It might be interesting in the future to decide in how far the approximation above affects the kinetic equation, especially in the case of two heavy neutrinos with highly degenerate masses.

OFF-SHELL KINETIC EQUATION: The equations describing the kinetic behaviour of g_{0h} are obtained by using the evolution equation (5.23) for $\delta\mathcal{S}_N$ and inserting the Lorentz decomposition (5.25). After expressing the different g_{ah} from eqs. (5.30)-(5.32) in terms of g_{0h} via the zeroth order constraint equation (5.29) and taking the Dirac trace, one ends up with

$$\partial_t g_{0h} = 2\frac{\partial_t f_\mathrm{F}}{1 - 2f_\mathrm{F}}\bar{g}_{0h} + \frac{\mathrm{i}}{2}\left[\mathrm{H}_N, g_{0h}\right] - \frac{1}{2}\left\{\Gamma_N, g_{0h}\right\} - \frac{1}{2}\frac{2}{1 - 2f_\mathrm{F}}\sum_{a=e,\mu,\tau}\frac{\mu_{\ell a} + \mu_\phi}{T}\{\tilde{\Gamma}_N^a, \bar{g}_{0h}\} , \tag{5.33}$$

that holds for a given helicity $h = \pm$. The individual terms

$$\mathrm{H}_N = 2g_w \left(\mathrm{Re}[Y^* Y^T] \frac{k \cdot \hat{\Sigma}_N^H}{k^0} - \mathrm{i}h \mathrm{Im}[Y^* Y^T] \frac{\tilde{k} \cdot \hat{\Sigma}_N^H}{k^0} \right) + \frac{1}{k^0} \left(\mathrm{Re}[M^\dagger M] + \mathrm{i}h \frac{|\mathbf{k}|}{k^0} \mathrm{Im}[M^\dagger M] \right) , \tag{5.34}$$

$$\Gamma_N = 2g_w \left(\mathrm{Re}[Y^* Y^T] \frac{k \cdot \hat{\Sigma}_N^{\mathcal{A}}}{k^0} - \mathrm{i}h \mathrm{Im}[Y^* Y^T] \frac{\tilde{k} \cdot \hat{\Sigma}_N^{\mathcal{A}}}{k^0} \right) , \tag{5.35}$$

$$(\tilde{\Gamma}_N^a)_{ij} = 2h g_w f_{\mathrm{F}} (1 - f_{\mathrm{F}}) \left(\mathrm{Re}[Y_{ia}^* Y_{aj}^T] \frac{\tilde{k} \cdot \hat{\Sigma}_N^{\mathcal{A}}}{k^0} - \mathrm{i}h \mathrm{Im}[Y_{ia}^* Y_{aj}^T] \frac{k \cdot \hat{\Sigma}_N^{\mathcal{A}}}{k^0} \right) , \tag{5.36}$$

are solely given by the equilibrium part of the reduced spectral and Hermitian self-energies $\hat{\Sigma}_N^{\mathcal{A}}$ and $\hat{\Sigma}_N^H$, respectively, i.e. the self-energies evaluated at zero chemical potential, cf. eq. (5.8). To that given order in the Yukawa couplings the deviation from equilibrium only appears in the term coming with (5.36). It considers the charges in the SM lepton sector as an input for the evolution equation of the heavy neutrino and will thus be referred to as the backreaction term. The contractions of $\hat{\Sigma}_N^{\mathcal{A}}$ and $\hat{\Sigma}_N^H$ with k and $\tilde{k}$ in Minkowski space are non-trivial and will be performed in section 5.3.

ON-SHELL KINETIC EQUATIONS: The kinetic equation (5.33) for g_{0h} is matrix valued in the heavy neutrino flavour space. Therefore, it is quite similar to density matrix equations that are often used in neutrino physics [143]. Note however that this it is defined for a general energy k^0 which does not necessarily put the heavy neutrinos on-shell. Consequently, the kinetic equation does not describe the evolution of particle number but is rather an equation for correlation functions. A specification to the on-shell case can be applied when using the narrow width limit for the heavy neutrinos quasiparticles, cf. the discussion in chapter 3. This approximation is justified due to the feeble coupling of the heavy neutrinos with the SM particles due to the smallness of the Yukawa couplings. In this case, the width is small enough to be approximated by a delta function. Hence, the phase space integrals are dominated by the quasiparticle poles Ω_i. These are defined as poles of the inverse effective Hamiltonian H_N^{-1} from (5.33) in a basis where H_N is diagonal. Eventually, when comparing with the zero-width solutions to the Wightman functions, cf. chapter 3, one can extract and approximate

$$\bar{g}_{0hij}(k) \simeq -\frac{1 - 2f_{\mathrm{F}}}{2} 2\pi \delta((k^0)^2 - \Omega_i^2) 2k^0 \delta_{ij} \, . \tag{5.37}$$

In low scale leptogenesis scenarios both the vacuum masses and the thermal masses are small compared to the relevant temperatures. Therefore one might use the relativistic approximation for the dispersion relation, such that $\delta((k^0)^2 - \Omega_i^2)$ simplifies to $\delta(k^2)$. Note, however, that we cannot neglect these masses in the term H_N in eq. (5.33). This is simply because these are responsible for the flavour oscillations, which create the asymmetries that eventually produce the baryon asymmetry. Further, we find that even in a low scale leptogenesis scenario LNV effects are important. These effects vanish in the ultrarelativistic limit $k^2 = 0$. Therefore, in the case of two almost degenerate heavy neutrinos, the mass shell is given by $k^2 = \bar{M}^2$. When making use of the relation $\mathrm{i}\delta S_N = -2S_N^{\mathcal{A}} \delta f$ and

using the KMS relation to relate $\bar{S}^+_N$ to $S^{\mathcal{A}} = \bar{S}^{\mathcal{A}}$ via $S^{\mathcal{A}}(1-2f_{\rm F}) = {\rm i}\bar{S}^+$, we can express g_{ah} in terms of $\bar{g}_{ah}$ and δf_{0h}:

$$g_{ah} = \frac{2}{1-2f_{\rm F}}\bar{g}_{ah}\delta f_{ah} \simeq 2\pi\delta(k^2-\bar{M}^2)2k^0\delta f_{ah}\,, \tag{5.38}$$

such that

$$\int \frac{{\rm d}k^0}{2\pi} g_{ah} = \delta f_{ah}\,. \tag{5.39}$$

When making use of eq. (5.26), this allows to write the equilibrium propagator and its deviation in a simple form

$$ {\rm i}\bar{S}^+_{Nij} \simeq 2\pi\delta(k^2-\bar{M}^2)\sum_h P_h(\not{k}+\bar{M})\frac{1-2f_{\rm F}}{2}\delta_{ij}\,, \tag{5.40}$$

$$ {\rm i}\delta S_{Nij} \simeq -2\pi\delta(k^2-\bar{M}^2)\sum_h P_h(\not{k}+\bar{M})\delta f_{0hij}\,. \tag{5.41}$$

With eq. (5.37), not only the different g_{ah} but also the full kinetic equation (5.33) can be expressed in terms of the deviation δf_{0h}. Note that we can limit our discussion on the case of particles, i.e. $\mathrm{sign}(k^0) = 1$, as the analogous equations for antiparticles, i.e. $\mathrm{sign}(k^0) = -1$ are directly recovered when making use of the Majorana condition (5.2) that implies

$$\delta f_{0h}(-k^0) = \delta f^*_{0h}(k^0)\,. \tag{5.42}$$

Integration of the kinetic equation (5.33) over k^0 yields the on-shell limit of the kinetic equations

$$\partial_t \delta f_{0h} = -\partial_t f_{\rm F} - \frac{\rm i}{2}\left[{\rm H}_N, \delta f_{0h}\right] - \frac{1}{2}\left\{\Gamma_N, \delta f_{0h}\right\} + \frac{1}{2}\sum_{a=e,\mu,\tau}\frac{\mu_{\ell a}+\mu_\phi}{T}\tilde{\Gamma}^a_N\,, \tag{5.43}$$

where we keep the same notation for ${\rm H}_N$, Γ_N and $\tilde{\Gamma}_N$ as in eqs. (5.34)-(5.36), although they are understood in the on-shell sense: $k^0 = |\mathbf{k}|$. Let us define helicity-even and helicity-odd parts of the deviations

$$\delta f^{\rm even}(k) = \frac{\delta f_{0+}(k) + \delta f_{0-}(k)}{2}\,, \tag{5.44}$$

$$\delta f^{\rm odd}(k) = \frac{\delta f_{0+}(k) - \delta f_{0-}(k)}{2}\,, \tag{5.45}$$

which will be useful later.

GENERALISATION TO AN EXPANDING UNIVERSE: The kinetic equation (5.43) for on-shell heavy neutrinos has only been derived in Minkowski space so far. The effect of the expanding universe can be implemented by using conformal coordinates [130], that are defined via the metric

$$g_{\mu\nu} = a(\eta)\mathrm{diag}(1,-1,-1,-1)\,, \tag{5.46}$$

with η the conformal time and $a(\eta)$ the scale factor such that ${\rm d}t = a(\eta){\rm d}\eta$. In a radiation-dominated universe we can relate the scale factor to the conformal time

$$a(\eta) = a_{\rm R}\eta\,, \tag{5.47}$$

via a quantity a_{R} that can be expressed in terms of the temperature T and the Hubble constant H

$$a_{\mathrm{R}} = m_{\mathrm{Pl}}\sqrt{\frac{45}{4\pi^3 g_\star}} = \frac{T^2}{H}\,, \tag{5.48}$$

when using the Friedmann equations. Here $m_{\mathrm{Pl}} = 1.22 \times 10^{19}\,\mathrm{GeV}$ is the Planck mass and $g_\star = 106.75$ counts the number of relativistic degrees of freedom. It is useful to choose a time coordinate that behaves antiproportionally to the temperature $z = T_{\mathrm{ref}}/T$, where the proportionality factor is some fixed reference temperature T_{ref} that can be chosen by convenience. An important scale for leptogenesis is the temperature of the EW sphaleron freeze-out. We consequently set T_{ref} to this temperature, such that the universe begins to expand at $z = 0$, while the EW sphalerons become suppressed at $z = 1$. Since $a_{\mathrm{R}}/a(\eta) = T$, it makes sense to interpret a_{R} as the comoving temperature. In these coordinates the equilibrium Fermi-Dirac distribution is given by

$$f^{\mathrm{eq}}(k) = \frac{1}{\mathrm{e}^{|\mathbf{k}|/a_{\mathrm{R}}} + 1}\,. \tag{5.49}$$

As f^{eq} does not depend on the conformal time its conformal time derivative vanishes $\frac{\mathrm{d}}{\mathrm{d}\eta} f'_{\mathrm{eq}} = 0$, such that

$$\frac{\mathrm{d}}{\mathrm{d}\eta}\delta f_{0hij} = -\frac{\mathrm{i}}{2}\left[\mathrm{H}_N, \delta f_{0h}\right]_{ij} - \frac{1}{2}\left\{\Gamma_N, \delta f_{0h}\right\}_{ij} + \frac{1}{2}\sum_{a=e,\mu,\tau}\frac{\mu_{\ell a} + \mu_\phi}{T}(\tilde{\Gamma}^a_N)_{ij}\,, \tag{5.50}$$

where the heavy neutrino flavour content is made explicit. The kinetic behaviour of the heavy neutrino is mainly given by the following three terms from eqs. (5.34)-(5.36). In conformal time and with on-shell heavy neutrinos these three terms are given by:

- **Effective Hamiltonian:** H_N is decomposed as $(\mathrm{H}_N)_{ij} = (\mathrm{H}^{\mathrm{vac}}_N)_{ij} + (\mathrm{H}^{\mathrm{th}}_N)_{ij}$ with the vacuum mass $\mathrm{H}^{\mathrm{vac}}_N$ and a thermal mass $\mathrm{H}^{\mathrm{th}}_N$ term, such that

$$(\mathrm{H}^{\mathrm{vac}}_N)_{ij} = \frac{a^2(\eta)}{|\mathbf{k}|}\left(\mathrm{Re}[M^\dagger M] + \mathrm{i}h\mathrm{Im}[M^\dagger M]\right)\,, \tag{5.51}$$

$$(\mathrm{H}^{\mathrm{th}}_N)_{ij} = 2g_w\left(\mathrm{Re}[Y^* Y^T]\frac{k\cdot\hat{\Sigma}^H_N}{k^0} - \mathrm{i}h\mathrm{Im}[Y^* Y^T]\frac{\tilde{k}\cdot\hat{\Sigma}^H_N}{k^0}\right)\,. \tag{5.52}$$

  With a complex vacuum mass matrix M, H_N is given in the most general form and describes the flavour oscillations of the heavy neutrinos. The thermal component $\hat{\Sigma}^H_N$ itself is given by two parts: On the one hand, there is the Hermitian part of the reduced self-energy of the heavy neutrino with the exchanged Higgs field. On the other hand, it also accounts for the temperature dependent EV of the Higgs field, cf. figure 5.3. Both components will be described in more detail and will also be quantified later in section 5.3

- **Damping term:** Γ_N accounts for the decay of the deviations δf_{0h} of the heavy neutrinos back to their equilibrium value and is given by

$$\Gamma_N = 2g_w\left(\mathrm{Re}[Y^* Y^T]\frac{k\cdot\hat{\Sigma}^{\mathcal{A}}_N}{k^0} - \mathrm{i}h\mathrm{Im}[Y^* Y^T]\frac{\tilde{k}\cdot\hat{\Sigma}^{\mathcal{A}}_N}{k^0}\right)\,, \tag{5.53}$$

  with the spectral part of the reduced self-energy $\hat{\Sigma}^{\mathcal{A}}_N$ of the heavy neutrino self-energy. A quantification of this self-energy will be provided in section 5.3.

- **Backreaction term:** When the heavy neutrinos start oscillating they produce asymmetries in the SM lepton sector in terms of the chemical potentials $\mu_{\ell a}$ and μ_ϕ, as we clear from section 5.4 on. The term responsible for such a creation will be referred to as the source term. The distribution of the heavy neutrino is, however, not independent of asymmetries in the SM lepton sector. Therefore, there is a so-called backreaction effect that is described by the term

$$\frac{\mu_{\ell a}+\mu_\phi}{T}(\tilde{\Gamma}^a_N)_{ij} \to 2hg_w\left(\mathrm{Re}[Y^*_{ia}Y^T_{aj}]\frac{\tilde{k}\cdot\hat{\Sigma}^{\mathcal{A}}_N}{k^0}-\mathrm{i}h\mathrm{Im}[Y^*_{ia}Y^T_{aj}]\frac{k\cdot\hat{\Sigma}^{\mathcal{A}}_N}{k^0}\right) \times\frac{\mathrm{e}^{|\mathbf{k}|/a_\mathrm{R}}}{(\mathrm{e}^{|\mathbf{k}|/a_\mathrm{R}}+1)^2}\frac{\mu_{\ell a}+\mu_\phi}{a_\mathrm{R}}\,. \tag{5.54}$$

INTRODUCING THE TRANSPORT COEFFICIENTS: As already mentioned, the kinetic equation (5.43) is determined by the reduced self-energies $\hat{\Sigma}^{\mathcal{A}}_N$ and $\hat{\Sigma}^H_N$ evaluated at zero chemical potential. Contractions of these self-energies with the four vectors k and $\tilde{k}$ describe transport coefficients, namely damping rates and thermal corrections to the heavy neutrino mass, and need to be evaluated. As the corresponding computation is non-trivial we will define the coefficients here and shift the evaluation to section 5.3. In ref. [2] the ultrarelativistic approximation $|\mathbf{k}|/k^0=\mathrm{sign}(k^0)$ is used that relates all equilibration rates to

$$\gamma(k)=\frac{2g_w}{a_\mathrm{R}}\frac{k\cdot\hat{\Sigma}^{\mathcal{A}}_N}{k^0}\,, \tag{5.55}$$

a quantity that does not allow for LNV. Expanding the relativistic approximation to the next non-vanishing order $\mathcal{O}(M_i^2/|\mathbf{k}|^2)$ not only LNC but also LNV rates appear, that both contribute to the equilibration process. The conserving rates are denoted by $\gamma_+(k)$ and correspond to $\gamma(k)$ from ref. [2], while $\gamma_-(k)$ are referred to as the LNV rates. To first non-vanishing order these are given by

$$\gamma_+(k)\equiv\frac{1}{a_\mathrm{R}}\frac{g_w}{k^0}\left(k+\tilde{k}\right)\cdot\hat{\Sigma}^{\mathcal{A}}_N\simeq\frac{2}{a_\mathrm{R}}\frac{g_w}{|\mathbf{k}|}\left(k\cdot\hat{\Sigma}^{\mathcal{A}}_N\right)\,, \tag{5.56}$$

$$\gamma_-(k)\equiv\frac{1}{a_\mathrm{R}}\frac{g_w}{k^0}\left(k-\tilde{k}\right)\cdot\hat{\Sigma}^{\mathcal{A}}_N\simeq\frac{1}{2a_\mathrm{R}}\frac{g_w}{|\mathbf{k}|}\frac{M_i^2}{|\mathbf{k}|}\left(\hat{\Sigma}^{\mathcal{A}0}_N+\hat{k}_i\cdot\hat{\Sigma}^{\mathcal{A}i}_N\right)\,. \tag{5.57}$$

This can be analogously applied or the Hermitian part $\hat{\Sigma}^H_N$. Note the two contributions of $\hat{\Sigma}^H_N$, cf. figure 5.3,

$$\hat{\Sigma}^H_N=\hat{\Sigma}^H_N|_\mathrm{th}+\hat{\Sigma}^H_N|_\mathrm{EV}\,, \tag{5.58}$$

with $\hat{\Sigma}^H_N|_\mathrm{th}$ the thermal contribution from the Higgs field in the symmetric phase of the SM and $\hat{\Sigma}^H_N|_\mathrm{EV}$ the EV for the Higgs background field from the beginning of the continuous EWSB on. Note that at tree level one has $\tilde{k}\cdot\hat{\Sigma}^H_N|_\mathrm{EV}=0$. We thus have

$$\mathfrak{h}^\mathrm{th}_+(k)\equiv\frac{1}{a_\mathrm{R}}\frac{g_w}{k^0}\left(k+\tilde{k}\right)\cdot\hat{\Sigma}^H_N|_\mathrm{th}\simeq\frac{2}{a_\mathrm{R}}\frac{g_w}{|\mathbf{k}|}\left(k\cdot\hat{\Sigma}^H_N|_\mathrm{th}\right)\,, \tag{5.59}$$

$$\mathfrak{h}^\mathrm{th}_-(k)\equiv\frac{1}{a_\mathrm{R}}\frac{g_w}{k^0}\left(k-\tilde{k}\right)\cdot\hat{\Sigma}^H_N|_\mathrm{th}\simeq\frac{1}{2a_\mathrm{R}}\frac{g_w}{|\mathbf{k}|}\frac{M_i^2}{|\mathbf{k}|}\left(\hat{\Sigma}^{H0}_N|_\mathrm{th}+\hat{k}_i\cdot\hat{\Sigma}^{Hi}_N|_\mathrm{th}\right)\,, \tag{5.60}$$

and

$$\frac{1}{2}\mathfrak{h}^\mathrm{EV}(k)\equiv\mathfrak{h}^\mathrm{EV}_+(k)=\mathfrak{h}^\mathrm{EV}_-(k)\equiv\frac{1}{a_\mathrm{R}}\frac{g_w}{k^0}\left(k\cdot\hat{\Sigma}^H_N|_\mathrm{EV}\right)\,. \tag{5.61}$$

KINETIC EQUATIONS FOR NUMBER DENSITIES: The kinetic equation (5.50) describing the equation of motion of the heavy neutrinos holds for each momentum mode $\mathbf{k}$ individually. Particularly, the backreaction term (5.54) creates a coupling between the individual modes. Trying to solve such a coupled system in order to obtain the full momentum dependence ends up in a huge complication, especially, when being interested in analytic approximations or in a fast numerical code. Therefore, we follow a convenient procedure [30, 44, 144] by reducing the system to number densities instead of momentum dependent distributions functions. This can be achieved by averaging over the momentum $\mathbf{k}$. Note that this yields $\mathcal{O}(1)$ errors in the final results, cf. e.g. ref. [145]. Nevertheless, this procedure is a step forward in understanding the generation of a matter-antimatter asymmetry via leptogenesis.

When integrating over three-momenta it is useful to introduce the equilibrium number density

$$n^{\mathrm{eq}} = \int \frac{\mathrm{d}^3k}{(2\pi)^3} f^{\mathrm{eq}}(k) = \frac{3}{4\pi^2} a_{\mathrm{R}}^3 \zeta(3)\,, \tag{5.62}$$

and helicity dependent deviations in the heavy neutrino flavour space

$$\delta n_{hij} = \int \frac{\mathrm{d}^3k}{(2\pi)^3} \delta f_{h0ij}(\mathbf{k})\,, \tag{5.63}$$

as well as the quantity

$$\tilde{n}^{\mathrm{eq}} = \int \frac{\mathrm{d}^3k}{(2\pi)^3} f^{\mathrm{eq}}(k)(1 - f^{\mathrm{eq}}(k)) = \frac{a_{\mathrm{R}}^3}{12}\,. \tag{5.64}$$

The helicity-even and helicity-odd parts of the deviations of the number densities n^{even} and n^{odd} are defined in analogy to the distribution functions, cf. eqs. (5.44) and (5.45). A complication arises when it comes to averaging products of a momentum dependent quantity and the distribution function. The most convenient way to solve this problem is to replace this quantity by its average value. Exemplary for the $1/|\mathbf{k}|$ term in the effective Hamiltonian this is

$$\left\langle \frac{1}{|\mathbf{k}|} \right\rangle \equiv \frac{1}{n^{\mathrm{eq}}} \int \frac{\mathrm{d}^3k}{(2\pi)^3} \frac{1}{|\mathbf{k}|} f^{\mathrm{eq}}(k) = \frac{\pi^2}{18 a_{\mathrm{R}} \zeta(3)}\,. \tag{5.65}$$

The procedure of averaging the self-energies is not straightforward such that its quantitative study is shifted to section 5.3. Nevertheless, in order to describe the momentum-average of a quantity $\mathcal{X}(k)$, that can be either $\gamma_\pm(k)$ or $\mathfrak{h}_\pm(k)$, we shortly discuss how these quantities need be averaged correctly. This being said, one should recall that these only appear with two different combinations of the equilibrium distribution f^{eq} and the deviation δf in the kinetic equation (5.50). Therefore, we introduce two different ways of momentum-averaging

$$\mathcal{X} \equiv \frac{1}{\delta n} \int \frac{\mathrm{d}^3k}{(2\pi)^3} \delta f(k) \mathcal{X}(k)\,, \tag{5.66}$$

$$\tilde{\mathcal{X}} \equiv \frac{1}{\tilde{n}^{\mathrm{eq}}} \int \frac{\mathrm{d}^3k}{(2\pi)^3} f^{\mathrm{eq}}(k)\left[1 - f^{\mathrm{eq}}(k)\right] \mathcal{X}(k)\,. \tag{5.67}$$

Depending on the quantity in the kinetic equation we use different strategies of averaging:

1. **Momentum-averaging:** The backreaction terms (5.54) is of the second type: $\tilde{\gamma}_{\pm}$. We find that one may neglect the term of second order $f^{\rm eq}(k)$ if $\tilde{\gamma}_{\pm}$ is not IR enhanced by powers smaller than $|\mathbf{k}|^{-2}$ for small $|\mathbf{k}|$. The same holds for $\tilde{n}^{\rm eq}$. This is true for $\tilde{\gamma}_{+}$, which is why

$$\tilde{\gamma}_{+} \simeq \frac{1}{n^{\rm eq}} \int \frac{\mathrm{d}^3 k}{(2\pi)^3} f^{\rm eq}(k) \gamma_{+}(k) \equiv \gamma_{+}^{\rm av} \,, \tag{5.68}$$

with the numerical value $\gamma_{+}^{\rm av} \simeq 0.012$ that has been derived in ref. [146] based on refs. [125, 147]. This approximation induces an error not larger than $\mathcal{O}(40\%)$. In contrast to $\tilde{\gamma}_{+}$, $\tilde{\gamma}_{-}$ receives an additional factor of $M^2/|\mathbf{k}|^2$. This IR enhancement requires to consider the complete expression

$$\tilde{\gamma}_{-} = \frac{1}{\tilde{n}^{\rm eq}} \int \frac{\mathrm{d}^3 k}{(2\pi)^3} f^{\rm eq}(k) \left[1 - f^{\rm eq}(k)\right] \gamma_{-}(k) \equiv \gamma_{-}^{\rm av} \,, \tag{5.69}$$

since the simplification from above cannot be used any more. The quantities $\gamma_{\pm}(k)$ and $\mathfrak{h}_{\pm}(k)$ both appear with the deviation δf and are thus of the first type. Assuming the heavy neutrinos to be in kinetic equilibrium, i.e. when the relation $\delta f(k)/f(k)^{\rm eq} \simeq \delta n/n^{\rm eq}$ is fulfilled, one can approximate the damping rate from eq. (5.53)

$$\gamma_{+} = \frac{1}{\delta n} \int \frac{\mathrm{d}^3 k}{(2\pi)^3} \delta f(k) \gamma_{+}(k) \simeq \frac{1}{n^{\rm eq}} \int \frac{\mathrm{d}^3 k}{(2\pi)^3} f^{\rm eq}(k) \gamma_{+}(k) = \gamma_{+}^{\rm av} \,, \tag{5.70}$$

and accordingly

$$\mathfrak{h}_{\pm}^{\rm th} = \frac{1}{\delta n} \int \frac{\mathrm{d}^3 k}{(2\pi)^3} \delta f(k) \mathfrak{h}_{\pm}^{\rm th}(k) \simeq \frac{1}{n^{\rm eq}} \int \frac{\mathrm{d}^3 k}{(2\pi)^3} f^{\rm eq}(k) \mathfrak{h}_{\pm}^{\rm th}(k) \,, \tag{5.71}$$

$$\mathfrak{h}^{\rm EV} = \frac{1}{\delta n} \int \frac{\mathrm{d}^3 k}{(2\pi)^3} \delta f(k) \mathfrak{h}^{\rm EV}(k) \simeq \frac{1}{n^{\rm eq}} \int \frac{\mathrm{d}^3 k}{(2\pi)^3} f^{\rm eq}(k) \mathfrak{h}^{\rm EV}(k) \,. \tag{5.72}$$

2. **Evaluation at the average momentum:** In case of the damping term γ_{-} from eq. (5.53) one cannot simply assume the heavy neutrino to be in kinetic equilibrium since the production is enhanced for soft momenta $|\mathbf{k}|$. Therefore, we limit ourselves to that momentum mode that most realistically represents the production of the heavy neutrinos, which is given by the average momentum

$$|\mathbf{k}_{\rm av}| \equiv \frac{1}{n^{\rm eq}} \int \frac{\mathrm{d}^3 k}{(2\pi)^3} |\mathbf{k}| f^{\rm eq}(k) = \frac{7\pi^4 T}{180\zeta(3)} \simeq 3.15\, T \,. \tag{5.73}$$

Consequently, we have

$$\gamma_{-} = \frac{1}{\delta n} \int \frac{\mathrm{d}^3 k}{(2\pi)^3} \delta f(k) \gamma_{-}(k) \simeq \gamma_{-}(|\mathbf{k}_{\rm av}|) \,. \tag{5.74}$$

The kinetic equation (5.50) for the deviation of the number density of the heavy neutrinos will be coupled to the evolution equation for the charge densities of the SM leptons. Therefore, it makes sense to relate the chemical potentials of the SM particles to their number densities. Due to fast gauge interactions one can assume that charged field are kept in

kinetic equilibrium. Consequently, we can describe a particle X by modified Fermi-Dirac and Bose-Einstein distribution functions to linear order in the chemical potentials

$$f_X = \frac{1}{\mathrm{e}^{\beta(k^0-\mu_X)} \pm 1} = f_X^{\mathrm{eq}} + \delta f_X \,, \tag{5.75}$$

$$\delta f_X = \frac{\mathrm{e}^{\beta k^0}}{(\mathrm{e}^{\beta k^0} \pm 1)^2} \mu_X \,. \tag{5.76}$$

The charge density of X, as the difference between the number density of particles and antiparticles, is then proportional to the chemical potential

$$q_X = \int \frac{\mathrm{d}^3 k}{(2\pi)^3} \left[f_X(|\mathbf{k}|) - (1 - f_X(-|\mathbf{k}|)) \right] = 2\mu_X \int \frac{\mathrm{d}^3 k}{(2\pi)^3} \delta f_X \,, \tag{5.77}$$

such that in comoving coordinates one has

$$q_X = \begin{cases} \frac{a_{\mathrm{R}}^2}{3} \mu_X & \text{for a massless bosons X} \\ \frac{a_{\mathrm{R}}^2}{6} \mu_X & \text{for a massless chiral fermions X} \end{cases} \,. \tag{5.78}$$

Eventually, the momentum-averaged evolution equation for the heavy neutrino number densities is given in terms of charge densities $q_{\ell a}$ and q_ϕ of the LH lepton doublets ℓ_{L}^a and the Higgs field ϕ, respectively,

$$\frac{\mathrm{d}}{\mathrm{d}z} \delta n_h = -\frac{\mathrm{i}}{2} [H_N^{\mathrm{th}} + z^2 H_N^{\mathrm{vac}}, \delta n_h] - \frac{1}{2} \{\Gamma_N, \delta n_h\} + \frac{1}{2} \sum_{a=e,\mu,\tau} \tilde{\Gamma}_N^a \left(q_{\ell a} + \frac{1}{2} q_\phi \right) \,, \tag{5.79}$$

with the momentum-independent components

$$H_N^{\mathrm{vac}} = \frac{\pi^2}{18\zeta(3)} \frac{a_{\mathrm{R}}}{T_{\mathrm{ref}}^3} \left(\mathrm{Re}[M^\dagger M] + \mathrm{i}h \mathrm{Im}[M^\dagger M] \right) \,, \tag{5.80}$$

$$H_N^{\mathrm{th}} = \frac{a_{\mathrm{R}}}{T_{\mathrm{ref}}} \left(\mathfrak{h}_+^{\mathrm{th}} \Upsilon_{+h} + \mathfrak{h}_-^{\mathrm{th}} \Upsilon_{-h} \right) + \mathfrak{h}^{\mathrm{EV}} \frac{a_{\mathrm{R}}}{T_{\mathrm{ref}}} \mathrm{Re}[Y Y^\dagger] \,, \tag{5.81}$$

$$\Gamma_N = \frac{a_{\mathrm{R}}}{T_{\mathrm{ref}}} \left(\gamma_+ \Upsilon_{+h} + \gamma_- \Upsilon_{-h} \right) \,, \tag{5.82}$$

$$\tilde{\Gamma}_N^a = h \frac{a_{\mathrm{R}}}{T_{\mathrm{ref}}} \left(\tilde{\gamma}_+ \Upsilon_{+h}^a - \tilde{\gamma}_- \Upsilon_{-h}^a \right) \,, \tag{5.83}$$

with

$$\Upsilon_{hij}^a = \mathrm{Re}[Y_{ia} Y_{aj}^\dagger] + \mathrm{i}h \mathrm{Im}[Y_{ia} Y_{aj}^\dagger] \,, \tag{5.84}$$

$$\Upsilon_{hij} = \sum_a \Upsilon_{hij}^a \,. \tag{5.85}$$

5.2 EVOLUTION OF LEPTON CHARGES

In this section quantum kinetic equations for SM leptons are derived in analogy to section 5.1. The relevant charge asymmetries are introduced in subsection 5.2.1 which are needed to describe the evolution of the SM asymmetries. The corresponding kinetic equations are derived in subsection 5.2.2 within the non-equilibrium CTP formalism. In subsection 5.2.3 spectator effects are discussed, which can significantly affect the produced baryon asymmetry due to redistribution of charges.

5.2.1 *Introducing the asymmetries*

It makes sense to introduce a flavour dependent quantity

$$\Delta_a = \frac{B}{3} - L_a \,, \tag{5.86}$$

that is conserved by all SM processes including EW sphaleron processes. Here, L_a are the individual lepton charges of flavour a given by the charges $q_{\ell a}$ of the LH lepton doublets ℓ^a_{L} and charges $q_{\mathrm{R}a}$ of the RH leptons e^a_{R}. The total lepton charge L is then given by the sum over all SM flavours

$$L = \sum_a L_a = \sum_a \left(g_w q_{\ell a} + q_{\mathrm{R}a}\right) \,. \tag{5.87}$$

However, L_a, L and so Δ_a are violated by the Yukawa couplings Y_{ia} and the Majorana mass M. Note that gauge interactions are fast compared to the Yukawa interaction which is due to the smallness of the couplings Y_{ia}. Consequently, the SM particles are kept in kinetic equilibrium and can thus be described by chemical potentials cf. eqs. (5.75)-(5.78). As Majorana particles, heavy neutrinos do not necessarily carry any charge. However, things change in the limit $T \gg M_i$, where helicity states of the heavy neutrinos begin to effectively act as particle and antiparticles. This allows to introduce the sterile charge

$$q_{Ni} \equiv \delta n_{+ii} - \delta n_{-ii} = 2\delta n^{\mathrm{odd}}_{ii} \,, \tag{5.88}$$

which, in the flavour basis where M is diagonal, is given as diagonal entry of the helicity-odd deviations of the number density from equilibrium. With the sterile charge q_N one can define a generalised lepton number

$$\tilde{L} = g_w \sum_a q_{\ell a} + \sum_i q_{Ni} \,, \tag{5.89}$$

which is motivated by looking at the Yukawa terms in the Lagrangian (2.46), where only the LH SM leptons couple to the heavy neutrinos. $\tilde{L}$ is approximately conserved in the ultrarelativistic limit $T \gg M_i$ up to terms of order M_i^2/T^2, i.e. the processes described by the transport coefficients γ_+ and $\mathfrak{h}^{\mathrm{th}}_+$ cannot violate $\tilde{L}$ in that limit, while γ_- and $\mathfrak{h}^{\mathrm{th}}_-$ do not conserve $\tilde{L}$, cf. eqs. (5.68)-(5.71) and eq. (5.74). Note that $\tilde{L}$ should not be confused with $\bar{L}$ from subsection 2.2.4, cf. ref. [3] for a more detailed discussion.

5.2.2 *Kinetic equations for lepton charges*

The derivation of the equations describing the evolutions of the SM charge densities happens analogously to the derivation of the kinetic equations of the heavy neutrino in section 5.1. However, at temperatures relevant for the generation of asymmetries off-diagonal correlations can be neglected because these are erased by μ and τ Yukawa couplings as described in more detail in the fully flavoured regime [49, 50, 124, 148, 149]. Therefore the evolution of the SM charge density is derived from the kinetic equation (3.49). For a SM flavour a it reads

$$\frac{\mathrm{d}}{\mathrm{d}t} q_{\ell a} = \int \frac{\mathrm{d}^4 k}{(2\pi)^4} \mathrm{tr}\left[\mathrm{i}\Sigma^{>}_{\ell a}(k) P_{\mathrm{L}} \mathrm{i}S^{<}_{\ell a}(k) - \mathrm{i}\Sigma^{<}_{\ell a}(k) P_{\mathrm{L}} \mathrm{i}S^{>}_{\ell a}(k)\right] \,. \tag{5.90}$$

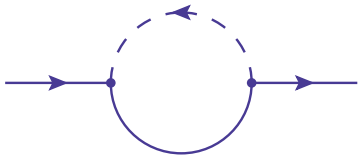

FIGURE 5.4: Self-energy diagram for SM leptons with a Higgs and a heavy neutrinos running in the loop.

The collision term, as the RH side of this equation depends on the SM lepton self-energy $\Sigma_{\ell a}$. In analogy to the heavy neutrino self-energy this can be derived as the functional derivative of the bubble diagram 5.2 such that

$$\mathrm{i}\Sigma^{cd}_{\ell a}(x,y) = cd\frac{\partial\Gamma_2}{\partial S^{dc}_{\ell a}(y,x)} = Y^*_{ia}Y^T_{aj}P_{\mathrm{R}}(\mathrm{i}S_N)^{cd}_{ij}(x,y)P_{\mathrm{L}}\mathrm{i}\Delta^{dc}_{\phi}(y,x)\,, \tag{5.91}$$

which is chosen such that it is diagonal in SU(2) flavour space. In Wigner space, cf. eq. (3.31), this transforms to

$$\mathrm{i}\not{\Sigma}^{cd}_{\ell a}(k) = Y^*_{ia}Y^T_{aj}\int\frac{\mathrm{d}^4k'}{(2\pi)^4}\frac{\mathrm{d}^4k''}{(2\pi)^4}(2\pi)^4\delta(k-k'-k'')P_{\mathrm{R}}\mathrm{i}S^{cd}_{Nij}(k')P_{\mathrm{L}}\mathrm{i}\Delta^{dc}_{\phi}(-k'')\,, \tag{5.92}$$

and is shown in figure 5.4. When inserting this expression for $\mathrm{i}\not{\Sigma}_{\ell a}$ into the collision term of eq. (5.90) and additionally making use of eqs. (5.4) and (5.5) the evolution equation can be recast into the form

$$\frac{\mathrm{d}}{\mathrm{d}t}q_{\ell a} = -\sum_{i,j}Y^*_{ia}Y^T_{aj}\int\frac{\mathrm{d}^4k}{(2\pi)^4}\mathrm{tr}\left[P_{\mathrm{L}}\mathrm{i}\hat{\Sigma}^{>}_{N\mathrm{R}a}(k)P_{\mathrm{R}}\mathrm{i}S^{<}_{Nij}(k) - P_{\mathrm{L}}\mathrm{i}\hat{\Sigma}^{<}_{N\mathrm{R}a}(k)P_{\mathrm{R}}\mathrm{i}S^{>}_{Nij}(k)\right]\,, \tag{5.93}$$

such that it only depends on the heavy neutrino quantities $\mathrm{i}\not{\Sigma}_{\ell a}$ and $\mathrm{i}S_N$. For small chemical potentials one can linearise this equation in the deviations $\mathrm{i}\delta\not{\Sigma}_{\ell a}$ and $\mathrm{i}\delta S_N$, which are driven by the chemical potentials of the SM lepton and the Higgs, such that

$$\begin{aligned}\frac{\mathrm{d}}{\mathrm{d}t}q_{\ell a} = &-\sum_{i,j}Y^*_{ia}Y^T_{aj}\int\frac{\mathrm{d}^4k}{(2\pi)^4}\mathrm{tr}\left[P_{\mathrm{L}}\mathrm{i}\delta\hat{\Sigma}^{>}_{N\mathrm{R}a}(k)P_{\mathrm{R}}\mathrm{i}S^{<}_{Nij}(k) - P_{\mathrm{L}}\mathrm{i}\delta\hat{\Sigma}^{<}_{N\mathrm{R}a}(k)P_{\mathrm{R}}\mathrm{i}S^{>}_{Nij}(k)\right]\\ &-\sum_{i,j}Y^*_{ia}Y^T_{aj}\int\frac{\mathrm{d}^4k}{(2\pi)^4}\mathrm{tr}\left[2P_{\mathrm{L}}\hat{\Sigma}^{\mathcal{A}}_{N}(k)P_{\mathrm{R}}\mathrm{i}\delta S_{Nij}(k)\right]\,,\end{aligned} \tag{5.94}$$

where we use eqs. (5.7) and (5.8) that hold for zero chemical potential in the second term. The first term can be simplified when making use of the linearised KMS relation (5.13). Applying the KMS relation in equilibrium (5.14) leads to

$$\begin{aligned}\frac{\mathrm{d}}{\mathrm{d}t}q_{\ell a} = &-4\sum_{i,j}Y^*_{ia}Y^T_{aj}\frac{\mu_{\ell a}+\mu_{\phi}}{T}\int\frac{\mathrm{d}^4k}{(2\pi)^4}\frac{f_{\mathrm{F}}(1-f_{\mathrm{F}})}{1-2f_{\mathrm{F}}}\mathrm{tr}\left[P_{\mathrm{L}}\mathrm{i}\hat{\Sigma}^{\mathcal{A}}_{N}(k)P_{\mathrm{R}}\mathrm{i}\bar{S}^{+}_{Nij}(k)\right]\\ &-\sum_{i,j}Y^*_{ia}Y^T_{aj}\int\frac{\mathrm{d}^4k}{(2\pi)^4}\mathrm{tr}\left[2P_{\mathrm{L}}\hat{\Sigma}^{\mathcal{A}}_{N}(k)P_{\mathrm{R}}\mathrm{i}\delta S_{Nij}(k)\right]\,.\end{aligned} \tag{5.95}$$

With the Lorentz decomposition (5.25) and with the zero width approximation, cf. eqs. (5.37) and (5.38) one can use eqs. (5.40) and (5.41) for the heavy neutrino propagator. There-

fore, when taking the Dirac trace and performing the sum over the helicity, as well as performing the k^0 integral into a sum over k^0 due to the delta function, one has

$$\frac{\mathrm{d}}{\mathrm{d}t}q_{\ell a} = -\sum_i Y^*_{ia}Y^T_{ai}\frac{\mu_{\ell a}+\mu_\phi}{T}\int\frac{\mathrm{d}^3k}{(2\pi)^3}\sum_{\mathrm{sign}(k^0)=\pm} f_{\mathrm{F}}(1-f_{\mathrm{F}})\frac{2k\cdot\hat{\Sigma}^{\mathcal{A}}_N\mathrm{sign}(k^0)}{\sqrt{|\mathbf{k}|^2+\bar{M}^2}}$$
$$+\sum_{i,j}Y^*_{ia}Y^T_{ai}\int\frac{\mathrm{d}^3k}{(2\pi)^3}\sum_{\mathrm{sign}(k^0)=\pm}\frac{(k+\tilde{k})\hat{\Sigma}^{\mathcal{A}}_N\delta f_{0+ij}+(k-\tilde{k})\hat{\Sigma}^{\mathcal{A}}_N\delta f_{0-ij}}{\sqrt{|\mathbf{k}|^2+\bar{M}^2}}\,, \tag{5.96}$$

where the term containing $\bar{M}$ is traceless. Performing the sum over $k^0 = \pm\sqrt{|\mathbf{k}|^2+\bar{M}^2}$ and using that $(k\pm\tilde{k})\hat{\Sigma}^{\mathcal{A}}_N \to -(k\mp\tilde{k})\hat{\Sigma}^{\mathcal{A}}_N$ under $k^0\to -k^0$ implies

$$\frac{\mathrm{d}}{\mathrm{d}t}q_{\ell a} = -\frac{T}{g_w}\sum_i Y^*_{ia}Y^T_{ai}\left(q_{\ell a}+\frac{1}{2}q_\phi\right)\frac{1}{\tilde{n}^{\mathrm{eq}}}\int\frac{\mathrm{d}^3k}{(2\pi)^3}f_{\mathrm{F}}(1-f_{\mathrm{F}})(\gamma_+(k)+\gamma_-(k))$$
$$+\frac{T}{g_w}\sum_{i,j}Y^*_{ia}Y^T_{aj}\sum_{h=\pm}\int\frac{\mathrm{d}^3k}{(2\pi)^3}\gamma_h(k)\left(\delta f_{+hij}-\delta f^*_{-hij}\right)\,. \tag{5.97}$$

We have used that $q_{\ell a}T = \mu_{\ell a}\,\tilde{n}^{\mathrm{eq}}$ and $q_\phi T = 2\mu_\phi\,\tilde{n}^{\mathrm{eq}}$, cf. eq. (5.64). In comoving coordinates we can express the evolution equation for the SM leptons as

$$\frac{\mathrm{d}}{\mathrm{d}z}q_{\ell a} = -\frac{\tilde{\gamma}_+ + \tilde{\gamma}_-}{g_w}\frac{a_{\mathrm{R}}}{T_{\mathrm{ref}}}\sum_i Y^*_{ia}Y^T_{ai}\left(q_{\ell a}+\frac{1}{2}q_\phi\right)+\frac{1}{T_{\mathrm{ref}}}\tilde{S}_a\,, \tag{5.98}$$

$$\tilde{S}_a = \frac{a_{\mathrm{R}}}{g_w}\sum_{h=\pm}\gamma_h\mathrm{tr}\left[(\delta n_{+h}-\delta n^*_{-h})\,\Upsilon^a_h\right]\,, \tag{5.99}$$

with the momentum-averaged rates $\gamma_\pm$ from eq. (5.70) and (5.74) and $\tilde{\gamma}_\pm$ from eqs. (5.68) and (5.69), respectively. Introducing the trace over the heavy neutrino indices, i.e. $\mathrm{tr}(\delta n\Upsilon) = \sum_{ij}(\delta n_{ij}\Upsilon_{ji})$, allows to write the $\tilde{S}_a$ term in a flavour covariant way. In some cases it might be useful to break this covariant form by extracting the δn_{ii} term from $\tilde{S}_a$ and shifting it into the first term of eq. (5.98). Therefore, the evolution of the SM leptons

$$\frac{\mathrm{d}q_{\ell a}}{\mathrm{d}z} = -\frac{1}{T_{\mathrm{ref}}}\sum_{h=\pm}W^h_a\left(q_{\ell a}+\frac{1}{2}q_\phi - hq_{Ni}\right)+\frac{1}{T_{\mathrm{ref}}}S_a\,, \tag{5.100}$$

is divided into a washout term with the operator

$$W^\pm_a = \frac{a_{\mathrm{R}}}{g_w}\tilde{\gamma}_\pm\sum_i Y_{ia}Y^\dagger_{ai}\,, \tag{5.101}$$

that describes the chemical equilibration of the charges with $q_{Ni} = 2\delta n^{\mathrm{odd}}_{ii}$, and into a source term, most conveniently expressed in term of the helicity-even and helicity-odd correlations,

$$S_a = 2\frac{a_{\mathrm{R}}}{g_w}\sum_{i\neq j}Y^*_{ia}Y_{ja}\sum_{h=\pm}\gamma_h\left[\mathrm{iIm}(\delta n^{\mathrm{even}}_{ij})+h\mathrm{Re}(\delta n^{\mathrm{odd}}_{ij})\right]\,, \tag{5.102}$$

that accounts for the generation of the SM charges through off-diagonal correlations δn_{ij}. Eventually, the differential equation (5.100) describing the evolution of SM forms a coupled system of differential equations for the SM lepton charges and the sterile charges with eq. (5.79). This coupled system can be solved by also transforming eq. (5.79) into helicity-even and helicity-odd parts and seeking for numerical solutions. It might however be beneficial to study the behaviour of this system analytically. Different parameter regions allow for approximate analytic solutions, cf. section 5.5 and 5.6.

5.2.3 *Effects from spectator fields*

Although ℓ_{L} and ϕ are the only particles of the SM that interact with the heavy neutrinos, the remaining SM particles can have some non-zero charge. Consequently, so-called spectator fields contribute to the chemical equilibration and redistribute charges during leptogenesis. As the washout is only sensitive to the L_a, the spectator processes are the reason for effectively hiding some asymmetries, such that they have an effect on the final result for the baryon asymmetry [150, 151]. Quantitatively, we incorporate the effect of the spectator fields by relating all the quantities appearing in the evolution equation of the lepton doublets to the asymmetries Δ_a, cf. eq. (5.86). The electron is the SM particle with the tiniest SM Yukawa coupling. As a consequence, at $T \lesssim 10^5\,\mathrm{GeV}$ all the SM Yukawa couplings have reached the state of chemical equilibrium [152]. This leads to constraints on the chemical potentials

$$\mu_{q_{\mathrm{L}}^a} - \mu_{u_{\mathrm{R}}^a} + \mu_\phi = 0\,, \tag{5.103}$$

$$\mu_{q_{\mathrm{L}}^a} - \mu_{d_{\mathrm{R}}^a} - \mu_\phi = 0\,, \tag{5.104}$$

$$\mu_{\ell_{\mathrm{L}}^a} - \mu_{e_{\mathrm{R}}^a} - \mu_\phi = 0\,, \tag{5.105}$$

where the index a labels the three SM generations. At temperatures relevant for the generation of asymmetries, both EW and strong sphalerons are in equilibrium and constrain the chemical potential further

$$g_s(\mu_{q_{\mathrm{L}}^1} + \mu_{q_{\mathrm{L}}^2} + \mu_{q_{\mathrm{L}}^3}) + \mu_{\ell_{\mathrm{L}}^1} + \mu_{\ell_{\mathrm{L}}^2} + \mu_{\ell_{\mathrm{L}}^3} = 0\,, \tag{5.106}$$

$$g_w(\mu_{q_{\mathrm{L}}^1} + \mu_{q_{\mathrm{L}}^2} + \mu_{q_{\mathrm{L}}^3}) - (\mu_{u_{\mathrm{R}}^1} + \mu_{u_{\mathrm{R}}^2} + \mu_{u_{\mathrm{R}}^3}) - (\mu_{d_{\mathrm{R}}^1} + \mu_{d_{\mathrm{R}}^2} + \mu_{d_{\mathrm{R}}^3}) = 0\,, \tag{5.107}$$

where $g_s = 3$ accounts for the three colour states. A last condition is given by the fact of a vanishing weak hypercharge

$$g_w Y_\phi q_\phi + \sum_{a=e,\mu,\tau} \left(g_w g_s Y_{q_{\mathrm{L}}^a} q_{q_{\mathrm{L}}^a} + g_w Y_{\ell_{\mathrm{L}}^a} q_{\ell_{\mathrm{L}}^a} + g_s Y_{u_{\mathrm{R}}^a} q_{u_{\mathrm{R}}^a} + g_s Y_{d_{\mathrm{R}}^a} q_{d_{\mathrm{R}}^a} + Y_{e_{\mathrm{R}}^a} q_{e_{\mathrm{R}}^a} \right) = 0\,. \tag{5.108}$$

It is now possible to relate the charge densities of the doublet leptons q_ℓ and of the Higgs boson q_ϕ to the asymmetries Δ by solving these equations. One obtains $q_\ell = A\Delta$ and $q_\phi = C\Delta$ with a matrix A and a vector C that are given by

$$A = \frac{1}{711} \begin{pmatrix} -221 & 16 & 16 \\ 16 & -221 & 16 \\ 16 & 16 & -221 \end{pmatrix}\,, \quad C = -\frac{8}{79} \begin{pmatrix} 1 & 1 & 1 \end{pmatrix}\,, \tag{5.109}$$

with the column vectors $q_\ell = (q_{\ell 1}, q_{\ell 2}, q_{\ell 3})^T$ as well as $\Delta = (\Delta_1, \Delta_2, \Delta_3)^T$ in flavour space. Accordingly, one may express the baryon asymmetry B and also the asymmetry in the doublet leptons in terms of Δ:

$$B = \frac{28}{79} \sum_a \Delta_a\,, \qquad B = -\frac{4}{3} \sum_a q_{\ell a}\,. \tag{5.110}$$

It is worth mentioning that this procedure recovers the well-known sphaleron conversion factor $B = \frac{28}{79}(B-L)$ [153]. An $\mathcal{O}(10\%)$ correction to this value arises due to the crossover nature of the EWSB as the EW sphalerons begin to continuously freeze out at temperatures higher than the EW scale [154, 155]. It might be interesting to include the time dependent rate of the EW sphaleron transitions in order to minimise this error. This will lead to temperature dependent conversion factor, which, however, is beyond the scope of this thesis.

5.3 DETERMINATION OF TRANSPORT COEFFICIENTS

Within the last sections the kinetic equations for the heavy neutrinos have been derived. Solution can be found by solving the coupled set of differential equations of both the heavy neutrinos (5.79) and the SM leptons (5.100). These equations depend on transport coefficients such as the damping rates $\gamma_\pm$, cf. eqs. (5.56) and (5.57), the thermal correction to the heavy neutrino mass $\mathfrak{h}^{\rm th}_\pm$, cf. eqs. (5.59) and (5.60), as well as on the modification of the heavy neutrino mass by the background Higgs EV $\mathfrak{h}^{\rm EV}$, cf. eq. (5.61), during the EWSB. These coefficients will be discussed and quantified in the following, while momentum-averaged expressions will be provided.

The effect from the Higgs EV is quantified in subsection 5.3.1, while the modification of the heavy neutrino mass due to thermal effects is discussed in subsection 5.3.2. In subsection 5.3.3 recent approaches to damping rates are mentioned and generalised. Particularly, a leading order derivation for LNV damping rates is provided within this subsection.

RELATIVISTIC APPROXIMATION: The coefficients such as the damping rates and the thermal masses depend on the combinations $k \pm \tilde{k}$. Since $(k \pm \tilde{k})\hat{\Sigma}^{\mathcal{A}}_N \to -(k \mp \tilde{k})\hat{\Sigma}^{\mathcal{A}}_N$ under $k^0 \to -k^0$ it is sufficient to use $\mathrm{sign}(k^0) = 1$. Further, we assume that momenta are sufficiently hard, i.e. $|\mathbf{k}| \sim T$. This allows us to perform a relativistic expansion in $M/|\mathbf{k}|$, such that

$$k^0 = \sqrt{|\mathbf{k}|^2 + M^2} = |\mathbf{k}| + \frac{M^2}{2|\mathbf{k}|} + \mathcal{O}\left(\frac{M^2}{|\mathbf{k}|^2}\right) . \tag{5.111}$$

To first non-vanishing order in $M/|\mathbf{k}|$ the combinations of k and $\tilde{k}$ are then given by

$$k + \tilde{k} \simeq \left(2|\mathbf{k}| + \frac{M^2}{2|\mathbf{k}|}\right)\begin{pmatrix}1\\ \hat{\mathbf{k}}\end{pmatrix} , \tag{5.112}$$

$$k - \tilde{k} \simeq \frac{M^2}{2|\mathbf{k}|}\begin{pmatrix}1\\ -\hat{\mathbf{k}}\end{pmatrix} . \tag{5.113}$$

This translates to the approximations shown in eqs. (5.56)-(5.57) and (5.59)-(5.60). Note that in ref. [2] an ultrarelativistic approximation, $|\mathbf{k}| = k^0\mathrm{sign}(k^0)$, has been used such that only terms up to $\mathcal{O}(M^2/|\mathbf{k}|^2)$ have been considered. In this case $k \simeq \tilde{k}$ and $\gamma_- = \mathfrak{h}^{\rm th}_- = 0$. We will extend this study up to the next non-vanishing order in $M^2/|\mathbf{k}|^2$ and consequently have to compute the terms γ_- and $\mathfrak{h}^{\rm th}_-$.

5.3.1 *The effect from the background Higgs field*

Due to the crossover nature of the SM the background Higgs field starts to continuously follow a temperature dependent Higgs field EV $v(T)$. The Hermitian part of the self-energy (5.11), which is shown in the bottom row of figure 5.3, can be solved at leading order. In this case, using the tree-level expression for the lepton propagator, the effect of the EV of the Higgs field on to the Hermitian self-energy is given by eq. (5.61) and reads

$$\mathfrak{h}^{\rm EV}(k,z) = \frac{2}{k^0}\frac{z^2v^2(z)}{T^2_{\rm ref}}a_{\rm R} , \tag{5.114}$$

and does not only depend on k but also in the coordinate z due to the temperature dependent EV. At tree-level the spectral self-energy vanishes exactly. Within this thesis we

neglect higher order effects such that there is no effect of the Higgs EV on the equilibration of the heavy neutrinos, while it only affects their effective thermal mass at leading order. It is interesting for future works to extend this study to the next non-vanishing order. Refs. [156, 157] have included the effect of the Higgs EV on the damping behaviour of the heavy neutrinos. As shown in eq. (5.72) the momentum-averaged contribution can be obtained by the integral over the equilibrium distribution

$$\mathfrak{h}^{\mathrm{EV}}(z) = \frac{1}{n^{\mathrm{eq}}} \int \frac{\mathrm{d}^3 k}{(2\pi)^3} \mathfrak{h}^{\mathrm{EV}}(k,z) f^{\mathrm{eq}}(k) = \frac{2\pi^2}{18\zeta(3)} \frac{z^2 v^2(z)}{T_{\mathrm{ref}}^2} \,. \tag{5.115}$$

A rather simple approximation for the temperature dependent Higgs EV can be applied [2]:

$$\frac{z^2 v^2(z)}{T_{\mathrm{ref}}^2} \simeq (-3.5 + 4.4z)\vartheta(z - z_v) \,, \tag{5.116}$$

where $z_v \simeq 0.8$ denotes the beginning of the EWSB, i.e. the time where $v(z)$ starts to be non-zero.

5.3.2 *Thermal correction to the right-handed neutrino mass*

The corrections to the heavy neutrino mass $\mathfrak{h}_{\pm}^{\mathrm{th}}$ are given via eqs. (5.59) and (5.60). These depend on the Hermitian part of the reduced self-energy $\hat{\Sigma}_N^H$, that is given eq. (5.9) and graphically illustrated in the top row of figure 5.3. This expression is of the same form as the self-energy expression for the SM leptons with gauge boson exchange, cf. eq. (3.92). In this case the computation of the Hermitian part of heavy neutrino self-energy happens analogously to the one of the SM leptons, cf. appendix A.2. It is additionally mentioned that the non-HTL contribution is subdominant for on-shell heavy neutrinos. The analytic expression in the HTL limit is most conveniently decomposed into the zeroth and into the spatial component

$$\hat{\Sigma}_N^{H0}|_{\mathrm{th}}(k) = \frac{T^2}{16|\mathbf{k}|} \log\left|\frac{k^0 + |\mathbf{k}|}{k^0 - |\mathbf{k}|}\right| , \tag{5.117}$$

$$\hat{\Sigma}_N^{Hi}|_{\mathrm{th}}(k) = \frac{T^2 k^0 k^i}{16|\mathbf{k}|^3} \log\left|\frac{k^0 + |\mathbf{k}|}{k^0 - |\mathbf{k}|}\right| - \frac{T^2 k^i}{8|\mathbf{k}|^2} \,. \tag{5.118}$$

This is the tree-level results as we use the zero-width approximation for the particles running in the loop. Additionally thermal masses and the chemical potentials of those are neglected. To first non-vanishing order in $M_i^2/|\mathbf{k}|^2$ the momentum dependent thermal correction to the heavy neutrino mass can then be expressed in terms of the (reduced) thermal mass of the heavy neutrino

$$\hat{m}_N^2 = k \cdot \hat{\Sigma}_N^H = \frac{T^2}{8} \,. \tag{5.119}$$

With eqs. (5.59) and (5.60) it follows that

$$\mathfrak{h}_{+}^{\mathrm{th}}(k) = \frac{2g_w}{k^0 T} \hat{m}_N^2 \simeq \frac{2g_w}{|\mathbf{k}|T} \hat{m}_N^2 \,, \tag{5.120}$$

$$\mathfrak{h}_{-}^{\mathrm{th}}(k) = \frac{1}{2} g_w \hat{m}_N^2 \frac{M_i^2}{|\mathbf{k}|^2} \frac{1}{k^0 T} \left[-1 + \log\left|\frac{k^0 + |\mathbf{k}|}{k^0 - |\mathbf{k}|}\right|\right] \,. \tag{5.121}$$

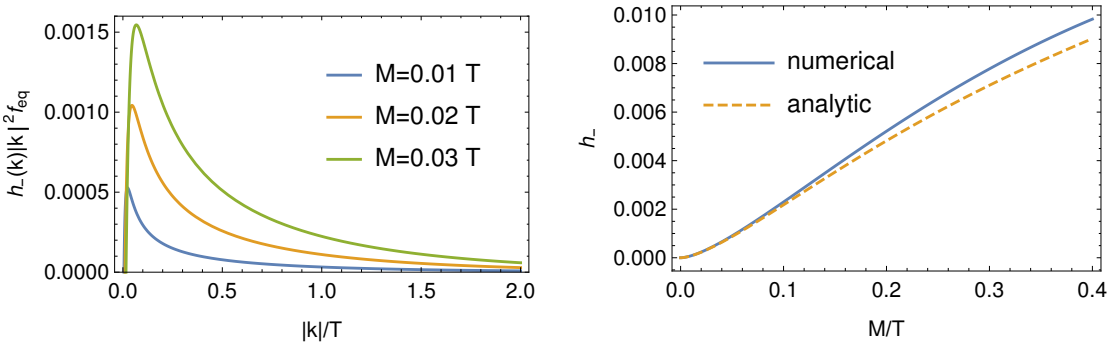

FIGURE 5.5: The left panel shows $|\mathbf{k}|^2\mathfrak{h}_-^{\text{th}}(k)f_{\text{eq}}(k)$ from eq. (5.121) as a function of $|\mathbf{k}|/T$ for different masses. The right panel compares the approximate solution (5.132) for the momentum-averaged LNV thermal correction $\mathfrak{h}_-$ to the full numerical solution.

Note that the non-reduced thermal mass of the heavy neutrino can be read of from eq. (5.8) and is given by

$$m_N^2 = k \cdot \Sigma_N^H = g_w \hat{m}_N^2 \left(Y^* Y^T P_{\text{R}} + Y Y^\dagger P_{\text{L}} \right) . \tag{5.122}$$

The thermal correction for a given momentum mode can be simply calculated from the expressions above. However, we are interested in a momentum-independent treatment of the coupled set of kinetic equations. The momentum-averaged value of $\mathfrak{h}_+^{\text{th}}(k)$ is obtained via eq. (5.71) and reads

$$\mathfrak{h}_+^{\text{th}} = \frac{1}{n^{\text{eq}}} \int \frac{\mathrm{d}^3 k}{(2\pi)^3} \mathfrak{h}_+^{\text{th}}(k) f^{\text{eq}}(k) = \frac{\pi^2}{36\zeta(3)} \simeq 0.23 \,. \tag{5.123}$$

In contrast to that, the approximation of the momentum-average of $\mathfrak{h}_-^{\text{th}}(k)$ is non-trivial for two reasons. First, it has a non-trivial dependence on k, particularly due to the logarithm. Second, $\mathfrak{h}_-^{\text{th}}(k)$ from eq. (5.121) is IR enhanced by a factor $|\mathbf{k}|^{-2}$ compared to $\mathfrak{h}_+^{\text{th}}(k)$ from eq. (5.120). This results in a logarithmic enhanced contribution for small momenta, which will be regulated by the heavy neutrino mass. In this case, small $|\mathbf{k}| \lesssim |\mathbf{k}_{\text{av}}| \simeq 3.15\, T$ are favoured, cf. left panel of figure 5.5, which in general could be at the size of the heavy neutrino mass. However, as we will show in the following, expanding in $M_i^2/|\mathbf{k}|^2$ turns out to be a useful expansion in the low scale leptogenesis scenario we consider in this thesis. This implies a limit on the heavy neutrino mass, $M_i \lesssim 50\,\text{GeV}$ and minimises the regime where the momentum drops below the heavy neutrino mass. In general, as we will compute $\mathfrak{h}_-^{\text{th}}$ as a function of M_i/T, the approximation will break down for larger M_i/T but turns out to be sufficient in low scale leptogenesis scenarios, cf. right panel of figure 5.5. With eq. (5.71) we have to compute

$$\mathfrak{h}_-^{\text{th}} = \frac{1}{n^{\text{eq}}} \int \frac{\mathrm{d}^3 k}{(2\pi)^3} \mathfrak{h}_-^{\text{th}}(k) f^{\text{eq}}(k) \,. \tag{5.124}$$

This adds a factor $|\mathbf{k}|^2 f^{\text{eq}}(k)$ that favours momenta of order $|\mathbf{k}_{\text{av}}| \simeq 3.15\, T$. Consequently, the error for small $|\mathbf{k}|$ gets decreased. As usual we have the freedom to choose $\mathbf{k} = |\mathbf{k}|\mathbf{e}_z$, such that all the angular integration gives a factor 4π. What we are then left with is

$$\mathfrak{h}_-^{\text{th}} \simeq \frac{g_w m_N^2 M_i^2}{3\zeta(3) T^4} \left[J_1\left(\frac{M_i}{T}\right) + J_2\left(\frac{M_i}{T}\right) \right] , \tag{5.125}$$

where the remaining one-dimensional integrals are solely contained in the following functions

$$J_1(x) = -\int_0^\infty \mathrm{d}y \frac{1}{\sqrt{y^2+x^2}} \frac{1}{\mathrm{e}^y+1}\,, \tag{5.126}$$

$$J_2(x) = \int_0^\infty \mathrm{d}y \frac{1}{\sqrt{y^2+x^2}} \log\left|\frac{\sqrt{y^2+x^2}+y}{\sqrt{y^2+x^2}-y}\right| \frac{1}{\mathrm{e}^y+1}\,. \tag{5.127}$$

These expressions can be calculated numerically for different masses M_i. However, we are interested in the parametric dependence of $\mathfrak{h}_-^{\mathrm{th}}$ on the mass M_i. This can be approximately obtained via partial integration such that

$$\begin{aligned} J_1(x) &= \frac{1}{2}\log(x) + \int_0^\infty \mathrm{d}y \log\left(\sqrt{y^2+x^2}+y\right) \frac{\mathrm{d}}{\mathrm{d}y}\left(\frac{1}{\mathrm{e}^y+1}\right) \\ &\simeq \frac{1}{2}\log(x) - \int_0^\infty \mathrm{d}y \log(2y) \frac{\mathrm{e}^y}{(\mathrm{e}^y+1)^2} \\ &\simeq \frac{1}{2}\log(x) - \frac{1}{2}(\log(\pi)-\gamma_{\mathrm{E}})\,, \end{aligned} \tag{5.128}$$

with the Euler–Mascheroni constant $\gamma_{\mathrm{E}} \simeq 0.58$. We have set x to zero in the second integral, which is valid due to an expansion in small $M_i^2/|\mathbf{k}|^2$. Before integrating J_2 by parts, we expand in small $M_i^2/|\mathbf{k}|^2$ such that

$$\begin{aligned} J_2(x) &\simeq \int_0^\infty \mathrm{d}y \frac{\log\left|1+\frac{4y^2}{x^2}\right|}{y\left(1+\frac{x^2}{2y^2}\right)} \frac{1}{\mathrm{e}^y+1} \\ &= \mathcal{J}(0,x) - \int_0^\infty \mathrm{d}y\, \mathcal{J}(y,x) \frac{\mathrm{d}}{\mathrm{d}y}\left(\frac{1}{\mathrm{e}^y+1}\right) \\ &= \frac{\pi^2}{48} + \int_0^\infty \mathrm{d}y\, \mathcal{J}(y,x) \frac{\mathrm{e}^y}{(\mathrm{e}^y+1)^2}\,, \end{aligned} \tag{5.129}$$

with the antiderivative

$$\mathcal{J}(y,x) \equiv \frac{1}{2}\left[\log\left|1+\frac{4y^2}{x^2}\right| \log\left|2+\frac{4y^2}{x^2}\right| + \mathrm{Li}_2\left(-1-\frac{4y^2}{x^2}\right)\right]. \tag{5.130}$$

Performing the remaining integral yields

$$J_2(x) \simeq -\frac{\pi^2}{48} + \frac{\log^2 2}{2} + \log 2\left(\log\frac{\pi}{2} - \gamma_{\mathrm{E}}\right) + 0.667 - \log x\,(\log\pi - \gamma_{\mathrm{E}}) + \frac{\log^2 x}{2}\,. \tag{5.131}$$

Eventually, the leading order parametric dependence on M_i with numerical coefficients is then given by

$$\mathfrak{h}_-^{\mathrm{th}} \simeq \left[2.30 - 0.47\log\left(z^2\frac{\bar{M}^2}{T_{\mathrm{ref}}^2}\right) + 3.47\log^2\left(z\frac{\bar{M}}{T_{\mathrm{ref}}}\right)\right] \times 10^{-2} \times z^2\frac{\bar{M}^2}{T_{\mathrm{ref}}^2}\,. \tag{5.132}$$

5.3.3 *Damping rates for right-handed neutrinos*

The damping rates $\gamma_\pm$ for the heavy neutrinos are defined in eqs. (5.56) and (5.57). These are determined by the spectral part of the reduced self-energies $\hat{\Sigma}_N^{\mathcal{A}}$ with the analytic expression (5.9). For the following discussion we differentiate between the LNC rate γ_+ and the LNV rate γ_-.

LNC RATES: The computation of the LNC rate has been studied in great detail in ref. [125] to leading order in the relevant couplings by relying in the CTP formalism. $2 \leftrightarrow 2$ scattering processes are accounted for by resumming either the Higgs field or the lepton doublet in the loop in self-energy type diagrams. Resummation of the lepton propagator is required in order to regulate IR divergences that otherwise would appear. Consequently, this instead ends up in a logarithmic contribution in the couplings. These scattering processes are enhanced by T^2/M^2 compared to (inverse) decays. These are given by a large amount of vertex-type diagrams and also by collinearly enhanced $1 \leftrightarrow 2$ processes, which requires the resummation of ladder diagrams where an arbitrary number of soft gauge bosons are inserted between the lepton and the Higgs propagator, cf. ref. [140]. The final result for the LNC rate γ_+ is valid up to leading order. With the procedure (5.70) the momentum-averaged rate has been numerically approximated to

$$\gamma_+^{\mathrm{av}} = \int \frac{\mathrm{d}^3 k}{(2\pi)^3} \gamma_+(k) f^{\mathrm{eq}}(k) \simeq 0.012\,. \tag{5.133}$$

Note, however, that this result applies for the damping term (5.82), while for the back-reaction term (5.83) an error of roughly $\sim 40\%$ arises due to the approximation used in eq. (5.68). Nevertheless, we make use of this numerical value for both the damping and the backreaction rate, and accept this uncertainty as it turns out to be still sufficient for our calculation.

LNV RATES: Note that the (inverse) decays contributing to the LNC rate (5.56) are suppressed by M^2/T^2 with respect to the $2 \leftrightarrow 2$ scatterings. However, these $1 \leftrightarrow 2$ processes turn out to dominate over the scattering processes within the computation of the LNV rate (5.57). The reason for this is that the leading contribution for both the scattering processes and the (inverse) decays is proportional to M^2/T^2 due to the factor $k - \tilde{k}$, cf. eq. (5.57). The spectral part of the $1 \leftrightarrow 2$ processes can be obtained by solving the expression (5.9) for the Wightman function

$$\hat{\Sigma}_N^<(k) = \int \frac{\mathrm{d}^4 p}{(2\pi)^4} \frac{\mathrm{d}^4 q}{(2\pi)^4} (2\pi)^4 \delta^4(q - k + p) \mathrm{i} S_\ell^<(p) \mathrm{i} \Delta_\phi^<(q)\,, \tag{5.134}$$

in the zero-width limit, cf. chapter 3,

$$\mathrm{i} S_\ell^<(p) \to -2\pi \delta(p^2 - m_\ell^2) f_\psi(p^0) \mathrm{sign}(p^0) P_{\mathrm{L}} \not{p}\,, \tag{5.135}$$

$$\mathrm{i} \Delta_\phi^<(q) \to 2\pi \delta(q^2 - m_\phi^2) f_\phi(q^0) \mathrm{sign}(q^0)\,, \tag{5.136}$$

and applying the KMS relation (5.14) afterwards. The corresponding Feynman diagram is shown in the top row of figure 5.3.

It is worth mentioning that at high temperatures one obtains the mass hierarchy $m_\phi^2 > m_\ell^2 > m_N^2$ given by the individual thermal masses that directly requires to use to modified dispersion relation of the Higgs field and the lepton. As a consequence, thermal masses must not be neglected. In general, even if the vacuum masses of the Higgs field and lepton are zero, their thermal masses allow for three different parametric channels:

- $M_i > m_\ell + m_\phi$ allows for the decay of the heavy neutrino when its mass is larger than the sum of the masses of the lepton and the Higgs field. For the leptogenesis scenario discussed in this thesis, i.e. for $M \lesssim 50\,\mathrm{GeV}$, this condition cannot be fulfilled.

- $m_\ell > M_i + m_\phi$ allows for the decay of the lepton due to the non-zero thermal mass only if m_ℓ is larger than the sum of the masses of the heavy neutrinos and the Higgs field. However, the condition $m_\ell > m_\phi$ is always false for the thermal masses given in eqs. (3.112)-(3.114).
- $m_\phi > M_i + m_\ell$ is the only channel that can be realised in the leptogenesis scenario discussed in this thesis, i.e. for $M_i \lesssim 50\,\text{GeV}$. The large thermal mass of the Higgs field, which is mainly due to the top quark contribution, allows the Higgs to decay into the lepton and the heavy neutrino. Since m_ϕ and m_ℓ are already determined by the temperature and the gauge couplings at these temperatures, this parametric regimes sets an upper bound on the applicability of our approximations, which depends on the temperature of the plasma due to the running couplings. Note that with the inclusion of the ladder diagrams there is no such an upper bound, cf. ref. [140].

The full integral can be truncated to a single integral

$$I_n(y) = \int_{\omega_-}^{\omega_+} \mathrm{d}x\, x^n \left[1 - f_\psi(x) + f_\phi(y-x)\right] , \tag{5.137}$$

for $n = 0, 1$, when making use of the delta functions, cf. appendix A.3 to get an insight of how to compute spectral self-energies. The remaining integral can be solved analytically, such that the momentum dependent spectral part of the self-energy with thermal masses in the regime $m_\phi > M_i + m_\ell$ is given by

$$\hat{\Sigma}_N^{\mathcal{A}0}(k) = \frac{T^2}{16\pi|\mathbf{k}|}\left[I_1(-\omega_+) - I_1(-\omega_-)\right] , \tag{5.138}$$

$$\hat{\Sigma}_N^{\mathcal{A}i}(k) = \frac{T^2}{16\pi|\mathbf{k}|}\frac{k^i}{|\mathbf{k}|}\left[\frac{k^0}{|\mathbf{k}|}\left[I_1(-\omega_+) - I_1(-\omega_-)\right] - \frac{M_i^2 + m_\ell^2 - m_\phi^2}{2|\mathbf{k}|T}\left[I_0(-\omega_+) - I_0(-\omega_-)\right]\right] , \tag{5.139}$$

with

$$I_0(\omega_\pm) \equiv \log(1 + \mathrm{e}^{\beta\omega_\pm}) - \log(-\mathrm{e}^{\beta k^0} + \mathrm{e}^{\beta\omega_\pm}) , \tag{5.140}$$

$$I_1(\omega_\pm) \equiv x(\log(1 + \mathrm{e}^{\beta\omega_\pm}) - \log(1 - \mathrm{e}^{\beta\omega_\pm - \beta k^0})) + \mathrm{Li}_2(-\mathrm{e}^{\beta\omega_\pm}) - \mathrm{Li}_2(\mathrm{e}^{\beta\omega_\pm - \beta k^0}) , \tag{5.141}$$

which has already been derived in ref. [125]. Since the spectral part of the self-energy is characterised by particles in the loop that are on-shell, non-trivial bounds on the integration limits of $I_{0,1}$ appear such that

$$\begin{aligned}\omega_\pm = {} & \frac{|k^0|}{2M_i^2}\left|M_i^2 + m_\ell^2 - m\phi^2\right| \\ & \pm \frac{\sqrt{(k^0)^2 - M_i^2}}{2M_i^2}\sqrt{M_i^4 + m_\ell^4 + m_\phi^4 - 2M_i^2 m_\ell^2 - 2M_i^2 m_\phi^2 - 2m_\ell^2 m_\phi^2} .\end{aligned} \tag{5.142}$$

Note that we are interested in solving the evolution equation of on-shell heavy neutrinos. Consequently we have specified the analytic solution to $k^2 = M_i^2$. The LNC rate is obtained by contracting $\hat{\Sigma}_N^{\mathcal{A}}$ with k. In this case the I_1 term completely disappears and the LNC rate only depends on I_0. In contrast to that, the LNV rate depends on both the I_0 and the I_1 term. With eqs. (5.57) and (5.138)-(5.141) the LNV damping rate of the heavy neutrino can now be calculated as a function of k.

Note that within this thesis only heavy neutrino masses smaller than $M_i \lesssim 50\,\text{GeV}$ are considered to ensure a relativistic treatment. The lowest temperature relevant for the generation of the baryon asymmetry is given by the EW sphaleron freeze-out temperature, i.e. $T \gtrsim 140\,\text{GeV}$. Consequently, we are able to make approximations that are valid for $M_i \lesssim 0.36\,T$. Note that this is a conservative approximation as usually the asymmetry is generated at higher temperatures around $z \sim 0.1$, or even earlier, such that the relevant masses are $M_i \ll 0.1\,T$. Further, as we will see in the following, a relevant scale, provided that the ladder diagrams [140] are neglected, is given by $m_\phi^2 - m_\ell^2$. These masses are only slowly running with the temperature. Hence, it is sufficient to evaluated these at the EW scale. With $m_\ell = 0.273\,T$ and $m_\phi = 0.682\,T$, one has $m_\phi^2 - m_\ell^2 \simeq 0.39\,T^2$ throughout the whole process. This allows to expand in small $M_i^2/(m_\phi^2 - m_\ell^2)$ and also M_i^2/m_ℓ^2. The non-trivial $|\mathbf{k}| = 0$ mode rate is given by

$$\begin{aligned}\gamma_-(|\mathbf{k}|=0) &= g_w \frac{\left(m_\phi^2 - m_\ell^2 - M_i^2\right)\sqrt{M_i^4 + m_\ell^4 + m_\phi^4 - 2M_i^2 m_\ell^2 - 2M_i^2 m_\phi^2 - 2m_\ell^2 m_\phi^2}}{32\pi M_i^3 \left[\sinh\left(\frac{M_i}{2T}\right) - \sinh\left(\frac{m_\ell^2 - m_\phi^2}{2M_i T}\right)\right]\operatorname{sech}\left(\frac{M_i}{2T}\right) T} \\ &= g_w \frac{\left(m_\phi^2 - m_\ell^2\right)^2}{32\pi M_i^3 T}\operatorname{csch}\left(\frac{m_\phi^2 - m_\ell^2}{2M_i T}\right) + \mathcal{O}\left(\frac{M_i^2}{m_\ell^2}, \frac{M_i^2}{m_\phi^2}\right). \end{aligned} \tag{5.143}$$

Another useful approximation, particularly interesting when extracting a simple dependence of γ_- on M_i, arises when expanding in small $M_i^2/|\mathbf{k}|^2$. With the considerations mentioned above this is valid for momenta $|\mathbf{k}| \gtrsim 0.36\,T$ in the very conservative approximation. In this case one has

$$\gamma_-(k) \simeq \frac{g_w T}{16\pi k^0}\frac{M_i^2}{|\mathbf{k}|^2}\left([I_1(-\omega_+) - I_1(-\omega_-)] + \frac{m_\phi^2 - m_\ell^2}{4|\mathbf{k}|T}\left[I_0(-\omega_+) - I_0(-\omega_-)\right]\right). \tag{5.144}$$

We can simplify eq. (5.144) even further by setting the heavy neutrino mass appearing in the $\omega_\pm$ from eq. (5.142) to zero, while γ_- only globally depends on M_i. In this case gives the limits

$$\lim_{M_i \to 0} \omega_- \to \frac{4|\mathbf{k}|^2 m_\ell^2 + |m_\phi^2 - m_\ell^2|^2}{4|\mathbf{k}||m_\phi^2 - m_\ell^2|} \simeq \frac{|m_\phi^2 - m_\ell^2|}{4|\mathbf{k}|} \equiv \tilde{\omega}_-\,, \tag{5.145}$$

while ω_+ goes to infinity, which further implies

$$\lim_{\omega_+ \to \infty} I_0(-\omega_+) = -|\mathbf{k}|\,, \tag{5.146}$$

$$\lim_{\omega_+ \to \infty} I_1(-\omega_+) = 0\,. \tag{5.147}$$

The approximation used in the second step in eq. (5.144) allows to write the rate in a simple form

$$\gamma_-(k) \simeq \frac{g_w T}{16\pi|\mathbf{k}|}\frac{M_i^2}{|\mathbf{k}|^2}\left[\mathrm{Li}_2\left(\mathrm{e}^{-\beta\tilde{\omega}_- - \beta|\mathbf{k}|}\right) - \mathrm{Li}_2\left(-\mathrm{e}^{-\beta\tilde{\omega}_-}\right)\right]. \tag{5.148}$$

In the limit of large $|\mathbf{k}|$, the thermal masses become negligible compared to $|\mathbf{k}|$. In this case ω_- can be neglected, such that the asymptotic behaviour is given by

$$\lim_{|\mathbf{k}| \to \infty} \gamma_-(|\mathbf{k}|) = g_w \frac{\pi T}{192}\frac{M_i^2}{|\mathbf{k}|^3}\,, \tag{5.149}$$

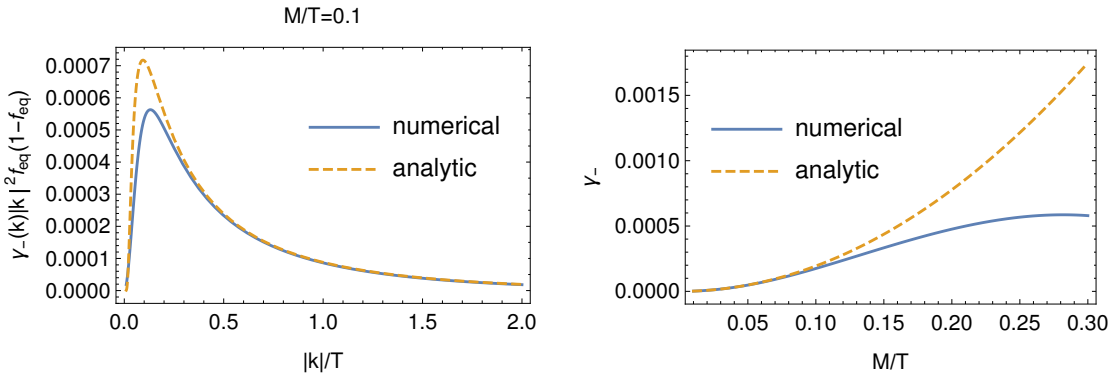

FIGURE 5.6: The left panel demonstrates the breakdown of the approximation $|\mathbf{k}|^2\gamma^-(k)f_{\rm eq}(1-f_{\rm eq})$ from eq. (5.148) for small $|\mathbf{k}|/T$ for a heavy neutrino mass $M_i/T = 0.1$. The right panel compares the approximate solution for the momentum-averaged LNV rate γ_- from eq. (5.151) to the full numerical solution.

where we use that $\mathrm{Li}_2(-1) = -\pi^2/12$. We have already mentioned that the approximation used to derive (5.148) breaks down for $|\mathbf{k}| \lesssim M_i$. This effect can be seen in left panel of figure 5.6, while for larger momenta the approximation is more valid.

Nevertheless, we are interested in a momentum-averaged description of the coupled set of differential equations (5.79) and (5.100). Particularly we use the momentum-averaged value for the backreaction term (5.83), while using the damping rate (5.82) at the average momentum $|\mathbf{k}_{\rm av}| \simeq 3.15\,T$, cf. eqs. (5.69),(5.73) and (5.74). Using eqs. (5.57) and (5.138)-(5.141) the LNV rate at the average momentum is simply evaluated to

$$\gamma_-(|\mathbf{k}_{\rm av}|) \simeq 9.7\times 10^{-4} z^2 \frac{\bar{M}^2}{T_{\rm ref}^2}\,, \tag{5.150}$$

which fulfils the required smallness of $M_i/|\mathbf{k}|$. The momentum-averaged rate, however, needs a non-trivial derivation for the following reasons. As we have seen above, $\gamma_-(k)$ has a complicated dependence on k. When using eq. (5.148), we see that is enhanced in the IR by a factor of $|\mathbf{k}|^2$ compared to $\gamma_+(k)$, which will not only end up in a logarithmic contribution but also the average momentum $|\mathbf{k}|$ is smaller than $|\mathbf{k}_{\rm av}| \simeq 3.15\,T$ for $\gamma_+(k)$, cf. left panel of figure 5.6. Due to this soft enhancement, special care has to be taken because the approximation based on small $M_i^2/|\mathbf{k}|^2$ used to derive eq. (5.148) breaks down if the momentum drops below the mass of the heavy neutrino. Consequently, the higher the mass the higher the error induced by the approximations. Using eq. (5.69), the momentum-averaged rate is computed via the integral

$$\gamma_-^{\rm av} = \frac{1}{\tilde{n}^{\rm eq}}\int \frac{{\rm d}^3k}{(2\pi)^3}\gamma_-(k) f^{\rm eq}(k)(1-f^{\rm eq}(k))\,, \tag{5.151}$$

where the thermal masses $m_\ell, m_\phi \neq 0$ act as regulators to soften the integral for small $|\mathbf{k}|$. Note that the error for small momenta $|\mathbf{k}|$ is decreased as the combination $|\mathbf{k}|^2 f^{\rm eq}(k)(1-f^{\rm eq}(k))$ favours momenta that are of order $|\mathbf{k}_{\rm av}| \simeq 3.15\,T$. Eventually, with eq. (5.148), numerical integration yields

$$\gamma_-^{\rm av} \simeq 2.1\times 10^{-2} z^2 \frac{\bar{M}^2}{T_{\rm ref}^2}\,. \tag{5.152}$$

A comparison between this approximated solution and the full numerical solution is shown in the right panel of figure 5.6. One can see that approximation works well for the relevant masses in the low scale leptogenesis scenario considered in this thesis, i.e. for $M_i \lesssim 0.1\,T$.

5.4 FULL SYSTEM OF DIFFERENTIAL EQUATIONS

This section begins with the discussion of the coupled set of differential equations that describes the leptogenesis scenario from CP-violating oscillations of two heavy RH neutrinos with masses in the GeV-range in subsection 5.4.1. Relevant time scales that not only describe the time of the first oscillations and the time of equilibration but also allow for an analytic treatment of two parameter regions are introduced in subsection 5.4.2. Further, a qualitative discussion of how LNV effects may have an impact on the baryon charge generation is provided in subsection 5.4.3.

5.4.1 *Coupled set of differential equations*

The time evolution in terms of the variable z of the deviation of number densities and off-diagonal flavour correlations of heavy neutrinos δn_h with helicity h from equilibrium is given by eq. (5.79). Together with the equation describing the time evolution of the SM charge densities (5.100), expressed in terms of the quantity Δ_a from eq. (5.86), it forms a coupled set of differential equation:

$$\frac{\mathrm{d}}{\mathrm{d}z}\delta n_h = -\frac{\mathrm{i}}{2}[H_N^{\mathrm{th}} + z^2 H_N^{\mathrm{vac}}, \delta n_h] - \frac{1}{2}\{\Gamma_N, \delta n_h\} + \frac{1}{2}\sum_{a,b=e,\mu,\tau} \tilde{\Gamma}_N^a (A_{ab} + C_b/2)\Delta_b\,, \tag{5.153}$$

$$\frac{\mathrm{d}}{\mathrm{d}z}\Delta_a = \sum_h \frac{\gamma_h^{\mathrm{av}}}{g_w}\frac{a_{\mathrm{R}}}{T_{\mathrm{ref}}}\sum_i Y_{ia}Y_{ai}^\dagger \left(\sum_b (A_{ab} + C_b/2)\Delta_b - h q_{Ni}\right) - \frac{S_a(\delta n_{hij})}{T_{\mathrm{ref}}}\,. \tag{5.154}$$

The matrix A and the vector C accounting for the spectator effects are given in eq. (5.109). H_N^{vac} from eq. (5.80) corresponds to the effective Hamiltonian in vacuum, while the thermal correction H_N^{th} is given by eq. (5.81). This contribution is due to the finite temperature background Higgs field: First, the LNC and LNV thermal corrections $\mathfrak{h}_+^{\mathrm{th}}$ and $\mathfrak{h}_-^{\mathrm{th}}$ to the heavy neutrino mass are given by eqs. (5.123) and (5.132), respectively. Second, the contribution from the Higgs EV $\mathfrak{h}^{\mathrm{EV}}$ during the crossover is shown in eq. (5.115), with the approximate form of the EV in eq. (5.116). The damping matrix Γ_N and the backreaction term $\tilde{\Gamma}_N^a$ in flavour space, given by eqs. (5.82) and (5.83), are the collision terms of this equation due to scattering with particles from the plasma. The LNC damping coefficient γ_+ has already been computed in ref. [146] and is given by γ_+^{av} from eq. (5.133), while the LNV coefficient γ_- has to be evaluated at the average momentum $|\mathbf{k}_{\mathrm{av}}| \simeq 3.15\,T$, cf. eq. (5.150). The source term S_a from eq. (5.102) is driven by the flavour oscillations δn_{hij} of the heavy neutrino for $i \neq j$. The LNC and LNV coefficients γ_+^{av} and γ_-^{av} for the backreaction term are given by eqs. (5.133) and (5.151), respectively. All these coefficients are given in their momentum-averaged form. The procedure of averaging is discussed in eqs. (5.70)-(5.74).

As already mentioned we have the freedom to choose a reference temperature T_{ref} by convenience. An interesting scale is given when the temperature drops below the freeze-out temperature of the EW sphalerons at $T_{\mathrm{ws}} \simeq 130\,\mathrm{GeV}$. For temperatures lower than T_{ws} all the generated baryon asymmetry is not equilibrated by the EW sphalerons any

more and is thus restored. Consequently, it is useful to choose $T_{\rm ref} = T_{\rm ws}$, such that the relevant baryon charge generating processes happen in the regime $z = 0$ to $z = 1$, while the freeze-out happens at $z = 1$.

5.4.2 *Time scales and relevant parameter regimes*

Besides the EW sphaleron freeze-out at $z \sim 1$, the system (5.153)-(5.154) features another two relevant time scales, the oscillation time scale $z_{\rm osc}$ and the equilibration time scale $z_{\rm eq}$. A separation of these two scale allows for approximate analytic solutions. The oscillation time scale corresponds to the time when the heavy neutrinos start to oscillate. It is given by the eigenvalues of $H_N^{\rm vac}$ from eq. (5.80). From $z = 0$ on the universe does not feature any heavy neutrinos. Consequently, they start getting produced out-of-equilibrium until they eventually reach equilibrium. The corresponding temperature scale is referred to as the equilibration time scale and is characterised by the eigenvalues of Γ_N from eq. (5.82). The relevant coefficients will be $\gamma_+ = \gamma_+^{\rm av}$ and $\gamma_-(|\mathbf{k}_{\rm av}|)$, cf. eqs. (5.133) and (5.150). It is worth mentioning that the inclusion of the LNV rate γ_- is only necessary for a small fraction of the leptogenesis parameter space. As we will see in the following sections, analytic approximations are performed for parameters for which LNV effects can be neglected. Note however that these approximate analytic solutions are just for illustrative purposes, while for the full parameter scan, that is needed for chapter 6 we use the full expression including LNV effects.

Due to the form of eq. (5.80), the matrix $H_N^{\rm vac}$ is diagonal in the same flavour basis where M is diagonal. We will refer this to the mass basis. On the contrary, looking at eq. (5.82), Γ_N is diagonal in the basis where Υ_{+h} is diagonal - the interaction basis. This holds if LNV are neglected as otherwise Υ_{-h} contributes with non-zero off-diagonal entries. In general Γ_N is not diagonal when $H_N^{\rm vac}$ is. This misalignment implies flavour oscillations of the heavy neutrinos. They are produced in the interaction basis and start to oscillate due to the commutator of $H_N^{\rm vac}$ in eq. (5.153). One might think that $H_N^{\rm th}$ from eq. (5.81) affects the oscillation time scale as it scales with T^2 with respect to $H_N^{\rm vac}$. Even though it becomes dominant at high temperatures this correction fails to initiate oscillations for two reasons. First, because there is no misalignment between the term that is driven by $\mathfrak{h}_\pm^{\rm th}$ and Γ_N. Second, the term $\mathfrak{h}^{\rm EV}$ only becomes non-zero for $z \gtrsim 0.8$, when oscillations in general have already started. Note that for n_s flavours of heavy neutrinos there are in total n_s equilibration time scales and $n_s(n_s-1)/2$ oscillation time scales. We will use the largest eigenvalue of the matrices $H_N^{\rm vac}$ and Γ_N for classifying the system qualitatively. The two relevant time scales are

$$z_{\rm osc} \simeq \left(a_{\rm R}|M_i^2 - M_j^2|\right)^{-1/3} T_{\rm ref}\,, \tag{5.155}$$

$$z_{\rm eq} \simeq T_{\rm ref}/(\gamma_+^{\rm av} a_{\rm R}||YY^\dagger||)\,, \tag{5.156}$$

for $i \neq j$, where the norm $||\cdot||$ of a Hermitian matrix is given by the absolute value of its largest eigenvalue. Note that we are considering the smallest equilibration time scale. Since $\gamma_+^{\rm av} \ll \gamma_-(|\mathbf{k}_{\rm av}|)$ is fulfilled in low scale leptogenesis scenarios for the relevant z, we use the larger rate $\gamma_+^{\rm av}$ for classifying the smallest equilibration scale. A separation of these two time scales allows for the physically interesting regimes that can also be analytically understood.

OSCILLATORY REGIME: Leptogenesis is said to happen in the oscillatory regime when $z_{\rm osc} \ll z_{\rm eq}$, i.e. when the largest oscillation time scale is still smaller than the fastest equilibration time scale. In this case the heavy neutrinos can perform a large number of oscillations before they finally reach equilibrium. The main baryon charge is generated during the first few oscillations and saturates when they oscillations become fast compared to the Hubble rate. Note, however, that this argument is only true when neglecting LNV effects. When LNV effects are included such a saturation is not achieved as the LNV damping rates are enhanced by z^2 compared to the LNC damping rate, cf. eqs. (5.133) and (5.150). In this case SM charges are continuously produced via the CP-violating oscillations of the heavy neutrinos until they equilibrate.

There are two advantages using analytic approximations. First, such a regime requires small Yukawa couplings. Hence, these couplings can be used as expansion parameters, which allows for a perturbative analysis. Second, particularly due to the smallness of the Yukawa couplings, it is possible to separate the process of leptogenesis into two different processes - the early generation of the asymmetry and the late washout due to the equilibration process. This strict decoupling ends up in a huge simplification when it comes to solving the system (5.153)-(5.154) in the oscillatory regime. Note again that the inclusion of LNV effects spoils this treatment if such effects stop being subdominant.

OVERDAMPED REGIME: On the opposite, the overdamped regime is classified by the fact that at least one heavy neutrino has reached equilibrium before a single oscillation has been performed. Note that the equilibration process and the generation of asymmetries are roughly happening at the same times. Consequently, it is not possible to make use of the procedure applied in the oscillatory regime as discussed above. Scenarios with such a overdamped behaviour are in general more interesting when it comes to experimental searches for heavy neutrinos. This is because the larger Yukawa couplings allow for larger mixings U^2_{ai}, cf. eq. (2.49), which increases the probability of an experimental discovery of the heavy neutrinos. Particularly in the case of two heavy neutrinos, the largest mixings U^2_{ai} can be achieved when the oscillations happen rather late such that the washout has limited time to erase all the asymmetries.

With eqs. (5.155) and (5.156) we can relate the mass difference to the Yukawa couplings in order to determine which regime is given by which choice of parameters. For $i \neq j$ this is given by

$$\frac{||YY^\dagger||\gamma_+^{\rm av} a_{\rm R}^{2/3}}{|M_i^2 - M_j^2|^{1/3}} \begin{cases} \ll 1 & \text{oscillatory} \\ \gg 1 & \text{overdamped} \end{cases} . \tag{5.157}$$

For the example plots presented in the following section we use the scenarios from table 5.1 and limit ourselves to NO.

5.4.3 *Effects from lepton number violating interactions*

Before examining the oscillatory and the overdamped regime in more detail, we shortly comment qualitatively on LNV effects and on how these can affect the baryon charge generation. This might be of interest for readers who are not particularly interested in approximate analytic solutions but rather want to qualitatively understand how leptogenesis from oscillations of heavy neutrinos works.

	I	II	III	IV	V
$\bar{M}$	1 GeV	50 GeV	1 GeV	10 GeV	10 GeV
ΔM^2	$2 \times 10^{-5}\bar{M}^2$	$1 \times 10^{-10}\bar{M}^2$	$1 \times 10^{-6}\bar{M}^2$	$5 \times 10^{-9}\bar{M}^2$	$1 \times 10^{-4}\bar{M}^2$
$\mathrm{Im}\omega$	2.16	0.32	5.01	6.00	5.00
U^2	2.2×10^{-9}	1.4×10^{-12}	6.6×10^{-7}	4.8×10^{-7}	6.5×10^{-8}

TABLE 5.1: Parameters used for the example plots in this work for the different scenarios. Further, NO is used and we use $\alpha_1 = 0$, $\alpha_2 = -\pi$, $\delta = 3\pi/2$ and $\mathrm{Re}\omega = 3\pi/4$. Scenarios I and II describe leptogenesis in the oscillatory regime, while II, III and V correspond to the overdamped regime. Regime I and III do not exhibit any significant effect from LNV processes, while II, IV and V are chosen such that LNV effects are not negligible.

In the low scale leptogenesis scenario we consider within this thesis the mass of the heavy neutrino is smaller than the mass of the W boson, which allows for a relativistic treatment of the relevant kinetic equations. Violation of the generalised lepton number $\tilde{L}$ is due to a non-zero Majorana mass M. One might naively think that LNV effects are subdominant in low scale leptogenesis models since the violation of $\tilde{L}$ is suppressed by M_i^2/T^2. Although we have shown that the LNV damping rates as well as LNV correction to the heavy neutrino thermal mass are small and suppressed by $z^2\bar{M}^2/T_{\mathrm{ref}}^2$ compared to the LNC transport coefficients, there exist parameter regions in the low scale leptogenesis in which such effects affect the evolution and generation of the asymmetries.

LEPTON NUMBER VIOLATION IN THE OSCILLATORY REGIME: In the oscillatory regime the equilibration of the two heavy neutrinos happens roughly at the same times, i.e. at $z_{\mathrm{eq}}^{+} \simeq T_{\mathrm{ref}}/(\gamma_{+}^{\mathrm{av}} a_{\mathrm{R}} ||YY^\dagger||)$ due to LNC processes. With eqs. (5.133) and (5.150) it is obvious that the LNV damping coefficients are suppressed compared to the LNC coefficients, cf. eq. (5.133) and consequently do not change the oscillation time scale. The effect from LNV process might become important for two reasons:

First, the LNV source can violate L and also $\tilde{L}$, such that the generated asymmetry cannot be deleted by LNC effects, through (inverse) decays already at $\mathcal{O}(|YY^\dagger|^2 M_i^2/T^2)$. As will we see in the following section, LNV effects will modify the behaviour of the off-diagonal components of the heavy neutrinos already at $\mathcal{O}(|YY^\dagger|)$. Therefore, the quick saturation of the lepton asymmetries, that are produced via the source term, is only valid when neglecting LNV processes. Thus, if LNV processes are included, the SM asymmetries produced by the source are prevented from a saturation that happens long before the equilibration of the heavy neutrinos. The charge produced by this source might be comparable to the generation of the baryon charge due to the incomplete washout if $M_i^2/T_{\mathrm{ref}}^2 z_{\mathrm{osc}}^2 \sim |YY^\dagger|$. With the naive seesaw relation $|Y_{ai}| \sim \sqrt{m_a \bar{M}_i}/v$ one can approximately argue that this effect becomes important if the asymmetry is produced at times $z \sim z_{\mathrm{osc}} \gtrsim \sqrt{m_a/\bar{M}} \sim 10^{-6}\sqrt{\mathrm{GeV}/\bar{M}}$. We find that especially for small mixing angles U^2 such an effect becomes non-negligible.

Second, independently from the LNV part of the source, an indirect violation of L and thus violation of B is due to the washout that diminishes the flavoured asymmetries with different rates. Hence, such an indirect LNV happens at $\mathcal{O}(|YY^\dagger|^3)$ even in the absence of LNV washout rates. Basically $\tilde{L}$ is conserved but some of the asymmetries can be hidden in q_{Ni} from EW sphaleron transition such that baryon number generation is due to a

change in Δ_a. Besides that, LNV can happen through LNV (inverse) decays. Naively one could argue that these are suppressed by $M_i^2/T_{\rm ref}^2 z_{\rm osc}^2$ compared to the LNC washout rates. However, since the washout is the more important the larger z is, a LNV washout can modify the baryon charge creation when having large heavy neutrino masses, i.e. when $1\,\text{GeV} \ll M_i \ll M_W$, where the upper bound is chosen in such way that the relativistic treatment from section 5.1 does not break down.

Eventually, we can conclude that there exist parameter regions where LNV becomes important. This requires to solve the evolution equations (5.153)-(5.154) numerically. Nevertheless, we find that most of the parameter region is such that LNV is subdominant.

LEPTON NUMBER VIOLATION IN THE OVERDAMPED REGIME: The overdamped regime is characterised by large Yukawa couplings. This happens naturally in the approximate $B-L$ conserving scenario, cf. subsection 2.2.4, where one of the eigenvalues of Υ_{+h} is much larger than the other. This argument also holds for Γ_N, that determines the equilibration of the heavy neutrinos. Consequently, the first heavy neutrino eigenstate equilibrates much earlier than the second one. As we will see in section 5.6, this fast equilibration allows to use quasi-static solutions, which relate the evolution of the first eigenstate as well as the off-diagonal correlation to the slowly evolving second heavy neutrino eigenstate. LNV effects can modify the baryon charge generation in three ways:

First, LNV processes can change the behaviour of how one heavy neutrino equilibrates. Particularly the equilibration for the feebly coupled eigenstate can happen either through mixing with the other eigenstate or through its own damping. In the absence of LNV effects this damping is tiny enough to be neglected due to the smaller eigenvalue of Υ_{+h}. However, when including LNV effects, eigenvalues of Υ_{-h} have to be taken into account. For the first heavy neutrino state this effect is subdominant. In contrast to that, the contribution of the second eigenvalue is of the order of the first eigenvalue times $\bar{M}^2/T^2$. In the case of small mass splittings and large Yukawa couplings, which turns out to delay the equilibration through that mixing, the second eigenvalue might be large enough by the LNV rate to initiate the equilibration of the second eigenstate. Since all the deviations of the heavy neutrinos from equilibrium are mainly determined by the second eigenstate, the whole system of equations (5.153)-(5.154) is affected by the early equilibration.

Second, the LNV part of the source can generate a non-zero $\tilde{L}$ which can only be washed out by the LNV washout. As the LNV washout is suppressed compared to the LNC washout, a sizeable amount of B due to the LNV source can remain even if the Yukawa couplings are large enough to diminish any baryon charge from the LNC source. This has an interesting consequence. When neglecting LNV effects, choosing the mass difference too large would end up in an early charge generation such that the washout has enough time to erase all the produced asymmetries. Consequently, the very large mixing angles are unfavoured for large mass splittings as the washout is too strong due to large Yukawa couplings. However, with the argumentation from above, larger mass splittings are more strongly correlated with large mixing angles when LNV processes are included.

Third, a violation of $\tilde{L}$ can occur through a LNV washout. Analogously to the oscillatory regime, this effect becomes more important when the masses are large, i.e. for the hierarchy $1\,\text{GeV} \ll M_i \ll M_W$.

Eventually, we find that the early equilibration of the feebly coupled heavy neutrino eigenstate can have a significant effect on the baryon charge generation, when having both highly degenerate masses and large Yukawa couplings.

5.5 OSCILLATORY REGIME

In this section analytic approximations to the BAU in the oscillatory regime are derived. This regime is characterised by off-diagonal oscillations of the heavy neutrinos that have to happen much earlier than their equilibration. Such a scenario comes in with two advantages that are helpful for an analytic treatment of the oscillatory regime. First, the separation of scales, i.e. $z_{\rm osc} \ll z_{\rm eq}$, allows for an independent treatment of the generation of the asymmetries in the different SM flavours and the washout, that eventually leads to a non-zero baryon charge. Second a weak and consequently late washout requires a smallness in the Yukawa couplings. This allows for a perturbative analysis in small Yukawa couplings $|YY^\dagger|$ such that the individual steps are characterised by different powers of Yukawa couplings.

The early oscillations together with the early charge generation is quantitatively discussed on subsection 5.5.1, while the late washout is addressed in subsection 5.5.2. For the parameters chosen in these subsection, there is no visible effect from LNV. Possible effects from LNV are covered in subsection 5.5.3.

Note however that treating the early oscillations with the resulting charge generation and the late washout separately is only valid for parameter choices for which LNV effects are subdominant. In comparison to the LNC source the generated charges through the LNV source do not saturate after the first oscillation. Rather a non-zero amount of $\tilde{L}$ is continuously produced until the heavy neutrino equilibrate. In the following two subsections 5.5.1 and 5.5.2, particularly for generating the relevant plots, we choose the parameter scenario I from table 5.1. In this case LNV are negligible. Nevertheless we keep the derivation as general as possible and only neglect the LNV rates when necessary.

PRODUCTION AT EARLY TIMES: Since the universe starts with zero abundance of heavy neutrinos, the heavy neutrino sector begins to be populated due to their own off-diagonal oscillations δn_{ijh} at $|YY^\dagger|$ for $i \neq j$. The source term (5.102) depends exactly on these correlations, such that the charge asymmetries Δ_a in the SM leptons are generated at order $|YY^\dagger|^2$. This production process happens at early times, i.e. at $z \sim z_{\rm osc}$. When only taking the LNC source into account, there are only asymmetries in the flavour states Δ_a but not in the total lepton number, i.e. $\sum_a \Delta_a = 0$, at order $|YY^\dagger|^2$.

WASHOUT AT LATE TIMES: For larger $z \gg z_{\rm osc}$, i.e. at $z \sim z_{\rm eq}$, the produced SM lepton charges relax back to equilibrium via scattering processes. At such late times effects from the off-diagonal correlation average out. In this case, the generation of Δ_a, cf. eq. (5.154) can be described by neglecting the source term S_a, while the kinetic equation for the heavy neutrino, cf. eq. (5.153) is solely driven by the backreaction term $\tilde{\Gamma}_N$ and the damping term Γ_N. The two reduced equations form a coupled set of differential equation properly describing the washout process. In general the corresponding rates are different for the individual flavours. Consequently, the washout process shifts parts of $\sum_a \Delta_a$ into $\sum_i q_{Ni}$ while preserving $\tilde{L}$. EW sphalerons do only couple to Δ_a and not to q_{Ni}. Therefore, a non-zero lepton charge is produced and transferred to a non-zero baryon charge at $|YY^\dagger|^3$. For successful baryogenesis, one needs to require at least one of the heavy neutrinos to be out-of-equilibrium before the EW sphalerons freeze out. Otherwise the baryon charge, that is directly coupled to the lepton charge, gets washed out by the fast EW sphaleron processes.

Note that the following analytic treatment holds for arbitrary n_s, i.e. not only for two almost mass degenerate heavy neutrinos, provided that the shortest oscillation time scale is still faster than the earliest equilibration time scale. Further, we are working in the mass basis, i.e. the flavour basis where M is diagonal. An exemplary plot for the evolution of the different particle densities, i.e. for $\delta n^{\rm even}_{11,22}$, $\delta n^{\rm odd}_{12}$, Δ_a and B, is given in figure 5.7.

5.5.1 *Oscillations at early times*

We will now solve this system (5.153)-(5.154) analytically. Therefore, we will elaborate shortly on the truncation of the differential equation. As already discussed, thermal corrections due to the effective Hamiltonian $H_N^{\rm th}$ dominate at high temperatures over the vacuum part $H_N^{\rm vac}$. However, these are diagonal in the same basis as the one where the heavy neutrinos are produced - the interaction basis. Consequently, there is no misalignment between the mass and the interaction basis. For this reason δn_h commutes with $H_N^{\rm th}$, such that the thermal correction to the effective Hamiltonian is not able to initiate oscillations. Thus, it is reasonable to neglect this effect. The second effect from the thermal correction is due to the crossover nature of the EWSB in the SM. The Higgs begins to settle a non-zero EV that might become important. However, this happens right before the EW sphalerons freeze out, i.e. for $z \gtrsim 0.8$, such that the source term is unaffected. During the production process at early time the backreaction term is of order $|YY^\dagger|^3$ and can consequently be neglected as a higher order effect. It will only become sizeable when the SM lepton charges have already been produced. The equation describing the evolution of the heavy neutrinos deviations can be simplified at $z \sim z_{\rm osc}$:

$$\frac{\mathrm{d}}{\mathrm{d}z}\delta n_h + \frac{\mathrm{i}}{2}z^2[H_N^{\rm vac}, \delta n_h] = -\frac{1}{2}\{\Gamma_N, \delta n_h\}\,. \tag{5.158}$$

We will use eq. (5.158) to describe the oscillations of the heavy neutrinos quantitatively and to show that the charges $q_{Ni} = 2n_i^{\rm odd}$ in the heavy neutrino sector are negligible at early times when neglecting LNV effects. Nevertheless, as the LNV processes conserve $g_w \sum_a q_{\ell a} - \sum_i q_{Ni}$, already at $\mathcal{O}(|YY^\dagger|^2)$ the sum of the LNV source over all SM flavours is non-vanishing and so $g_w \sum_a q_{\ell a} = \sum q_{Ni} \neq 0$. Solutions to eq. (5.158) are obtained when solving for helicity-even and helicity-odd deviations. With eqs. (5.80) and (5.82) the corresponding equations to solve arise from eq. (5.158):

$$\begin{aligned}\frac{\mathrm{d}}{\mathrm{d}z}\delta n_{ij}^{\rm odd} + \mathrm{i}\Omega_{ij}z^2\delta n_{ij}^{\rm odd} = \\ -\sum_{h=\pm}\frac{\gamma_h}{2}\frac{a_{\rm R}}{T_{\rm ref}}\left(\{\mathrm{Re}[YY^\dagger], \delta n^{\rm odd}\} + h\{\mathrm{iIm}[YY^\dagger], \delta n^{\rm even}\}\right)_{ij}\,,\end{aligned} \tag{5.159}$$

$$\begin{aligned}\frac{\mathrm{d}}{\mathrm{d}z}\delta n_{ij}^{\rm even} + \mathrm{i}\Omega_{ij}z^2\delta n_{ij}^{\rm even} = -\frac{\mathrm{d}}{\mathrm{d}z}n^{\rm eq}\delta_{ij} \\ -\sum_{h=\pm}\frac{\gamma_h}{2}\frac{a_{\rm R}}{T_{\rm ref}}\left(\{\mathrm{Re}[YY^\dagger], \delta n^{\rm even}\} + h\{\mathrm{iIm}[YY^\dagger], \delta n^{\rm odd}\}\right)_{ij}\,,\end{aligned} \tag{5.160}$$

where

$$\Omega_{ij} = \frac{a_{\rm R}}{T_{\rm ref}^3}\frac{\pi^2}{36\zeta(3)}(M_i^2 - M_j^2)\,, \tag{5.161}$$

determines the oscillation frequency. Since we are working in the mass basis, we have the freedom of choosing the mass matrix M to be real and diagonal. Solutions at order

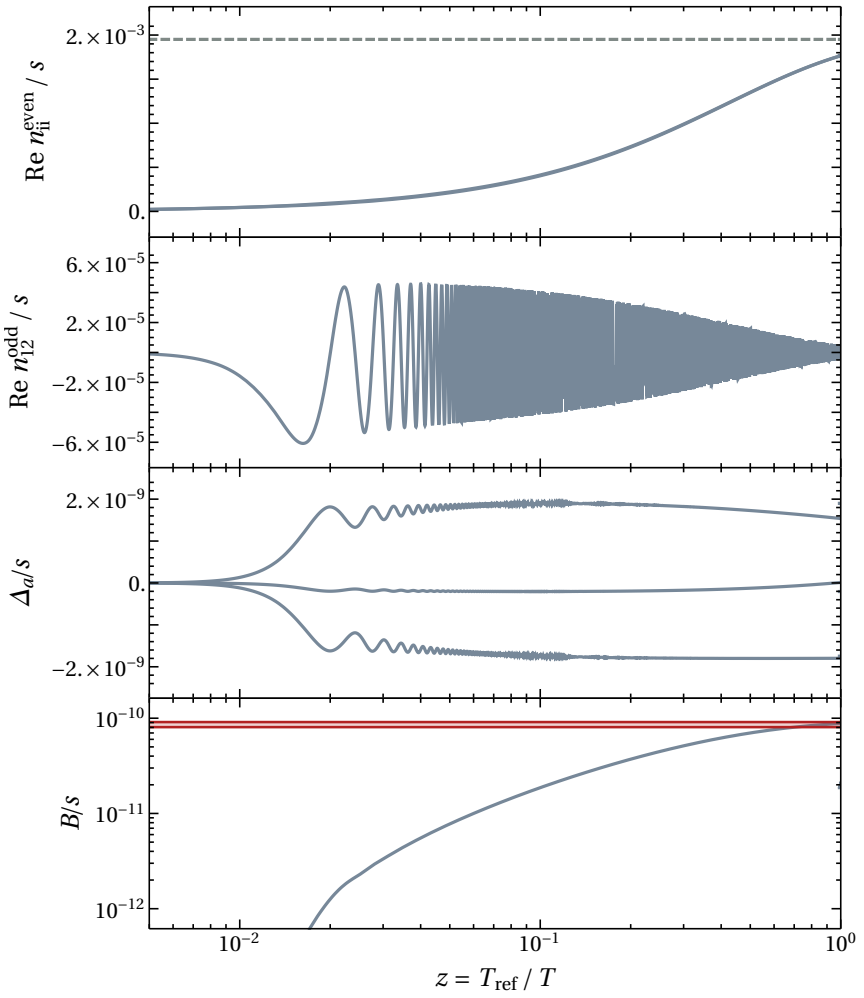

FIGURE 5.7: This plot is similar to figure 1 from ref. [2] but extended in the first panel, where the evolution of the heavy neutrino number density towards the equilibrium value (grey, dashed) is shown. The number density is given as the real part of the diagonal components of the helicity-even contribution n_{ii}^{even}. Further, the evolution of the CP-violating oscillations of the heavy neutrinos, characterised by the real part of the helicity-odd off-diagonal contribution, is illustrated in the second panel. The oscillations of these correlations n_{12}^{odd} act as the source for the flavoured asymmetries Δ_a as shown in the third panel. After the first oscillation the frequency starts increasing until the effect of the SM lepton charge production averages out. Note that at this stage no baryon asymmetry has been created as the LNV source is suppressed compared to the LNC source for the parameter scenario I from table 5.1. Only after the washout starts diminishing the SM lepton asymmetries back to their equilibrium value a non-zero baryon charge B arises. This $B \neq 0$ will be washed out expect when at least one of the Δ_a remains out-of-equilibrium at $z = 1$, the time when the EW sphalerons become inactive. The baryon charge is shown in the fourth panel, where the error bars of the experimental observed value is indicated by the red band.

$|YY^\dagger|$ will drive the source term (5.102). This source determines the amount of SM lepton asymmetries Δ_a at $|YY^\dagger|^2$. Thus, we are left with solving for $\delta n_{ij}^{\rm even}$ and $\delta n_{ij}^{\rm odd}$ with $i \neq j$ in order to determine the source.

OSCILLATIONS OF HEAVY NEUTRINOS: It is convenient to solve the system (5.158) for both the helicity-even and the helicity-odd parts of the distributions. We make use of the relation $z_{\rm osc} \ll z_{\rm eq}$ that allows to solve the system in a perturbative expansion. The smallness of the Yukawa allows to neglect of the RH sides of eqs. (5.168)-(5.169) at zeroth order, i.e. at $\mathcal{O}(|YY^\dagger|^0)$:

$$\frac{\mathrm{d}}{\mathrm{d}z}\delta n_{ij}^{\rm odd} + \mathrm{i}\Omega_{ij}^2 \delta n_{ij}^{\rm odd} = 0\,, \tag{5.162}$$

$$\frac{\mathrm{d}}{\mathrm{d}z}\delta n_{ij}^{\rm even} + \mathrm{i}\Omega_{ij} z^2 \delta n_{ij}^{\rm even} = -\frac{\mathrm{d}}{\mathrm{d}z} n^{\rm eq}\delta_{ij}\,. \tag{5.163}$$

At this order, assuming that there is no initial heavy neutrino content in the very early universe, i.e. $\delta n_{ij}^{\rm odd}(z=0) = \delta n_{ij}^{\rm even}(z=0) = 0$, only the diagonal solution for the even part is non-vanishing

$$\delta n_{ii}^{\rm even} = -n^{\rm eq} + \mathcal{O}(|YY^\dagger|)\,, \qquad \delta n_{ii}^{\rm odd} = \mathcal{O}(|YY^\dagger|)\,. \tag{5.164}$$

The off-diagonal solutions, that are responsible for the flavour oscillations, first appear at $\mathcal{O}(|YY^\dagger|)$. With these solutions that are valid at $\mathcal{O}(|YY^\dagger|^0)$, we can replace $\delta n_{hij} \to -n^{\rm eq}\delta_{ij}$ in eqs. (5.168)-(5.169). Thus, solutions at $\mathcal{O}(|YY^\dagger|^1)$ are given by solving the system

$$\frac{\mathrm{d}}{\mathrm{d}z} n_{ij}^{\rm odd} + \mathrm{i}\Omega_{ij} z^2 n_{ij}^{\rm odd} = \mathrm{i}\mathrm{Im}[YY^\dagger]_{ij}\left(G^+ - G^- z^2\right)\,, \tag{5.165}$$

$$\frac{\mathrm{d}}{\mathrm{d}z} n_{ij}^{\rm even} + \mathrm{i}\Omega_{ij} z^2 n_{ij}^{\rm even} = \mathrm{Re}[YY^\dagger]_{ij}\left(G^+ + G^- z^2\right)\,. \tag{5.166}$$

Since this system is not coupled, solutions for the helicity-odd and helicity-even deviations are obtained independently. In both cases

$$G^+ = \gamma_+ \frac{a_{\rm R}}{T_{\rm ref}} n^{\rm eq}\,, \qquad G^- = \hat{\gamma}_- \frac{a_{\rm R}}{T_{\rm ref}} n^{\rm eq}\,, \tag{5.167}$$

determines the amplitude of the oscillations, where the z-dependence of $\gamma_- \equiv \hat{\gamma}_- z^2$ is factored out. This is because LNV rates, in contrast to the LNC rates, are not constant in z but proportional to z^2 to first non-vanishing order in M/T, cf. the discussion in section 5.3. Solutions to eqs. (5.165) and (5.166) are given by

$$n_{ij}^{\rm odd}(z) = \mathrm{i}\mathrm{Im}[YY^\dagger]_{ij}\left(G^+\mathcal{F}_{ij}^+(z) - G^-\mathcal{F}_{ij}^-(z)\right)\,, \tag{5.168}$$

$$n_{ij}^{\rm even}(z) = \mathrm{Re}[YY^\dagger]_{ij}\left(G^+\mathcal{F}_{ij}^+(z) + G^-\mathcal{F}_{ij}^-(z)\right)\,, \tag{5.169}$$

where the z-dependence is contained in

$$\mathcal{F}_{ij}^+(z) = \frac{(-1)^{1/6}}{\Omega_{ij}^{1/3} 3^{2/3}}\left[\Gamma\left(\frac{1}{3}\right) - E_{1/3}\left(-\frac{\mathrm{i}}{3}\Omega_{ij} z^3\right)\right]\exp\left(-\frac{\mathrm{i}}{3}\Omega_{ij} z^3\right)\,, \tag{5.170}$$

$$\mathcal{F}_{ij}^-(z) = \frac{1}{\mathrm{i}\Omega_{ij}}\left[1 - \exp\left(-\frac{\mathrm{i}}{3}\Omega_{ij} z^3\right)\right]\,, \tag{5.171}$$

with

$$E_n(x) = \int_1^\infty \mathrm{d}t\, \frac{\mathrm{e}^{-xt}}{t^n}\,, \tag{5.172}$$

under the assumption of zero initial sterile charge. $\mathcal{F}^\pm$ describes the oscillation of the heavy neutrinos via eqs. (5.168)-(5.169). Particularly, as we will see later, it is $\mathrm{Im}[\mathcal{F}^\pm]$ that drives the source term. The higher the z the faster the oscillation become. $\mathcal{F}^+$ oscillates around zero with increasing frequency such that its average value decreases to zero. In contrast to that the average value of $\mathcal{F}^+$ does not vanish for large z but converges to $1/|\Omega_{ij}|$. This has essential consequences for the charge generation, as will be discussed later.

The upper panel of figure 5.9 compares the helicity-odd solutions (5.168) and (5.169) to the numerical solution. It is obvious that the larger the z the worse the approximate solutions becomes. This is mainly due to the neglect of the backreaction. However, the production of the SM charges is primarily determined by the first oscillations, such that this offset is unimportant for the charge generation. For the parameter scenario I from table 5.1 these solution are dominated by G^+ and $\mathcal{F}^+$ since $\gamma_+ \gg \gamma_-$, such that the effect of the LNV can be neglected for these parameters.

HEAVY NEUTRINO CHARGES: While off-diagonal solutions δn_{ij} for $i \neq j$, cf. eqs. (5.168) and (5.169), are crucial for the generation of charge asymmetries in the SM lepton sector, the diagonal entries of the helicity-odd and helicity-even components $\delta n_{ii}^{\mathrm{odd}}$ and $\delta n_{ii}^{\mathrm{even}}$ in the mass basis determine the charge of the heavy neutrinos at early times. In order to quantify the evolution of these quantities, we solve eq. (5.159) and (5.160) for diagonal entries and discuss the effect of LNV processes. In this case the oscillatory term containing the heavy neutrino masses vanishes. Further, the hermiticity of $YY^\dagger$ forces $\mathrm{iIm}[YY^\dagger]_{ii} = 0$. When using the hermiticity property of n_{ij}, i.e. $n_{ij} = n_{ij}^\dagger$ and $n_{ij} = n_{ji}^*$, we end up at

$$\frac{\mathrm{d}}{\mathrm{d}z}\delta n_{ii}^{\mathrm{odd}}(z) = -(\Gamma_N)_i \delta n_{ii}^{\mathrm{odd}}(z) + F_i^{\mathrm{odd}}(z)\,, \tag{5.173}$$

$$\frac{\mathrm{d}}{\mathrm{d}z}\delta n_{ii}^{\mathrm{even}}(z) = -(\Gamma_N)_i \delta n_{ii}^{\mathrm{even}}(z) + F_i^{\mathrm{even}}(z)\,, \tag{5.174}$$

with

$$(\Gamma_N)_i = (\gamma_+ + \gamma_-)\frac{a_{\mathrm{R}}}{T_{\mathrm{ref}}}\mathrm{Re}[\mathrm{YY}^\dagger]_{ii} \simeq \gamma_+ \frac{a_{\mathrm{R}}}{T_{\mathrm{ref}}}\mathrm{Re}[\mathrm{YY}^\dagger]_{ii}\,, \tag{5.175}$$

$$F_i^{\mathrm{odd}}(z) = -\sum_{h=\pm}\gamma_h \frac{a_{\mathrm{R}}}{T_{\mathrm{ref}}}\sum_{j\neq i}\left(\mathrm{Re}[YY^\dagger]_{ij}\mathrm{Re}[\delta n_{ji}^{\mathrm{odd}}] - h\mathrm{Im}[YY^\dagger]_{ij}\mathrm{Im}[\delta n_{ji}^{\mathrm{even}}]\right)\,, \tag{5.176}$$

$$F_i^{\mathrm{even}}(z) = -\sum_{h=\pm}\gamma_h \frac{a_{\mathrm{R}}}{T_{\mathrm{ref}}}\sum_{j\neq i}\left(\mathrm{Re}[YY^\dagger]_{ij}\mathrm{Re}[\delta n_{ji}^{\mathrm{even}}] - h\mathrm{Im}[YY^\dagger]_{ij}\mathrm{Im}[\delta n_{ji}^{\mathrm{odd}}]\right)\,. \tag{5.177}$$

Note that the relations always hold at a given order in $|YY^\dagger|$. The solutions for the off-diagonal components (5.168) and (5.169) at order $|YY^\dagger|$ imply

$$\mathrm{Re}[\delta n_{ji}^{\mathrm{odd}}] = -\mathrm{Im}[YY^\dagger]_{ij}\left(G^+\mathrm{Im}[\mathcal{F}_{ij}^+] - G^-\mathrm{Im}[\mathcal{F}_{ij}^-]\right)\,, \tag{5.178}$$

$$\mathrm{Im}[\delta n_{ji}^{\mathrm{even}}] = -\mathrm{Re}[YY^\dagger]_{ij}\left(G^+\mathrm{Im}[\mathcal{F}_{ij}^+] + G^-\mathrm{Im}[\mathcal{F}_{ij}^-]\right)\,. \tag{5.179}$$

These relations can be inserted back into $F_i^{\rm odd}(z)$. When making use of symmetry properties of the various tensors one has

$$F_i^{\rm odd}(z) = -2\hat{\gamma}_-\gamma_+\frac{a_{\rm R}^2}{T_{\rm ref}^2}n^{\rm eq}\sum_{j\neq i}{\rm Re}[YY^\dagger]_{ij}{\rm Im}[YY^\dagger]_{ij}{\rm Im}[\mathcal{F}_{ij}^-(z) - z^2\mathcal{F}_{ij}^+(z)]\,, \tag{5.180}$$

where γ_- is decomposed into a z-independent component $\hat{\gamma}_-$ and a z^2 contribution, such that $\gamma_-(z) = z^2\hat{\gamma}_-$, as discussed earlier. At $\mathcal{O}(|YY^\dagger|^2)$, we can neglect the decay term $(\Gamma_N)_i$ as it is already $\mathcal{O}(|YY^\dagger|)$ and because $\delta n_{ii}^{\rm odd}$ is vanishing at zeroth order in the Yukawas, cf. eq. (5.164). It follows that the sterile charge is only non-vanishing when considering LNV effects at $\mathcal{O}(|YY^\dagger|^2)$. Therefore, when including LNV processes the washout has to be included already at early times since it is not decoupled from the charge generation any more. It can be shown that for two heavy neutrinos the sterile charge is exactly vanishing at all order on the Yukawa couplings provided that LNV effects are neglected. This allows the neglect of the washout and use $q_{Ni} = 0$ as the input for the late washout equations, cf. ref. [2] for a more detailed discussion.

Solutions for the helicity-even parts $\delta n_{ii}^{\rm even}$ can be obtained recursively by integrating eq. (5.174). The obtained result at a given order $|YY^\dagger|^n$ is inserted back into eq. (5.174) again to obtain the result at order $|YY^\dagger|^{n+2}$. In each step of this recursive procedure the initial condition $\delta n_{ii}^{\rm even}(0) = -n^{\rm eq}$, cf. eq. (5.164), has to be fulfilled. At order $|YY^\dagger|^2$ the dependence on $F_i^{\rm even}$ vanishes such that

$$\delta n_{ii}^{\rm even}(z) = -n^{\rm eq}\left(1 - (\Gamma_N)_i z + (\Gamma_N)_i^2\frac{z^2}{2} + \mathcal{O}\left(|YY^\dagger|^3\right)\right)\,, \tag{5.181}$$

while the higher orders $\delta n_{ii}^{\rm even}$ depends non-trivially on $F_i^{\rm even}$. Note that $F_i^{\rm even}$ is a function of the off-diagonal correlations and consequently, with eqs. (5.169), oscillates around zero. In the oscillatory regime, where a perturbative analysis in the Yukawas is allowed, a useful approximation of $\delta n_{ii}^{\rm even}$ is given by solving eq. (5.174) when neglecting $F_i^{\rm even}$ as it only appears at order $|YY^\dagger|^3$. In this case $\delta n_{ii}^{\rm even}$ converges to

$$\delta n_{ii}^{\rm even}(z) \to -n^{\rm eq}\left(1 - (\Gamma_N)_i z + (\Gamma_N)_i^2\frac{z^2}{2} - \dots\right) \to -n^{\rm eq}{\rm e}^{-(\Gamma_N)_i z}\,, \tag{5.182}$$

such that it equilibrates with rate $(\Gamma_N)_i$ to its equilibrium vale $n^{\rm eq}$ according to

$$n_{ii}^{\rm even}(z) = n^{\rm eq}\left(1 - {\rm e}^{-(\Gamma_N)_i z}\right)\,. \tag{5.183}$$

Note however that $\delta n_{ii}^{\rm even}$ starts oscillating due to $F_i^{\rm even}$ and consequently starts deviating from (5.182) for $z \gtrsim z_{\rm osc}$. The equilibration process of $\delta n_{ii}^{\rm even}$ is shown in the first panel of figure 5.7, while the approximate solution (5.182) is compared to the full numerical solution in figure 5.8. One directly recognises that the usage of the approximation (5.182) is justified in the oscillatory regime, simply because the oscillations are too tiny to be observed.

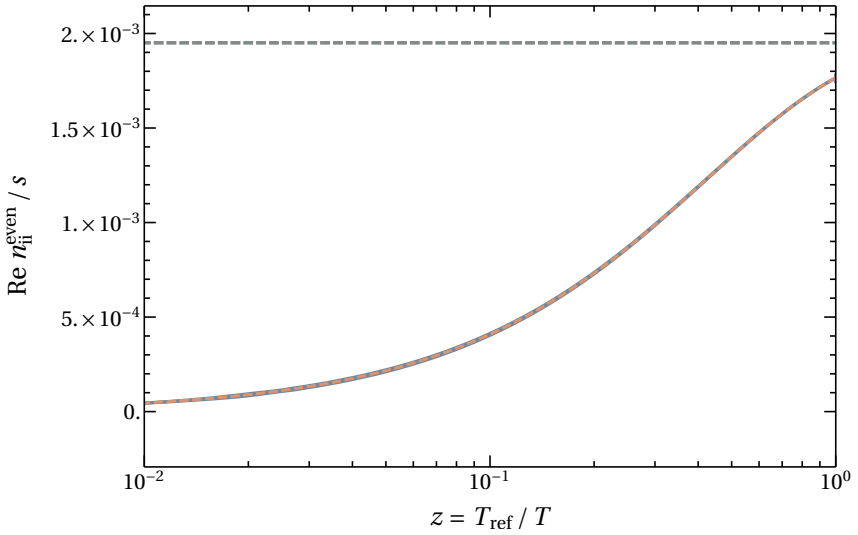

FIGURE 5.8: Comparison of the approximate helicity-even diagonal solution n_{ii}^{even} (orange, dashed) from eq. (5.182) to the full numerical solution (blue), also shown in the top panel of figure 5.7, in the oscillatory regime equilibrating to the equilibrium value n^{eq} (grey, dashed). Here, the parameter scenario I from table 5.1 is used.

CHARGE ASYMMETRIES IN THE LEPTON DOUBLETS: With the off-diagonal components (5.168) and (5.169) the source (5.102) can be decomposed as $S_a = S_a^{\text{PF}} + S_a^{\text{LNV}}$ with the PF source

$$\begin{aligned} S_a^{\text{PF}}(z) &= 2\mathrm{i}\frac{\gamma_+^2}{g_w}\frac{a_{\text{R}}^2}{T_{\text{ref}}}n^{\text{eq}}\sum_{\substack{i,j,c\\ i\neq j}} Y_{ai}^\dagger Y_{ic} Y_{cj}^\dagger Y_{ja}\left(\text{Im}\left[\mathcal{F}_{ij}^+(z)\right] + z^2\text{Im}\left[\mathcal{F}_{ij}^-(z)\right]\frac{\hat{\gamma}_-^2}{\gamma_+^2}\right) \\ &\simeq 2\mathrm{i}\frac{\gamma_+^2}{g_w}\frac{a_{\text{R}}^2}{T_{\text{ref}}}n^{\text{eq}}\sum_{\substack{i,j,c\\ i\neq j}} Y_{ai}^\dagger Y_{ic} Y_{cj}^\dagger Y_{ja}\text{Im}\left[\mathcal{F}_{ij}^+(z)\right] , \end{aligned} \tag{5.184}$$

where we have expanded in small $\hat{\gamma}_-^2/\gamma_+^2$, and the LNV source

$$S_a^{\text{LNV}}(z) = 2\mathrm{i}\frac{\gamma_+\hat{\gamma}_-}{g_w}\frac{a_{\text{R}}^2}{T_{\text{ref}}}n^{\text{eq}}\sum_{\substack{i,j,c\\ i\neq j}} Y_{ai}^\dagger Y_{ic}^* Y_{cj}^T Y_{ja}\left(z^2\text{Im}\left[\mathcal{F}_{ij}^+(z)\right] + \text{Im}\left[\mathcal{F}_{ij}^-(z)\right]\right) , \tag{5.185}$$

that fulfil $\sum_a S_a^{\text{PF}} = 0$ and $\sum_a S_a^{\text{LNV}} \neq 0$.

The separation of scales in the oscillatory regime, $z_{\text{osc}} \ll z_{\text{eq}}$, allows to neglect the washout at $z \sim z_{\text{osc}}$ both for the kinetic equation of the heavy neutrinos (5.153) and for the evolution of the SM leptons, as given by eq. (5.154). This, however, is only true when neglecting the LNV source since it continuously creates SM charges and does not saturate until the heavy neutrinos equilibrate. When including LNV effects, the generation of charges and their washout cannot be separated any more. We will consequently neglect LNV effects and discuss the effect of the LNV process later on.

As shown above, $q_{Ni} \simeq 0$ at this scale when neglecting LNV effects. Consequently, we can assume that no baryon asymmetry is produced during the first oscillations and

further conclude that $\Delta_a \simeq -q_{\ell a}$. The flavoured lepton charge densities are then given by integrating over the source term (5.184)

$$q_{\ell a}(z) = \int_0^z \frac{\mathrm{d}z'}{T_{\rm ref}} S_a(\delta n_{ij}^{\rm odd}, \delta n_{ij}^{\rm even}) \,. \tag{5.186}$$

The solution for the off-diagonal components at order $|YY^\dagger|$ from eqs. (5.168) and (5.169) can be inserted into the source term (5.184). Within the source only the off-diagonal solutions δn_{ijh} depend on z. Since we have factored out all the z-dependence into the function $\mathcal{F}_{ij}^+$ from eq. (5.170), the remaining integral that needs to be solved is given by

$$\int_0^z \mathrm{d}z' \,\mathrm{Im}\left[\mathcal{F}_{ij}^+(z')\right] = \frac{z^2}{2} \mathrm{Im}\,{}_2\mathrm{F}_2\left(\left\{\frac{2}{3}, 1\right\}; \left\{\frac{4}{3}, \frac{5}{3}\right\}; -\frac{\mathrm{i}}{3}|\Omega_{ij}|z^3\right) \mathrm{sign}(M_i^2 - M_j^2) \,, \tag{5.187}$$

where an analytic solution is available in terms of the generalised hypergeometric function

$${}_p\mathrm{F}_q(\{a_1, \ldots, a_p\}; \{b_1, \ldots, b_q\}; w) = \sum_{k=0}^{\infty} \prod_{i=1}^{p} \frac{\Gamma(k + a_i)}{\Gamma(a_i)} \prod_{j=1}^{q} \frac{\Gamma(b_j)}{\Gamma(k + b_j)} \frac{w^k}{k!} \,, \tag{5.188}$$

for $p, q \in \mathbb{N}_0$ and complex $w \in \mathbb{C}$, with $\Gamma(x)$ the Gamma function. Right after the first few oscillations, i.e. for z larger than $z_{\rm osc}$, the charges Δ_a are going to saturate close to their maximal values $\Delta_a^{\rm sat}$, cf. the bottom panel figure 5.9. In the following we will thus compute $q_{\ell a}^{\rm sat}$ by taking the limit

$$q_{\ell a}(z) = \int_0^z \frac{\mathrm{d}z'}{T_{\rm ref}} S_a \simeq \int_0^\infty \frac{\mathrm{d}z'}{T_{\rm ref}} S_a \equiv q_{\ell a}^{\rm sat} \,. \tag{5.189}$$

As the diagonal sterile charges q_{Ni} are negligible at early times, the only asymmetries present in the plasma at $|YY^\dagger|^2$ are the flavoured asymmetries Δ_a in the SM fields. To compute these, the limit $z \to \infty$ of eq. (5.187) is taken and leads to

$$\int_0^\infty \mathrm{d}z \,\mathrm{Im}\left[\mathcal{F}_{ij}^+(z)\right] = -\frac{\pi^{\frac{1}{2}}\Gamma(\frac{1}{6})}{2^{\frac{2}{3}}3^{\frac{4}{3}}|\Omega_{ij}|^{\frac{2}{3}}} \mathrm{sign}(M_i^2 - M_j^2) \,. \tag{5.190}$$

When putting all the elements together the asymptotic values for the flavoured charge asymmetries are given by

$$\begin{aligned} \frac{q_{\ell a}^{\rm sat}}{s} = -\frac{\Delta_a^{\rm sat}}{s} &= -\frac{\mathrm{i}}{g_\star^{\frac{5}{3}}} \frac{3^{\frac{13}{3}}5^{\frac{5}{3}}\Gamma(\frac{1}{6})\zeta(3)^{\frac{5}{3}}}{2^{\frac{8}{3}}\pi^{\frac{41}{6}}} \sum_{\substack{i,j,c \\ i\neq j}} \frac{Y_{ai}^\dagger Y_{ic} Y_{cj}^\dagger Y_{ja}}{\mathrm{sign}(M_i^2 - M_j^2)} \left(\frac{m_{\rm Pl}^2}{|M_i^2 - M_j^2|}\right)^{\frac{2}{3}} \frac{\gamma_+^2}{g_w} \\ &\simeq \sum_{\substack{i,j,c \\ i\neq j}} \frac{\mathrm{Im}[Y_{ai}^\dagger Y_{ic} Y_{cj}^\dagger Y_{ja}]}{\mathrm{sign}(M_i^2 - M_j^2)} \left(\frac{m_{\rm Pl}^2}{|M_i^2 - M_j^2|}\right)^{\frac{2}{3}} \times 3.4 \times 10^{-4} \frac{\gamma_+^2}{g_w} \,, \end{aligned} \tag{5.191}$$

where the expression is divided by the comoving entropy density $s = 2\pi^2 g_\star a_{\rm R}^3/45$. One can show that the total lepton charge vanishes, i.e. $\sum_a \Delta_a^{\rm sat} = 0$, at the given order of $|YY^\dagger|^2$. This is not surprising as we are using the LNC source (5.184) that does not allow any $\tilde{L}$ generation. Thus, since we have shown that $q_{Ni} = 0$ at $\mathcal{O}(|YY^\dagger|)$ also $\sum_a \Delta_a^{\rm sat}$ has to be zero. The bottom panel of figure 5.9 compares the approximate solution of Δ_a, that is given by inserting (5.168) and (5.169) into eq. (5.186) with the source (5.184) and

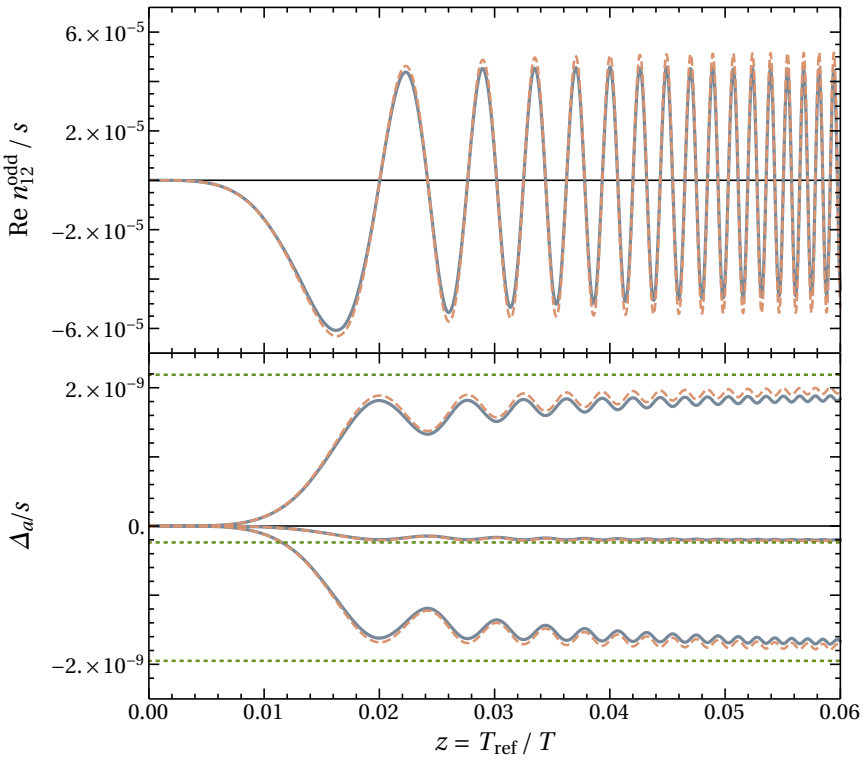

FIGURE 5.9: Similar to figure 3 from ref. [2], the analytic approximations (orange, dashed) are compared to the full numerical solution (blue, solid) for the off-diagonal correlation $\delta n_{12}^{\mathrm{odd}}$, cf. eqs. (5.168) and (5.169), in the upper panel and for the flavoured charge densities Δ_a in the lower panel. Here, parameter scenario I from table 5.1 is used for which LNV effects are negligible. The different Δ_a are obtained by inserting the correlations (5.168) and (5.169) into the source (5.184) and evaluating the integral (5.186) according to eq. (5.187). Further, the quick saturation of Δ_a to (5.191) after the first oscillations is shown via the green, dashed lines in the bottom panel. Note that particularly for the derivation of eq. (5.191) we have neglected backreaction effects of δn as well as thermal masses. Note that the oscillatory regime is characterised by oscillations that happen such early that the washout of Δ_a can be neglected. The approximations shown here are valid at order $|YY^\dagger|^2$, which implies the sum of the three Δ_a to vanish. LNV and thus a non-zero B only appears at $|YY^\dagger|^3$ when washout effects are included.

using the analytic integral solution (5.187), to the full numerical solution. It is obvious that Δ_a quickly reaches the saturated value (5.191). Since we have neglected the washout of the SM lepton charges, the approximate solution gets worse for larger z. Due to the separation of scales in the oscillatory regime, i.e. $z_{\rm osc} \ll z_{\rm eq}$, we can use $\Delta_a^{\rm sat}$ as an input for the washout equation. This will be shown in the following.

5.5.2 *Washout at late times*

At late times $z \sim z_{\rm eq}$, when the generation of the lepton doublet charges via heavy neutrino oscillations has already been completed, these oscillations can be neglected. This is due to the fact that either these oscillation frequency continuously increases until it is so rapid that the effect on the charge generation averages out or that the heavy neutrinos have already decayed. Note that this only applies when neglecting LNV effects, which otherwise would prevent the charges to from a quick saturation after the first oscillations. The neglect of the oscillations has two consequences. First, the source term in the evolution equation (5.154) for the charge lepton doublets can be dropped. Second, the equation (5.153) for the heavy neutrinos charge is purely described by the decay term Γ_N and the backreaction term $\tilde{\Gamma}_N$, while $H_N^{\rm vac}$ as the oscillation term together with the effective Hamiltonian $H_N^{\rm th}$ can be neglected. The system describing the late washout can be truncated to the following form

$$g_w \frac{{\rm d}\Delta_a}{{\rm d}z} = \frac{a_{\rm R}}{T_{\rm ref}} \sum_i Y_{ia} Y_{ai}^\dagger \sum_{h=\pm} \left(\tilde{\gamma}_h \sum_b (A_{ab} + C_b/2)\Delta_b - h\gamma_h q_{Ni} \right) , \tag{5.192}$$

$$\frac{{\rm d}q_{Ni}}{{\rm d}z} = -\frac{a_{\rm R}}{T_{\rm ref}} \sum_a Y_{ia} Y_{ai}^\dagger \sum_{h=\pm} h \left(h\gamma_h q_{Ni} - \tilde{\gamma}_h \sum_b (A_{ab} + C_b/2)\Delta_b \right) . \tag{5.193}$$

The approximate solution (5.191) to the charge densities $\Delta_a^{\rm sat}$ and $q_N = 0$, that are generated through the oscillations at $z \sim z_{\rm osc} \ll z_{\rm eq}$, are used as the initial conditions for solving the system of eqs. (5.192) and (5.193) when neglecting LNV effects. We also take account of the effect of spectator fields by using the matrix A and the vector C, cf. eq. (5.109). Note that spectator fields have mostly been neglected in different studies, corresponding to $C = 0$ and $A = -1$. However, it turns out that the spectator fields modify these equation and consequently can change the result for the baryon charge B significantly, particularly in leptogenesis scenarios where the asymmetries are PF [152]. This is because this asymmetry is due to an incomplete cancellation of the flavoured charges Δ_a, which turns out to be highly sensitive to the effect of spectator fields. This effect is demonstrated in figure 5.10.

Note that the sum of eqs. (5.192) and (5.193) describes the conservation of $\tilde{L}$ during the washout that is only broken when including the LNV rates γ_-:

$$\frac{\rm d}{{\rm d}z} \left(g_w \sum_a \Delta_a - \sum_i q_{Ni} \right) = 2 \frac{a_{\rm R}}{T_{\rm ref}} \sum_i (YY^\dagger)_{ii} \left(\gamma_- q_{Ni} - \tilde{\gamma}_- \sum_b (A_{ab} + C_b/2)\Delta_b \right) . \tag{5.194}$$

In order to solve the coupled system of eqs. (5.192)-(5.193) it makes sense to reduce it to a linear first-order differential equation for $(3 + n_s)$-dimensional vectors $(q_\ell^T, q_N^T)^T$, in the general case of n_s heavy neutrino flavours, such that

$$\frac{\rm d}{{\rm d}z} \begin{pmatrix} q_\ell(z) \\ q_N(z) \end{pmatrix} = \frac{a_{\rm R}}{T_{\rm ref}} \sum_{h=\pm} K_h \begin{pmatrix} q_\ell(z) \\ q_N(z) \end{pmatrix} , \qquad K_h = \begin{pmatrix} K^{\ell\ell} & K_h^{\ell N} \\ K_h^{N\ell} & K^{NN} \end{pmatrix} . \tag{5.195}$$

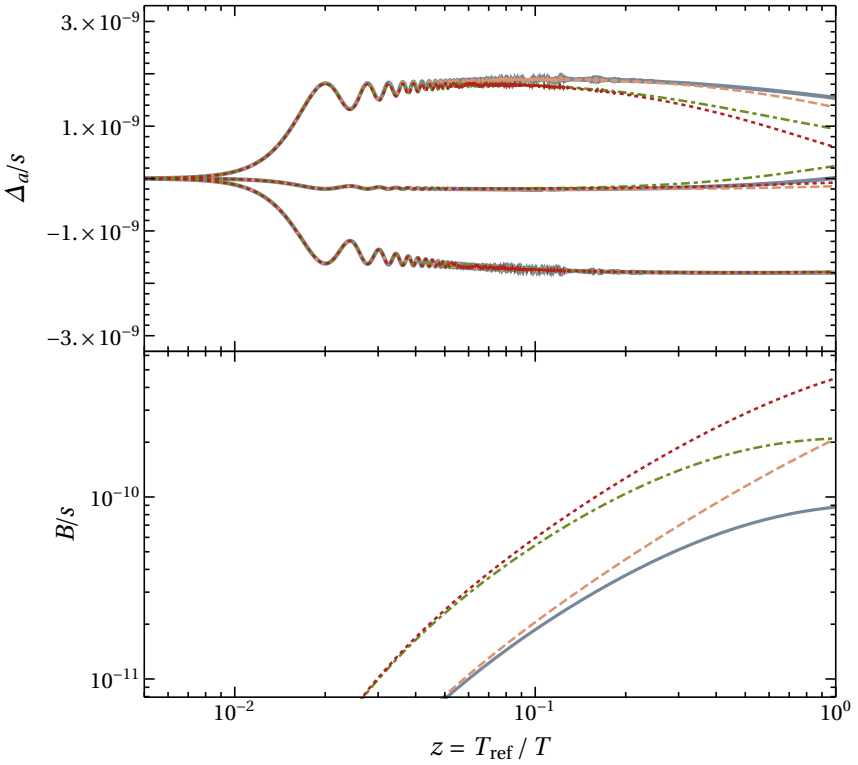

FIGURE 5.10: Comparison of the full numerical solution for the different flavoured asymmetries Δ_a/s (top panel) and for the baryon asymmetry B/s (lower panel) with backreaction and spectator effects included (blue, solid) to the setup with only spectator effects (orange, dashed), only backreaction (green, dot-dashed) and neither of these two effects (red, dotted) included. Here, parameter scenario I from table 5.1 is used.

The components of the matrices $K_h^{\ell\ell}, K_h^{\ell N}, K_h^{N\ell}$ and K_h^{NN} are given by

$$\left(K_h^{\ell\ell}\right)_{ab} = \frac{\tilde{\gamma}_h}{g_w}\sum_{k=1}^{n_s} Y_{ak}^\dagger Y_{ka}\left(A_{ab}+\frac{1}{2}\right), \qquad \left(K_h^{\ell N}\right)_{aj} = -h\frac{\gamma_h}{g_w}Y_{aj}^\dagger Y_{ja},$$
$$\left(K_h^{N\ell}\right)_{ib} = h\tilde{\gamma}_h\sum_{d=1}^{3} Y_{id}Y_{di}^\dagger\left(A_{db}+\frac{1}{2}C_b\right), \qquad \left(K_h^{NN}\right)_{ij} = -\gamma_h\sum_{d=1}^{3} Y_{id}Y_{di}^\dagger\delta_{ij}, \tag{5.196}$$

with $a, b = 1, 2, 3$ the SM lepton flavours and $i, j = 1, 2, \ldots, n_s$ the heavy neutrino flavours. Solution can be found by diagonalising the Matrix K_h

$$K_h^{\text{diag}} = \mathrm{T}_h^{-1} K_h \mathrm{T}_h, \tag{5.197}$$

with a transformation matrix T_h, where the eigenvectors of K_h are the column vectors. In the following we only consider the LNC processes by setting $h = 1$ in eqs. (5.192) and (5.193). Since γ_+ and $\tilde{\gamma}_+$ are not z-dependent in the first non-vanishing order in M^2/T^2, we can write

$$\begin{pmatrix} q_\ell(z) \\ q_N(z) \end{pmatrix} = \mathrm{T}_+ \exp\left(\frac{a_{\mathrm{R}}}{T_{\text{ref}}} K_+^{\text{diag}}(z-\tilde{z})\right)\mathrm{T}_+^{-1}\begin{pmatrix} q_\ell^{\text{init}} \\ q_N^{\text{init}} \end{pmatrix}. \tag{5.198}$$

$q_\ell^{\text{init}} = q_\ell^{\text{sat}}$ and $q_N^{\text{init}} = 0$ are the vectors of asymmetries that have been created during the oscillation process at early times $\tilde{z} \sim z_{\text{osc}}$, cf. eq. (5.191). At $z_{\text{osc}} \ll z_{\text{eq}}$ the generated charges saturate very quickly, cf. figure 5.9, compared to the time where the washout process becomes important. Therefore, we can assume these initial conditions to be produced at zero time, i.e. it makes sense to take the limit $\tilde{z} \to 0$ of eq. (5.198). This system can be solved for the individual asymmetries $\Delta_a = -q_{\ell a}$. While $\sum_a \Delta_a^{\text{sat}} = 0$, the washout implies an incomplete cancellation between the different Δ_a, which directly relates to a non-zero baryon charge $B \sim \sum_a \Delta_a \neq 0$, cf. eq. (5.110). Note that the LNC washout conserves $\tilde{L}$. For this reason any production of $\sum_a \Delta_a$ is due to some shift in $\sum q_{Ni}$ such that the change in $\tilde{L}$ is zero, cf. eq. (5.194) when setting $\gamma_- = \tilde{\gamma}_- = 0$. Since the EW sphalerons do not couple to the heavy neutrinos, the baryon charge is only sensitive to $\sum_a \Delta_a$.

A comparison between this approximate analytic procedure of the washout of the different Δ_a and the full numerical solution is shown in the top panel of figure 5.11. Note that the washout term, i.e. the first term proportional to Δ_a in eq. (5.192), will wash out all the asymmetry in the different Δ_a and will consequently erase all the baryon asymmetry that has been produced. The only way to protect the baryon charge from being washed out is the keep at least one of the Δ_a out-of-equilibrium before the EW sphalerons freeze out. In this case the non-zero baryon charge gets frozen in and is consequently given by

$$B = \frac{28}{79}\lim_{z\to 1}\sum_a \Delta_a(z). \tag{5.199}$$

A comparison between the analytic approximation to the baryon charge B and the full numerical solution is shown in the bottom panel of figure 5.11.

5.5.3 *Lepton number violating effects*

This subsection is not intended to provide an analytic procedure to approximately describe the generation of the baryon asymmetry. It rather should make the reader aware that there

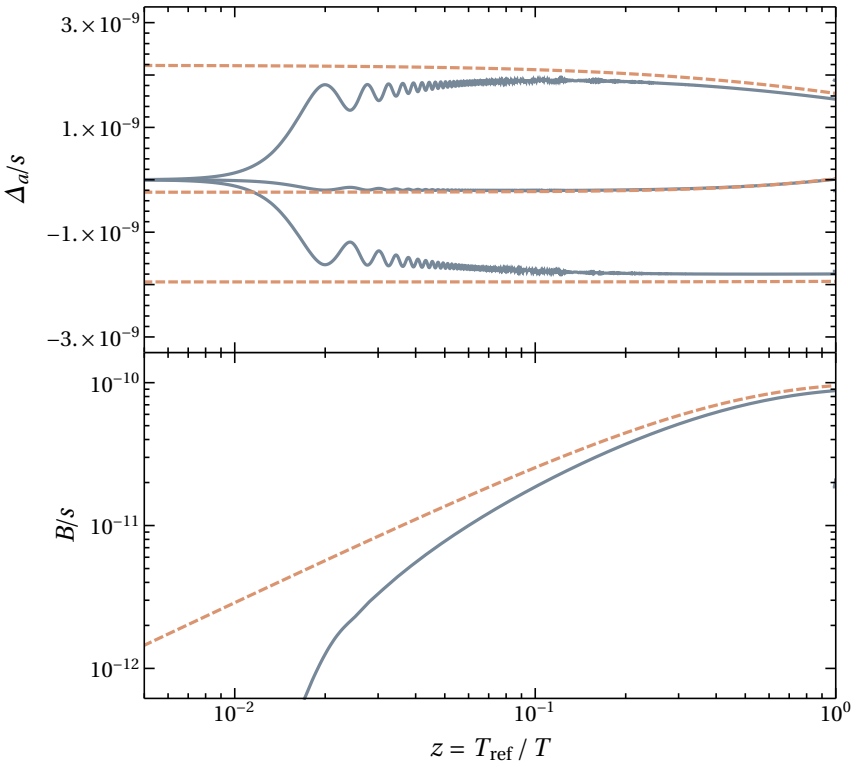

FIGURE 5.11: The top panel demonstrates the washout of the different asymmetries Δ_a in the oscillatory regime. An incomplete cancellation of these happens due to washout rates that are in general different for the individual flavours. This implies a generation of a non-zero baryon charge according to eq. (5.110). The approximate analytic procedure (orange, dashed), cf. eqs. (5.198) and (5.191), is compared to the full numerical solution (blue, solid). Here, parameter scenario I from table 5.1 is used.

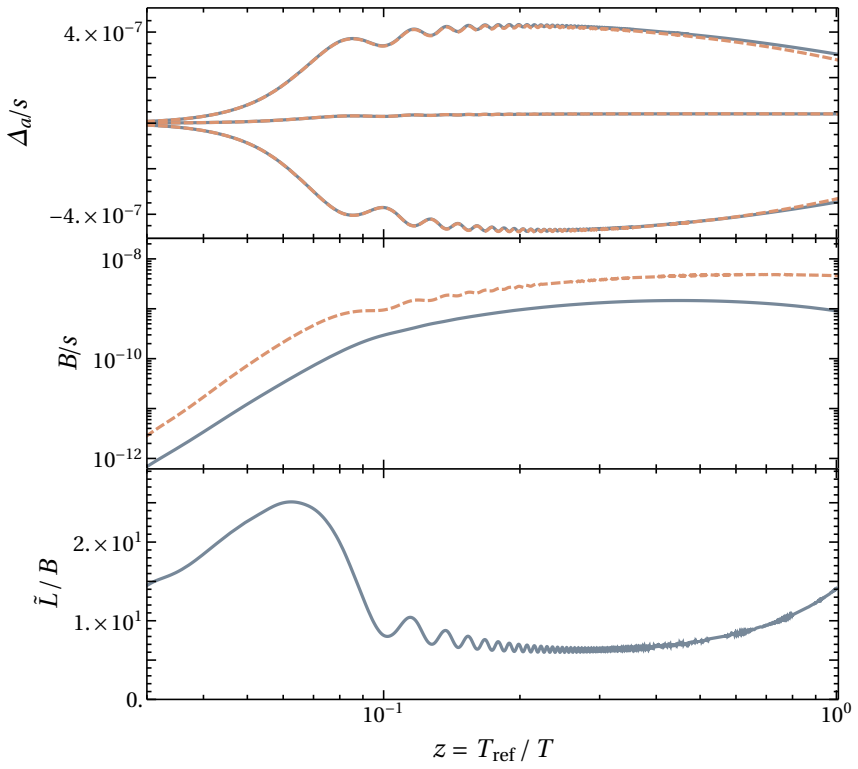

FIGURE 5.12: Evolution of the SM charges (first panel) and the baryon asymmetry (second panel) when neglecting LNV effects (blue, solid) and including LNV effects (orange, dashed). The third panel shows the ratio $\tilde{L}/B$ that measures the magnitude of LNV. Here, parameter scenario II from table 5.1 is used.

exists parameter regions for which LNV effects are important and cannot be neglected and help to qualitatively understand how LNV effects can affect the baryon charge creation in the oscillatory regime.

When neglecting LNV effects the generation of both the SM and the sterile charges can be separated from their washout. This is true because we have shown that there is no initial charge of q_{Ni} at $\mathcal{O}(|YY^\dagger|^2)$ and because of the quick saturation of Δ_a long before the washout becomes active. Things change when allowing for LNV processes. In this case the source does not make the asymmetries Δ_a saturate after the first oscillations. They rather keep growing until the heavy neutrinos equilibrate. Therefore, even when the washout starts acting on the charges, new charges are still produced via the source terms S_a^{LNV} and F_i^{odd}, cf. eqs. (5.185) and (5.180), due to off-diagonal correlations δn_{ij}. Note that particularly S_a^{LNV} creates $g_w \sum_a q_{\ell a} + \sum_i q_{Ni} \neq 0$ and thus violates $\tilde{L}$. Figure 5.12 illustrates the effect of including LNV processes.

While the LNC washout preserves $\tilde{L}$, the LNV washout washes $\tilde{L}$ out. Due to the hierarchy $\gamma_+ \gg \gamma_-$ and $\tilde{\gamma}_+ \gg \tilde{\gamma}_-$, the LNV washout does only allows for a tiny change of $\tilde{L}$ for $z \gtrsim z_{\mathrm{eq}}$. In figure 5.12 this effect is visible in the first panel when the orange, dashed line starts deviating slightly from the blue, solid line. In the following discussion, we neglect γ_- and $\tilde{\gamma}_-$ in the washout for simplicity reasons. As a consequence the washout

does not violate $\tilde{L}$. The equations describing the washout are obtained analogously to eqs. (5.192) and (5.193) and generalised to

$$g_w \frac{\mathrm{d}\Delta_a}{\mathrm{d}z} = \gamma_+ \frac{a_\mathrm{R}}{T_\mathrm{ref}} \sum_i Y_{ia} Y^\dagger_{ai} \left(\sum_b (A_{ab} + C_b/2)\Delta_b - q_{Ni} \right) - g_w \frac{S_a^\mathrm{LNV} + S_a^\mathrm{PF}}{T_\mathrm{ref}} , \tag{5.200}$$

$$\frac{\mathrm{d}q_{Ni}}{\mathrm{d}z} = -\gamma_+ \frac{a_\mathrm{R}}{T_\mathrm{ref}} \sum_a Y_{ia} Y^\dagger_{ai} \left(q_{Ni} - \sum_b (A_{ab} + C_b/2)\Delta_b \right) + \frac{S_i^N}{T_\mathrm{ref}} , \tag{5.201}$$

with $S_i^N = 2F_i^\mathrm{odd} T_\mathrm{ref}$, cf. eq. (5.180) and $\tilde{\gamma}_+ \simeq \gamma_+$. Note that the two source terms are only valid at $\mathcal{O}(|YY^\dagger|^2)$. Therefore, it does not include the decay of the off-diagonal correlations through the heavy neutrino production. Thus, the equation from above is only valid for $z \lesssim z^\mathrm{eq}$. $\tilde{L}$ is conserved by the washout and is only violated via the sources such that its evolution is given by the integral

$$\tilde{L}(z) = -\int_0^z \frac{\mathrm{d}z'}{T_\mathrm{ref}} \left(g_w \sum_a S_a^\mathrm{LNV}(z') + \sum_i S_i^N(z') \right) . \tag{5.202}$$

With eqs. (5.168), (5.169) and (5.170), (5.171) one can show that

$$g_w \frac{S_a^\mathrm{LNV}(z)}{T_\mathrm{ref}} = 8\gamma_+ \hat{\gamma}_- \frac{a_\mathrm{R}^2}{T_\mathrm{ref}^2} n^\mathrm{eq} \mathrm{Re}[YY^\dagger]_{12} \mathrm{Im}[YY^\dagger]_{12} \mathrm{Im}\left[\mathcal{F}_{12}^-(z) + z^2 \mathcal{F}_{12}^+(z) \right] , \tag{5.203}$$

$$\frac{S_a^N(z)}{T_\mathrm{ref}} = -8\gamma_+ \hat{\gamma}_- \frac{a_\mathrm{R}^2}{T_\mathrm{ref}^2} n^\mathrm{eq} \mathrm{Re}[YY^\dagger]_{12} \mathrm{Im}[YY^\dagger]_{12} \mathrm{Im}\left[\mathcal{F}_{12}^-(z) - z^2 \mathcal{F}_{12}^+(z) \right] , \tag{5.204}$$

such that the dependence of the generalised lepton number on $\mathcal{F}^-$ vanishes:

$$\tilde{L}(z) = -8\gamma_+ \hat{\gamma}_- \frac{a_\mathrm{R}^2}{T_\mathrm{ref}^2} n^\mathrm{eq} \mathrm{Re}[YY^\dagger]_{12} \mathrm{Im}[YY^\dagger]_{12} \int_0^z \mathrm{d}z' \, (z')^2 \mathrm{Im}\left[\mathcal{F}_{12}^+(z') \right] . \tag{5.205}$$

After the first oscillations, i.e. when $z \gg z_\mathrm{osc}$, $\tilde{L}$ can be approximated by its average value

$$\tilde{L}(z) \simeq 8\gamma_+ \hat{\gamma}_- \frac{a_\mathrm{R}^2}{T_\mathrm{ref}^2} n^\mathrm{eq} \mathrm{Re}[YY^\dagger]_{12} \mathrm{Im}[YY^\dagger]_{12} \frac{z}{|\Omega_{ij}|} . \tag{5.206}$$

Qualitatively one can conclude that LNV in the oscillatory regime becomes the more important the larger the heavy neutrino mass $\bar{M}$ and the more degenerate the heavy neutrinos are. Further, the baryon charge generation is dominated by the LNV source compared to the incomplete LNC washout when keeping the Yukawa couplings small. Such a scenario appears when looking for small mixing angles close to the seesaw line, which happens when the oscillations happen rather late and where the washout is very weak.

A comparison between the full result and the approximated value for $\tilde{L}$ for small $z \ll z_\mathrm{eq}$ is presented in figure 5.13.

BARYON CHARGE GENERATION THROUGH THE LNV SOURCE ONLY: Although we have found an approximate analytic solution for $\tilde{L}$ that holds for $z \lesssim z_\mathrm{eq}$ in the last paragraph, describing the evolution of the baryon asymmetry quantitatively is non-trivial, simply because we do not know how Δ_a and q_{Ni} evolve separately. Therefore, we consider the case where all the lepton asymmetry is produced via the LNV source and consequently neglect the washout. This allows to find approximate analytic solution for the baryon

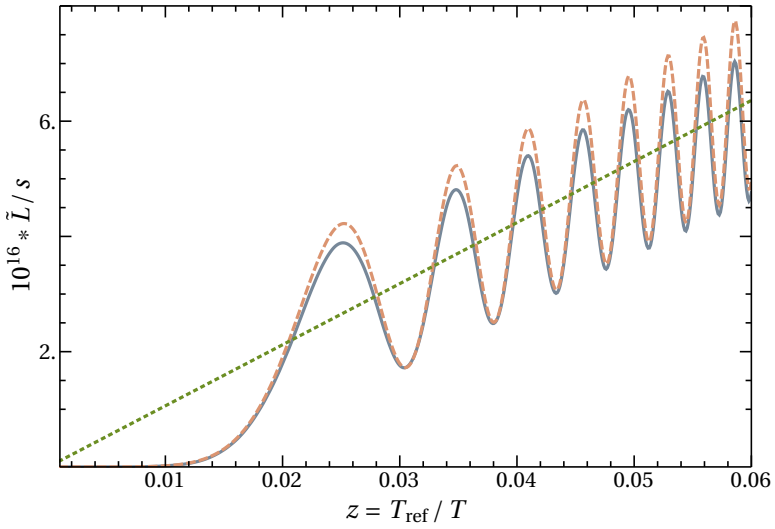

FIGURE 5.13: Generalised lepton number $\tilde{L}$ generation through LNV sources for the parameter scenario II from table 5.1. The full numerical solution (blue) is compared to the approximate result (5.205) (orange, dashed) and to the averaged approximation (5.206) (green, solid).

charge generation. In order to do so, we define a charge complementary to $\tilde{L}$ that is given by

$$\begin{aligned}\tilde{L}^{\text{LNV}} &= g_w \sum_a \Delta_a + \sum_i q_{Ni} = -\int_0^z \frac{\mathrm{d}z'}{T_{\text{ref}}} \left(g_w \sum_a S_a^{\text{LNV}}(z') - \sum_i S_i^N(z') \right) \\ &= -8\gamma\hat{\gamma}_- \frac{a_{\text{R}}^2}{T_{\text{ref}}^2} n^{\text{eq}} \text{Re}[YY^\dagger]_{12} \text{Im}[YY^\dagger]_{12} \int_0^z \mathrm{d}z' \, \text{Im}\left[\mathcal{F}_{12}^-(z')\right] \\ &\to -8\gamma\hat{\gamma}_- \frac{a_{\text{R}}^2}{T_{\text{ref}}^2} n^{\text{eq}} \text{Re}[YY^\dagger]_{12} \text{Im}[YY^\dagger]_{12} \left(-\frac{z}{|\Omega_{ij}|} + \frac{\Gamma\left(\frac{1}{3}\right)}{2\Omega_{ij}^{4/3} 3^{1/6}} \right) . \end{aligned} \tag{5.207}$$

In the last step we have replaced the oscillatory term due to $\mathcal{F}_{12}^-$ by its average value. Such a replacement is valid for $z \gg z_{\text{osc}}$. Eventually, the baryon charge in the absence of a washout can be approximated as

$$\begin{aligned} B &= \frac{2}{3g_w} \left(\tilde{L} + L^{\text{LNV}} \right) \\ &\simeq -8 \frac{2}{3g_w} \gamma\hat{\gamma}_- \frac{a_{\text{R}}^2}{T_{\text{ref}}^2} n^{\text{eq}} \text{Re}[YY^\dagger]_{12} \text{Im}[YY^\dagger]_{12} \left(\frac{\Gamma\left(\frac{1}{3}\right)}{2|\Omega^{4/3}|_{ij} 3^{1/6}} - \frac{2z}{|\Omega_{ij}|} \right) . \end{aligned} \tag{5.208}$$

Note that this approximation does not include the decay of the source term due to the equilibration of the heavy neutrinos, which would imply that B actually saturates at $z \sim z^{\text{eq}}$. Therefore, the approximation breaks down for $z \gtrsim z^{\text{eq}}$. A comparison plot is shown in figure 5.14.

Eventually, we can conclude that there exist parameter regions for which LNV effects cannot be neglected for the baryon charge generation. We are able to qualitatively understand the baryon charge generation and approximately quantify the evolution of $\tilde{L}$ for z before the equilibration of the heavy neutrinos. However, finding a procedure that analyt-

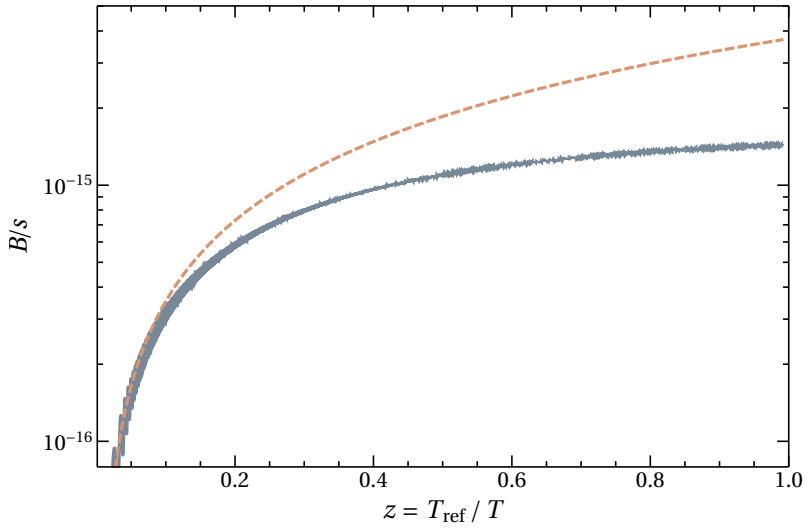

FIGURE 5.14: Generation of baryon asymmetry through LNV sources while neglecting washout effects for the parameter scenario II from table 5.1. The full numerical result (blue) is compared to the approximate solution (5.208) (orange, dashed). The approximate solution overestimates the baryon asymmetry for $z \gtrsim z^{\mathrm{eq}}$ since it does not consider the equilibration of the off-diagonal correlations of the heavy neutrinos.

ically computes the baryon asymmetry as done in the PF case is challenging and might be interesting for future works.

5.6 OVERDAMPED REGIME

In contrast to the oscillatory regime from section 5.5 there are parameter choices, particularly phenomenologically interesting, which yield to an equilibration of one of the heavy neutrino interaction eigenstate before the first oscillation has been completed. Such a behaviour is called overdamped and is demonstrated in figure 5.15. The parameters used for the different plots in this section are chosen such that LNV effects on the source term and on the generation of the baryon asymmetry are subdominant. Nevertheless the discussion, particularly the derivation of the source term, is kept as general as possible. Possible effects from LNV on the baryon charge creation are mentioned when necessary.

Subsection 5.6.1 demonstrates how large Yukawa couplings, i.e. mixing angles larger than the naive seesaw relation (2.58), are achieved in the symmetry protected scenario in the flavour basis where Υ_{+h} is diagonal. The generation of the asymmetry through the off-diagonal oscillations within the quasi-static approximation is quantitatively discussed in subsection 5.6.2. The time evolution of the SM charges, particularly a procedure to obtain an approximate analytic solution for the baryon charge, is addressed in subsection 5.6.3, while LNV processes are neglected. In subsection 5.6.4 three interesting scenarios are presented, such as a flavour asymmetric washout, an early equilibration through LNV effects and relatively large mass splittings, which are allowed when including LNV effects.

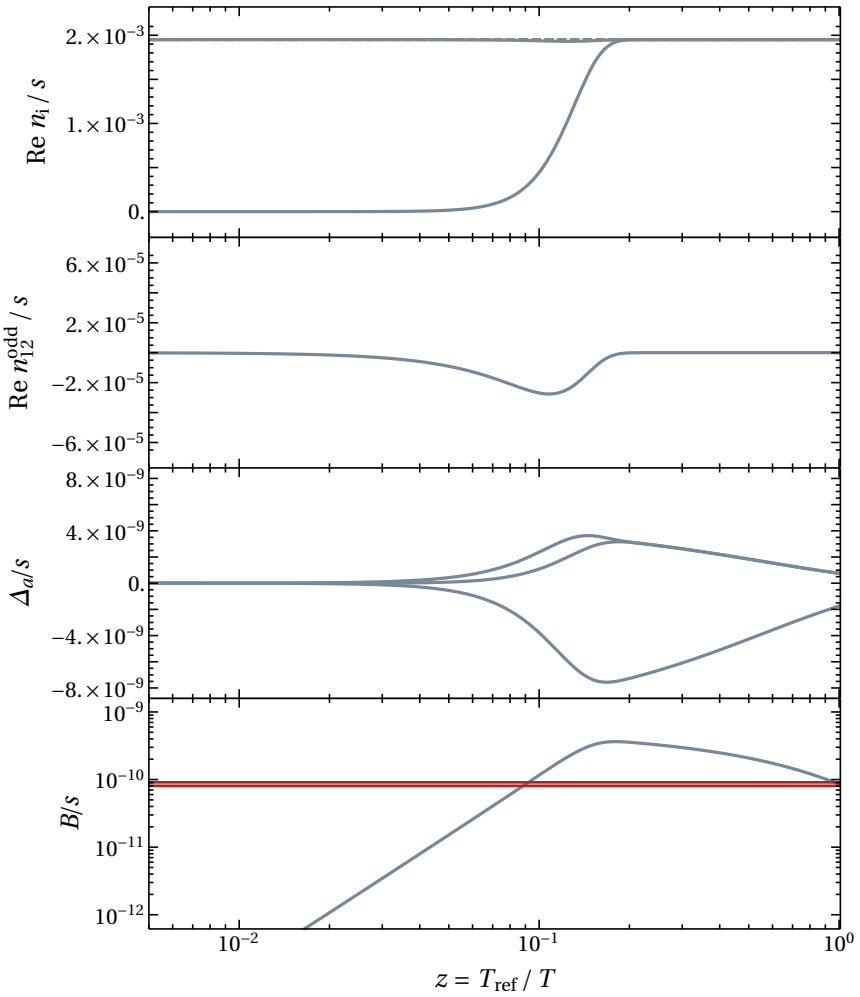

FIGURE 5.15: This plot is similar to figure 6 from ref. [2]. However, it is extended in the first panel, where the equilibration of the two heavy neutrino eigenstates (grey, dashed) is shown. We use parameter scenario III from table 5.1. The evolution of the CP-violating oscillations of the heavy neutrinos are characterised by the real part of the helicity-odd off-diagonal contribution, as being shown in the second panel. The oscillations of these correlations n_{12}^{odd} are the source for the flavoured asymmetries Δ_a as illustrated in the third panel. In comparison to the oscillatory regime, cf. figure 5.7, the oscillations do not start much earlier than the equilibration but begin rather late. When the washout starts pushing the SM lepton asymmetries back to their equilibrium value a non-zero baryon charge B emerges. This $B \neq 0$ will only survive when at least one of the Δ_a remains out-of-equilibrium until the EW sphalerons become inactive at $z = 1$. The baryon charge with the error bars of the experimental observed value (red band) is shown in the fourth panel.

5.6.1 *Large mixing angles and the interaction flavour basis*

Two scenarios which can account for the overdamped behaviour are those in which either the Yukawa couplings Y_{ia} are much larger than the ones implied by the naive seesaw expectation (2.58), or where the masses of the heavy neutrino are such degenerate that the oscillations happen at times comparable to the EW sphaleron freeze-out. These scenarios usually happen in the symmetry protected scenario with an approximate $B-L$ conservation, cf. section 2.2.4, with $\epsilon, \mu \ll 1$. Such a scenario has interesting features when it comes to the decay behaviour of the heavy neutrinos. According to eq. (5.82) the decay rate of the heavy neutrinos is characterised by the eigenvalues of the matrix Υ_{+h} and also by Υ_{-h} when including LNV effects. This motivates to treat the overdamped regime in the basis where Υ_{+h} is diagonal. It is useful for the following discussion to define the two linear combinations

$$Y_a \equiv \frac{1}{\sqrt{2}} \left(Y_{1a} + \mathrm{i} Y_{2a}\right) , \tag{5.209}$$

$$\epsilon_a \equiv \frac{1}{\sqrt{2}} \left(Y_{1a} - \mathrm{i} Y_{2a}\right) , \tag{5.210}$$

that fulfil $\sum_a |Y_a|^2 \gg \sum_a |\epsilon_a|^2$ and consequently allows for an expansion in small $|\epsilon_a|$. Note that ϵ_a are of order $\sqrt{\epsilon}$ with ϵ as the small LNV parameter introduced in eq. (2.59). The matrix

$$\mathcal{U} \simeq \frac{1}{\sqrt{2}} \begin{pmatrix} \mathrm{i}(1+\chi) & -(1-\chi) \\ 1 & 1 \end{pmatrix} , \qquad \text{with} \qquad \chi \equiv \frac{2\sum_a \epsilon_a Y_a^*}{\sum_a |Y_a|^2} + \mathcal{O}(\epsilon_a^2) , \tag{5.211}$$

diagonalises Υ_{+h}, according to

$$\Upsilon^{\mathrm{diag}} = \mathcal{U}^\dagger \Upsilon_{+h} \mathcal{U} \simeq \begin{pmatrix} \sum_a |Y_a|^2 & 0 \\ 0 & \mathcal{O}(\epsilon_a^2) \end{pmatrix} , \tag{5.212}$$

where the diagonal entries of Υ_{+h} define the eigenvalues. Since the decay rate is proportional to these eigenvalues, the first interaction eigenstate equilibrates quickly compared to the second that only couples feebly to the plasma with. We will show in the following that the production of the second eigenstate is not only given by its own equilibration but also by oscillations with the heavy neutrino instead. Note that the usage of eq. (5.212) implies that the off-diagonal components $\Upsilon_{12}^{\mathrm{diag}} = \Upsilon_{21}^{\mathrm{diag}} = 0$ vanish in the interaction basis. It is worth mentioning that $\mathcal{U}$ from eq. (5.211) does not fully diagonalise Υ_{-h} unless the exact limit $\epsilon_a \to 0$ holds. At $\mathcal{O}(\epsilon_a^2)$ one has

$$\Upsilon^{\mathrm{LNV}} = \mathcal{U}^\dagger \Upsilon_{-h} \mathcal{U} \simeq \begin{pmatrix} \mathcal{O}(\epsilon_a^2) & -2\sum_a \epsilon_a^* Y_a \\ -2\sum_a \epsilon_a Y_a^* & \sum_a |Y_a|^2 \end{pmatrix} , \tag{5.213}$$

where the off-diagonal entries of Υ_{-h} in the interaction basis are of order $\mathcal{O}(\epsilon_a Y_a^*)$. We use the superscript LNV since this quantity comes with the LNV equilibration rates. This will be clear in the following.

The perturbative treatment from the oscillatory regime cannot be used to analytically describe the overdamped regime simply because the larger decay rate is not small enough to be treated as a tiny perturbation parameter when compared to the vacuum oscillations. Nevertheless, as we will show in the following, appropriate analytic solutions are obtained

by making use of quasi-static approximations, similar to refs. [57, 63], and by expanding in the smaller eigenvalue. Note again that within this section we will work in the interaction basis of the heavy neutrinos and further only consider positive helicity deviations such that $\delta n_{ij} \equiv \delta n_{ijh}$ for $h = +$. This implies $\Upsilon_{+h} = YY^\dagger$ and $\Upsilon_{-h} = Y^*Y^T$. The evolution for the negative helicity deviation are obtained via complex conjugation of the kinetic equation, i.e. using the complex conjugate quantities of Γ_N, H_N^{vac} and H_N^{th}. Analogously to eq. (5.212), working in the interaction basis allows to express the mass matrix M in terms of the small LNV parameter μ and the average mass $\bar{M}$ from eq. (2.59) and (2.60), respectively, such that the combination of the mass matrix $\mathcal{U}^\dagger(MM^\dagger)\mathcal{U} = \tilde{M}\tilde{M}^\dagger$ in the interaction basis (denoted by tilde) appearing in the effective Hamiltonian in vacuum (5.80) is written as

$$\tilde{M}\tilde{M}^\dagger \simeq \bar{M}^2 \begin{pmatrix} 1+\mu^2+2\text{Re}(\chi)(2\mu-\mu^2) & 2\mu \\ 2\mu & 1+\mu^2-2\text{Re}(\chi)(2\mu-\mu^2) \end{pmatrix}, \tag{5.214}$$

with $\chi \sim \mathcal{O}(\epsilon_a)$ from eq. (5.211). In the exact $B-L$ conserving limit, i.e. for $\epsilon_a \to 0$, the mass and the interaction basis are maximally misaligned such that

$$\tilde{M}\tilde{M}^\dagger = \frac{1}{2}\begin{pmatrix} M_1^2+M_2^2 & M_2^2-M_1^2 \\ M_2^2-M_1^2 & M_1^2+M_2^2 \end{pmatrix} + \mathcal{O}(\epsilon_a)\,. \tag{5.215}$$

5.6.2 *Generation of asymmetries in the lepton sector*

According to eq. (5.154) the generation of the flavoured SM asymmetries Δ_a is due to the source (5.102) that is driven by the off-diagonal correlations δn_{hij}. Since we are working in the interaction basis it makes sense to use the flavour covariant form of the source from eq. (5.99) instead. A decomposition into a LNC or PF and into LNV part implies

$$\tilde{S}_a = \tilde{S}_a^{\text{PF}} + \tilde{S}_a^{\text{LNV}}\,, \tag{5.216}$$

$$\tilde{S}_a^{\text{PF}} = \gamma_+ \frac{a_{\text{R}}}{g_w}\text{tr}\left[\delta n_+ \Upsilon_+^a - (\delta n_- \Upsilon_-^a)^*\right], \tag{5.217}$$

$$\tilde{S}_a^{\text{LNV}} = \gamma_- \frac{a_{\text{R}}}{g_w}\text{tr}\left[\delta n_- \Upsilon_+^a - (\delta n_+ \Upsilon_-^a)^*\right], \tag{5.218}$$

where we use $(\Upsilon_{-h}^a)^* = \Upsilon_{+h}^a$. Note that only $\sum_a S_a^{\text{LNV}}$ is non-zero, while $\sum_a S_a^{\text{PF}} \neq 0$. Treating the backreaction as a higher order effect, cf. eq. (5.153), we have to solve the differential equation

$$\frac{\text{d}}{\text{d}z}\delta n_{ij} = -\frac{\text{i}}{2}[H_N^{\text{th}} + z^2 H_N^{\text{vac}}, \delta n]_{ij} - \frac{1}{2}\{\Gamma_N, \delta n\}_{ij}\,, \tag{5.219}$$

for δn_{ij}. Using eq. (5.212) together with eqs. (5.80) and (5.81) we can express the equilibration rate as well as the thermal corrections up to order $\mathcal{O}(\epsilon_a)$

$$\Gamma_N \simeq \frac{a_{\text{R}}}{T_{\text{ref}}}\sum_a |Y_a|^2 \begin{pmatrix} \gamma_+ & 0 \\ 0 & \gamma_- \end{pmatrix}, \tag{5.220}$$

$$H_N^{\text{th}} \simeq \frac{a_{\text{R}}}{T_{\text{ref}}}\sum_a |Y_a|^2 \begin{pmatrix} \mathfrak{h}_+^{\text{th}} & 0 \\ 0 & \mathfrak{h}_-^{\text{th}} \end{pmatrix} + \frac{\mathfrak{h}^{\text{EV}}}{2}\frac{a_{\text{R}}}{T_{\text{ref}}}\sum_a |Y_a|^2 \begin{pmatrix} 1 & 0 \\ 0 & 1 \end{pmatrix}, \tag{5.221}$$

while the effective Hamiltonian in vacuum is not necessarily diagonal in this basis

$$H_N^{\rm vac} = \frac{\pi^2}{18\zeta(3)}\frac{a_{\rm R}}{T_{\rm ref}^3}\bar{M}^2\begin{pmatrix}\mu^2+1 & 2\mu\\ 2\mu & \mu^2+1\end{pmatrix}. \tag{5.222}$$

As a consequence, the difference $(H_N^{\rm vac})_{11}-(H_N^{\rm vac})_{22}$ vanishes in the exact $B-L$ conserving limit. However, in order to be more general, we do not neglect this difference in the following discussion. We have decomposed Γ_N and $H_N^{\rm th}$ into the LNC and LNV contributions, that are both diagonal in the same basis, as well into the effect arising from the Higgs EV. Hence, the system of evolution equations without the backreaction effect is given by

$$\frac{{\rm d}\delta n_{11}}{{\rm d}z} = -(\Gamma_N)_{11}\delta n_{11} - \frac{\rm i}{2}z^2\left[(H_N^{\rm vac})_{12}\delta n_{21} - (H_N^{\rm vac})_{12}^*\delta n_{12}\right], \tag{5.223}$$

$$\frac{{\rm d}\delta n_{22}}{{\rm d}z} = -(\Gamma_N)_{22}\delta n_{22} - \frac{\rm i}{2}z^2\left[(H_N^{\rm vac})_{12}^*\delta n_{12} - (H_N^{\rm vac})_{12}\delta n_{21}\right], \tag{5.224}$$

for the diagonal contributions. The correlation is determined via

$$\begin{aligned}\frac{{\rm d}\delta n_{12}}{{\rm d}z} = &-\frac{1}{2}\left((\Gamma_N)_{11}+(\Gamma_N)_{22}\right)\delta n_{12} - \frac{\rm i}{2}\left((H_N^{\rm th})_{11}-(H_N^{\rm th})_{22}\right)\delta n_{12}\\ &- \frac{\rm i}{2}z^2\sum_k\left[(H_N^{\rm vac})_{1k}\delta n_{k2} - \delta n_{1k}(H_N^{\rm vac})_{k2}\right].\end{aligned} \tag{5.225}$$

Note that due to $\sum_a^2|\epsilon_a|^2/\sum_a|Y_a|^2 \ll 1$ in the overdamped regime and due to the smallness of the LNV rates compared to the LNC rates, one has the hierarchy $(\Gamma_N)_{11} \ll (\Gamma_N)_{22}$, such that the first heavy neutrino eigenstates equilibrates much faster than the second one and hence reaches its quasi-static value before the first oscillation

$$\frac{z_{\rm eq}}{z_{\rm osc}} = \frac{\sqrt[3]{|M_1^2-M_2^2|/a_{\rm R}^2}}{\gamma_+^{\rm av}\sum_a|Y_a|^2} \ll 1\,. \tag{5.226}$$

QUASI-STATIC APPROXIMATION: The quasi-static approximation as an effect of the fast equilibration of the first heavy neutrino eigenstate and its flavour correlations to the second heavy neutrino eigenstate implies

$${\rm d}\delta n_{11}/{\rm d}z \,=\, {\rm d}\delta n_{12}/{\rm d}z \,=\, {\rm d}\delta n_{21}/{\rm d}z \,\simeq\, 0\,, \tag{5.227}$$

and consequently relates δn_{11}, δn_{12} and $\delta n_{21} = \delta n_{12}^*$ directly to δn_{22} via

$$\delta n_{11} = \frac{z^4|(H_N^{\rm vac})_{12}|^2}{\mathcal{N}(z)}\frac{{\rm tr}(\Gamma_N)}{(\Gamma_N)_{11}}\delta n_{22}\,, \tag{5.228}$$

$$\delta n_{12} = -\frac{z^2(H_N^{\rm vac})_{12}\left({\rm i}\,{\rm tr}(\Gamma_N)+\Delta H_N^{\rm th}+z^2\Delta H_N^{\rm vac}\right)}{\mathcal{N}(z)}\delta n_{22}\,, \tag{5.229}$$

with the denominator

$$\mathcal{N}(z) \equiv {\rm tr}(\Gamma_N)^2 + (\Delta H_N^{\rm th})^2 + 2z^2\Delta H_N^{\rm th}\Delta H_N^{\rm vac} + z^4(\tilde{H}_N^{\rm vac})^2\,,$$

where we use the following notations

$${\rm tr}(\Gamma_N) \equiv (\Gamma_N)_{11}+(\Gamma_N)_{22}\,, \tag{5.230}$$

$$\Delta H_N^{\rm th} \equiv (H_N^{\rm th})_{11}-(H_N^{\rm th})_{22}\,, \tag{5.231}$$

$$\Delta H_N^{\rm vac} \equiv (H_N^{\rm vac})_{11}-(H_N^{\rm vac})_{22}\,, \tag{5.232}$$

$$(\tilde{H}_N^{\rm vac})^2 \equiv \frac{{\rm tr}(\Gamma_N)}{(\Gamma_N)_{11}}|(H_N^{\rm vac})_{12}|^2 + (\Delta H_N^{\rm vac})^2\,. \tag{5.233}$$

Note that due to eq. (5.221), $\Delta H_N^{\rm th}$ does not depend on the Higgs EV in the symmetric limit. Eqs. (5.228)-(5.229) allow for the differential equation for the weakly coupled state δn_{22} that does not depend on the correlations δn_{11} any more

$$\begin{aligned}\frac{{\rm d}\delta n_{22}}{{\rm d}z} &= -\left[(\Gamma_N)_{22} + {\rm tr}(\Gamma_N)\frac{z^4|(H_N^{\rm vac})_{12}|^2}{\mathcal{N}(z)}\right]\delta n_{22} \\ &= -\left[(\Gamma_N)_{22} + {\rm tr}(\Gamma_N)\frac{|(H_N^{\rm vac})_{12}|^2}{(\tilde{H}_N^{\rm vac})^2}\frac{z^4}{(z^2+\tilde{z}_{\rm c}^2)(z^2+\tilde{z}_{\rm c}^{*2})}\right]\delta n_{22}\,, \end{aligned} \tag{5.234}$$

where we have introduced the parameter

$$\tilde{z}_{\rm c} = \sqrt{\frac{\Delta H_N^{\rm th}}{\tilde{H}_N^{\rm vac}}\left[\frac{\Delta H_N^{\rm vac}}{\tilde{H}_N^{\rm vac}} + {\rm i}\sqrt{\frac{|(H_N^{\rm vac})_{12}|^2}{(\tilde{H}_N^{\rm vac})^2}\frac{{\rm tr}(\Gamma_N)}{(\Gamma_N)_{11}} + \frac{{\rm tr}(\Gamma_N)^2}{(\Delta H_N^{\rm th})^2}}\right]}\,, \tag{5.235}$$

as the poles of $\mathcal{N}(z)$. Note that the hierarchy $\gamma_- \ll \gamma_+$ as well as $\mathfrak{h}_-^{\rm th} \ll \mathfrak{h}_+^{\rm th}$ allows to approximate

$${\rm tr}(\Gamma_N) \simeq (\Gamma_N)_{11}\,, \qquad \Delta H_N^{\rm th} \simeq (H_N^{\rm th})_{11}\,. \tag{5.236}$$

Up to $\mathcal{O}(\epsilon_a)$ the effect from the Higgs EV appears a diagonal matrix in eq. (5.221). This diagonal matrix has no contribution due to the commutator of eq. (5.219). Hence, the thermal correction, which only enters as the difference $\Delta H_N^{\rm th}$ in eq. (5.225), is insensitive on the Higgs EV at $\mathcal{O}(\epsilon_a)$. With the absolute value

$$|\tilde{z}_{\rm c}| = \sqrt{\frac{\Delta H_N^{\rm th}}{\tilde{H}_N^{\rm vac}}}\sqrt[4]{1+\frac{{\rm tr}(\Gamma_N)^2}{(\Delta H_N^{\rm th})^2}}\,, \tag{5.237}$$

a new time scale arises that indicates the time when the vacuum part of the Hamiltonian $z^2 H_N^{\rm vac}$ starts becoming comparable to the thermal contribution $H_N^{\rm th}$. With approximations above one can show that

$$|\tilde{z}_{\rm c}| = \sqrt{\frac{\Delta H_N^{\rm th}}{\tilde{H}_N^{\rm vac}}}\sqrt[4]{1+\frac{\gamma_+^2}{(\mathfrak{h}_+^{\rm th})^2}} \sim z_{\rm osc}\sqrt{\frac{z_{\rm osc}}{z_{\rm eq}}\frac{\mathfrak{h}_+^{\rm th}}{\gamma_+}} \gg z_{\rm osc}\,, \tag{5.238}$$

Although we have neglected $(\Gamma_N)_{22}$ compared to $(\Gamma_N)_{11}$, we cannot simply neglect $(\Gamma_N)_{22}$ in eq. (5.224) since it can affect the equilibration of the second heavy neutrino eigenstate.

SOLUTIONS TO THE WEAKLY COUPLED HEAVY NEUTRINO STATE: With the differential equation (5.234) solutions are given by

$$\begin{aligned}\delta n_{22}(z) &= \delta n_{22}(0)\exp\left\{-\int_0^{z'}(\Gamma_N)_{22}(z'){\rm d}z' - (\Gamma_N)_{11}\frac{|(H_N^{\rm vac})_{12}|^2}{(\tilde{H}_N^{\rm vac})^2}\left[z - \frac{{\rm Im}\left(\tilde{z}_{\rm c}^3\arctan\frac{z}{\tilde{z}_{\rm c}}\right)}{{\rm Im}\tilde{z}_{\rm c}^2}\right]\right\} \\ &\simeq \delta n_{22}(0)\exp\left(-(\hat{\Gamma}_N)_{22}\frac{z^3}{3} - (\Gamma_N)_{11}\frac{|(H_N^{\rm vac})_{12}|^2}{(\tilde{H}_N^{\rm vac})^2}\frac{z^5}{5|\tilde{z}_{\rm c}|^4}\right)\,, \end{aligned} \tag{5.239}$$

where the approximation in the second step holds in the regime where $z \ll |\tilde{z}_{\rm c}|$ and is obtained by using the expansion $\arctan(x) = x - x^3/3 + x^5/5 + \mathcal{O}(x^7)$ and the relation ${\rm Im}(1/c)/{\rm Im}(c) = -1/|c|^2$ for $c \in \mathbb{C}$. Further, we have used that leading order contribution

to the LNV rate γ_- is of order $\mathcal{O}(z^2)$, such that we can decompose $(\Gamma_N)_{22}(z) \simeq (\hat{\Gamma}_N)_{22} z^2$ with the z-independent quantity $(\hat{\Gamma}_N)_{22}$. Note that in the $B-L$ conserving limit one has $\Delta H_N^{\rm vac} \simeq 0$ and consequently $|(H_N^{\rm vac})_{12}|^2 \simeq (\tilde{H}_N^{\rm vac})^2$. Therefore eq. (5.239) gives rise to two time scales

$$z_{N_2}^{\mathrm{eq},(\Gamma_N)_{11}} \equiv |\tilde{z}_c| \sqrt[5]{\frac{5}{(\Gamma_N)_{11}|\tilde{z}_{\rm c}|} \frac{|(H_N^{\rm vac})_{12}|^2}{(\tilde{H}_N^{\rm vac})^2}} \simeq |\tilde{z}_{\rm c}|^{4/5} (\Gamma_N)_{11}^{-1/5} , \tag{5.240}$$

$$z_{N_2}^{\mathrm{eq},(\Gamma_N)_{22}} \simeq (\hat{\Gamma}_N)_{22}^{-1/3} , \tag{5.241}$$

where $z_{N_2}^{\mathrm{eq},(\Gamma_N)_{11}}$ describes the equilibration process of the second heavy neutrino eigenstate N_2 through oscillations with the fast equilibrating eigenstate N_1. In contrast to that, $z_{N_2}^{\mathrm{eq},(\Gamma_N)_{22}}$ is the equilibrium time scale happening due to the LNV rate $(\Gamma_N)_{22}$. It follows that the heavy neutrino state N_2 will equilibrate before $|\tilde{z}_{\rm c}|$, which justifies the usage of eq. (5.239) a posteriori. These two equilibration time scales can be written as

$$z_{N_2}^{\mathrm{eq},(\Gamma_N)_{11}} \simeq \left(\frac{405\zeta^2(3)(\mathfrak{h}_+^{\rm th})^2}{\pi^4 \gamma_+} \frac{T_{\rm ref}^5}{a_{\rm R} \bar{M}^4} \frac{\sum_a |Y_a|^2}{\mu^4} \right)^{1/5} , \tag{5.242}$$

$$z_{N_2}^{\mathrm{eq},(\Gamma_N)_{22}} \simeq \left(\frac{a_{\rm R}}{T_{\rm ref}} \hat{\gamma}_- \sum_a |Y_a|^2 \right)^{-1/3} . \tag{5.243}$$

The ratio $z_{N_2}^{\mathrm{eq},(\Gamma_N)_{22}} / z_{N_2}^{\mathrm{eq},(\Gamma_N)_{11}}$ determines when the LNV processes are important. One might naively think that LNV effects are subdominant in low scale leptogenesis models since $(\Gamma_N)_{22}$ is suppressed by a factor of $\bar{M}^2/T_{\rm ref}$ compared to $(\Gamma_N)_{11}$. However, N_2 can equilibrate via the LNV rate at $z_{N_2}^{\mathrm{eq},(\Gamma_N)_{22}} \ll z_{N_2}^{\mathrm{eq},(\Gamma_N)_{11}}$, i.e. for small $\mu \ll 1$ and large Yukawa couplings, what delays the equilibration through the mixing. Nevertheless, there exist a huge fraction of the low scale leptogenesis parameter space, where the effect from LNV decays can be neglected. Hence, if $z \ll \tilde{z}_c$ and $z_{N_2}^{\mathrm{eq},(\Gamma_N)_{11}} \ll z_{N_2}^{\mathrm{eq},(\Gamma_N)_{22}}$, the equilibration process of the weakly coupled second heavy neutrino eigenstate N_2 can be described via

$$\delta n_{22}(z) \simeq \delta n_{22}(0) \exp\left(- \frac{z^5}{\left(z_{N_2}^{\mathrm{eq},(\Gamma_N)_{11}} \right)^5} \right) . \tag{5.244}$$

In a parameter region where LNV effects are subdominant, e.g. for parameter scenario III from table 5.1, both the equilibration of N_2 and the fast equilibration of N_1 are shown in figure 5.16, where the approximate result (5.244) for δn_{22} and with eq. (5.228) also the approximate evolution of δn_{11} are shown. Note, however, that the approximation (5.244) breaks down for $z_{N_2}^{\mathrm{eq},(\Gamma_N)_{11}} \sim z_{N_2}^{\mathrm{eq},(\Gamma_N)_{22}}$, where the decay of N_2 is mainly due to the equilibration rate $(\Gamma_N)_{22}$. This can be achieved by increasing $|\tilde{z}_c|$, i.e. when decreasing the mass splitting μ. Such a tuning is particularly important when aiming to reach large U_a^2, where the equilibration due to $(\Gamma_N)_{22}$ can have significant effects.

THE SOURCE OF THE ASYMMETRY: The source term (5.216)

$$S_a^{\rm PF} = 2\gamma_+ \frac{a_{\rm R}}{g_w} \mathrm{Re}\left[(\delta n_{+\,12} - \delta n^*_{-\,12}) (\Upsilon_+^a)_{21} \right] , \tag{5.245}$$

$$S_a^{\rm LNV} = -2\gamma_- \frac{a_{\rm R}}{g_w} \mathrm{Re}\left[(\delta n_{+\,12} - \delta n^*_{-\,12}) (\Upsilon_-^a)_{21} \right] , \tag{5.246}$$

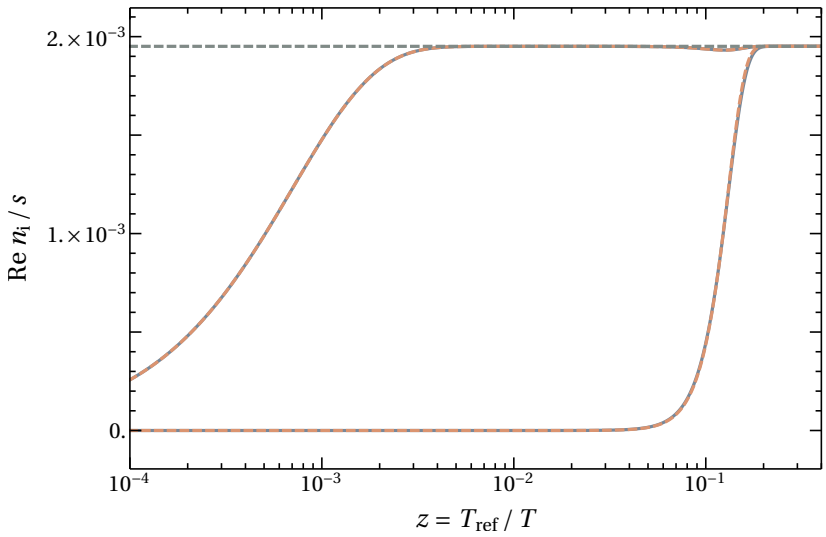

FIGURE 5.16: The fast and slow equilibration processes in the overdamped regime for the two heavy neutrinos n_{11} and n_{22}, respectively, in the interaction basis towards their equilibrium value n^{eq} (grey, dashed). The approximate solutions (orange, dashed), cf. eqs. (5.244) and (5.228), agree very well with the full numerical solution (blue). Here, parameter scenario III from table 5.1 is used.

which is responsible for the generation of the SM lepton asymmetry, is caused by the CP-odd correlation, cf. eq. (5.229),

$$\begin{aligned}\delta n_{+\,12} - \delta n^{*}_{-\,12} &= -2\mathrm{i}\,\mathrm{tr}(\Gamma_N)\frac{(H_N^{\mathrm{vac}})_{12}}{(\tilde{H}_N^{\mathrm{vac}})^2}\frac{z^2}{(z^2+\tilde{z}_{\mathrm{c}}^2)(z^2+\tilde{z}_{\mathrm{c}}^{*2})}\delta n_{22}(z)\\ &\simeq -2\mathrm{i}\,(\Gamma_N)_{11}\frac{(H_N^{\mathrm{vac}})_{12}}{(\tilde{H}_N^{\mathrm{vac}})^2}\frac{z^2}{|z^2+\tilde{z}_{\mathrm{c}}^2|^2}\delta n_{22}(z)\,,\end{aligned} \tag{5.247}$$

such that with eq. (5.239) the source is directly determined

$$\frac{S_a^{\mathrm{PF}}(z)}{T_{\mathrm{ref}}} = 4\frac{\gamma_+^2}{g_w}\frac{a_{\mathrm{R}}^2}{T_{\mathrm{ref}}^2}\sum_b |Y_b|^2\frac{(H_N^{\mathrm{vac}})_{12}}{(\tilde{H}_N^{\mathrm{vac}})^2}\mathrm{Im}\left[(\Upsilon_+^a)_{21}\right]\frac{z^2}{|z^2+\tilde{z}_{\mathrm{c}}^2|^2}\delta n_{22}(z)\,, \tag{5.248}$$

$$\frac{S_a^{\mathrm{LNV}}(z)}{T_{\mathrm{ref}}} = -4\frac{\hat{\gamma}_-\gamma_+}{g_w}\frac{a_{\mathrm{R}}^2}{T_{\mathrm{ref}}^2}\sum_b |Y_b|^2\frac{(H_N^{\mathrm{vac}})_{12}}{(\tilde{H}_N^{\mathrm{vac}})^2}\mathrm{Im}\left[(\Upsilon_-^a)_{21}\right]\frac{z^4}{|z^2+\tilde{z}_{\mathrm{c}}^2|^2}\delta n_{22}(z)\,, \tag{5.249}$$

with $\mathrm{Im}[(\Upsilon_+^a)_{21}] = \mathrm{Im}[Y_{2a}Y_{a1}^{\dagger}]$. Note that we cannot simply neglect the smaller eigenvalue $|\epsilon_a|$ since the source is only non-vanishing at first order in ϵ_a. As a consequence of the quasi-static approximation (5.227), the source directly depends on the deviation of the weakly coupled state δn_{22}. Further, since $\gamma_- \ll \gamma_+$, the LNV source for a given flavour is small compared to the LNC source: $S_a^{\mathrm{LNV}} \ll S_a^{\mathrm{PF}}$. Therefore, the baryon asymmetry being produced during the washout due to incomplete cancellations between the SM asymmetries is dominated by S_a^{PF}. Nevertheless, S_a^{LNV} already creates a baryon asymmetry independently of the washout since $B \sim \sum_a S_a^{\mathrm{LNV}} \neq 0$ with

$$\sum_a \frac{S_a^{\mathrm{LNV}}(z)}{T_{\mathrm{ref}}} = 8\frac{\hat{\gamma}_-\gamma_+}{g_w}\frac{a_{\mathrm{R}}^2}{T_{\mathrm{ref}}^2}\sum_b |Y_b|^2\frac{(H_N^{\mathrm{vac}})_{12}}{(\tilde{H}_N^{\mathrm{vac}})^2}\mathrm{Im}\left[\sum_a \epsilon_a Y_a^*\right]\frac{z^4}{|z^2+\tilde{z}_{\mathrm{c}}^2|^2}\delta n_{22}(z)\,. \tag{5.250}$$

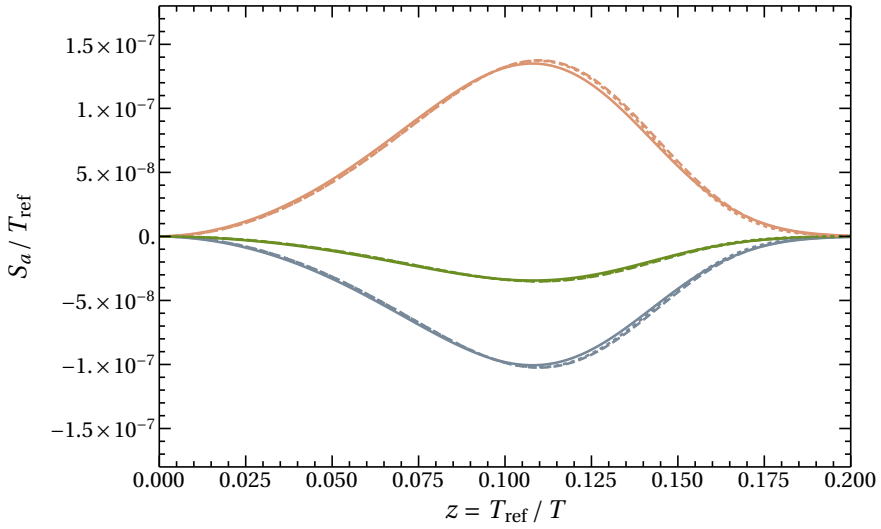

FIGURE 5.17: Source S_a for the SM asymmetries Δ_a for the three lepton flavours e (blue), μ (orange) and τ (green). The numerical solution (solid) is compared to the source with approximate analytic solutions for δn_{22} from the first row of eq. (5.239) (dashed) and also to the approximated source (5.251) (dotted). Here, parameter scenario III from table 5.1 is used.

This can be verified by using $B \sim \sum_a \mathrm{Im}[(\Upsilon^a_-)_{21}] = \mathrm{Im}[\Upsilon^{\mathrm{LNV}}_{21}] = -2\mathrm{Im}[\sum_a \epsilon_a Y_a^*] \neq 0$, while $\sum_a S_a^{\mathrm{PF}} \sim \sum_a \mathrm{Im}[(\Upsilon^a_+)_{21}] = \mathrm{Im}[\Upsilon^{\mathrm{diag}}_{21}] = 0$. For parameter regions where the LNV effects on the equilibration of δn_{22} are negligible, the evolution of the source term S_a is shown in figure 5.17 and the numerical solution is compared to the approximate analytic solution

$$\begin{aligned}\frac{S_a}{s\,T_{\mathrm{ref}}} &\simeq -\frac{45\sqrt{5}}{g_\star^{3/2} g_w 4\pi^{7/2}} \frac{\gamma_{\mathrm{av}}^2}{\mathfrak{h}_{\mathrm{th}}^2} \frac{m_{\mathrm{Pl}} \bar{M}^2 \mu}{T_{\mathrm{ref}}^3} \frac{\mathrm{Im}[Y_a^* \epsilon_a]}{\sum_b |Y_b|^2} z^2 \exp\left(-\frac{z^5}{\left(z_{N_2}^{\mathrm{eq},(\Gamma_N)_{11}}\right)^5}\right) \\ &\simeq -5.65 \times 10^{-7} \times \frac{m_{\mathrm{Pl}} \bar{M}^2 \mu}{T_{\mathrm{ref}}^3} \frac{\mathrm{Im}[Y_a^* \epsilon_a]}{\sum_b |Y_b|^2} z^2 \exp\left(-\frac{z^5}{\left(z_{N_2}^{\mathrm{eq},(\Gamma_N)_{11}}\right)^5}\right) . \end{aligned} \tag{5.251}$$

that is valid for $\mu \ll 1$ but still large enough that $z_{N_2}^{\mathrm{eq},(\Gamma_N)_{11}} \ll z_{N_2}^{\mathrm{eq},(\Gamma_N)_{22}}$.

GENERATION OF ASYMMETRY THROUGH THE HIGGS EV: While in the oscillatory regime the asymmetries Δ_a are mainly produced at early times, one can neglect the effect from the Higgs EV. However, in the overdamped regime, oscillations happen rather late such that the Higgs EV can have an effect on the asymmetry production. We find that even in the exact mass degenerate case, i.e. $\mu = 0$, the Higgs EV gives rise to a non-zero source. In order to show this, one has to keep in mind that even though the $\mathfrak{h}^{\mathrm{EV}}$ term in ΔH_N^{th} vanishes, a contribution of $(H_N^{\mathrm{th}})_{12} \sim \frac{1}{2}\frac{a_{\mathrm{R}}}{T_{\mathrm{ref}}} \mathfrak{h}^{\mathrm{EV}}(z) \epsilon_a Y_a^*$ arises since $\mathrm{Re}(YY^\dagger)$ is not completely diagonal in the basis where Υ_{+h} is diagonal. A deeper quantitative discussion might be interesting for future works.

VALIDITY OF THE QUASI-STATIC APPROXIMATION: In the overdamped regime the first heavy neutrino eigenstate equilibrates much faster than the second one, i.e. the

relation $(\Gamma_N)_{11}^{-1} \ll z$ holds for times z where the second heavy neutrino eigenstate has still not equilibrated. Therefore, unless δn_{22} effects the behaviour of δn_{11} drastically, δn_{11} can be treated to be quasi-static. In the following we will show that the smallness of the derivative $\mathrm{d}\delta n_{22}/\mathrm{d}z$ implies that $\mathrm{d}\delta n_{11}/\mathrm{d}z$ and $\mathrm{d}\delta n_{12}/\mathrm{d}z$ remain small at all relevant scales as well, such that the quasi-static approximations (5.227) are justified.

We have argued that the equilibration of δn_{22} happens at times $z_{N_2}^{\mathrm{eq},(\Gamma_N)_{11}} \ll |\tilde{z}_c|$. Eq. (5.244) then implies that the derivative $\mathrm{d}\delta n_{22}/\mathrm{d}z$ is small for $z \ll |\tilde{z}_c|$. Since the change in δn_{11} and δn_{12} after the equilibration of δn_{11} is only induced by changes in δn_{22}, we only have to show that $\mathrm{d}\delta n_{11}/\mathrm{d}z$ and $\mathrm{d}\delta n_{12}/\mathrm{d}z$ are small for times $z \ll |\tilde{z}_c|$. In this regime eqs. (5.228) and (5.229) simplify to

$$\delta n_{11} \simeq \frac{z^4}{|\tilde{z}_c|^4} \frac{|(H_N^{\mathrm{vac}})_{12}|^2}{(\tilde{H}_N^{\mathrm{vac}})^2} \frac{\mathrm{tr}(\Gamma_N)}{(\Gamma_N)_{11}} \delta n_{22}\,, \tag{5.252}$$

$$\delta n_{12} \simeq -\frac{z^2}{|\tilde{z}_c|^4} \left(\mathrm{i}(\Gamma_N)_{11} + \Delta H_N^{\mathrm{th}}\right) \frac{|(H_N^{\mathrm{vac}})_{12}|^2}{(\tilde{H}_N^{\mathrm{vac}})^2} \frac{\mathrm{tr}(\Gamma_N)}{(\Gamma_N)_{11}} \delta n_{22}\,, \tag{5.253}$$

Performing the derivative of these two equations after z justifies the use of the quasi-static approximation (5.227)

$$\frac{\mathrm{d}\delta n_{11}}{\mathrm{d}z} = \frac{4}{z}\delta n_{11} + \frac{\mathrm{d}\delta n_{22}}{\mathrm{d}z}\frac{\delta n_{11}}{\delta n_{22}} \ll (\Gamma_N)_{11}\delta n_{11}\,, \tag{5.254}$$

$$\frac{\mathrm{d}\delta n_{12}}{\mathrm{d}z} = \frac{2}{z}\delta n_{12} + \frac{\mathrm{d}\delta n_{22}}{\mathrm{d}z}\frac{\delta n_{12}}{\delta n_{22}} \ll (\Gamma_N)_{11}\delta n_{12}\,, \tag{5.255}$$

when making use of the fact that $\mathrm{d}\delta n_{22}/\mathrm{d}z$ is small and that $(\Gamma_N)_{11}^{-1} \ll z$ holds for the relevant z, as argued above.

5.6.3 *Evolution of lepton charges in absence of lepton number violation*

In contrast to the oscillatory regime, the evolution of the SM charges cannot be inferred by the source only. In terms of the larger eigenvalue it can be concluded that at least one flavour of Δ_a is of the same order Y_a as the quickly equilibrating heavy neutrino δn_{11}. Therefore, the washout and equilibration do not happen much later than the first oscillation. Rather the washout and the production of the charge happen at roughly the same time. Consequently, there is no saturation of the SM charge for small z. In order to solve for Δ_a, one needs to consider both the source and the backreaction term.

In the following we neglect LNV effects, and discuss possible implications later on. In this case it is possible to obtain an approximate analytic solution for the evolution of the baryon charge in the overdamped regime. Note that in this case $\tilde{L}$ remains zero throughout all times, which directly relates the baryon asymmetry to the sterile charges

$$B(z) = \frac{28}{79}\sum_a \Delta_a(z) = \frac{28}{79}\frac{2}{g_w}\left(\delta n_{11}^{\mathrm{odd}}(z) + \delta n_{22}^{\mathrm{odd}}(z)\right)\,. \tag{5.256}$$

We have already mentioned that the source term is only non-vanishing at first order in the smaller eigenvalue ϵ_a. Therefore, in order to correctly describe the evolution of the

SM charges, the system has to be solved to first order ϵ_a. To this order the helicity-odd deviation δn_{11} can be obtained from the following differential equations

$$\begin{aligned}\frac{\mathrm{d}\delta n_{11}}{\mathrm{d}z} = &-(\Gamma_N)_{11}\delta n_{11} - \frac{\mathrm{i}}{2}z^2\left[(H_N^{\mathrm{vac}})_{12}\delta n_{21} - (H_N^{\mathrm{vac}})^*_{12}\delta n_{12}\right] \\ &+ \frac{1}{2}\sum_{a,b}\frac{a_{\mathrm{R}}}{T_{\mathrm{ref}}}|Y_a|^2\tilde{\gamma}_+\left(A_{ab}+\frac{C_b}{2}\right)\Delta_a\,,\end{aligned} \tag{5.257}$$

and also depend on Δ_a due to the backreaction term. In contrast to that, the differential equation for δn_{22} remains unaffected since the backreaction is suppressed by ϵ_a. Since Δ_a is first order in ϵ_a, the neglect of the washout when calculating the sterile charges is justified at zeroth order in ϵ_a. With the charges $q_{Ni} \equiv 2\delta n^{\mathrm{odd}}_{ii}$ the evolution of the asymmetries Δ_a in the interaction basis is given by

$$\frac{\mathrm{d}\Delta_a}{\mathrm{d}z} = \frac{\tilde{\gamma}_+}{g_w}\frac{a_{\mathrm{R}}}{T_{\mathrm{ref}}}|Y_a|^2\sum_b(A_{ab}+C_b/2)\Delta_b - \frac{S_a}{T_{\mathrm{ref}}} - 2\frac{\gamma_+}{g_w}\frac{a_{\mathrm{R}}}{T_{\mathrm{ref}}}|Y_a|^2\delta n^{\mathrm{odd}}_{11}\,. \tag{5.258}$$

Analogously to the previous subsection, we can perform the quasi-static approximation. This allows to write the differential equation for $\delta n^{\mathrm{odd}}_{22}$ as

$$\begin{aligned}\frac{\mathrm{d}\delta n^{\mathrm{odd}}_{22}}{\mathrm{d}z} = &-(\Gamma_N)_{11}\frac{|(H_N^{\mathrm{vac}})_{12}|^2}{(\tilde{H}_N^{\mathrm{vac}})^2}\frac{z^4}{|z^2+\tilde{z}_c^2|^2} \\ &\times\left(\delta n^{\mathrm{odd}}_{22} - \sum_{b,c}\frac{|Y_b|^2}{2\sum_d|Y_d|^2}\left(A_{bc}+\frac{C_c}{2}\right)\Delta_c\right)\,,\end{aligned} \tag{5.259}$$

while $\delta n^{\mathrm{odd}}_{11}$ is replaced by its quasi-static value

$$\begin{aligned}\delta n^{\mathrm{odd}}_{11} = &\frac{|(H_N^{\mathrm{vac}})_{12}|^2}{(\tilde{H}_N^{\mathrm{vac}})^2}\frac{z^4}{|z^2+\tilde{z}_c^2|^2}\delta n^{\mathrm{odd}}_{22} \\ &+\sum_{b,c}\frac{|Y_b|^2}{2\sum_d|Y_d|^2}\left(A_{bc}+\frac{C_c}{2}\right)\Delta_c\left(1-\frac{z^4}{|z^2+\tilde{z}_c^2|^2}\frac{|(H_N^{\mathrm{vac}})_{12}|^2}{(\tilde{H}_N^{\mathrm{vac}})^2}\right)\,.\end{aligned} \tag{5.260}$$

Consequently, we can express $\delta n^{\mathrm{odd}}_{11}$ in terms of Δ_a and the derivative of $\delta n^{\mathrm{odd}}_{22}$

$$\delta n^{\mathrm{odd}}_{11} = \sum_{b,c}\frac{|Y_b|^2}{2\sum_d|Y_d|^2}\left(A_{bc}+\frac{C_c}{2}\right)\Delta_c - \frac{\mathrm{d}\delta n^{\mathrm{odd}}_{22}}{\mathrm{d}z}\left(\frac{a_{\mathrm{R}}}{T_{\mathrm{ref}}}\sum_a|Y_a|^2\gamma_+\right)^{-1}\,. \tag{5.261}$$

When neglecting the derivative $\mathrm{d}\delta n^{\mathrm{odd}}_{22}/\mathrm{d}z$, the baryon asymmetry is determined via

$$B(z) \simeq \frac{28}{79}\frac{2}{g_w}\left(\sum_{b,c}\frac{|Y_b|^2}{2\sum_d|Y_d|^2}\left(A_{bc}+\frac{C_c}{2}\right)\Delta_c(z) + \delta n^{\mathrm{odd}}_{22}(z)\right)\,. \tag{5.262}$$

Therefore, we need to know the evolution of $\delta n^{\mathrm{odd}}_{22}(z)$ and $\Delta_a(z)$. In general $\delta n^{\mathrm{odd}}_{22}(z)$ is obtained by solving eq. (5.259), where one needs to know the evolution of $\Delta_a(z)$. However, it turns out to be a good approximation to neglect $\delta n^{\mathrm{odd}}_{22}$ for times before the feebly coupled eigenstate equilibrates. After equilibration we can fix it to its quasi-static value, that is given by neglecting the RH side of eq. (5.259). Note that the quasi-static values for $\delta n^{\mathrm{odd}}_{11}$, which is given by eq. (5.261) when neglecting the derivative term, and $\delta n^{\mathrm{odd}}_{22}$ are equal

$$\delta n^{\mathrm{odd}}_{11,22} \to \sum_{b,c}\frac{|Y_b|^2}{2\sum_d|Y_d|^2}\left(A_{bc}+\frac{C_c}{2}\right)\Delta_c(z)\,, \tag{5.263}$$

such that

$$B(z) \simeq \frac{28}{79} \sum_{b,c} \frac{|Y_b|^2}{g_w \sum_d |Y_d|^2} \left(A_{bc} + \frac{C_c}{2} \right) \Delta_c(z) \left(1 + \theta \left(z - z_{N_2}^{\mathrm{eq},(\Gamma_N)_{11}} \right) \right) . \tag{5.264}$$

Consequently, $B(z)$ follows the evolution of $\Delta_a(z)$, which needs to be determined in the following. Eq. (5.261) can be inserted into eq. (5.258) to obtain

$$\frac{\mathrm{d}\Delta_a}{\mathrm{d}z} = \sum_b \tilde{W}_{ab} \Delta_b - \frac{S_a(z)}{T_{\mathrm{ref}}} - \frac{2}{g_w} \frac{|Y_a|^2}{\sum_d |Y_d|^2} \frac{\mathrm{d}\delta n_{22}^{\mathrm{odd}}}{\mathrm{d}z} , \tag{5.265}$$

with an effective washout matrix

$$\tilde{W}_{ab} = \frac{a_{\mathrm{R}}}{T_{\mathrm{ref}}} \frac{\gamma_+}{g_w} |Y_a|^2 \sum_c \left(\delta_{ac} - \frac{|Y_c|^2}{\sum_d |Y_d|^2} \right) A_{cb} . \tag{5.266}$$

It turns out to be a good approximation when neglecting the derivative $\mathrm{d}\delta n_{22}^{\mathrm{odd}}/\mathrm{d}z$ here, as it is small for $z \ll \tilde{z}_c$. Solutions are then given by

$$\Delta_a(z) \simeq \sum_{b,c=1,2} v_{ab}^T \mathrm{e}^{w_b z} \int_0^z \mathrm{d}z' \, \mathrm{e}^{-w_b z'} v_{bc} \frac{S_c(z')}{T_{\mathrm{ref}}} . \tag{5.267}$$

Here, v_{bc} are the set of eigenvectors of $\tilde{W}_{ab}$ and $w_{1,2}$ are the two corresponding non-vanishing eigenvalues. Note that in the absence of LNV processes there must be a vanishing eigenvalue. For the parameter scenario III from table 5.1 a comparison between the full numerical solution and the approximation (5.262) for Δ_a and B is presented in figure 5.18. The approximation agrees with the numerical solution for $z \gtrsim z_{N_2}^{\mathrm{eq},(\Gamma_N)_{11}}$ up to $\mathcal{O}(50\%)$, and is even more accurate for $z \lesssim z_{N_2}^{\mathrm{eq},(\Gamma_N)_{11}}$.

5.6.4 *Interesting scenarios in the overdamped regime*

In the following three interesting scenarios are qualitatively discussed.

SCENARIO I: LARGE MIXING ANGLES: Increasing the size of the Yukawa couplings does not only give larger mixing angles U_a^2 but also leads to a stronger washout. If the washout becomes too strong, the asymmetries Δ_a and thus the baryon asymmetry are washed out too early to be consistent with the experimental measured BAU. Consequently, there is an upper limit for the different mixing angles U_a^2. In order to preserve the baryon asymmetry from the washout one can further delay its washout by decreasing the mass splitting. In this case the baryon asymmetry is produced right before the EW sphaleron freeze-out, while the washout has no time to effectively wash out the asymmetry. The largest possible mixing angles are then obtained when delaying the production and further requiring the washout to be as weak as possible by keeping the magnitude of the Yukawa couplings large. Note that in order to have large mixing angles we cannot simply decrease the washout rate by lowering the Yukawa couplings. However, one can decrease the effective washout strength by requiring a certain flavour mixing pattern. These are different for the two neutrino mass orderings and are limited by neutrino oscillation data. For NO this is realised when the electron couples minimally. See appendix B for a detailed discussion. In contrast to that the electron has to couple maximally for IO, while the muon or the tau couple minimally.

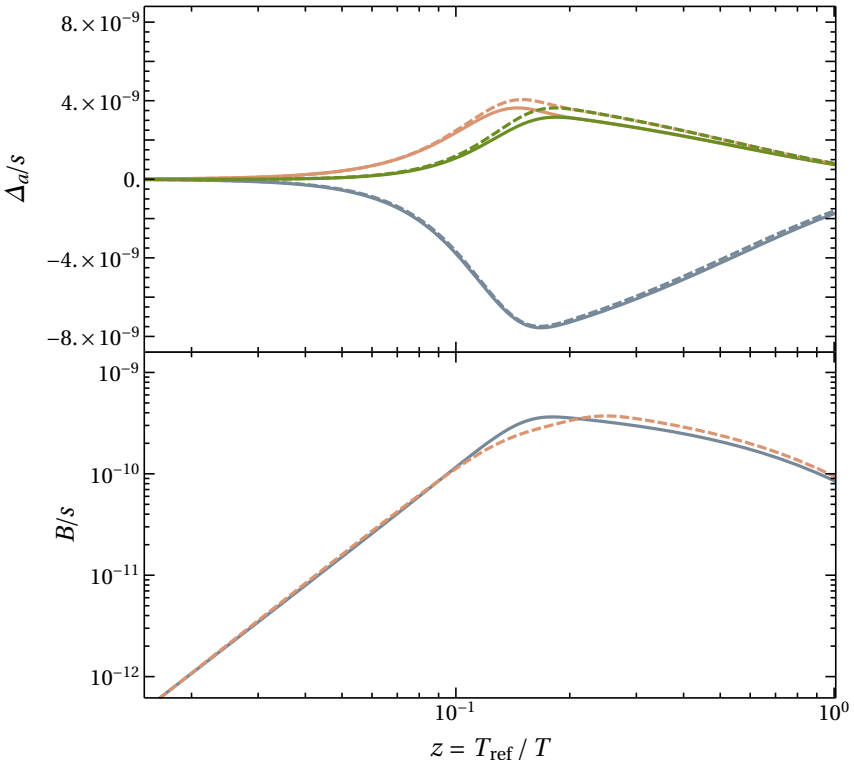

FIGURE 5.18: The numerical solution (solid) is compared to the approximate analytic solutions (dashed). The upper panel shows the SM asymmetries Δ_a for the three lepton flavours e (blue), μ (orange) and τ (green). The lower panel illustrates the validity of the analytic approximation to the baryon asymmetry. Here, parameter scenario III from table 5.1 is used.

In the following, we assume a highly flavour asymmetric washout for NO. Without loss of generality we can assume that the washout rate for Δ_1 is much smaller than the equilibration rate of the feebly coupled heavy neutrino eigenstate, while the washout rates for Δ_2 and Δ_3 are much larger than that equilibration rate, i.e. $\gamma_+|Y_1|^2 a_{\mathrm{R}}/T_{\mathrm{ref}} \ll 1/z_{N_2}^{\mathrm{eq},(\Gamma_N)_{11}}$ and $\gamma_+|Y_{2,3}|^2 a_{\mathrm{R}}/T_{\mathrm{ref}} \gg 1/z_{N_2}^{\mathrm{eq},(\Gamma_N)_{11}}$. In this case $\tilde{W}_{ab}$ has not only a zero eigenvalue due to conservation of $\tilde{L}$ but also a tiny eigenvalue due to the negligible washout of Δ_1. This leads to the relation $\Delta_1 = -2\Delta_{2,3}$ as soon as $\Delta_{2,3}$ reach their quasi-static value. This usually happens when the feebly coupled heavy neutrino eigenstate equilibrates, i.e. when the source term and the derivative in eq. (5.265) can be neglected. However, in the case of a strong washout of $\Delta_{2,3}$, this happens at very early times. A simple solution for the baryon asymmetry is then obtained from eq. (5.264) when neglecting $|Y_1|^2 \ll |Y_{2,3}|^2$ and using $\Delta_1 = -2\Delta_{2,3}$, such that

$$B(z) \simeq \frac{28}{79}\frac{\Delta_1(z)}{6g_w}\left(1 + \vartheta\left(z - z_{N_2}^{\mathrm{eq},(\Gamma_N)_{11}}\right)\right) . \tag{5.268}$$

An analytic expression for the evolution of the weakly washed out SM particle $\Delta_1(z)$ is given by approximately solving eq. (5.267) when neglecting the eigenvalue w_b within the integral. A more detailed study, where this approximate analytic solution is compared to the full numerical solution for both neutrino mass orderings is presented at the end of section 4 in ref. [2]. An exemplary plot showing the evolution of the asymmetries Δ_a and the baryon asymmetry for parameters chosen such that U^2 is maximal and being consistent with leptogenesis, is presented for NO in figure 5.19.

SCENARIO II: EARLY EQUILIBRATION: We have already mentioned that LNV effects are able to let the feebly coupled heavy neutrino eigenstate equilibrate early. According to eqs. (5.242) and (5.243) such a scenario can be achieved for large Yukawa couplings and a high mass degeneracy. Further, the higher the chosen mass of the heavy neutrino the more effective the impact of LNV becomes. The early equilibration then directly implies an early damping of the source as it is related to that heavy neutrino with the smaller eigenvalue through the quasi-static approximation. Therefore, both the SM asymmetries Δ_a and the baryon charge are affected by the early equilibration as well, such that LNV effects are able to highly change the baryon asymmetry. Note that this effect even occurs when neglecting the LNV source and the LNV washout, as the whole dynamic is changed through the early equilibration of the feebly coupled eigenstate together with the quasi-static approximation. An exemplary plot is given in figure 5.20 for the parameter scenario IV from table 5.1.

SCENARIO III: LARGE MASS SPLITTINGS: Provided that LNV processes are neglected, no sufficient amount of baryon charge is generated when having too large mass splittings for the heavy neutrinos. This is because the comparably strong washout has enough time to wash out all the produced charges. However, when including LNV effects, a non-zero generalised lepton number can be produced via the LNV source or via the LNV washout. Even if there is no early equilibration, as mentioned in the last paragraph, the amount of the baryon asymmetry that remains at the time when the EW sphalerons freeze out can be much higher when including LNV effects than without them. This is because the non-zero generalised lepton number is preserved by the LNC washout and is only diminished by the LNV washout. The lower panel figure 5.20 shows the evolution of the

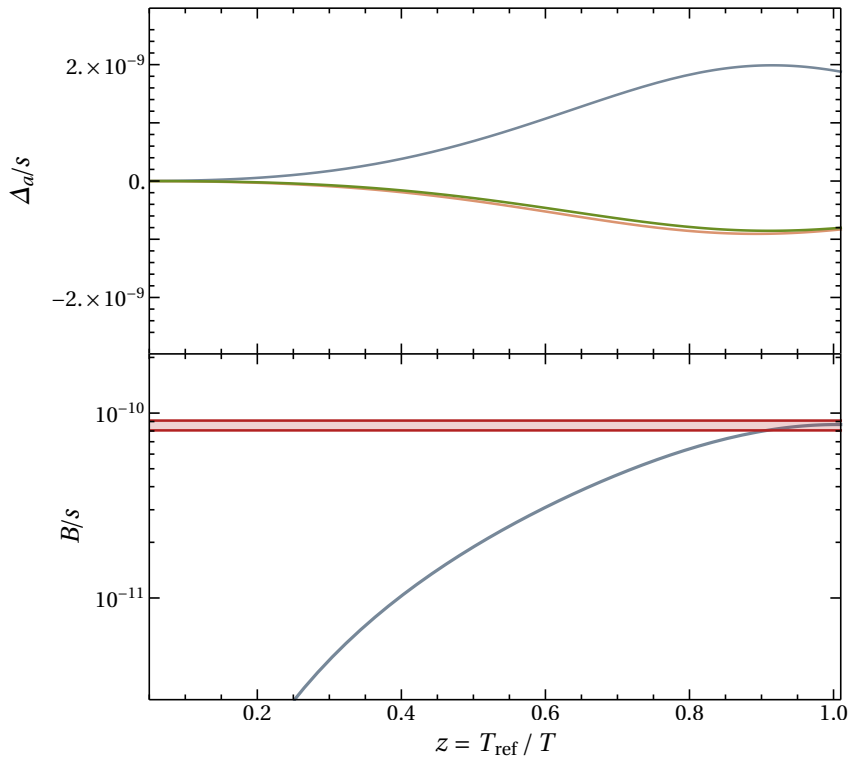

FIGURE 5.19: The evolution of the asymmetries Δ_a and the baryon asymmetry B for NO for $\bar{M} = 1\,\text{GeV}$. The additional parameters are chosen such that this scenario could explain the observed baryon asymmetry and such that U^2 is maximal, i.e. $U^2 = 1.09 \times 10^{-6}$. The late generation of the baryon charge is given by the degeneracy $\Delta M^2 = 4{\times}10^{-8}\bar{M}^2$, while the remaining parameters $\alpha_1 = 0$, $\alpha_2 = 0$, $\delta = \pi/2$ and $\text{Re}\omega = 5\pi/4 + 5.26\text{i}$ are chosen such that this example leads to a maximally flavour asymmetric washout. Within this example LNV effects are neglected. However, for that heavy neutrino mass they do not seem to change the output significantly.

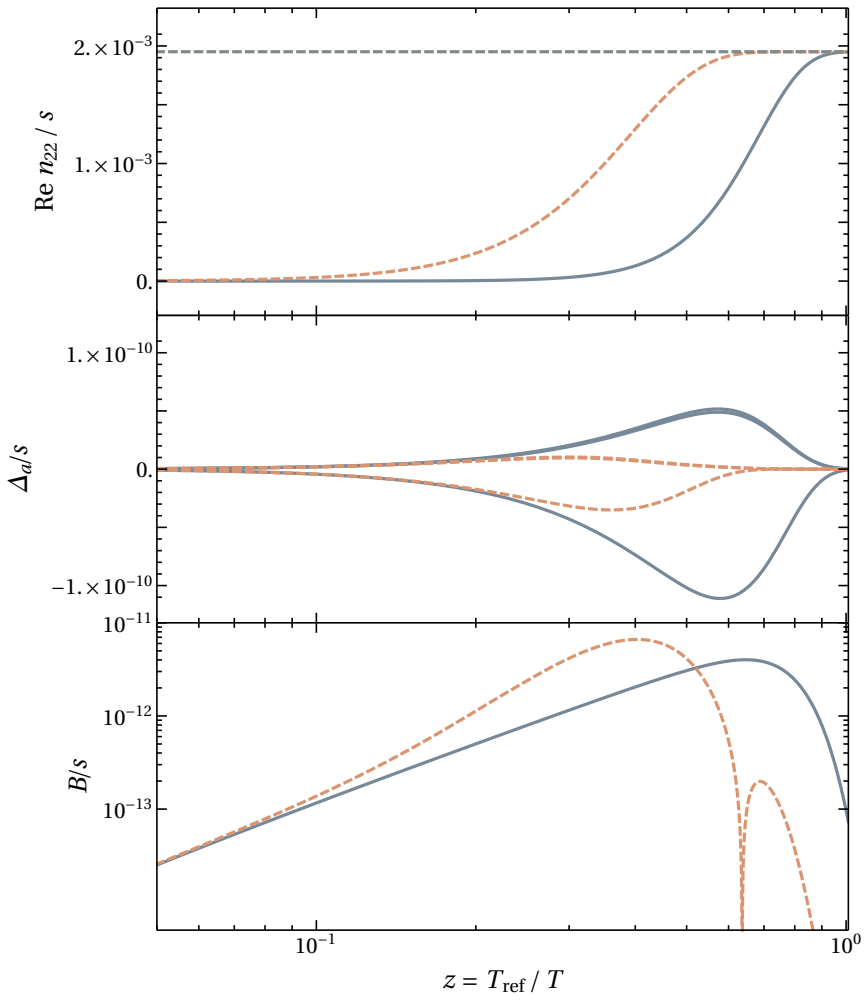

FIGURE 5.20: Equilibration of $\delta_{22}^{\mathrm{odd}}$ (first panel), as well as the evolution of the SM charges (second panel) and the baryon asymmetry (third panel) when neglecting LNV effects (blue, solid) and including LNV effects (orange, dashed). Here, parameter scenario IV from table 5.1 is chosen, which yields to an early equilibration of the feebly coupled heavy neutrino eigenstate.

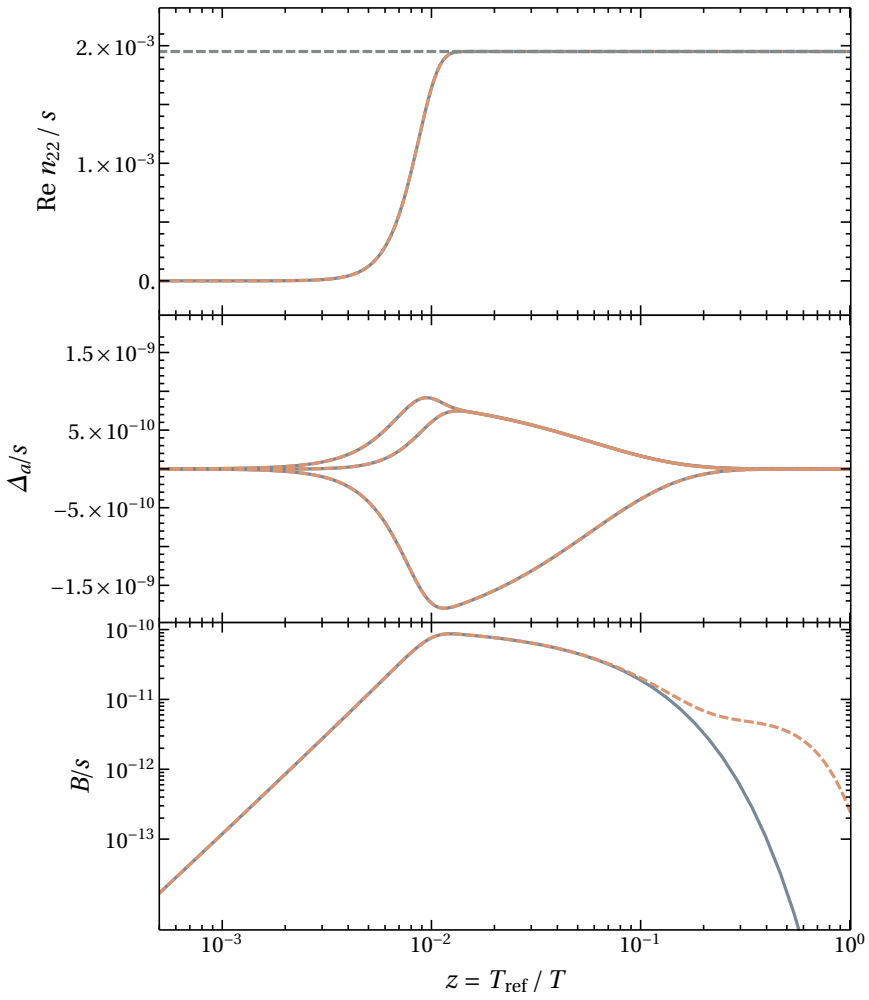

FIGURE 5.21: Equilibration of $\delta_{22}^{\mathrm{odd}}$ (first panel), as well as the evolution of the SM charges (second panel) and the baryon asymmetry (third panel) when neglecting LNV effects (blue, solid) and including LNV effects (orange, dashed). Here, parameter scenario V from table 5.1 is chosen.

baryon charge with and without LNV effects for the parameter scenario V from table 5.1. Note that for this choice, the evolution of the asymmetries Δ_a are almost unaffected by LNV effects. The Yukawa couplings are chosen such that the washout significantly erases the baryon charge in the absence of LNV effects. Nevertheless, a sizeable baryon asymmetry remains due to LNV processes. This is because the generalised lepton number can only be washed out by the LNV washout, which in general is much weaker than the LNC washout. As a consequence, the inclusion of LNV effects can allow for larger mass splitting that are consistent with leptogenesis.

6

TESTING THE LOW SCALE SEESAW AND LEPTOGENESIS

Heavy RH neutrinos with masses at the GeV-scale can not only account for the BAU via leptogenesis [17] but can also generate the light neutrino masses via the seesaw mechanism [18–23]. Several constraints on the flavour mixing pattern, their CP properties and on the mass spectrum are imposed under the requirement to fulfil these phenomena. In this chapter both bounds from past experiments, including searches for physics beyond the SM, and constraints from neutrino oscillation data [116] are taken into account. We refer to refs. [1, 16, 46, 92, 158, 159, 159–163] for pedagogical reviews in terms experimental constraints and perspectives. Further, the potential of future experiments to discover heavy neutrinos is studied. In particular, the parameter space for masses between 5 GeV and 50 GeV is confronted with the discovery potential of heavy neutrinos via displaced vertex searches at future lepton colliders such as FCC-ee [3, 68, 70, 72, 96], ILC [3, 70, 71, 97–99] and CEPC [3, 70, 100]. Besides the potential discovery of heavy neutrinos, the precision of measuring the coupling to all SM flavours due to large achievable number of displaced vertex events is investigated. Provided that heavy neutrinos are found in future experiments, the results can be used to decide of these are the common origin of the BAU and the light neutrino masses. If, additionally, the Dirac phase δ in the PMNS matrix (2.25) is measured to sufficient precision in neutrino oscillation experiments, such as NOνA [101] or DUNE [93–95], all model parameters of the type-I seesaw mechanism are in general determinable [1]. As a consequence, the low scale seesaw is a fully testable theory of baryogenesis and the light neutrino masses. This chapter is based on refs. [1, 3, 4, 6, 7].

Section 6.1 explains how neutrino oscillation data and other constraints, such as direct and indirect constrains, can be used to test the low scale seesaw mechanism as the origin of the light neutrino masses. Additional constraints arise in the possible case that the heavy neutrinos can account for the observed BAU via leptogenesis, as shown in section 6.2. In section 6.3 the perspective of future experiments such as FCC-ee, ILC and CEPC to probe the parameter space is determined, and how these can constrain the model parameters. Provided that heavy neutrinos are detected in the future, it is shortly discussed in section 6.4 how testable the low scale seesaw mechanism is. Additional informations, such as full expressions for the active-sterile mixing angles and a discussion about parameter invariances, are provided in appendix B.

6.1 TESTING THE SEESAW MECHANISM

Accounting for the experimentally observed properties of the light SM neutrino directly constraints the properties of the heavy neutrinos. In the near future all the unconstrained parameters of the light neutrinos can be measured expect for the Majorana phases. We

show that, if the resolution of the experiment allows for an independent measurement of the mixing of the heavy neutrinos to the individual SM flavours, it is possible to reconstruct all model parameters of the seesaw Lagrangian. However, the major part of the parameter space that also satisfies the leptogenesis constraints requires mass splittings ΔM that can be too small in order to be experimentally resolved. Consequently, only U_a^2 instead of U_{ai}^2 is observable, cf. eqs. (2.49) and (2.50) in chapter 2. Nevertheless, U_a^2 depends on the light neutrino mixing angles and can be used as a to probe the seesaw mechanism and consequently the origin of neutrino masses, even if the masses of heavy neutrino cannot be resolved individually. Recall that table 2.2 lists the best fit values of the neutrino oscillation data from November 2017 (NuFIT v3.1) [116].

Based on refs. [1, 6, 7], subsection 6.1.1 describes how neutrino oscillation data constrains both the flavour mixing ratios U_a^2/U^2 and the minimal U_a^2, while subsection 6.1.2 shortly discusses how past, direct and indirect, search experiments as well as observations from cosmology can constrain U_a^2.

6.1.1 *Constraints from neutrino oscillation data*

The seesaw equation (2.35) can be translated to the naive expectation (2.58) that relates the active-sterile mixing angles, see eq. (2.49), of a heavy neutrino with flavour i to the SM leptons with flavour a. In this case, the magnitude of the mixing is basically given by the heavy neutrino mass and by the light neutrino masses, cf. table 2.2. In this case, eq. (2.35) suggests that the active-sterile mixing angles need to be small in order to be in agreement with the smallness of the light neutrino masses. However, there might be cancellations in the light neutrino mass matrix m_ν such that the eigenvalues of m_ν are tiny despite comparably large Yukawa couplings resulting in large mixings U^2. In this case, mixing angles larger than the estimate (2.58) can be achieved in a technically natural way. This is particularly interesting when it comes to collider searches for the heavy neutrinos. Such cancellation can appear e.g. in models with an exact $B - L$ symmetry. This symmetry protected scenario is shortly discussed in subsection 2.2.4 and allows for an expansion in the small parameters μ and ϵ, see eq. (2.59). Throughout this chapter we limit ourselves to two almost degenerate heavy neutrino states, i.e. $\mu \simeq 0$, and keep only the leading order terms in ϵ. This is justified because particularly low scale leptogenesis mechanisms with large mixing angles, i.e. with small ϵ, that increase the chance of an experimental discovery of the heavy neutrinos, favour very small mass splitting μ. Further, this allows to express all the physical observables in terms of $\bar{M}$. An extension to three flavours is possible and has e.g. been performed in ref. [89].

FLAVOUR MIXING RATIOS: We find that leptogenesis with two heavy neutrinos requires a high mass degeneracy, i.e. $\mu \ll 1$, in order to be consistent with the observed BAU, especially when aiming for large mixing angles U^2, or $\epsilon \ll 1$, that lie within the reach of future experiments. Not all experiments in the future can resolve such a mass splitting with a sufficient precision. Consequently, these are not able to measure the individual heavy neutrinos, i.e. the mixing angles $U_{a1}^2 \simeq U_{a2}^2$ are not observable but only the sum $U_a^2 = \sum_i U_{ai}^2$, cf. eq. (2.49) for a definition of these mixing angles. To leading order in small solar mass differences, i.e. $\sqrt{m_\odot/m_{\text{atm}}}$, by following refs. [121, 159, 164],

and keeping terms of order $1/\epsilon$ the total mixing can be deduced from the full expression given in appendix B.1:

$$U^2 \simeq \frac{1}{2\bar{M}} m_{\text{atm}} e^{2\text{Im}\omega} \text{ for NH}\,, \tag{6.1}$$

$$U^2 \simeq \frac{1}{\bar{M}} m_{\text{atm}} e^{2\text{Im}\omega} \text{ for IH}\,. \tag{6.2}$$

The relations for the flavoured mixings U_a^2 in case of NO to the first non-vanishing order of $\sqrt{m_\odot/m_{\text{atm}}}$ read

$$U_e^2 \simeq e^{2\text{Im}\omega} \frac{m_{\text{atm}}}{2\bar{M}} \sin^2\theta_{13}\,, \tag{6.3}$$

$$U_\mu^2 \simeq e^{2\text{Im}\omega} \frac{m_{\text{atm}}}{2\bar{M}} \cos^2\theta_{13} \sin^2\theta_{23}\,, \tag{6.4}$$

$$U_\tau^2 \simeq e^{2\text{Im}\omega} \frac{m_{\text{atm}}}{2\bar{M}} \cos^2\theta_{13} \cos^2\theta_{23}\,. \tag{6.5}$$

The approximate value $\theta_{23} \simeq \pi/4$ makes U_μ^2 and U_τ^2 to be comparable in size, while the relative smallness of θ_{13} suppresses U_e^2 with respect to U_μ^2 and U_τ^2. Within this approximation of small $m_\odot/m_{\text{atm}}$ the only free parameter is $\text{Im}\omega$ since $\bar{M}$ can be measured kinematically. As a consequence, the set of equations is overconstrained. In case of IO, θ_{13} and $\theta_{23} - \pi/4$ can be neglected to obtain simple relations:

$$U_e^2 \simeq e^{2\text{Im}\omega} \frac{m_{\text{atm}}}{2\bar{M}} \left[1 + \xi \sin\left(\frac{\alpha_2 - \alpha_1}{2}\right) \sin(2\theta_{12})\right], \tag{6.6}$$

$$U_\mu^2 \simeq e^{2\text{Im}\omega} \frac{m_{\text{atm}}}{4\bar{M}} \left[1 - \xi \sin\left(\frac{\alpha_2 - \alpha_1}{2}\right) \sin(2\theta_{12})\right], \tag{6.7}$$

$$U_\tau^2 \simeq U_\mu^2\,. \tag{6.8}$$

Within the approximation of small $m_\odot/m_{\text{atm}}$, a measurement of U_e^2 and U_μ^2 would not only allow to determine $\text{Im}\omega$, but also the physical Majorana phase difference $\alpha_2 - \alpha_1$. Note that these simplified relations can be useful to gain a rough qualitative understanding of the mixing angles and particular their parametric dependences. However, at the desired quantitative level the dependence of U_a^2 on the Dirac phase δ and on the Majorana phases $\alpha_{1,2}$ have to be taken into account. This is because $m_\odot/m_{\text{atm}}$, θ_{13} and $\theta_{23} - \pi/4$ turn out to be not small enough to allow for such an approximation, e.g. $\sqrt{m_\odot/m_{\text{atm}}} \sim 1/2$. This requires to use the full expressions from appendix B.1. We find that for $\mu, \epsilon \ll 1$ the flavour ratios U_a^2/U^2 do not depend on $\text{Im}\omega$. The possible range of U_a^2/U^2 that is consistent with neutrino oscillation data can be obtained by varying the phases α_2 and δ. Note that in the scenario of two heavy neutrinos the lightest SM neutrino needs to be massless. This allows to set $\alpha_1 = 0$, which can e.g. be read off from the eq. (B.1). We relate the flavour mixing ratio U_e^2/U^2 to U_μ^2/U^2 for both neutrino mass ordering in figure 6.1.

SEESAW LINES: The seesaw mechanism does not only constrain the flavour ratios U_a^2/U^2 but also gives a lower bound on the individual U_a^2. This is due to the fact that for any mass $\bar{M}$ the Yukawa couplings have to be small enough in order to be still able to explain the light neutrino masses. This can be seen from the naive seesaw equation (2.58). In the limit of $\mu \ll 1$ these so-called seesaw lines are given by $U_a^2 \sim 1/\bar{M}$ and happen for certain combinations of $(\alpha, \delta, \text{Im}\omega)$. See appendix B.1 for a detailed discussion including eqs. (B.34)-(B.39). Note that the symmetry protected scenario, as described in

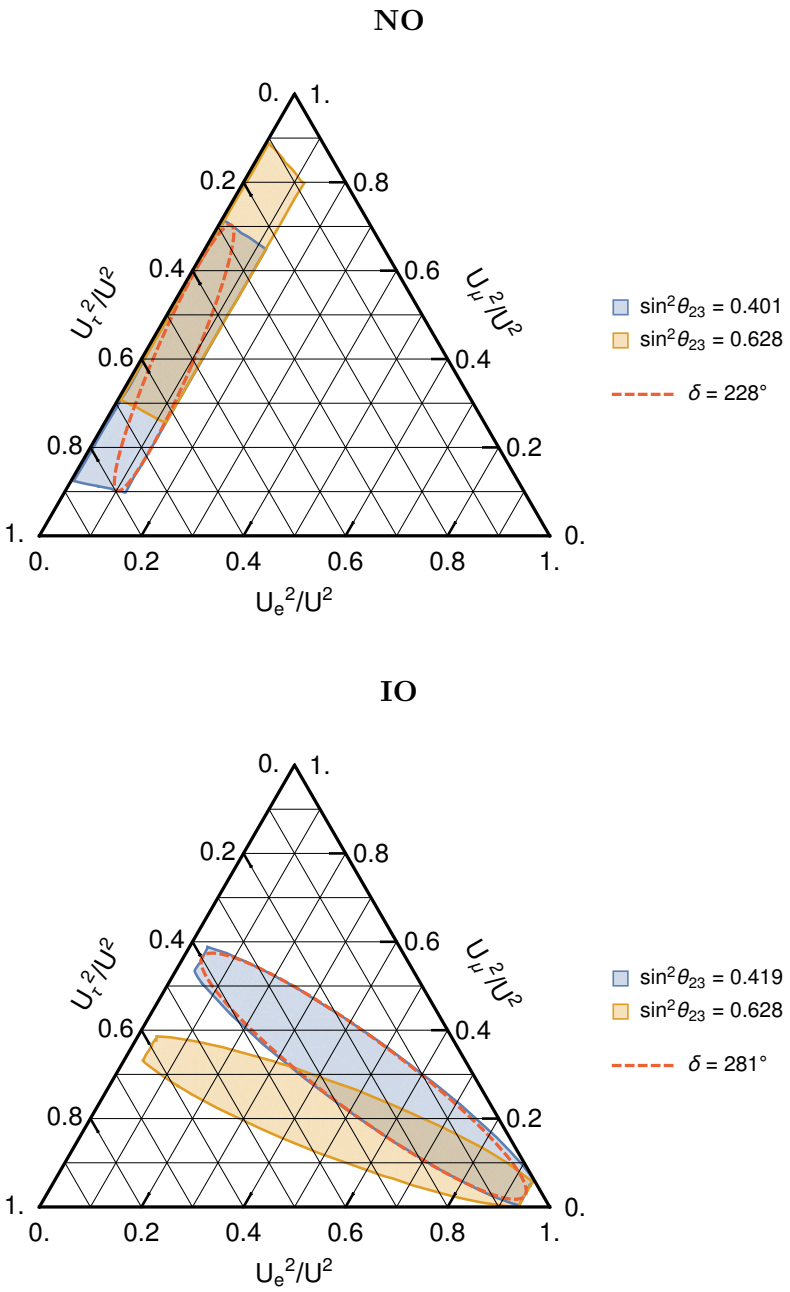

FIGURE 6.1: This plot is an updated versions of figure 1 from ref. [1] and describes the allowed range of U_a^2/U^2 indicated by the coloured regions. This range is obtained by varying the phases in U_ν after the light neutrino mixing angles and the light neutrino masses are fixed to their best fit values as given in table 2.2. Note that $\sum_a U_a^2/U^2 = 1$ fixes U_τ^2/U^2. In the upper panel NO is assumed, while in the lower panel IO is chosen. The 3σ range for θ_{23} is given by $0.401 \lesssim \sin^2\theta_{23} \lesssim 0.628$ for NO and by $0.419 \lesssim \sin^2\theta_{23} \lesssim 0.628$ for IO [116]. The orange and blue regions are given as the limits of this experimental uncertainty. Provided that the Dirac phase δ is measured in the future to a sufficient precision, the plotted regions will reduce to ellipses in the U_e^2/U^2-U_μ^2/U^2 plane. With the best fit value [116] $\delta = 228°$ and $\delta = 281°$ for NO and IO, respectively, this is shown by the red dashed lines. This figure assumes the limit $\epsilon, \mu \ll 1$. Thus, the flavour ratios U_a^2/U^2 do not depend on Imω. For non-small ϵ, i.e. for smaller Imω, both the size and the shape of the coloured region change.

subsection 2.2.4, allows for Yukawa couplings that are not constraint from above, such that there is no upper bound for U_a^2 from neutrino oscillation data. However, as shown in figures 6.2-6.5, leptogenesis imposes an upper bound U_a^2 since the washout must not be too strong in order to explain the observed BAU. We find that lower bounds on the U_a^2 are given by leptogenesis and not by the seesaw constraints for small masses $\bar{M}$. However, for larger masses $\bar{M}$, the lower bounds for the different U_a^2 converge to the corresponding seesaw lines. This effect can e.g. be seen in figures 6.2-6.5.

6.1.2 *Other constraints*

We shortly summarise other constraints than the ones from neutrino oscillation data which will set bounds on the range of U_{ai}^2 or particularly on U_a^2 for a given average mass $\bar{M}$. Detailed studies are given in refs. [1, 162] for two almost mass degenerate heavy neutrinos. The different constraints can be grouped into direct constraints, indirect constraints and constraints from cosmology. In ref. [1] a parameter scan is presented that finds the allowed range of U_a^2 that is consistent with past experiments. Those constraints are located at very large Imω that are much above the maximally allowed U^2 by leptogenesis. Therefore, this requires the use of the radiatively corrected Casas-Ibarra parametrisation, as introduced in ref. [119], instead of eq. (2.52).

DIRECT CONSTRAINTS: In general heavy neutrinos take part in all processes which involve SM neutrinos, if the processes is kinematically allowed, but with an amplitude suppressed with the mixing angle, cf. eq. (2.47). We refer the seek for heavy neutrinos in processes where they are being produced and appear as real particles to as direct searches. For the parameter scan negative results from the following direct search experiments are taken into account, NA3 [165], PS191 [166], CHARM [167, 168], DELPHI [169], L3 [170], TINA [171], CHARMII [172], NuTeV [173] LHCb [174], ATLAS [175], CMS [176], BELLE [177], BEBC [178], FMMF [179], E949 [180], PIENU [181], NOMAD [182], besides constraints from Kaon decays [183, 184]. Particularly for peak searches below the Kaon mass, the summary given in ref. [158] is used, while for PS191 the reinterpretation given in ref. [159] is used to obtain the direct constraints.

INDIRECT CONSTRAINTS: Even if the heavy neutrinos do not appear as real particles, constraints can be deduced from indirect searches in which the heavy neutrinos appear as virtual states. One of the strongest constraints is given by the neutrino oscillation data. It does not only constrain or determine the mixing angles θ_{ab} and the mass differences $m_\odot$, $m_{\rm atm}$, but will also allow to measure the Dirac phase δ to a high precision. As already discussed in subsection 6.1.1, we find that a detection of heavy neutrinos and the consequent measurement of the individual U_a^2 can provide informations about the Majorana phases $\alpha_{1,2}$ and the Dirac phase δ. Further, we find lower bounds on U_a^2 that are given in terms of the seesaw lines (B.34)-(B.39). The constraints from direct searches, as discussed above, can be combined with indirect constraints, such as as constraints from $0\nu\beta\beta$ decays [185, 186], violation of CKM unitarity [187–192], LNV decays [193, 194], lepton universality [187, 195, 196], and constraints from EW precision data [197–199]. A detailed discussion is given in ref. [162].

CONSTRAINTS FROM COSMOLOGY: Before turning our attention to constraints from leptogenesis we shortly comment on a cosmological effect that also limits the mixings U_a^2. The requirement that heavy neutrinos, which come into thermal equilibrium in the early universe [200], must have decayed before the formation of light elements in BBN [201], imposes constraint on the lifetime of the heavy neutrinos, i.e. their lifetime must be shorter than 0.1 s. This argument is based on the decay rates provided in refs. [87, 144].

COMBINED CONSTRAINTS: Neutrino oscillation data, direct and indirect searches as well the BBN individually constrain the $\bar{M} - U_a^2$ plane. One would naively expect that the total excluded region is given by superimposing these regions. However, we find that the synergy of these constraints imply non-trivial combined constraints that are much stronger than these. The global constrained are given in figures 2-3 of ref. [1] and are shown as the grey region in figures 6.2-6.5.

6.2 CONSTRAINTS FROM LEPTOGENESIS

In the previous section we have found that strong constraints on the flavour mixing pattern of the heavy neutrinos, particularly for large U^2, are imposed by the requirement to explain the light neutrino masses via the seesaw mechanism. Further, other constraints such as those from direct and indirect searches as well as from BBN have been discussed, which put constraints on the mass spectrum of the heavy neutrinos. Besides that, additional constraints arise when simultaneously requiring the heavy to explain the observed BAU. In order to investigate the testability of leptogenesis with two heavy neutrinos, upper and lower bounds for U^2 and the different U_a^2 that are consistent with the observed BAU and the light neutrino masses are provided based on refs. [1, 6, 7]. These are compared to both the disfavoured regions by the combined constraints and to proposed sensitivity lines of future experiments. As a generalisation of refs. [1, 6, 7], we further discuss how flavour effects further constrain the parameter space, in particular U_a^2/U^2, due to the importance of flavour asymmetric washout rates for large U^2, cf. appendix B.1. Note that large U^2 happen in the overdamped regime, particularly in the symmetry protected scenario, which is why LNV effects are in general not negligible. Therefore, we perform a parameter scan that includes these effects by using the set of equations (5.153) and (5.154). More details about how such a parameter scan is performed are given in ref. [3].

In subsection 6.2.1 lower and upper bounds on the individual mixings U_a^2 that are consistent with leptogenesis are compared to both the region that is excluded by the combined constrained and to future experiments that might be able to test low scale leptogenesis. The effect of leptogenesis on the flavour ratios U_a^2/U^2 is discussed in subsection 6.2.2.

6.2.1 *Testability in future experiments*

When trying to answer the question if the heavy neutrinos will be discovered in future experiments it is important to compare the expected sensitivity of such experiments to the allowed parameter region, that can both explain the light neutrino masses and also account for the predicted value for the BAU. For that reason it is convenient to plot U^2 and also the various U_a^2 over $\bar{M}$. When binning the whole range of $\bar{M}$ logarithmically, the largest and smallest possible value for the corresponding mixing is extracted. The data

points can then be connected to an upper bound and a lower bound. We limit ourselves to masses in the range $0.1\,\text{GeV} \lesssim \bar{M} \lesssim 50\,\text{GeV}$ for two reasons. First, constraints from the BBN that all heavy neutrinos must decay faster than 0.1 s puts strong bound on the minimal mass, such that $0.1\,\text{GeV} \lesssim \bar{M}$ is an appropriate choice. Second, $\bar{M} \gtrsim 50\,\text{GeV}$ are in general testable but cause the relativistic treatment of the kinetic equations from chapter 5 to break down.

The possibility of future experiments to see signatures of heavy neutrinos for the different U_a^2 and the total U^2 is displayed in figures 6.2-6.5 and in figure 6.8 for FCC-ee, ILC and CEPC. These figures are updated versions of figures 4-7 from ref. [1]. Note that for the upper and lower bound lines for the BAU we do not take LNV effects into account. Although the baryon asymmetry is in general affected by such effects, which makes them non-negligible for many certain parameter choices, we find that the error on the upper bound for the BAU is of $\mathcal{O}(1)$, see figure 6.8 for U^2 with heavy neutrino masses larger than 5 GeV for comparison. The leptogenesis lower bound converges quickly to the seesaw line, i.e. for small masses. This happens even before the combined constraint is solely given by the seesaw line. Therefore, the leptogenesis lower bound is only affected by LNV effects in the region that is already disfavoured by global constraints.

Heavy neutrinos with masses smaller than the mass of the B meson can be searched for at proposed fixed target experiments such as T2K [88], NA62 [88–90] and SHiP [69, 91, 92] or even in LBNE [93–95]. In addition, B-factories [82–86] is capable to test the low scale leptogenesis parameter space. Provided that the heavy neutrinos are heavier than the B mesons but still lighter than the W boson, searches can be performed via lepton [67–74] and hadron colliders [74–81]. A review of signature searches for heavy neutrinos at colliders is provided in ref. [74].

A more careful study of experiments such as FCC-ee at the Z-pole and ILC as well as CEPC is provided in section 6.3. The testability interpretation of the other experiments, i.e. those from figures 6.2-6.5, has to be taken with care since it is suffering particularly from the following issue. A certain U_a^2 for a given heavy neutrino mass $\bar{M}$ and SM flavour a might be consistent with an observation in an experiment and also with successful leptogenesis. However, as different sets of model parameters that lead to this specific U_a^2 can in general correspond to different U_b^2 for $b \neq a$, this does not necessarily imply that those heavy neutrinos that are discovered in the experiments are able to generate the observed BAU. A more precise approach to treat the testability is given by both calculating the sensitivity of the experiment for every set of seesaw parameters and determining if this set is able to predict the BAU. We discuss this scenario particularly for the colliders FCC-ee, ILC and CEPC in section 6.3.

6.2.2 *Flavour mixing patterns*

As already discussed in detail in chapter 5, the overdamped regime is characterised by large Yukawa couplings that not only result in a sizeable production of asymmetries but also make this regime suffer from a strong washout. Since both the washout rates and the damping rates depend on the same Yukawa couplings, a complete washout of the SM asymmetries and consequently of B can only avoided for a given hierarchy in the magnitude of the washout rates. Thus, it is expected that leptogenesis with large mixings U^2 can only be realised in the case of certain flavour mixing patterns, that allow for such

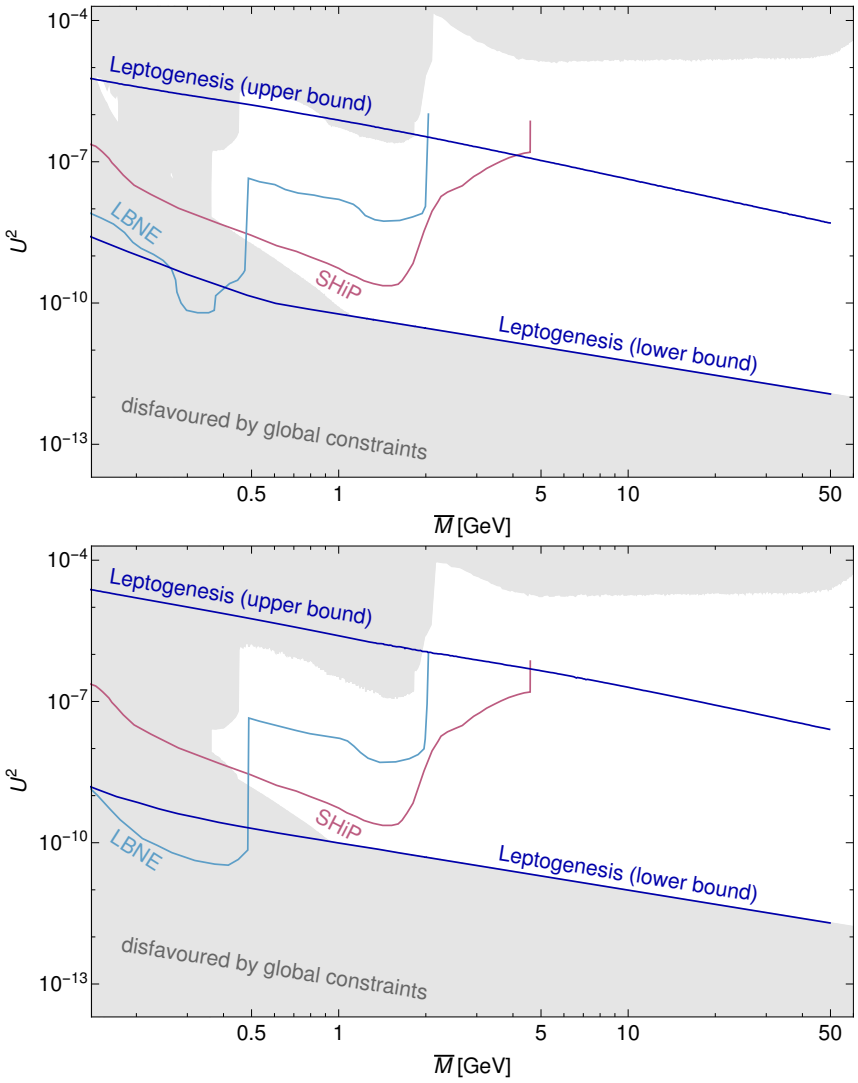

FIGURE 6.2: These plots are updated versions of figure 4 from ref. [1] and show the limits on the total U^2 as a function of $\bar{M} = (M_1 + M_2)/2$ for NO (top panel) and IO (bottom panel) that is consistent with leptogenesis and neutrino oscillation data. The parameter region that is disfavoured by global constraints, as discussed in section 6.1, is given by the grey area. The upper and lower bounds on the mixing (blue lines) are compared to the maximally achieved sensitivities of future experiments: The SHiP lines (purple) correspond to the 90% c.l. upper limits for 0.1 background events in 2×10^{20} proton target collisions for a ratio of $U_e^2 : U_\mu^2 : U_\tau^2 \sim 52 : 1 : 1$ [91, 202]. The LBNE/DUNE sensitivity (light blue) is given under the assumption of an exposure of 5×10^{21} protons on target for a detector length of 30 m [94]. The expected achieved sensitivities of FCC-ee, ILC and CEPC, which can effectively probe the parameter space for $\bar{M} \gtrsim 5$GeV via displaced vertex searches [3], are given in figure 6.8.

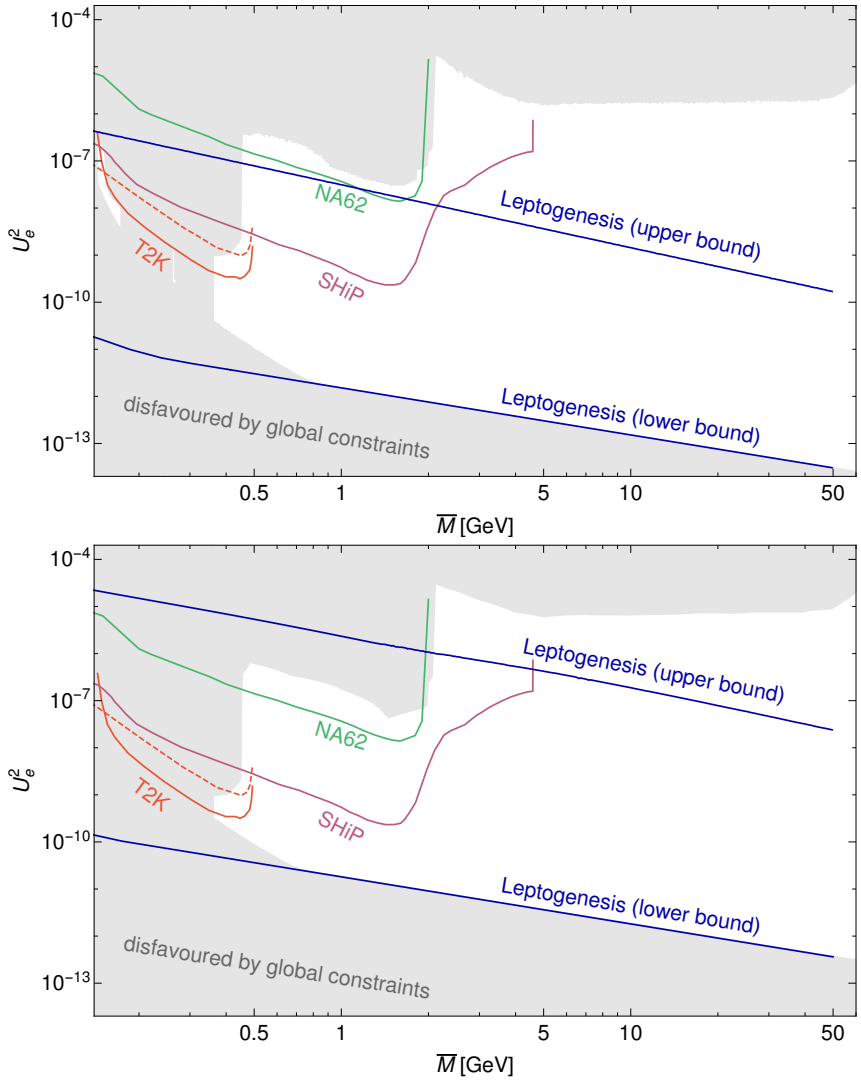

FIGURE 6.3: These plots are updated versions of figure 5 from ref. [1] and show the limits on the total U^2 as a function of $\bar{M} = (M_1 + M_2)/2$ for NO (top panel) and IO (bottom panel) that is consistent with leptogenesis and neutrino oscillation data. The parameter region that is disfavoured by global constraints, as discussed in section 6.1, is given by the grey area. The upper and lower bounds on the mixing (blue lines) are compared to the maximally achieved sensitivities of future experiments: The SHiP lines (purple) correspond to the 90% c.l. upper limits for 0.1 background events in 2×10^{20} proton target collisions for a ratio of $U_e^2 : U_\mu^2 : U_\tau^2 \sim 52 : 1 : 1$ [91, 202]. An estimate of the T2K sensitivity is provided in ref. [88] with 10^{21} protons on target at 90% c.l. with full volume for both the $K^+ \to e^+ N \to e^+ e^- \pi^+$ two-body decays (red, solid) and the $K^+ \to e^+ N \to e^+ e^- e^+ \nu_e$ three-body decays (red, dashed) [88].The expected limit of the NA62 experiment on U_e^2 via $K^+ \to \pi^+ \nu \bar{\nu}$ with about 10^{13} 400 GeV protons on target is given by the turquoise line for the scenario $U_e^2 : U_\mu^2 : U_\tau^2 \sim 1 : 0 : 0$ [89].

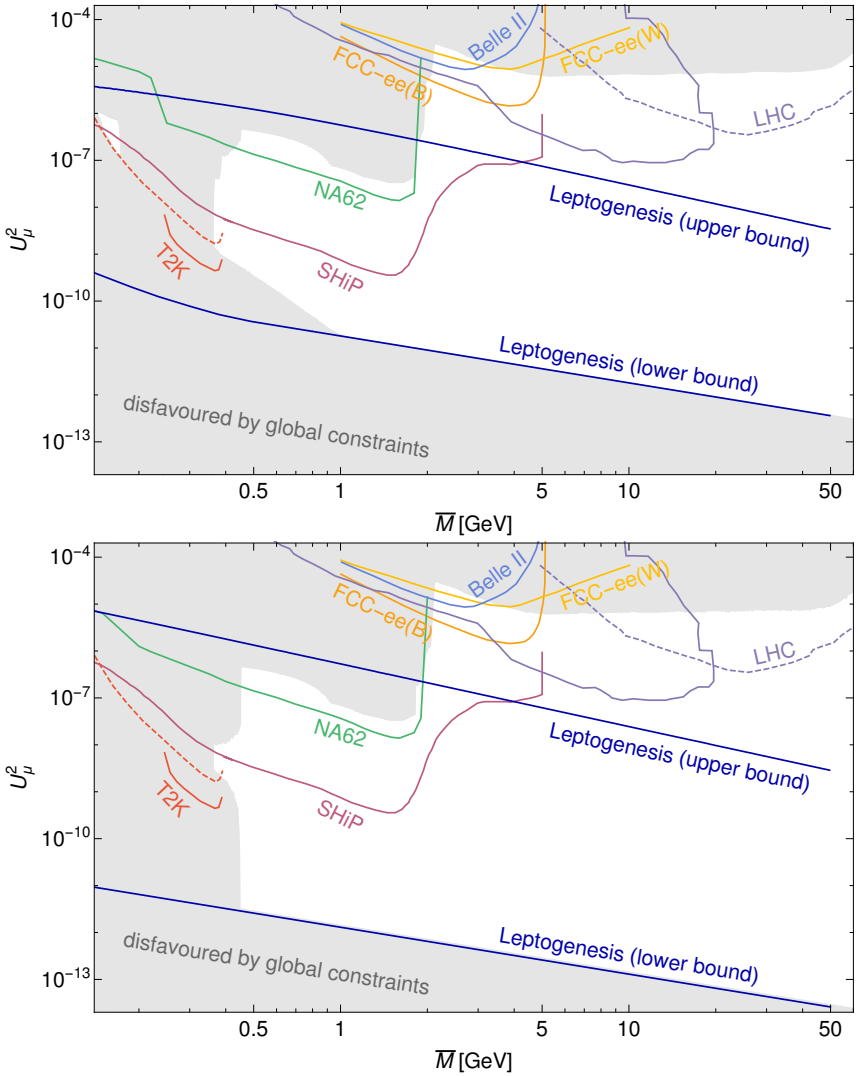

FIGURE 6.4: These plots are updated versions of figure 6 from ref. [1] and show the limits on the total U^2 as a function of $\bar{M} = (M_1 + M_2)/2$ for NO (top panel) and IO (bottom panel) that is consistent with leptogenesis and neutrino oscillation data. The parameter region that is disfavoured by global constraints, as discussed in section 6.1, is given by the grey area. The upper and lower bounds on the mixing (blue lines) are compared to the maximally achieved sensitivities of future experiments: The SHiP lines (purple) correspond to the 90% c.l. upper limits for 0.1 background events in 2×10^{20} proton target collisions for a ratio of $U_e^2 : U_\mu^2 : U_\tau^2 \sim 1 : 26 : 3.8$ [91, 202]. The estimated sensitivity of displaced vertex searches at LHCb during the high-luminosity run with $380\,\text{fb}^{-1}$ is given in black, see ref. [203]. The expected limit of the NA62 experiment on U_μ^2 via $K^+ \to \pi^+\nu\bar{\nu}$ with about 10^{13} 400 GeV protons on target is given by the turquoise line for the scenario $U_e^2 : U_\mu^2 : U_\tau^2 \sim 0 : 1 : 0$ [89]. The sensitivity of T2K has been estimated in ref. [88] with 10^{21} protons on target at 90% c.l. for full volume in case of $K^+ \to \mu^+ N \to \mu^+\mu^-\pi^+$ two-body decays (red, solid) and $K^+ \to \mu^+ N \to \mu^+\mu^- e^+\nu_e$ three-body decays (red, dashed) [88]. LNV decays of 5×10^{10} B^+ mesons at Belle II (blue) and 2×10^8 W bosons (yellow) at the FCC-ee can put limits on U_μ^2 [86]. The expected sensitivity from B meson decay at the FCC-ee corresponds to the light orange line [86]. The limits on U_μ^2 from displaced lepton jet (solid) and prompt trilepton (dashed) searches for $300\,\text{fb}^{-1}$ and $\sqrt{s} = 13\,\text{TeV}$ at the LHC [76] are given as violet lines.

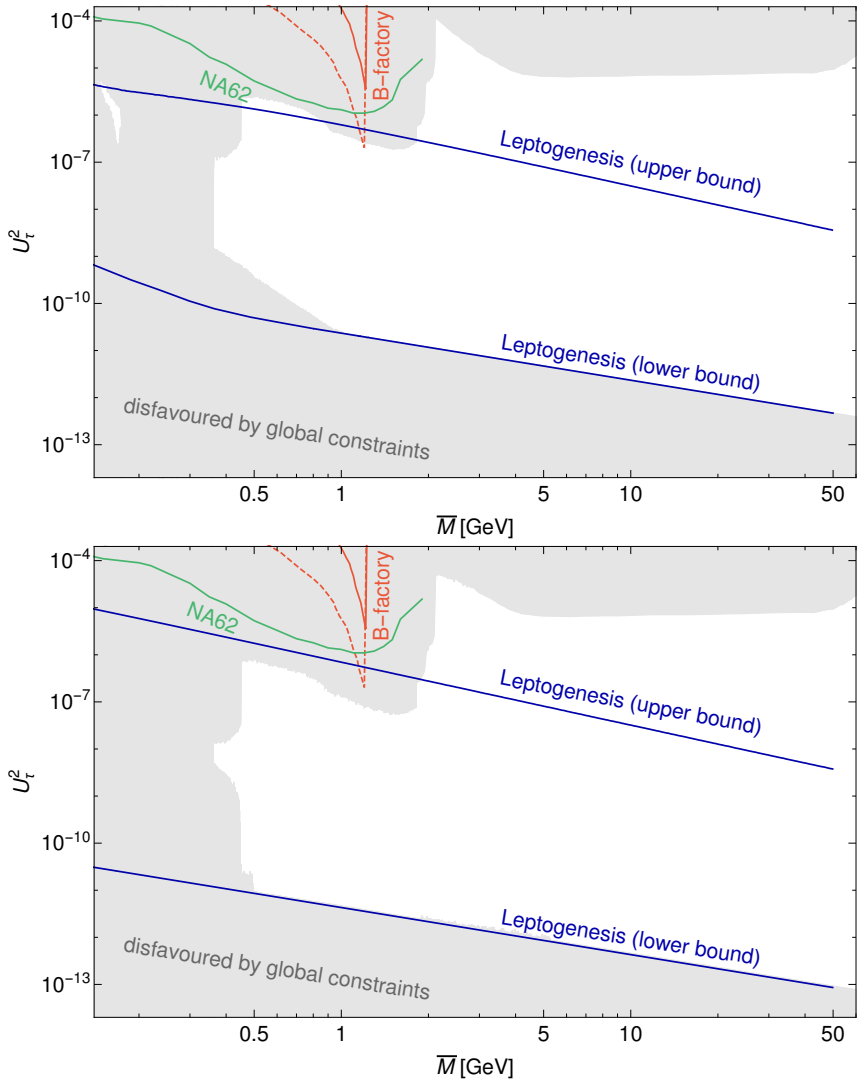

FIGURE 6.5: These plots are updated versions of figure 7 from ref. [1] and show the limits on the total U^2 as a function of $\bar{M} = (M_1 + M_2)/2$ for NO (top panel) and IO (bottom panel) that is consistent with leptogenesis and neutrino oscillation data. The parameter region that is disfavoured by global constraints, as discussed in section 6.1, is given by the grey area. The upper and lower bounds on the mixing (blue lines) are compared to the maximally achieved sensitivities of future experiments: For a kinematic analysis of 10^6 $\tau^- \to \nu\pi^-\pi^+\pi^-$ decays at B-factories [82] the conservative and the most optimistic 95% c.l. limits in U_τ^2 are given by the solid red and the dashed red lines. The expected limit of the NA62 experiment on U_τ^2 via $K^+ \to \pi^+\nu\bar{\nu}$ with about 10^{13} 400 GeV protons on target is given by the turquoise line for the scenario $U_e^2 : U_\mu^2 : U_\tau^2 \sim 0 : 0 : 1$ [89].

a hierarchy. We refer to appendix B.1 for a more detailed discussion. An interesting question that will be addressed within this subsection is the following:

If U^2 is fixed to a specific value, what is the range of U_a^2/U^2 that generates the observed BAU?

For a given flavour ratio U_a^2/U^2, that is allowed by neutrino oscillation data, cf. figure 6.1, we are interested in the maximally allowed U^2 consistent with leptogenesis constraints. As these flavour ratios are fixed uniquely by choosing the phases α_2 and δ, the only free parameters are ΔM, ω and the discrete $\xi = \pm 1$. Note that the dependence on the heavy neutrino mass and on Reω disappears for large Imω or $\epsilon \ll 1$, while we further consider $\mu \simeq 0$. Results are plotted in figure 6.6 for an average heavy neutrino mass $\bar{M} = 30\,\text{GeV}$. Figures 8-10 from ref. [1] show the dependence on different heavy neutrinos masses and also provide a magnified view for the corners of large U^2. In contrast to that, the present study includes LNV effects.

Everything within the black lines can be explained with neutrino oscillation data. We find for both neutrino mass hierarchies that the larger U^2 can only be realised when requiring the washout to be strongly flavour asymmetric, i.e. large U^2 regions are pushed to the corner of the areas. In case of NO, this happens for $\alpha_2 = -2\delta + \pi$, when the electron couples minimally $U_e^2/U^2 \simeq 0.006$, while for IO the electron has to couple maximally $U_e^2/U^2 \simeq 0.94$, which corresponds to $\alpha_2 - \alpha_1 \equiv \alpha_2 = \pi$. See appendix B.1 for a more detailed discussion. The effect of the relative coupling of the muon U_μ^2/U^2 with respect to the coupling of the tauon U_τ^2/U^2 in these corners is subdominant. A special feature happens for IO. We find, as visible in figure 6.6, that the scenario of equal mixings $U_e^2 = U_\mu^2 = U_\tau^2$ does not allow for large mixings U^2. In absence of LNV effects, such a scenario fails to account for the observed BAU, as leptogenesis requires a flavour asymmetric washout in order to generate a sufficient amount of leptons charges. This effect has been shown in figure 9 of ref. [1]. Note that this suppression is only visible for IO since the parameter region is already excluded by neutrino oscillation data in case of NO.

6.3 LEPTOGENESIS AT FUTURE LEPTON COLLIDERS: FCC-EE, ILC AND CEPC

Based on refs. [3, 4], this section discusses the perspectives of probing the low scale leptogenesis in the minimal seesaw model with two heavy neutrinos at future experiments. We are particularly focusing on the proposed lepton colliders such as FCC-ee, ILC and CEPC. Our discussion is based on heavy neutrinos with masses in the range $5\,\text{GeV} < \bar{M} < 50\,\text{GeV}$, i.e. on heavy neutrinos that are lighter than the W boson but heavier than B mesons. This regime is interesting as it allows for the decay of real EW gauge bosons in order to produce a large amount of heavy neutrinos. Note that for masses below 5 GeV heavy neutrinos can be produced via meson decays and in fixed target experiments. In this case, SHiP, B-factories and NA62 seem to be more promising, see in particular figure 6.2. The potential of lepton colliders probing the leptogenesis parameter space has been investigated in refs. [1, 68, 69, 71, 204, 205]. We aim to improve those outcomes as described in the following three points:

- In contrast to previous studies, such as ref. [1], we do not only include LFV effects from thermal scatterings but also effects from LNV decays and inverse decays. See chapter 5 for a detailed analysis.

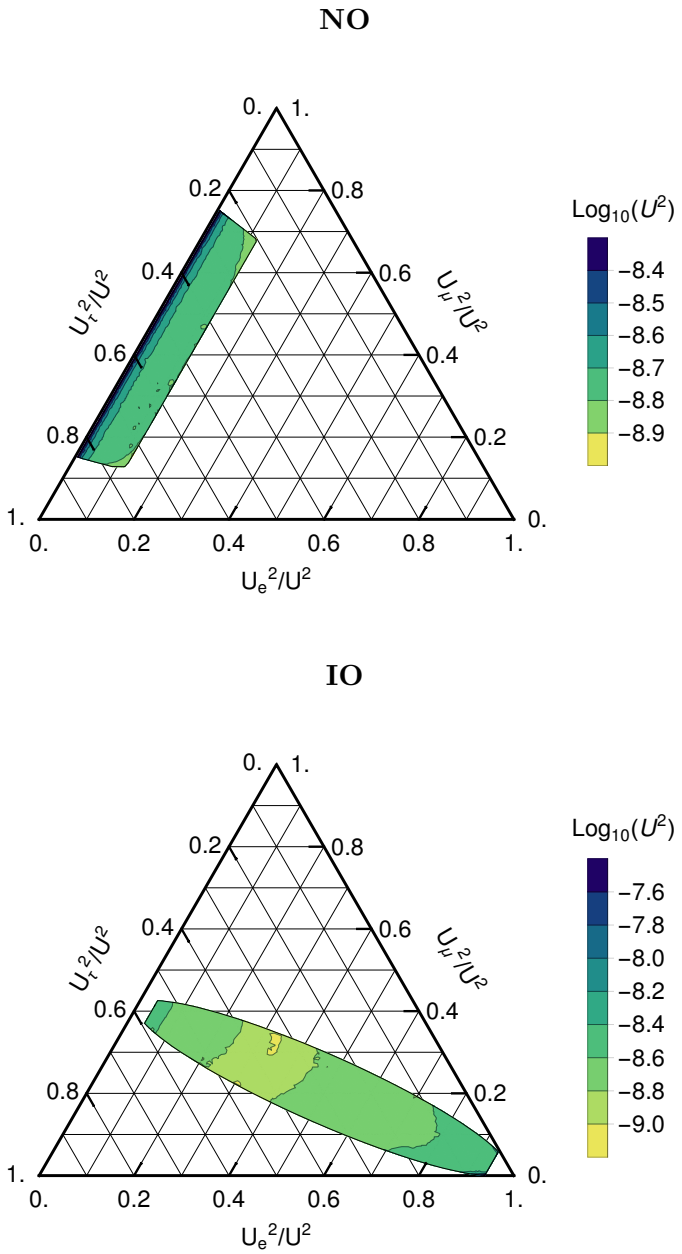

FIGURE 6.6: This plot is taken from ref. [3] and generalises figures 8-9 from ref. [1] by including LNV effects. The neutrino oscillation data allows for the region within the black lines. The largest mixing angle U^2 that is consistent with both the seesaw constraints and the observed BAU is indicated by the corresponding colour from the plot legend. The top panel corresponds to NO, while the bottom panel describes IO for two heavy neutrinos with an average mass $\bar{M} = 30\,\text{GeV}$. The largest viable mixing angles arise in the case of a highly flavour asymmetric flavour pattern, i.e. for $U_a^2 \ll U^2$. Figures 8-10 from ref. [1] show the dependence on different heavy neutrinos masses and also provide a magnified view for the corners of large U^2.

- There is a crucial fact that most of the previous studies are missing: Leptogenesis and the sensitivities of the experiments do not just depend on the total mixing U^2 but rather on the relative magnitudes of the mixing of the individual flavours U_e^2, U_μ^2 and U_τ^2. Therefore, estimates on the potential of future experiments by comparing the viable leptogenesis parameter space on the $\bar{M} - U_a^2$ planes to the projected experimental sensitivities on the same planes, such as figures 6.2-6.5, are not fully consistent. This is due to the fact that experimental sensitivities do not only depend on U^2 but also on the different U_a^2. Therefore, a certain U_μ^2 for a given mass $\bar{M}$ might be consistent with an observation in an experiment and also with a successful leptogenesis. However, as the U_μ^2 can correspond to different U_e^2, such a case does not necessarily guarantee that those heavy neutrinos that are discovered in the experiments are able to generate the observed BAU. Within the following analysis both the expected number of events in a given experiment and the BAU is computed for each combination of leptogenesis parameters. This procedure manifests the consistent check if both requirements are fulfilled simultaneously.

- We provide an estimate on the precision with which experiments are able to measure the magnitude of the individual mixings U_a^2. If heavy neutrinos will be discovered in future experiments, it is the relative size of the U_a^2 compared to the total mixing U^2 that provides a strong test of the generation of light neutrinos masses and the BAU within the minimal seesaw model.

Subsection 6.3.1 briefly discusses how heavy neutrinos can be tested at future colliders such as FCC-ee, ILC and CEPC. In subsection 6.3.2 potential discoveries of heavy neutrinos at these colliders are investigated, while subsection 6.3.3 describes with which precision the heavy neutrino flavour structure can be measured.

6.3.1 *Measurement of the low scale seesaw parameters at colliders*

The following discussion should be understood as a short summary of section 4 in ref. [3]. An instructive review is given in ref. [74]. In order to test if a hypothetical signal at future lepton collider coincides with the prediction from leptogenesis in a minimal seesaw scenario a precise knowledge of the flavour mixings U_a^2 is crucial. It is this mixing that determines the interaction strength of the heavy neutrinos with the surrounding SM leptons and thus determines the lifetime, cf. the Lagrangian term (2.47). For heavy neutrinos with masses between a few GeV and the mass of the W boson, the feeble mixing gives rise to relatively long lifetimes that lie in the range between picoseconds up to nanoseconds [206]. As a consequence, heavy neutrinos live long enough to travel a substantial distance before decaying in the detector, ending up in a displaced vertex. A schematic illustration is given in figure 6.7. Such signatures are exotic in a way that they allow for highly sensitive tests of the mixing angles for heavy neutrinos with masses below the mass of the W boson. Particularly interesting are future lepton colliders with high luminosities. For the following discussion about displaced vertex searches we limit ourselves on LNC signatures, i.e. we work in the $B - L$ conserving limit with $\epsilon, \mu \to 0$ as described in subsection 2.2.4. This is justified since the region of successful leptogenesis that is accessible by experiments requires large mixings, and consequently corresponds to the symmetry protected scenario. Note that small deviations from this scenario are not drastically impacting the production

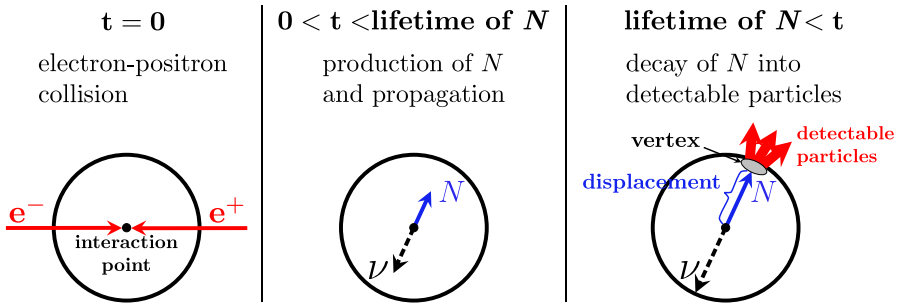

FIGURE 6.7: The feeble mixing of the heavy neutrinos to the SM leptons ends up in long lifetimes. This yields exotic signatures in form of displaced vertices, the visible displacement of the vertex from the interaction point. Such signatures allow to look for heavy neutrinos down to smallest active-sterile mixings. This figure is taken from ref. [3].

and decay rates, which is why results from ref. [73] for displaced vertex searches in the symmetric limit are considered.

The following three proposed future lepton colliders with their different specific physics programs are studied:

- Under these three colliders the FCC-ee is the most powerful when it comes to the luminosity. It is planned to have a high integrated luminosity of 110 ab^{-1} in the Z-pole run.
- The ILC is planned to run both at the Z-pole and also at 500 GeV center of mass energy with integrated luminosities of $\mathcal{L} = 0.1\,\mathrm{ab}^{-1}$ and $\mathcal{L} = 5\,\mathrm{ab}^{-1}$, respectively.
- Besides the ILC, also the CEPC is going to run at two energies, both at the Z-pole and also at 240 GeV center of mass energy with an integrated luminosity of $\mathcal{L} = 0.1\,\mathrm{ab}^{-1}$ and $\mathcal{L} = 5\,\mathrm{ab}^{-1}$, respectively.

PRODUCTION OF HEAVY NEUTRINOS: In general, heavy neutrino production at lepton colliders happens in processes where electron and positrons decay into an electron neutrino and a heavy neutrino $e^+e^- \to \nu N$. These processes can either happen in the s-channel and in the t-channel. The s-channel production is dominant at the Z-pole run, where the intermediate particle is the Z-boson. For center of mass energies of both 240 GeV and 500 GeV it is the t-channel process, where the W boson is exchanged, that dominates the production of the heavy neutrinos. As a consequence, the cross sections $\sigma_{\nu N}$ at the Z-pole only depend on the total U^2, while the productions above the Z-pole are sensitive to U_e^2.

DECAY CHANNELS OF HEAVY NEUTRINOS: There are four possible decay channels for the heavy neutrinos: the semileptonic channel ($N \to \ell_\mathrm{L} jj$), the leptonic channel ($N \to \ell_\mathrm{L}\ell_\mathrm{L}\nu$), the hadronic channel ($N \to jj\nu$), and the invisible channel ($N \to \nu\nu\nu$). We are particularly interested in probing the flavour mixing angle U_a^2. For this reason, the semileptonic decays providing a charged lepton of flavour a seem to be the most promising ones in order to test the flavour patterns. A detailed discussion about the expected number of events, that depends on the probability of particle decays within the detector, the branching ratio and the cross section, is given in section 4 of ref. [3]. In the present work

we randomise over the fundamental model parameters. Every set of these parameters leads to certain mixings U_a^2 that can be directly translated to the expected number of events via the methods described in ref. [3].

GUARANTEED AND POTENTIAL DISCOVERY: With the discussion above, the total number of expected displaced vertex events should depend on U^2 for collider searches at the Z-pole. In contrast, in case of W boson exchanges in the t-channel, these expected numbers also depend on U_e^2. Therefore, the total rate depends on U_e^2 differently as on U_μ^2 and U_τ^2. As a consequence, the total number of expected events cannot be fixed solely by U^2 and $\bar{M}$. For a fixed U^2 there exists two scenarios. First, the guaranteed discovery, where all the model parameters that lead to that U^2 can explain leptogenesis. Second, the potential discovery, where there exists at least one set of parameters for the given U^2 that is in agreement with leptogenesis. In both cases we require the expected number of events to be four or higher in order to call such an event a discovery. The distinction is particularly interesting for ILC and CEPC for center of mass energies above the Z-pole, cf. the dashed lines in figure 6.8.

6.3.2 *Sensitivities for different right-handed neutrino masses*

The region in the $\bar{M} - U^2$ plane that is consistent with leptogenesis and with neutrino oscillations data as well as for which a detection of heavy neutrinos via displaced vertex searches is possible is given in figure 6.8.

The experimentally disfavoured region is shown in grey and corresponds to the combined global constraints, cf. the discussion in section 6.1. The upper bound is mainly given by constraints from DELPHI [169, 207]. Note that constraint from displaced vertex searches from LHCb, cf. ref. [203], are not taken into account. In the mass region of 5 GeV and 10 GeV, these are only marginally more sensitive. However, these do not directly probe U^2 but mainly U_μ^2. The lower bound is given by the seesaw line, i.e. it is due to the fact that the Yukawa couplings have to be small enough in order to explain the light neutrino masses. We find that the leptogenesis lower bound is below that seesaw line, which is why we do not plot it here. The leptogenesis upper bound, i.e. the maximal U^2 for a given $\bar{M}$ that can explain the observed BAU is shown in blue.

We distinguish between NO (left column) and IO (right column). Further, we limit the discussion to masses in the range $\bar{M} < 50$ GeV because the uncertainty in the set of equation (5.153) and (5.154) that describes leptogenesis increases, particularly the relativistic approximation breaks down, for larger masses. The collider sensitivity lines correspond to a detection of heavy neutrinos with at least four events. We find that FCC-ee covers the largest part of the parameter space that is consistent with leptogenesis. Therefore, it is most capable to probe heavy neutrinos. Further, ILC and CEPC turn out to perform better for IO than for NO, in particular the runs with higher center of mass energies. In contrast, there are too little events for ILC and CECP in case of NO. This can be explained with the constraints from neutrinos oscillation data. As figure 6.1 shows, the electron coupling to the heavy neutrinos is suppressed compared to the muon and tauon mixing. Since the electron corresponds to the dominant production channel for runs with center of mass energies above the Z-pole, the number of events are small.

Note that ILC and CEPC with higher center of mass energies do not only depend on the total U^2 but also on the U_e^2. The solid lines tells that for the given U^2 there are

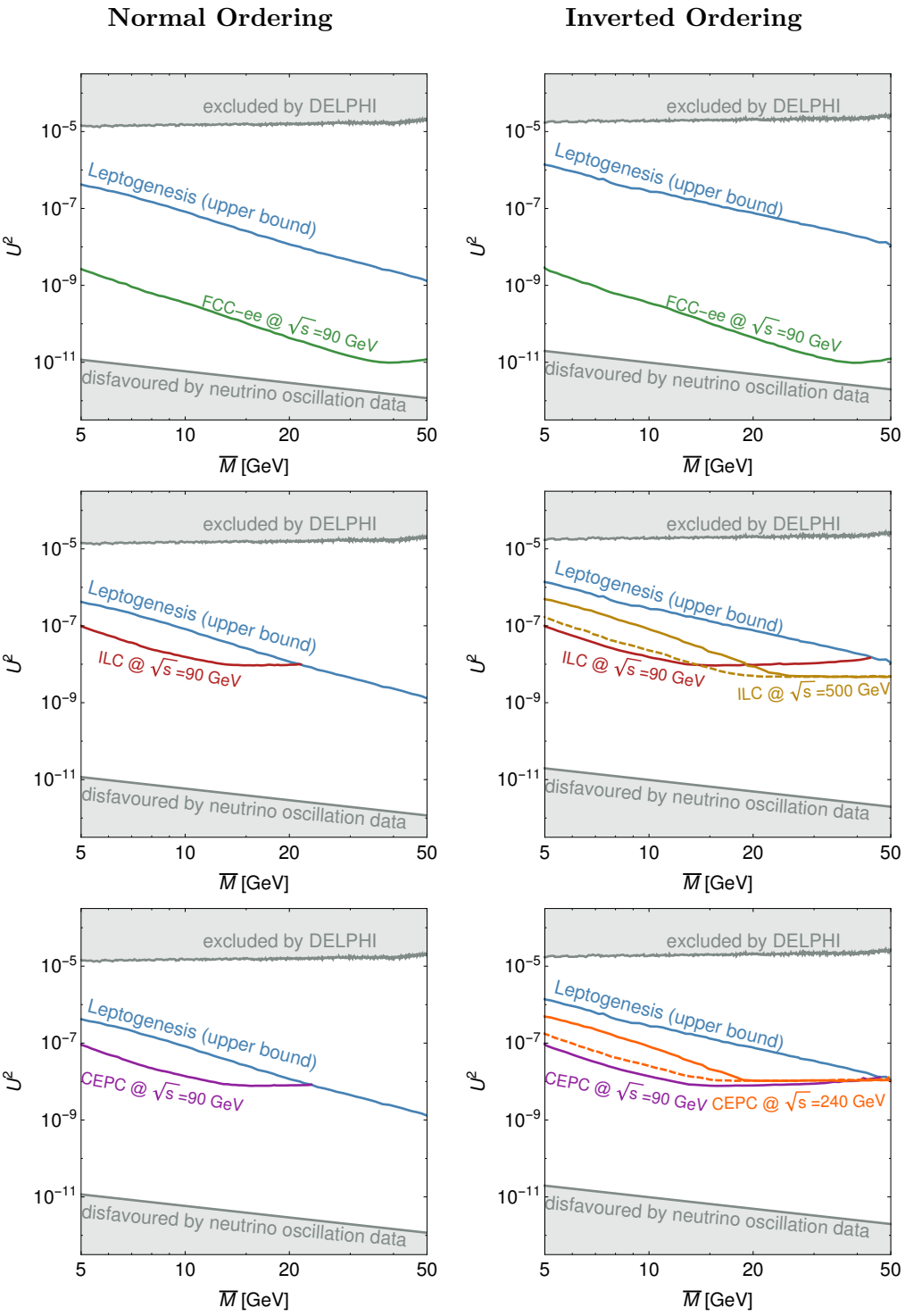

FIGURE 6.8: This plot is taken from ref. [3]. The largest possible U^2 for given average heavy neutrino mass $\bar{M}$ that is consistent with leptogenesis is shown in blue. Upper bounds on U^2, for which at least four displaced vertex events from heavy neutrinos consistent with leptogenesis are expected at future lepton colliders such as FCC-ee, are displaced by the coloured lines. Solid lines correspond to a guaranteed discovery, while the dashed lines correspond to a potential discovery. The top grey area is excluded by DELPHI, while the bottom grey area, the seesaw line, is disfavoured by neutrino oscillation data. Note that in this mass range the lower bound from leptogenesis is lower than the seesaw line. A more detailed discussion is given in the main text of subsection 6.3.2.

parameter points that can explain the BAU. In contrast, the dashed line means that all the parameter points which lead to the given U^2 can explain leptogenesis. Therefore, the solid line describes a potential discovery, while the dashed line corresponds to a guaranteed discovery. See section 6.4 and appendix B.1 for a detailed discussion about the parameter degeneracies.

It is worth mentioning that CEPC is planned for a much shorter run time at the Z-pole compared to FCC-ee since the priority given the Higgs measurements, i.e. at 240 GeV. If the CEPC run time is increased, we expect sensitivities close to the ones of FCC-ee. A comparison plot is shown in figure 4 from ref. [3].

Note that large number of events from displaced vertices can be observed, particularly at FCC-ee, see figures B.1. As discussed in the next subsection, such large numbers can allow for accurate measurements of the flavour composition.

6.3.3 *Precision for the different flavour ratios*

Precision values with which FCC-ee, ILC and CEPC are able to measure the flavour ratios U_a^2/U^2 are shown in figures 6.9 and 6.10. The capability of these experiments to measure a huge number of displaced vertex events, see figures B.1-B.3, does not only allow for a detection of heavy neutrinos but also able to measures the flavour dependent mixings U_a^2/U^2.

Within figures 6.9 and 6.10 we use almost mass degenerate heavy neutrinos with an average mass of $\bar{M} = 30\,\text{GeV}$. The individual coloured regions indicate the precision with which the experiments are able to measure the flavour ratios. Ref. [3] provides a detailed discussion about the precision measurement by using Poisson statistics when relating the expected number of events for a given SM flavour a to semileptonic events. In this case we follow an conservative approach, i.e. we take the lowest achievable precision value for each bin in the $U_a^2/U^2 - U^2$ plane. Note that the precision for U_a^2/U^2 does not only depend on the flavour a but also on the other flavours $b \neq a$. This effect is not straightforward, which is why we do not show it explicitly in the plots.

As discussed before, neutrino oscillation data forces the flavour ratio U_e^2/U^2 to be small for NO, cf. figure 6.1. Therefore, the other flavour ratios are measured with a higher precision. In contrast to that, the best precision is given for U_e^2/U^2 for IO. Within the different experiments, see figures 6.9 and 6.10, FCC-ee allows for the best precisions, i.e. at the percent level, which is due to a large number of events. In case of IO there are parts in the parameter space which can be tested with a precision up to 5% at ILC and CEPC. Note that for masses lower than $\bar{M} = 30\,\text{GeV}$ more events can be measured, which allows for even better precisions.

A feature of IO is that there are prominent spikes, see e.g. figure 6.9. These are due to leptogenesis at large U^2, which requires a flavour asymmetric washout, as discussed in more detail in appendix B.1. Since neutrino oscillation data for two heavy neutrinos puts certain limits on the flavour ratios U_a^2/U^2, see figure 6.1, the electron has to couple maximally. In this case we find $U_e^2/U^2 \simeq 0.94$, what explains the spike in the bottom left panel of figure 6.9. Thus, the requirement $U_\mu^2/U^2, U_\tau^2/U^2 \ll U_e^2/U^2$ explains the peaks for the other two plots in the lower panel of figure 6.9. Note that the maximal height of these peaks must be equally high for all the flavours. In comparison, such peaks are not visible for NO. This is because, neutrino oscillation data combined with large U^2 from

leptogenesis require the electron to couple minimally, i.e. we find $U_e^2/U^2 \simeq 0.006$. Thus, the allowed range for the other flavour ratios is quite large.

HOW TO INTERPRET THESE PLOTS: Provided that heavy neutrinos are discovered in future experiments, a measurement of the flavour ratios U_a^2/U^2 combined with constraints from neutrino oscillation data can allow to test if these are responsible for the light neutrino masses. Figures 6.9 and 6.10 provide an estimate of how precise a measurement of U_a^2/U^2 can be performed at the future colliders FCC-ee, ILC and CEPC. If all three flavour ratios U_a^2/U^2 are measured with a sufficient precision, figure 6.6 then allows, with the given precision, to see if these flavour ratios are within the given areas that are allowed be neutrino oscillation data. This does either support or falsify the hypothesis that heavy neutrinos are the origin of the light neutrino masses and that they can simultaneously explain the observed BAU.

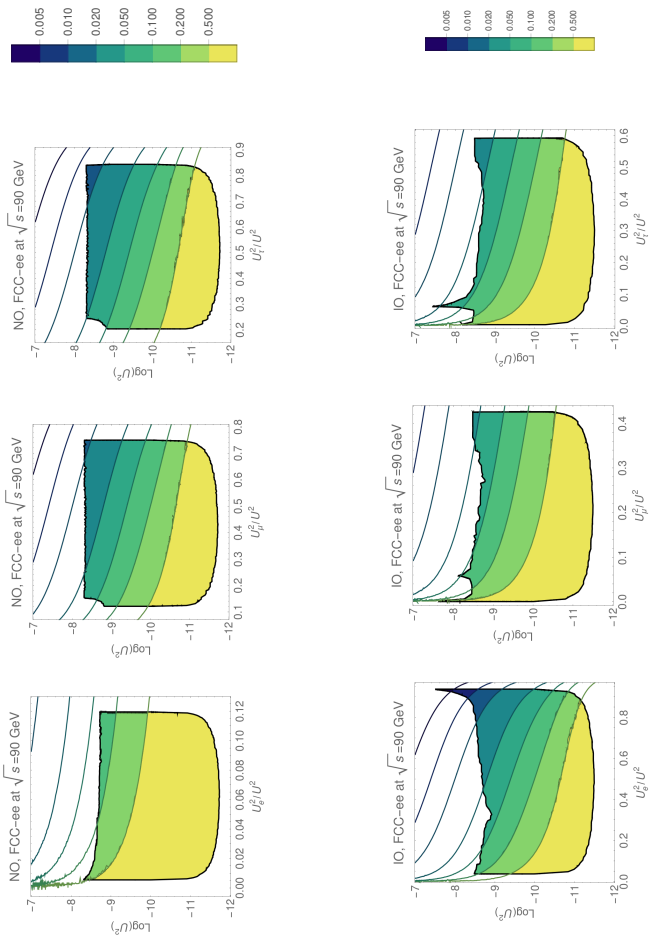

FIGURE 6.9: This plot is taken from ref. [3] and shows the maximally achieved precision with which U_a^2/U^2 with $a = e, \mu, \tau$ can be measured at the FCC-ee at a center of mass energy of $\sqrt{s} = 90\,\text{GeV}$. NO and IO are shown in the top and the bottom line, respectively. Leptogenesis works within the black contour. Two almost mass degenerate heavy neutrinos with $M = 30\,\text{GeV}$ are considered. A detailed discussion is given in the main text of subsection 6.3.3.

6.4 TESTABILITY OF THE MODEL

Leptogenesis with two heavy neutrino requires them to be almost mass degenerate in order to able to explain the observed BAU via leptogenesis, cf. chapter 5 for a detailed discussion. With a potential detection of heavy neutrinos in future experiments it is desirable to gain a full reconstruction of the fundamental parameters appearing in the low scale seesaw Lagrangian (2.46). Within this chapter we have assumed that future experiments are not able to resolve such a mass degeneracy. Therefore, only U_a^2 can be measured for the three SM flavours instead of U_{ai}^2. If heavy neutrinos are detected in future experiments, figure 6.1 together with the analytic expressions from appendix B.1 imply that a measurement of the individual U_a^2 allows to extract $\mathrm{Im}\omega$. However, α and δ cannot be uniquely obtained from such a measurement due to degeneracies as described in appendix B.1. Further, ΔM and $\mathrm{Re}\omega$ as the remaining crucial parameters for leptogenesis cannot be inferred from such as measurement neither. See refs. [1, 7] for a detailed discussion.

Nevertheless, an independent measurement of δ would not only help to predict the heavy neutrino flavour patterns but would also proof the fact that there is CP violation in the lepton sector of the SM. This is in general possible at future neutrino oscillation experiments, such as NOνA or DUNE. In principle it is also possible to determine $\mathrm{Re}\omega$ if $0\nu\beta\beta$ decays are observed, cf. refs. [1, 7] for discussions, provided that $\bar{M}$ is smaller than a few GeV [208–210]. Ref. [3] describes which ΔM are possible within successful leptogenesis and provide possible ways of how to determine them future experiments.

In the following we discuss under which circumstances the low scale seesaw is a fully testable theory of light neutrino masses and leptogenesis.

RECONSTRUCTION OF THE PARAMETERS: Provided that the masses of the two heavy neutrinos can be resolved in some experiment, a measurement of all U_{ai}^2 implies a determination of the phases (δ, α_2) and the complex angle ω uniquely up to the physical transformation $(\delta, \alpha_2, \mathrm{Re}\omega) \to (-\delta, 2\pi - \alpha_2, -\mathrm{Re}\omega)$, cf. appendix B.1, while $\bar{M}$ and ΔM could be determined from the kinematics. A sufficiently precise measurement of δ at future neutrino oscillation experiments combined with mass resolutions that are allow for independent measurements of U_{a1}^2 and U_{a2}^2, would allow to fully reconstruct all the fundamental parameters in the Lagrangian.

Given a resolution that is too low to distinguish the different heavy neutrino states, this only allows for a measurement of the three U_a^2. This comes along with a physical invariance, in contrast to the unphysical one in appendix B.1, under another transformation on the phases, which, however, has no analytic form since it requires solving trigonometric functions from appendix B.1. Note that this degeneracy cannot be broken by a measurement of δ. In such an approximate degenerate case $M_1 \simeq M_2 \simeq \bar{M}$ and in the limit $\epsilon \to 0$, the dependence of U_a^2 on $\mathrm{Re}\omega$ vanishes. Thus, both ΔM and $\mathrm{Re}\omega$ cannot be constrained by the oscillation data and a measurement of U_a^2 alone. However, it is possible to uniquely fix $\mathrm{Im}\omega$ by measuring U_a^2 as U^2 does not depend on ξ. Note that for $\epsilon \ll 1$ the flavour ratios U_a^2/U^2 are independent of ω and $\bar{M}$ but are completely fixed the phases (α, δ). As a consequence, the possible determination of δ with a sufficient high precision combined with the measurement of the individual U_a^2 can provide a powerful test of the seesaw mechanism as the origin of the light neutrino masses, simply because not every set $(U_e^2, U_\mu^2, U_\tau^2)$ can be achieved by varying the different phases (α_2, δ) and $\mathrm{Im}\omega$, see figure 6.1.

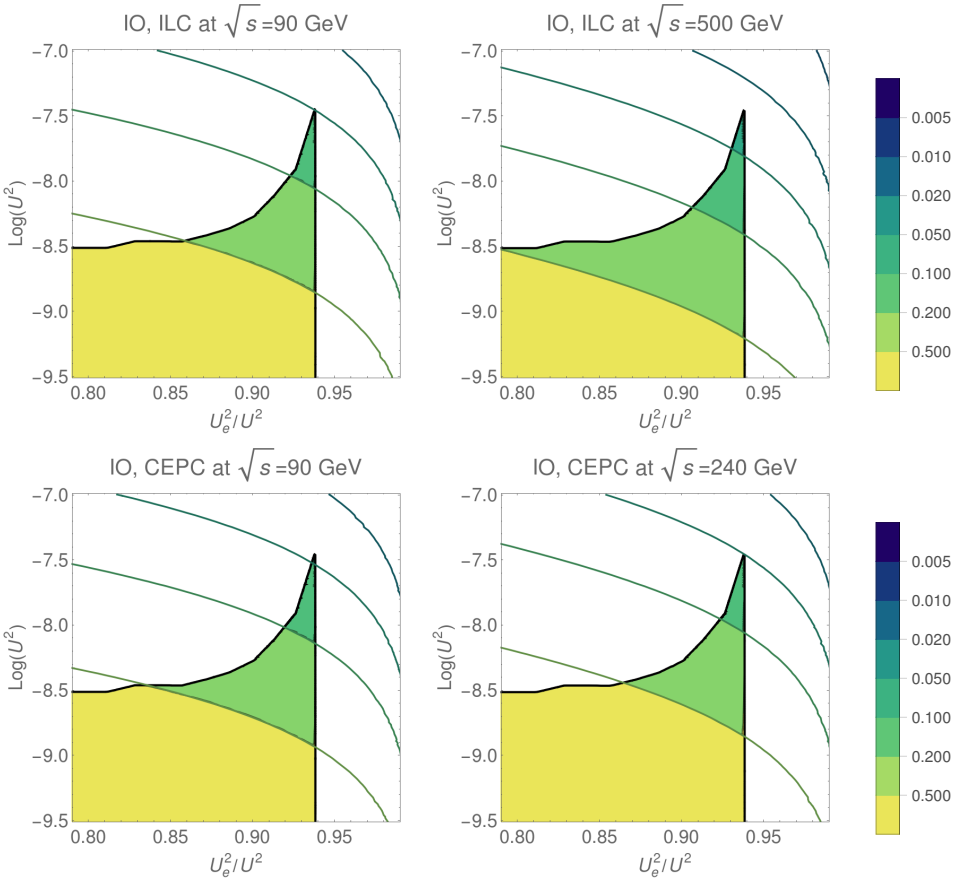

FIGURE 6.10: This plot is taken from ref. [3] and shows the maximally achieved precision with which U_a^2/U^2 with $a = e, \mu, \tau$ can be measured at the ILC at a center ofmass energy of $\sqrt{s} = 90\,\text{GeV}$ (top, left) and $\sqrt{s} = 500\,\text{GeV}$ (top, right), respectively, as well as at the CEPC at a center of mass energy of $\sqrt{s} = 90\,\text{GeV}$ (bottom, left) and $\sqrt{s} = 240\,\text{GeV}$ (bottom, right), respectively. NO is shown in the top line, while IO is given in the lower line. Leptogenesis works within the black contour. Two almost mass degenerate heavy neutrinos with $M = 30\,\text{GeV}$ are considered. In contrast to figure 6.9, only these four channels can be tested with precision higher than 50%. All the other channels, e.g. the ones that test U_μ^2/U^2 and U_τ^2/U^2 at the CEPC and ILC are not shown here because the maximally achieved precision for all U^2 consistent with leptogenesis is below 50%. A more detailed discussion is given in the main text of subsection 6.3.3.

7

CONCLUSION

7.1 SUMMARY

Both the observed BAU and the neutrino flavour oscillations are phenomena that cannot be explained by the SM alone. Within this thesis we have worked on two well-motivated models that can solve these puzzles: EW baryogenesis and leptogenesis from oscillations of GeV-scale heavy RH neutrinos in the early universe. All the calculations have been done within non-equilibrium field theory based on the CTP approach by Schwinger and Keldysh. Kinetic equations have been derived from the 2PI effective action. This formalism implicitly provides the correct description of the physical screening for the different particles. In particular, the particles receive a finite width and a thermal mass due to interactions with the surrounding plasma. Therefore, IR divergences, that appear in several tree-level scattering diagrams, are directly regulated. In general, these kinetic equations are not easy to solve. A convenient way to solve these equations is to transform them into Wigner space. In this case the observables such as the two-point functions only depend on the momentum k and on the average macroscopic space-time coordinate x that is e.g. given by background fields, such as the bubbles of broken symmetry during the EWPT. For the processes discussed in this thesis, the change of x is smaller than the typical energy scale of the particles in the plasma $|\mathbf{k}| \sim T$, such that $\partial_x \ll |\mathbf{k}|$. Therefore, a simplification arises when truncating the relevant equations to first non-vanishing order in gradients.

One possible way to explain the observed BAU is given by EW baryogenesis that happens during the EWPT. Provided that the PT is strongly first-order, which is only viable when extending the SM by new fields that couple significantly to the SM, CP-violating interaction with the walls of bubbles with broken EW symmetry lead to CP asymmetries, that diffuse ahead of the walls. Particularly asymmetries of LH fermions are transferred into asymmetries in the baryons via EW sphalerons, that are fast in the symmetric phase. As soon as the expanding bubbles sweep up these asymmetries, these are prevented from being washed out since the rate of EW sphaleron transitions is suppressed in the broken phase. When solving a network of diffusion equations, one finds that the final asymmetry is sensitive to the diffusion constants of the different SM particles. The determination of the diffusion constants happens when solving a Boltzmann-like transport equation in the CTP formalism. The diffusion constants are inverse-proportionally related to the collision term that takes account of all the scattering information. Within a leading order study in the couplings, i.e. when only considering $2 \leftrightarrow 2$ scattering processes, the collision term is divided into one-loop self-energy diagrams and two-loop vertex type diagrams. The self-energy type diagrams are IR enhanced for processes from the exchange of gauge bosons and fermions. This is due to HTL contributions in the t-channel. As an implicit feature of the CTP formalism fully resummed propagators exhibit a finite width behaviour due

to continuous interactions with the surrounding plasma and also account for the thermal mass shell. Relevant diffusion constants are computed based on a variational approach by refs. [132, 133]. The outcomes of chapter 3 and 4 are the following:

- Resummed propagators, that are dressed by particle interactions with the plasma, are derived from first principles in the 2PI CTP formalism. The spectral self-energies give rise to an effective width, while the Hermitian self-energies enter the dispersion relation. We list a complete set of one-loop self-energies for the SM particles. The Hermitian parts are computed in the HTL limit. In contrast, full analytic solutions to the spectral parts are computed. In particular, an analytic expression for the spectral part of both transverse and longitudinal gauge boson self-energies is provided.

- The IR enhanced self-energy type contributions are softened by the use of the dressed propagators. Therefore, the main contribution is given when momenta of the exchanged particles are of the order of the HTL parts of the Hermitian self-energies, i.e. for $|\mathbf{q}| \sim gT$. This leads to leading logarithmic contribution to the diffusion constants. We find that not only transverse and longitudinal modes of the gauge bosons but also fermions and plasminos are equally important.

- It turns out that the individual contributions from the vertex-type diagrams are divergent for soft momentum exchanges. However, we find certain symmetry properties that lead to a cancellation of these divergences when summing up all the relevant contributions. To leading order in the coupling it is then sufficient to use free propagators instead of fully resummed ones. Consequently, those diagrams only give a leading linear contribution to the diffusion constants, that is subdominant compared to the leading logarithmic contribution from the self-energy type diagrams.

- In contrast to previous results [139] we find that diffusion constants for the RH leptons are by a factor of approximately two larger, which eventually slightly enhances the final generated baryon charge. In addition, the diffusion constant for the Higgs is calculated.

Another well-motivated scenario that can explain the BAU is obtained by extending the SM by heavy RH neutrinos. These can not only generate the BAU via leptogenesis but can also explain the light neutrino masses via the type-I seesaw mechanism. In the first proposed scenarios of leptogenesis [17] this happens via CP-violating decays of superheavy RH neutrinos. To be in agreement with neutrino oscillation data the mass of the lightest RH neutrino needs to be larger than 10^9 GeV. Even though resonant leptogenesis scenarios can push this limit down to the TeV-scale it is difficult to test these scenarios in near future experiments. In terms of such a detection we consider the scenario that generates the BAU via oscillations of heavy RH neutrinos during their production. We limit our discussion to the minimal model of two almost mass degenerate heavy neutrinos in the low GeV-range that leaves the lightest SM neutrino massless. Baryogenesis happens in three regimes that are classified by three time-scales: the oscillation time-scale z_{osc} determines the time of the first oscillation, z_{eq} corresponds to the time when the first RH comes into equilibrium with the primordial plasma. Eventually, z_{ws} determines the time of the EW sphaleron freeze-out, after which B becomes a conserved quantity. An analytic understanding of the baryon charge generation is given in the following regimes:

In the oscillatory regime, i.e. for $z_{\rm osc} \ll z_{\rm eq} < z_{\rm ws}$, lepton flavour asymmetries are produced within the first few oscillations at $z \simeq z_{\rm osc}$. In the absence of LNV effects there is no total lepton charge at this stage. However, the LFV washout leads to a transfer of the different flavour asymmetries L_a into the sterile sector such that the generalised lepton number is still conserved but L is indirectly violated. Since the EW sphalerons only couple to LH leptons, L is partially transferred into B. One needs to require that the washout is incomplete such that at least one of the heavy neutrinos remains out-of-equilibrium at $z \simeq z_{\rm ws}$ as otherwise B would be completely washed out. Such a late washout compared to the early oscillations is only possible when the Yukawa couplings are sufficiently small. This allows for a perturbative treatment of this regime.

In the approximate $B-L$ conserving limit, cancellations in the Yukawa matrices allow for mixing angles that are much larger than the naive seesaw expectation (2.58). This scenario is preferred in the overdamped regime where the strongly coupled heavy neutrino interaction state equilibrates long before any oscillation has happened. In contrast, there is a feebly coupled eigenstate that decouples from the theory in the exact $B-L$ conserving limit. Approximate analytic solutions can be found by relying on a quasi-static approximation for the evolution the strongly coupled eigenstate. This allows to express the evolution of the heavy neutrinos and also the flavoured asymmetries in terms of the weakly coupled eigenstate. Due to the large Yukawa couplings the washout is rather strong and might erase all generated asymmetries before the EW sphaleron freeze-out. In case of two heavy neutrinos, this can be prevented if the mass degeneracy of the heavy neutrinos is increased, which leads to a later washout at $z \sim z_{\rm ws}$. Therefore, there is no time for the washout to effectively erase the asymmetries. In contrast to the oscillatory regime, parameter choices that lead to the overdamped behaviour give rise to large active-sterile mixing angles, increasing the chance of an experimental detection of heavy neutrinos in near future experiments.

Based on refs. [2] and some discussions of refs. [1, 3] the results of chapter 5 are the following:

- Evolution equations for heavy neutrinos and SM leptons have been derived from first principles within the non-equilibrium CTP formalism. Thermal masses, backreaction effects from the asymmetries that are generated via the heavy neutrino oscillation, as well as spectator effects turn out to be important and are taken into account in our study.

- Effects that violate the generalised lepton number via $1 \leftrightarrow 2$ (inverse) decays are included and the corresponding transport coefficients are computed in a momentum-averaged framework. We find parameter regions in which such effects are important and can have a sizeable effect on the baryon charge generation. Particularly in the overdamped regime, these can lead to an early equilibration of the feebly coupled eigenstate such that washout has more time to erase the generated asymmetries.

- For both the oscillatory and the overdamped regime we find approximate analytic solutions that are consistent up to $\mathcal{O}(1)$ correction when being compared with the numerical solutions.

In order to decide if the heavy neutrinos are the common origin of the light neutrino masses and the observed BAU, it is of great interest to detect them in future experiments.

Consistency of these two phenomena imposes constraints on their masses, their coupling to the SM particles and on their CP-violating properties. The fact that leptogenesis from oscillations of heavy neutrinos allows for masses in the GeV-range makes the seesaw a testable model. Given the minimal model that extends the SM by only two heavy neutrinos only comes with four new parameters, i.e. the heavy neutrino masses $M_{1,2}$ and the complex mixing angle ω. An experimental discovery is most likely for large mixing angles U^2. These are consistent with the light neutrino masses if heavy neutrinos are almost mass degenerate, such that $\Delta M \ll \bar{M}$. This is naturally motivated as the seesaw Lagrangian in this case features an approximate $B - L$ symmetry.

Not all future experiments are capable to resolve the two different heavy neutrinos, i.e. the mass difference ΔM cannot be measured. Therefore, a detection of heavy neutrino could only determine U_a^2 instead of U_{ai}^2. Further, the large U^2 that are favoured by experiments for a discovery signal require large Imω. In this case, the observables are insensitive to Reω and ΔM, as crucial parameters for leptogenesis. It is shown that leptogenesis is not fully testable if the mass resolution is too weak, in the sense that all fundamental parameters can be reconstructed, even if the Dirac phase will be measured by neutrino oscillation experiments to s sufficient precision. Nevertheless, a measurement of heavy neutrinos can constrain the parameter space severely and provides a consistency check of the light neutrino mass generation via the seesaw mechanism and the baryon charge generation via leptogenesis.

Particular focus has been placed on the future collider FCC-ee in the electron positron mode with in integrated luminosity of $\mathcal{L} = 110\,\text{ab}^{-1}$ for the Z-pole run, the ILC running at both the Z-pole and at a center of mass energy energy of $\sqrt{s} = 500\,\text{GeV}$ with $\mathcal{L} = 0.1\,\text{ab}^{-1}$ and $\mathcal{L} = 5\,\text{ab}^{-1}$, respectively, as well as the CEPC with $\mathcal{L} = 0.1\,\text{ab}^{-1}$ and $\mathcal{L} = 5\,\text{ab}^{-1}$ at the Z-pole and at $\sqrt{s} = 240\,\text{GeV}$, respectively. These experiments are very sensitive via displayed vertex searches in the parameter region where heavy neutrinos can explain both the BAU and the light neutrino masses.

The outcomes of chapter 6, based on ref. [3], concerning the test of the low scale seesaw and leptogenesis are the following:

- In case of large degeneracies in the heavy neutrino masses and for comparably large Imω, the flavour ratios U_a^2/U^2 are determined solely by the light neutrino parameters. Besides the Majorana phase α, these parameters might be determined in the near future.

- Combined constraints from past experiments, such as direct and indirect searches, and the requirement of not jeopardising the successful predictions of the BBN can strongly constrain the parameter regions for U_a^2.

- The viable range for the mixings U_a^2 consistent with leptogenesis and neutrino oscillation data is found and is compared to the reach of future experiments, in particular to FCC-ee, ILC and CEPC.

- The FCC-ee can test a substantial part of the leptogenesis parameter space at the Z-pole run. The ILC and CEPC are also able to test a significant part of the low scale seesaw parameter space for IO when running with center of mass energies of $\sqrt{s} = 500\,\text{GeV}$ and $\sqrt{s} = 240\,\text{GeV}$, respectively. For NO the Z-pole run of both ILC and CEPC can discover heavy neutrinos.

- Due to large number of displayed vertex events, particularly the FCC-ee is able to test the flavour ratios U_a^2/U^2 with a precision at the percent level. A precision of 10% to 5% is anticipated for ILC and CEPC for IO. A sufficient measurement of these ratios can provide a consistency check of the light neutrino mass generation.

- A measurement of the individual U_a^2 will be a powerful test of the minimal low scale leptogenesis. This even holds if the mass degeneracy that is necessary for successful leptogenesis is too large to be resolved and if $\mathrm{Im}\omega \gg 1$, which makes the U_a^2 be insensitive to ΔM and $\mathrm{Re}\omega$. For given U^2 and $\bar{M}$ the requirement of fulfilling leptogenesis imposes constraints on U_a^2/U^2. A detection of heavy neutrinos within these regions can be circumstantial evidence for leptogenesis.

7.2 OUTLOOK

Different aspects regarding the computation of the diffusion constants, cf. chapter 4 need be investigated in future works:

- The calculation of the diffusion constant do not take flavour changing Yukawa interactions into account. This effect seems to affect the found results at $\mathcal{O}(1)$ and has to be included in future works.

- We neglect close-to-collinear effects that are due to an arbitrary number of soft scatterings during the emission. This so-called Landau-Pomeranchuk-Migdal (LPM) effect, cf. e.g. ref. [140], might affect the diffusion constants at leading linear order. However, we expect that the numerical values for the diffusion constants are not affected sizeably by these effects since the leading logarithmic contributions dominate.

The discussion about leptogenesis from oscillations of heavy RH neutrino, cf. chapter 5, suffers from the following issues which need to be clarified in future works:

- The derivation of the evolution equations is based on a momentum-averaged approach. Due to the fact that the heavy neutrinos are out-of-equilibrium after their production, such a treatment is expected to induce an error of $\mathcal{O}(1)$.

- Particularly when relating the different charges to each other via spectator effects, we assume that all the SM Yukawa interactions are in equilibrium. However, this is only true for temperatures $T \lesssim 10^5\,\mathrm{GeV}$ when the electron has eventually equilibrated. This may overlap with the regime that is physically interesting, since the oscillations of the heavy neutrinos may have already started at these temperatures.

- We use the simplified assumption of a sudden freeze-out of the EW sphalerons. However, EWSB in the SM happens via a crossover. This does not only modify the spectator effects but also affects the baryon charge generation in the strongly overdamped regime during the crossover.

- While the approximate analytic solutions in the oscillatory regime hold for an arbitrary number of heavy neutrinos, the treatment of the overdamped regime is based on two heavy neutrinos. Extensions to three or more heavy neutrinos might be of interest for phenomenological studies.

- A suppression of the baryon asymmetry can be caused by the Higgs EV if the asymmetry is generated during the crossover at $z \sim z_{\mathrm{ws}}$. Although only a small fraction of the parameter space is actually affected by this effect, it is important to resolve this issue in future works.
- Our discussion is based on a relativistic treatment. Therefore, for heavy neutrino masses close to the EW scale this approximation begins to break down.

Heavy neutrinos can not only explain the light neutrino masses via the seesaw mechanism but can also account for the observed baryon asymmetry of the universe via leptogenesis. Future experiments, such as FCC-ee, ILC and CEPC, are capable to test a substantial part of the viable parameter space. Provided that heavy neutrinos are discovered in the future, a measurement of the magnitude of their couplings to the SM leptons can allow for a determination of all model parameters in some parts of the parameter region. This would make the seesaw mechanism a fully testable theory of baryogenesis and neutrino masses.

A

TECHNICALITIES FOR QUASIPARTICLES AT FINITE TEMPERATURE

This appendix provides additional calculations that are needed to correctly describe the properties of quasiparticles at finite temperatures.

Section A.1 investigates the decomposition of gauge bosons into transverse and longitudinal modes at high temperatures. In sections A.2 and A.3 detailed computations of the Hermitian and spectral self-energies are given, from which the HTL approximated expressions of chapter 3, that describe the dispersion relation and damping behaviour of quasiparticles, can be deduced. Section A.1 provides an integral technique, motivated by ref. [211], that is useful to numerically evaluate the contribution of the diffusion constants that arises from vertex type diagrams, cf. chapter 4.

A.1 GAUGE BOSONS AT FINITE TEMPERATURE

The following discussion about gauge bosons at finite temperatures is based on ref. [128]. Note that the Ward identity

$$k^\mu \Pi^{ab}_{\mu\nu}(k) = 0\,, \tag{A.1}$$

for the gauge boson self-energy is not only fulfilled at zero temperature but also at finite temperature.[1] At non-zero temperature $\Pi_{\mu\nu}(k)$ is not only a linear combination of the symmetric tensors $g_{\mu\nu} = \mathrm{diag}(1,-1,-1,-1)$ and $k_\mu k_\nu$ but also depends on the plasma vector $u_\mu = (u^0, \mathrm{u})$ that is due to the local rest frame of the thermal medium. It fulfils $u^\alpha u_\alpha = 1$ and allows for the symmetric tensors $u_\mu u_\nu$, $k_\mu u_\nu + u_\mu k_\nu$ and $g_{\mu\nu}$. The local frame of the medium breaks Lorentz invariance and allows for non-zero thermal masses for the gauge bosons. Further, in addition to the two transverse modes, a longitudinal mode arises at finite temperatures, such that the self-energy

$$\Pi^{ab}_{\mu\nu}(k) = P^{\mathrm{T}}_{\mu\nu}(k)\Pi^{ab}_{\mathrm{T}}(k) + P^{\mathrm{L}}_{\mu\nu}(k)\Pi^{ab}_{\mathrm{L}}(k)\,, \tag{A.2}$$

can be expressed in terms of the transverse and longitudinal projectors

$$P^{\mathrm{T}}_{\mu\nu}(k) = \bar{g}_{\mu\nu} + \frac{\bar{k}_\mu \bar{k}_\nu}{|\mathbf{k}|^2}\,, \tag{A.3}$$

$$P^{\mathrm{L}}_{\mu\nu}(k) = -\frac{1}{k^2|\mathbf{k}|^2}(|\mathbf{k}|^2 u_\mu + \omega \bar{k}_\mu)(|\mathbf{k}|^2 u_\nu + \omega \bar{k}_\nu)\,, \tag{A.4}$$

1 Ref. [212] states that the HTL parts of the gauge boson self-energies satisfy the Ward identity in both abelian and non-abelian gauge theories. However, beyond the HTL approximation the Ward identity is only fulfilled in abelian theories. When looking at eqs. (3.96)-(3.98), one can verify analytically that this argument also holds in non-abelian theories at least at one-loop order.

with $\bar{g}_{\mu\nu} = g_{\mu\nu} - u_\mu u_\nu$ and $\bar{k}_\mu = k_\mu - \omega u_\mu$ and the two Lorentz scalars

$$\omega = k^\alpha u_\alpha \,, \tag{A.5}$$

$$|\mathbf{k}| = \sqrt{\omega^2 - k^2} \,. \tag{A.6}$$

The projectors are directly transverse with respect to the four momentum k^μ

$$k_\mu P^{\mu\nu}(k) = k_\mu Q^{\mu\nu}(k) = 0 \,, \tag{A.7}$$

and consequently fulfil eq. (A.1) by construction. Further, the projectors fulfil the orthogonality relations

$$(P_\mathrm{T})^\mu_\alpha (P_\mathrm{T})^\alpha_\nu = (P_\mathrm{T})^\mu_\nu \,, \quad (P_\mathrm{L})^\mu_\alpha (P_\mathrm{L})^\alpha_\nu = (P_\mathrm{L})^\mu_\nu \,, \quad (P_\mathrm{T})^\mu_\alpha (P_\mathrm{L})^\alpha_\nu = (P_\mathrm{L})^\mu_\alpha (P_\mathrm{T})^\alpha_\nu = 0 \,, \tag{A.8}$$

while the traces are correspond to the number of degrees of freedom:

$$(P_\mathrm{T})^{\mu\nu}(P_\mathrm{T})_{\mu\nu} = (P_\mathrm{T})^\mu_\mu = 2 \,, \tag{A.9}$$

$$(P_\mathrm{L})^{\mu\nu}(P_\mathrm{L})_{\mu\nu} = (P_\mathrm{L})^\mu_\mu = 1 \,. \tag{A.10}$$

Note that within this thesis we work in the frame of the medium without loss of generality, such that we use $u_\mu = (1, \mathbf{0})$ and hence $\omega = k^0$. This implies the simple expressions $\bar{g}_{\mu\nu} = \mathrm{diag}(0, -1, -1, -1)$ and $\bar{k} = (0, \mathbf{k})$. Eventually, the transverse and longitudinal parts can be solely written in terms of the two contractions Π_{00} and $\Pi_{\mu\nu} g^{\mu\nu}$:

$$\Pi_\mathrm{L} = -\frac{k^2}{|\mathbf{k}|^2} u^\mu u^\nu \Pi_{\mu\nu} = -\frac{k^2}{|\mathbf{k}|^2} \Pi_{00} \,, \tag{A.11}$$

$$\Pi_\mathrm{T} = -\frac{1}{2}\Pi_\mathrm{L} + \frac{1}{2} g^{\mu\nu} \Pi_{\mu\nu} \,. \tag{A.12}$$

A.2 COMPUTATION OF HERMITIAN SELF-ENERGIES

The Hermitian self-energies are obtained by solving eq. (3.16). It is more convenient to write the self-energies in terms of the (anti-)time-ordered self-energies. These can be expressed in terms of the tree-level (anti-)time-ordered functions (3.79) and (3.80), which have a temperature dependent and a vacuum part. While the pure temperature parts cancel in the Hermitian self-energy, the combination of temperature dependent and vacuum parts survive. Note that the Hermitian self-energies also have a pure vacuum contribution, which can be neglected in the present study. The mixed term give rise to principal values

$$\mathrm{PV}\frac{1}{x} \equiv \frac{1}{2}\left(\frac{1}{x + \mathrm{i}\epsilon} + \frac{1}{x - \mathrm{i}\epsilon}\right) \,. \tag{A.13}$$

As an expansion in the coupling finite width effects are neglected, which is a justified assumption in the SM due to small couplings. Further, thermal masses are neglected as an higher order effect in the temperature.

In contrast to the spectral self-energies, all the diagrams displayed in figures 3.4, 3.5 and 3.6 do contribute to the Hermitian parts. The evaluation of the tadpole and seagull contributions is rather trivial compared to the sunset contributions. This is because these are already of the HTL form. The computation of the sunset diagrams can be simplified

up to one-dimensional integrals over the outer momenta. As these are non-trivial to solve, these are eventually evaluated in the HTL limit, whole keeping a subdominant remainder. In this case the decomposition can be employed,

$$G^H = G^{H\,\mathrm{HTL}} + G^{H\,\mathrm{rem}}\,, \tag{A.14}$$

where only $G^{H\,\mathrm{HTL}}$ is evaluated analytically.

HIGGS FIELD: The one-loop self-energy expression for the Higgs is given by eq. (3.86) with the sunset contributions (3.87) and (3.88), as well as by the tadpole and seagull contributions (3.90) and (3.91). With the considerations above the Hermitian self-energy for the Higgs field is given by

$$\begin{aligned}\Pi_\phi^H(k) = &-G_\phi \int \frac{\mathrm{d}^4p}{(2\pi)^4}\frac{\mathrm{d}^4q}{(2\pi)^4}(2\pi)^4\delta^4(q-p-k)(k+q)^2 \\ &\times\left[\mathrm{PV}\frac{1}{p^2}2\pi\delta(q^2)f_\phi(|\mathbf{q}|)+\mathrm{PV}\frac{1}{q^2}2\pi\delta(p^2)f_V(|\mathbf{p}|)\right] \\ &+2N_c h_t^2\int \frac{\mathrm{d}^4p}{(2\pi)^4}\frac{\mathrm{d}^4q}{(2\pi)^4}(2\pi)^4\delta^4(q-p-k)p\cdot q \\ &\times\left[\mathrm{PV}\frac{1}{p^2}2\pi\delta(q^2)f_\psi(|\mathbf{q}|)+\mathrm{PV}\frac{1}{q^2}2\pi\delta(p^2)f_\psi(|\mathbf{p}|)\right] \\ &+(4G_\phi+6\lambda)\int\frac{\mathrm{d}^4p}{(2\pi)^4}2\pi\delta(p^2)f_\mathrm{B}(|\mathbf{p}|)\,.\end{aligned} \tag{A.15}$$

The non-sunset contributions, i.e. the last line of eq. (A.15), can be solved when making use of the freedom to choose the spatial momentum to point into z-direction. Thus, the angle integrals contribute with a factor 4π. The zeroth component integral can be truncated via the delta function that puts the particles on-shell. The last integral is then given by

$$\int_0^\infty \mathrm{d}|\mathbf{p}||\mathbf{p}|f_\mathrm{F}(|\mathbf{p}|) = \frac{\pi^2}{12}T^2\,, \tag{A.16}$$

$$\int_0^\infty \mathrm{d}|\mathbf{p}||\mathbf{p}|f_\mathrm{B}(|\mathbf{p}|) = \frac{\pi^2}{6}T^2\,. \tag{A.17}$$

In case of the sunset diagrams, the four-dimensional delta function can be used to truncate one of the four-dimensional integrals. Analogously, the one-dimensional delta functions that put the particles on-shell eliminate the remaining zeroth component integral. The remaining three-dimensional integral can be further truncated in analogy to the non-sunset contributions when making use of the freedom to choose the spatial momentum to point into z-direction. However, the polar angle integral, i.e. the $\mathrm{d}\cos\theta$ integral, can be performed analytically in the principal value sense, while the azimuthal integral contributes with a factor 2π.

Eventually, the whole system can be reduced to a single integral over the outer three-momentum. The term that is of the from of eqs. (A.16) and (A.17) can be calculated can be evaluated accordingly and is referred to as the HTL contribution

$$\Pi_\phi^{H\,\mathrm{HTL}}(k) = \left(\frac{G_\phi}{4}+\frac{N_c h_t^2}{12}+\frac{\lambda}{2}\right)T^2\,, \tag{A.18}$$

while the remainder is given by

$$\Pi_\phi^{H\,\mathrm{rem}}(k) = \frac{k^2}{16\pi^2|\mathbf{k}|}\int_0^\infty d|\mathbf{p}|L_-(|\mathbf{p}|)\left(4G_\phi f_\phi(|\mathbf{p}|)+2N_c h_t^2 f_\psi(|\mathbf{p}|)\right), \tag{A.19}$$

$$L_\pm(|\mathbf{p}|) = \log\left|\frac{|\mathbf{p}|+\omega_+}{|\mathbf{p}|+\omega_-}\right| \pm \log\left|\frac{|\mathbf{p}|-\omega_+}{|\mathbf{p}|-\omega_-}\right|, \tag{A.20}$$

with $\omega_\pm = (k^0 \pm |\mathbf{k}|)/2$. Note that the Hermitian self-energies are used to regulate the spectral propagators, such as eq. (3.52), in order to prevent them from an IR divergence for small k^2, where k is the off-shell momentum of the Hermitian self-energy. In this case k^2 usually dominates over $\Pi^H(k)$ for non-small k^2. For smaller k^2, Π^H becomes important, namely when k is smaller than the soft scale: $k^2 \gg g^2T^2$. Therefore, it is sufficient to use the HTL approximation. This allows to assume hard loop-momenta $|\mathbf{p}| \gg |\mathbf{k}|, |k^0|$ and further $|\mathbf{p}|^2 \gg k^2$. Within this approximation one has

$$L_-(|\mathbf{p}|) \simeq 2\frac{|\mathbf{k}|}{|\mathbf{p}|}, \qquad L_+(|\mathbf{p}|) \simeq -2\frac{k^0|\mathbf{k}|}{|\mathbf{p}|^2}. \tag{A.21}$$

Thus, $\Pi_\phi^{H\,\mathrm{rem}}$ receives contributions of order k^2 and $k^2\log T$, see also ref. [128]. As a consequence, one can conclude that $\Pi_\phi^{H\,\mathrm{HTL}}$ dominates over $\Pi_\phi^{H\,\mathrm{rem}}$ at high temperatures.

FERMIONS: In analogy to the Higgs field the Hermitian fermion self-energy is given by eqs. (3.92) and (3.16),

$$\begin{aligned}\not{\Sigma}_\psi^H(k) = 2G_\psi P_{\mathrm{R,L}}\int\frac{\mathrm{d}^4p}{(2\pi)^4}\frac{\mathrm{d}^4q}{(2\pi)^4}(2\pi)^4\delta^4(q-p-k)\not{q} \\ \times\left[\mathrm{PV}\frac{1}{p^2}2\pi\delta(q^2)f_\psi(|\mathbf{q}|)+\mathrm{PV}\frac{1}{q^2}2\pi\delta(p^2)f_V(|\mathbf{p}|)\right],\end{aligned} \tag{A.22}$$

and is most conveniently computed by solving the scalar components Σ^0 and Σ^i separately. The HTL contributions are given by terms of the form of eqs. (A.16) and (A.17) and read

$$\Sigma_\psi^{H0\,\mathrm{HTL}}(k) = \frac{G_\psi T^2}{16|\mathbf{k}|}\log\left|\frac{k^0+|\mathbf{k}|}{k^0-|\mathbf{k}|}\right|, \tag{A.23}$$

$$\Sigma_\psi^{Hi\,\mathrm{HTL}}(k) = \frac{G_\psi T^2}{16|\mathbf{k}|}\frac{k^0k^i}{|\mathbf{k}|^2}\log\left|\frac{k^0+|\mathbf{k}|}{k^0-|\mathbf{k}|}\right| - \frac{G_\psi T^2}{8|\mathbf{k}|}\frac{k^i}{|\mathbf{k}|}. \tag{A.24}$$

The remainder are given by

$$\begin{aligned}\Sigma_\psi^{H0\,\mathrm{rem}}(k) = \frac{G_\psi}{8\pi^2|\mathbf{k}|}\int_0^\infty d|\mathbf{p}|\Big[|\mathbf{p}|L_+(|\mathbf{p}|)(f_\psi(|\mathbf{p}|)+f_V(|\mathbf{p}|)) \\ -k^0L_-(|\mathbf{p}|)f_V(|\mathbf{p}|)\Big],\end{aligned} \tag{A.25}$$

$$\begin{aligned}\Sigma_\psi^{Hi\,\mathrm{rem}}(k) = \frac{G_\psi}{8\pi^2|\mathbf{k}|}\frac{k^i}{|\mathbf{k}|}\int_0^\infty d|\mathbf{p}|\Big[-|\mathbf{k}|L_-(|\mathbf{p}|)f_V(|\mathbf{p}|) \\ +\left(\frac{k^0}{|\mathbf{k}|}|\mathbf{p}|L_+(|\mathbf{p}|)-\frac{k^2}{2|\mathbf{k}|}L_-(|\mathbf{p}|)\right)(f_\psi(|\mathbf{p}|)+f_V(|\mathbf{p}|))\Big],\end{aligned} \tag{A.26}$$

and are subdominant at high temperatures with the same arguments as used for the remainder of the Hermitian self-energy of the Higgs field.

When describing the evolution of number densities of heavy neutrinos in a low scale leptogenesis scenario, cf. chapter 5, Hermitian parts of fermionic self-energies appear for on-shell heavy neutrinos ($p^2 = M^2$) in the form

$$k \cdot \Sigma^H(k) = \frac{|Y|^2}{8} T^2 - \frac{|Y|^2}{8\pi^2} \frac{k^2 T}{|\mathbf{k}|} \int_0^\infty \mathrm{d}|\mathbf{p}| f_\mathrm{B}(2|\mathbf{p}|) L_-(|\mathbf{p}|)\,, \tag{A.27}$$

such that the dependence on L_+ vanishes. The second term can be evaluated with the procedure presented in the appendix of ref. [128]. Eventually, up to $\mathcal{O}(1/T^2)$, the full expression is given by

$$k \cdot \Sigma^H(k) \simeq \frac{|Y|^2}{8} T^2 + \frac{|Y|^2}{8\pi^2} M^2 \left[1 - \gamma_\mathrm{E} - \frac{|p^0|}{|\mathbf{p}|} \log \left| \frac{|p^0| + |\mathbf{p}|}{|p^0| - |\mathbf{p}|} \right| + \frac{1}{2} \log \left(\frac{4\pi^2 T^2}{M^2} \right) \right], \tag{A.28}$$

with $p^0 = \sqrt{|\mathbf{p}|^2 + M^2}\,\mathrm{sign}(p^0)$, $|p^0| \geq |\mathbf{p}|$ and the Euler–Mascheroni constant $\gamma_\mathrm{E} \simeq 0.58$. Note for simplicity flavour effects have been neglected in the sense that there is only one heavy neutrino that couples to one SM lepton through an one-dimensional Yukawa coupling Y. A generalisation to more flavours can be done analogously. For masses smaller than the typical temperature scale, the non-HTL expression, i.e. the second term of the equation above, is subdominant. This justifies the usage of the HTL approximation for heavy neutrinos in low scale leptogenesis scenarios since their mass M is required to be below the EW scale.

GAUGE BOSONS: The Hermitian gauge boson self-energy is given by the decomposition (3.95) together with eqs. (3.96)-(3.102) and (3.16)

$$\begin{aligned}
\Pi^H_{\mu\nu} = {} & 2N_\psi g^2 C^F \int \frac{\mathrm{d}^4 p}{(2\pi)^4} \mathrm{PV} \frac{1}{(k+p)^2} T_{\mu\nu} 2\pi\delta(p^2) f_\psi(|\mathbf{p}|) \\
& + 2N_\phi g^2 C^F \int \frac{\mathrm{d}^4 p}{(2\pi)^4} \mathrm{PV} \frac{1}{(k+p)^2} U_{\mu\nu} 2\pi\delta(p^2) f_\phi(|\mathbf{p}|) \\
& + g^2 C_2^A \int \frac{\mathrm{d}^4 p}{(2\pi)^4} \mathrm{PV} \frac{1}{(k+p)^2} G_{\mu\nu} 2\pi\delta(p^2) f_V(|\mathbf{p}|) \\
& - (3g^2 C_2^A + 2g^2 C^F) g_{\mu\nu} \int \frac{\mathrm{d}^4 p}{(2\pi)^4} 2\pi\delta(p^2) f_\mathrm{B}(|\mathbf{p}|)\,.
\end{aligned} \tag{A.29}$$

According to eqs. (A.11) and (A.11) one has to solve for the two contractions $\Pi^H_{\mu\nu} g^{\mu\nu}$ and Π^H_{00}. In analogy to the evaluation of the Hermitian self-energy for the Higgs field and for the fermions, one ends up at

$$\Pi^H_{\mu\nu}(k) g^{\mu\nu} = g^2 C^F N_\psi K_\psi(k^0, |\mathbf{k}|) + g^2 C^F K_\phi(k^0, |\mathbf{k}|) + g^2 C_2^A K_V(k^0, |\mathbf{k}|)\,, \tag{A.30}$$

$$\Pi^H_{00}(k) = g^2 C^F N_\psi H_\psi(k^0, |\mathbf{k}|) + g^2 C^F H_\phi(k^0, |\mathbf{k}|) + g^2 C_2^A H_V(k^0, |\mathbf{k}|)\,, \tag{A.31}$$

where

$$K_\psi = -\int_0^\infty \frac{\mathrm{d}|\mathbf{p}|}{2\pi^2} \left[4|\mathbf{p}| + \frac{k^2}{2|\mathbf{k}|} L_-(|\mathbf{p}|) \right] f_\psi(|\mathbf{p}|)\,, \tag{A.32}$$

$$K_\phi = -\int_0^\infty \frac{\mathrm{d}|\mathbf{p}|}{2\pi^2} \left[4|\mathbf{p}| - \frac{k^2}{4|\mathbf{k}|} L_-(|\mathbf{p}|) \right] f_\phi(|\mathbf{p}|)\,, \tag{A.33}$$

$$K_V = -\int_0^\infty \frac{\mathrm{d}|\mathbf{p}|}{2\pi^2} \left[4|\mathbf{p}| + \frac{5}{4} \frac{k^2}{|\mathbf{k}|} L_-(|\mathbf{p}|) \right] f_V(|\mathbf{p}|)\,, \tag{A.34}$$

and

$$H_\psi = -\int_0^\infty \frac{\mathrm{d}|\mathbf{p}|}{2\pi^2}\left[2|\mathbf{p}|\left(1-\frac{k^0}{|\mathbf{k}|}\log\left|\frac{\omega_+}{\omega_-}\right|\right)+\frac{1}{|\mathbf{k}|}M(|\mathbf{p}|)\right]f_\psi(|\mathbf{p}|)\,, \tag{A.35}$$

$$H_\phi = -\int_0^\infty \frac{\mathrm{d}|\mathbf{p}|}{2\pi^2}\left[2|\mathbf{p}|\left(1-\frac{k^0}{|\mathbf{k}|}\log\left|\frac{\omega_+}{\omega_-}\right|\right)+\frac{1}{|\mathbf{k}|}M(|\mathbf{p}|)+\frac{|\mathbf{k}|}{4}L_-(|\mathbf{p}|)\right]f_\phi(|\mathbf{p}|)\,, \tag{A.36}$$

$$H_V = -\int_0^\infty \frac{\mathrm{d}|\mathbf{p}|}{2\pi^2}\left[2|\mathbf{p}|\left(1-\frac{k^0}{|\mathbf{k}|}\log\left|\frac{\omega_+}{\omega_-}\right|\right)+\frac{1}{|\mathbf{k}|}M(|\mathbf{p}|)-\frac{|\mathbf{k}|}{4}L_-(|\mathbf{p}|)\right]f_V(|\mathbf{p}|)\,, \tag{A.37}$$

with L_- from eq. (A.20) and with

$$M(|\mathbf{p}|) = \sum_\pm \pm(|\mathbf{p}|\pm\omega_+)(|\mathbf{p}|\pm\omega_-)\log\left|\frac{|\mathbf{p}|\pm\omega_+}{|\mathbf{p}|\pm\omega_-}\right|\,, \tag{A.38}$$

for $\omega_\pm = (k^0 \pm |\mathbf{k}|)/2$. We have shown that L_- does not contribute to the HTL contribution of the Hermitian gauge boson self-energy. However, provided that $|\mathbf{p}| \gg |\mathbf{k}|, k^0, \sqrt{|k^2|}$, we can approximate

$$M(|\mathbf{p}|) \simeq 2|\mathbf{k}||\mathbf{p}|\,. \tag{A.39}$$

Therefore, the terms containing $M(|\mathbf{p}|)$ contribute to the HTL expression. When evaluating eqs. (A.16) and (A.17) and making use of eqs. (A.11) and (A.12), one eventually obtains

$$\Pi_{\mathrm{L}}^{H\,\mathrm{HTL}}(q) = \left(\frac{1}{2}C^F N_\psi + C^F N_\phi + C_2^A\right)\frac{g^2T^2}{3}\left(\frac{(q^0)^2}{|\mathbf{q}|^2}-1\right)\left(1-\frac{q^0}{2|\mathbf{q}|}\log\left|\frac{q^0+|\mathbf{q}|}{q^0-|\mathbf{q}|}\right|\right)\,, \tag{A.40}$$

$$\Pi_{\mathrm{T}}^{H\,\mathrm{HTL}}(q) = -\left(\frac{1}{2}C^F N_\psi + C^F N_\phi + C_2^A\right)\frac{g^2T^2}{6} - \frac{1}{2}\Pi_{\mathrm{L}}^H(q^0,|\mathbf{q}|)\,. \tag{A.41}$$

The Hermitian parts of the self-energies for the Higgs field, the fermions and the gauge bosons in the HTL limit are given in the main text in eqs. (3.108), (3.109), (3.110) and (3.111).

A.3 COMPUTATION OF SPECTRAL SELF-ENERGIES

When calculating the spectral self-energies to one-loop order only the sunset type diagrams in figures 3.4, 3.5 and 3.6 contribute. Analytic expressions are given by eqs. (3.87) and (3.88) for the Higgs field, by eq. (3.92) for fermions and by eqs. (3.96), (3.97) and (3.98) for gauge bosons. As the spectral part of the self-energy is given by the difference of the Wightman functions, see eq. (3.15), the particles in the loop are put on their mass shell. This implies constraints on the outer momenta, which are in general different for the s-channel and the t-channel, i.e. for $k^2 \geq 0$ and $k^2 < 0$, respectively, where k is the outer momentum, which in general is not on-shell. Note that we neglect the width of the particles running in the loop. This is justified in the SM due to small couplings. Further thermal masses are neglected as higher order effects. Analytic expressions for the Wightman functions are then given by the tree-level propagators (3.75)-(3.78) and (3.81).

The computation can be simplified to one remaining integral over the outer momentum when making use of the different delta functions. In case of one massless boson and one massless fermion running in the loop these integrals are of the form

$$I_n(y^0,y) = \int_{\frac{y^0-y}{2}}^{\frac{y^0+y}{2}} \mathrm{d}x\, x^n \left[1 - f_{\mathrm{F}}(x) + f_{\mathrm{B}}(y^0-x)\right] - \vartheta(y^2-(y^0)^2)\int_{-\infty}^{\infty} \mathrm{d}x\, x^n \left[1 - f_{\mathrm{F}}(x) + f_{\mathrm{B}}(y^0-x)\right], \tag{A.42}$$

while for two massless fermions or bosons in the loop, respectively, one has

$$J_n^{\mathrm{F,B}}(y^0,y) = \int_{\frac{y^0-y}{2}}^{\frac{y^0+y}{2}} \mathrm{d}x\, x^n \left[1 \mp f_{\mathrm{F,B}}x) \mp f_{\mathrm{F,B}}(y^0-x)\right] - \vartheta(y^2-(y^0)^2)\int_{-\infty}^{\infty} \mathrm{d}x\, x^n \left[1 \mp f_{\mathrm{F,B}}(x) \mp f_{\mathrm{F,B}}(y^0-x)\right]. \tag{A.43}$$

Note that the Heaviside step function ϑ allows that the corresponding terms are only present in the t-channel, i.e. for $(y^0)^2 < y^2$. This decomposition makes the different boundaries for the s- and t-channel obvious. Note that for massive particles these boundaries become more complicated. The solutions are functions of logarithms and polylogarithms, defined as $\mathrm{Li}_n(z) = \sum_{j=1}^{\infty} \frac{z^j}{j^n}$ for a complex number z, and read

$$I_0(y^0,y) = \log\left|\frac{1+\mathrm{e}^{\frac{1}{2}(y^0+y)}}{1+\mathrm{e}^{\frac{1}{2}(y^0-y)}}\right| + \log\left|\frac{1-\mathrm{e}^{\frac{1}{2}(y^0+y)}}{1-\mathrm{e}^{\frac{1}{2}(y^0-y)}}\right| - y - \vartheta(y^2-(y^0)^2)y^0\,, \tag{A.44}$$

$$I_1(y^0,y) = \mathrm{Re}\Big[x(\log(1+\mathrm{e}^x) - \log(1-\mathrm{e}^{x-y^0})) + \mathrm{Li}_2(-\mathrm{e}^x) - \mathrm{Li}_2(\mathrm{e}^{x-y^0})\Big]_{x=\frac{1}{2}(y^0-y)}^{x=\frac{1}{2}(y^0+y)} - \vartheta(y^2-(y^0)^2)\frac{(y^0)^2-\pi^2}{2}\,, \tag{A.45}$$

as well as

$$J_0^{\mathrm{F}} = 2\log\frac{1+\mathrm{e}^{\frac{y^0+y}{2}}}{1+\mathrm{e}^{\frac{y^0-y}{2}}} - y - \vartheta(y^2-(y^0)^2)y^0\,, \tag{A.46}$$

$$J_1^{\mathrm{F}} = \Big[x\log\frac{1+\mathrm{e}^x}{1+\mathrm{e}^{x-y^0}} + \mathrm{Li}_2(-\mathrm{e}^x) - \mathrm{Li}_2(-\mathrm{e}^{x-y^0})\Big]_{x=\frac{y0-y}{2}}^{x=\frac{y0+y}{2}} - \vartheta(y^2-(y^0)^2)\frac{(y^0)^2}{2}\,, \tag{A.47}$$

$$J_2^{\mathrm{F}} = \Big[x^2\log\frac{1+\mathrm{e}^x}{1+\mathrm{e}^{x-y^0}} + 2x\,\mathrm{Li}_2(-\mathrm{e}^x) - 2x\,\mathrm{Li}_2(-\mathrm{e}^{x-y^0}) - 2\,\mathrm{Li}_3(-\mathrm{e}^x) + 2\,\mathrm{Li}_3(-\mathrm{e}^{x-y^0})\Big]_{x=\frac{y0-y}{2}}^{x=\frac{y0+y}{2}} - \vartheta(y^2-(y^0)^2)\frac{(y^0)^3+\pi^2y^0}{3}\,, \tag{A.48}$$

and

$$J_0^{\mathrm{B}} = 2\log\left|\frac{1-\mathrm{e}^{\frac{y^0+y}{2}}}{1-\mathrm{e}^{\frac{y^0-y}{2}}}\right| - y - \vartheta(y^2-(y^0)^2)y^0\,, \tag{A.49}$$

$$J_1^{\mathrm{B}} = \mathrm{Re}\Big[x\log\frac{1-\mathrm{e}^x}{1-\mathrm{e}^{x-y^0}} + \mathrm{Li}_2(\mathrm{e}^x) - \mathrm{Li}_2(\mathrm{e}^{x-y^0})\Big]_{x=\frac{y0-y}{2}}^{x=\frac{y0+y}{2}} - \vartheta(y^2-(y^0)^2)\frac{(y^0)^2}{2}\,, \tag{A.50}$$

$$J_2^{\mathrm{B}} = \mathrm{Re}\Big[x^2\log\frac{1-\mathrm{e}^x}{1-\mathrm{e}^{x-y^0}} + 2x\,\mathrm{Li}_2(\mathrm{e}^x) - 2x\,\mathrm{Li}_2(\mathrm{e}^{x-y^0}) - 2\,\mathrm{Li}_3(\mathrm{e}^x) + 2\,\mathrm{Li}_3(\mathrm{e}^{x-y^0})\Big]_{x=\frac{y0-y}{2}}^{x=\frac{y0+y}{2}} - \vartheta(y^2-(y^0)^2)\frac{(y^0)^3-2\pi^2y^0}{3}\,. \tag{A.51}$$

In terms of these functions the spectral self-energies for different particles are given by

$$\Pi_{\phi}^{\mathcal{A}}(k) = -\frac{G_\phi}{8\pi}\frac{k^2}{|\mathbf{k}|}J_0^{\mathrm{B}}\left(\frac{k^0}{T},\frac{|\mathbf{k}|}{T}\right) + \frac{N_c h_t^2}{16\pi}\frac{k^2}{|\mathbf{k}|}J_0^{\mathrm{F}}\left(\frac{k^0}{T},\frac{|\mathbf{k}|}{T}\right). \tag{A.52}$$

and

$$\Sigma_{\psi}^{\mathcal{A}0}(k) = \frac{G_\psi T^2}{8\pi|\mathbf{k}|}I_1\left(\frac{k^0}{T},\frac{|\mathbf{k}|}{T}\right), \tag{A.53}$$

$$\Sigma_{\psi}^{\mathcal{A}i}(k) = \frac{G_\psi T^2}{8\pi|\mathbf{k}|}\left[\frac{k^0}{|\mathbf{k}|}I_1\left(\frac{k^0}{T},\frac{|\mathbf{k}|}{T}\right) - \frac{(k^0)^2-|\mathbf{k}|^2}{2|\mathbf{k}|T}I_0\left(\frac{k^0}{T},\frac{|\mathbf{k}|}{T}\right)\right]\frac{k^i}{|\mathbf{k}|}, \tag{A.54}$$

as well as

$$\Pi_{\mu\nu}^{(\psi)\mathcal{A}}(k)g^{\mu\nu} = -\frac{k^2 T}{8\pi|\mathbf{k}|}g^2 C^F J_0^{\mathrm{F}}, \tag{A.55}$$

$$\Pi_{00}^{(\psi)\mathcal{A}}(k) = \frac{T^3}{8\pi|\mathbf{k}|}g^2 C^F\left[-\frac{k^2}{2T^2}J_0^{\mathrm{F}} + \frac{2k^0}{T}J_1^{\mathrm{F}} - 2J_2^{\mathrm{F}}\right], \tag{A.56}$$

for the chiral fermion insertion,

$$\Pi_{\mu\nu}^{(\phi)\mathcal{A}}(k)g^{\mu\nu} = -\frac{k^2 T}{16\pi|\mathbf{k}|}g^2 C^F J_0^{\mathrm{B}}, \tag{A.57}$$

$$\Pi_{00}^{(\phi)\mathcal{A}}(k) = \frac{T^3}{16\pi|\mathbf{k}|}g^2 C^F\left[\frac{(k^0)^2}{T^2}J_0^{\mathrm{B}} - \frac{4k^0}{T}J_1^{\mathrm{B}} + 4J_2^{\mathrm{B}}\right], \tag{A.58}$$

for the Higgs boson contribution and lastly for the gauge bosons including ghosts running in the loop

$$\Pi_{\mu\nu}^{(V)\mathcal{A}}(k)g^{\mu\nu} = \frac{5k^2 T}{16\pi|\mathbf{k}|}g^2 C_2^A J_0^{\mathrm{B}}, \tag{A.59}$$

$$\Pi_{00}^{(V)\mathcal{A}}(k) = \frac{T^3}{16\pi|\mathbf{k}|}g^2 C_2^A\left[\frac{(2k^2-(k^0)^2)}{T^2}J_0^{\mathrm{B}} - \frac{4k^0}{T}J_1^{\mathrm{B}} + 4J_2^{\mathrm{B}}\right]. \tag{A.60}$$

The non-vanishing HTL expressions, i.e. those expression that give rise to the parts of the spectral self-energy that is proportional to T^2, only appear in the t-channel as these are parts of the terms that come with the Heaviside step function ϑ, and are given by

$$I_1^{\mathrm{HTL}} = \frac{\pi^2}{2}, \qquad J_2^{\mathrm{F\,HTL}} = -\frac{\pi^2 y^0}{3}, \qquad J_2^{\mathrm{B\,HTL}} = 2\frac{\pi^2 y^0}{3}, \tag{A.61}$$

such that the spectral self-energy of the Higgs field vanishes in the HTL approximation. The spectral parts of the self-energies for the fermions and gauge bosons in the HTL limit are given in the main text in eqs. (3.122) and (3.123).

A.4 HOW TO COMPUTE VERTEX-TYPE CONTRIBUTIONS TO THE COLLISION TERM

When dealing with vertex type diagrams, particularly when computing diffusion constants as in chapter 4, integrals of the form

$$\begin{aligned}\mathcal{J} = &\int\frac{\mathrm{d}^4p_1}{(2\pi)^4}\int\frac{\mathrm{d}^4p_2}{(2\pi)^4}\int\frac{\mathrm{d}^4p_3}{(2\pi)^4}\int\frac{\mathrm{d}^4p_4}{(2\pi)^4}(2\pi)^4\delta^4(p_1+p_2-p_3-p_4)\\ &\times(2\pi)^4\delta(p_1^2)\delta(p_2^2)\delta(p_3^2)\delta(p_4^2)\mathrm{sign}(p_1^0)\mathrm{sign}(p_2^0)\mathrm{sign}(p_3^0)\mathrm{sign}(p_4^0)\mathcal{F}(p_1^0,p_2^0,p_3^0,p_4^0),\end{aligned} \tag{A.62}$$

appear and have to solved numerically, see the contraction (4.85) and (4.88). It is convenient to define a new coordinate $r = p_1 + p_2 = p_3 + p_4 = |\mathbf{r}|\mathbf{e}_z$ that can be chosen such that it points in the z-direction without loss of generality. The four-dimensional delta function can be used to get rid of the p_3 integral. This allows to express p_3 as well as p_2 in terms of r and p_1. p_1 and p_4 can be written as

$$\mathbf{p}_{1,4} = |\mathbf{p}_{1,4}| \begin{pmatrix} \sin\theta_{1,4}\cos\phi_{1,4} \\ \sin\theta_{1,4}\sin\phi_{1,4} \\ \cos\phi_{1,4} \end{pmatrix} . \tag{A.63}$$

The four-dimensional integral over p_2 is transformed into an integral over r^0 and $|\mathbf{r}|$. With $\delta(p_{1,4}^4)$ the $p_{1,4}^0$ integrals can be evaluated as sums over $\pm p_{1,4}^0$. $\delta(p_{2,3}^4)$ can be used to get rid of the $\cos\theta_{1,4}$ integrals. However, since $|\cos\theta_{1,4}| \leq 1$, this implies boundaries that can be put into two window functions

$$\mathcal{W}(p_{1,4}^0, |\mathbf{p}_{1,4}|) = \vartheta\left(1 - \left|\frac{2r^0 p_{1,4}^0 - r_0^2 + |\mathbf{r}|^2}{2|\mathbf{r}||\mathbf{p}_{1,4}|}\right|\right) , \tag{A.64}$$

with the Heaviside step function ϑ. In total one is left with

$$\begin{aligned} \mathcal{J} = \frac{1}{8(2\pi)^7} \int_0^\infty \mathrm{d}|\mathbf{p}_1| \int_0^\infty \mathrm{d}|\mathbf{p}_4| \int_0^\infty \mathrm{d}|\mathbf{r}| \int_{-\infty}^\infty \mathrm{d}r^0 \int_0^{2\pi} \mathrm{d}\phi_1 \int_0^{2\pi} \mathrm{d}\phi_4 \\ \times \sum_{p_1^0 = \pm|\mathbf{p}_1|} \sum_{p_4^0 = \pm|\mathbf{p}_4|} \mathrm{sign}(p_1^0)\mathrm{sign}(p_4^0)\mathrm{sign}(r^0 - p_1^0)\mathrm{sign}(r^0 - p_4^0) \\ \times \mathcal{W}(p_1^0, |\mathbf{p}_1|)\mathcal{W}(p_4^0, |\mathbf{p}_4|)\mathcal{F}(p_1^0, r^0 - p_1^0, r^0 - p_4^0, p_4^0) . \end{aligned} \tag{A.65}$$

For the processes considered in this thesis, the only dependence on the azimuthal angle is given by terms of the form $\cos(\phi_1 - \phi_2)$. The corresponding azimuthal integrals make such term vanish. Therefore, one can get rid of these integrals by multiplying $\mathcal{J}$ with 4π while setting $\phi_1 = 0$ and $\phi_4 = \pi/2$. Eventually, this implies

$$\begin{aligned} \mathcal{J} = \frac{1}{4(2\pi)^6} \int_0^\infty \mathrm{d}|\mathbf{p}_1| \int_0^\infty \mathrm{d}|\mathbf{p}_4| \int_0^\infty \mathrm{d}|\mathbf{r}| \int_{-\infty}^\infty \mathrm{d}r^0 \\ \times \sum_{p_1^0 = \pm|\mathbf{p}_1|} \sum_{p_4^0 = \pm|\mathbf{p}_4|} \mathrm{sign}(p_1^0)\mathrm{sign}(p_4^0)\mathrm{sign}(r^0 - p_1^0)\mathrm{sign}(r^0 - p_4^0) \\ \times \mathcal{W}(p_1^0, |\mathbf{p}_1|)\mathcal{W}(p_4^0, |\mathbf{p}_4|)\mathcal{F}(p_1^0, r^0 - p_1^0, r^0 - p_4^0, p_4^0)|_{\phi_1=0,\phi_4=\pi/2} . \end{aligned} \tag{A.66}$$

When calculating diffusion constants for particles one can assume $\mathrm{sign}(p_1^0) = 1$. The remaining three signum functions give rise to three scenarios, see table 4.1, and allow for the decomposition

$$\mathcal{J} = \mathcal{J}_a + \mathcal{J}_b + \mathcal{J}_c . \tag{A.67}$$

Scenario a, given by $\mathrm{sign}(p_1^0) = \mathrm{sign}(p_2^0) = \mathrm{sign}(p_3^0) = \mathrm{sign}(p_4^0)$, describes $\phi\phi \to \phi\phi$ or $\phi V \to \phi V$ and analogously for fermions. Further it implies that $r^0 \geq |\mathbf{p}_{1,4}|$ such that

$$\begin{aligned} \mathcal{J}_a = \frac{1}{4(2\pi)^6} \int_0^\infty \mathrm{d}|\mathbf{p}_1| \int_0^\infty \mathrm{d}|\mathbf{p}_4| \int_0^\infty \mathrm{d}|\mathbf{r}| \int_{-\infty}^\infty \mathrm{d}r^0 \\ \times \vartheta(r^0 - |\mathbf{p}_1|)\vartheta(r^0 - |\mathbf{p}_4|)\mathcal{W}(|\mathbf{p}_1|, |\mathbf{p}_1|)\mathcal{W}(|\mathbf{p}_4|, |\mathbf{p}_4|) \\ \times \mathcal{F}(|\mathbf{p}_1|, |r^0 - \mathbf{p}_1|, |r^0 - |\mathbf{p}_4||, |\mathbf{p}_4|)|_{\phi_1=0,\phi_4=\pi/2} . \end{aligned} \tag{A.68}$$

Scenario b, given by $\mathrm{sign}(p_1^0) = -\mathrm{sign}(p_2^0) = \mathrm{sign}(p_3^0) = -\mathrm{sign}(p_4^0)$, describes $\phi\bar{\phi} \to \phi\bar{\phi}$ or $\phi V \to \phi V$ and analogously for fermions. Further it implies that $-|\mathbf{p}_4| < r^0 < |\mathbf{p}_1|$ such that

$$\begin{aligned}\mathcal{J}_b = \frac{1}{4(2\pi)^6}\int_0^\infty \mathrm{d}|\mathbf{p}_1|\int_0^\infty \mathrm{d}|\mathbf{p}_4|\int_0^\infty \mathrm{d}|\mathbf{r}|\int_{-\infty}^\infty \mathrm{d}r^0 \\ \times \vartheta(|\mathbf{p}_1| - r^0)\vartheta(r^0 + |\mathbf{p}_4|)\mathcal{W}(|\mathbf{p}_1|, |\mathbf{p}_1|)\mathcal{W}(-|\mathbf{p}_4|, |\mathbf{p}_4|) \\ \times \mathcal{F}(|\mathbf{p}_1|, -|r^0 - |\mathbf{p}_1||, |r^0 + |\mathbf{p}_4||, -|\mathbf{p}_4|)|_{\phi_1=0,\phi_4=\pi/2}\,. \end{aligned} \tag{A.69}$$

Scenario c, given by $\mathrm{sign}(p_1^0) = -\mathrm{sign}(p_2^0) = -\mathrm{sign}(p_3^0) = \mathrm{sign}(p_4^0)$, describes $\phi\bar{\phi} \to \phi\bar{\phi}$ or $\phi\bar{\phi} \to VV$ and analogously for fermions. Further it implies that $r^0 < |\mathbf{p}_{1,4}|$ such that

$$\begin{aligned}\mathcal{J}_c = \frac{1}{4(2\pi)^6}\int_0^\infty \mathrm{d}|\mathbf{p}_1|\int_0^\infty \mathrm{d}|\mathbf{p}_4|\int_0^\infty \mathrm{d}|\mathbf{r}|\int_{-\infty}^\infty \mathrm{d}r^0 \\ \times \vartheta(|\mathbf{p}_1| - r^0)\vartheta(|\mathbf{p}_4| - r^0)\mathcal{W}(|\mathbf{p}_1|, |\mathbf{p}_1|)\mathcal{W}(|\mathbf{p}_4|, |\mathbf{p}_4|) \\ \times \mathcal{F}(|\mathbf{p}_1|, -|r^0 - |\mathbf{p}_1||, -|r^0 - |\mathbf{p}_4||, |\mathbf{p}_4|)|_{\phi_1=0,\phi_4=\pi/2}\,. \end{aligned} \tag{A.70}$$

Note that $\mathcal{J}_a = \mathcal{J}_b$ when having $2 \leftrightarrow 2$ scattering processes that involve two scalars (fermions) and two gauge bosons as external particles since these describe the same processes $\phi V \to \phi V$ ($\psi V \to \psi V$). Analogously one has $\mathcal{J}_b = \mathcal{J}_c$ for processes with external particles of the same species since these also account for the same process, i.e. $\phi\bar{\phi} \to \phi\bar{\phi}$ ($\psi\bar{\psi} \to \psi\bar{\psi}$). In the latter case $\mathcal{J}_a = 0$ since $\phi\phi \to \phi\phi$ ($\psi\psi \to \psi\psi$) should not contribute to the diffusion process.

B

REMARKS ON THE TEST OF THE SEESAW AND LEPTOGENESIS

This appendix is based on refs. [1, 3] and provides additional informations that are particularly needed for chapter 6.

In section B.1 full expressions for the active-sterile mixing angles are given including a discussion about a flavour asymmetric washout, the seesaw line are determined and physical as well as unphysical parameter degeneracies are mentioned. Section B.2 provides detailed information about the expected number of events in experiments such as FCC-ee, ILC and CEPC.

B.1 ACTIVE-STERILE MIXING ANGLES

In the case of two heavy neutrino there are six mixing angles U_{ai}^2, which can be expressed in terms of the parameters of the seesaw Lagrangian (2.46) with the Casas-Ibarra parametrisation from eq. (2.52) and the fundamental parameters introduced in subsections 2.1.2 and 2.2.3. We collect the quantities that have already been measured with a sufficient precision into constants a_i and b_i. On the one hand, these are expressed in term of the light neutrino masses m_a for $a, b = 1, 2, 3$ with the mass of the lightest neutrino $m_0 = 0$ and the mixing angles θ_{ab}, where s_{ab} and c_{ab} are shorthand notations for $\sin\theta_{ab}$ and $\cos\theta_{ab}$. Note that s_{ab} and c_{ab} are understood as the positive real roots of s_{ab}^2 and c_{ab}^2, as given in table 2.2. Further $\xi = \pm$ is included. On the other hand, we keep the parametrical dependence on the unconstrained parameters, such as the complex angle $\mathrm{Re}\omega$, $\mathrm{Im}\omega$, the Majorana phases $\alpha_{1,2}$ and also the Dirac phase δ explicit.

In case of NO each of the U_{ai}^2 are insensitive to α_1 as $m_1 = m_0 = 0$, such that

$$\frac{M_1 U_{e1}^2 + M_2 U_{e2}^2}{\cosh(2\mathrm{Im}\omega)} = a_1^+ - a_2 \sin\left(\frac{\alpha_2}{2} + \delta\right) \tanh(2\mathrm{Im}\omega)\,, \tag{B.1}$$

$$\frac{M_1 U_{\mu 1}^2 + M_2 U_{\mu 2}^2}{\cosh(2\mathrm{Im}\omega)} = a_3^+ - a_4 \cos(\delta) - \left[a_5 \sin\left(\frac{\alpha_2}{2}\right) - a_6 \sin\left(\frac{\alpha_2}{2} + \delta\right)\right] \tanh(2\mathrm{Im}\omega)\,, \tag{B.2}$$

$$\frac{M_1 U_{\tau 1}^2 + M_2 U_{\tau 2}^2}{\cosh(2\mathrm{Im}\omega)} = a_7^+ + a_4 \cos(\delta) + \left[a_5 \sin\left(\frac{\alpha_2}{2}\right) + a_8 \sin\left(\frac{\alpha_2}{2} + \delta\right)\right] \tanh(2\mathrm{Im}\omega)\,, \tag{B.3}$$

and

$$\frac{M_1U_{e1}^2 - M_2U_{e2}^2}{\cos(2\mathrm{Re}\omega)} = a_1^- - a_2\cos\left(\frac{\alpha_2}{2}+\delta\right)\tan(2\mathrm{Re}\omega)\,, \tag{B.4}$$

$$\frac{M_1U_{\mu1}^2 - M_2U_{\mu2}^2}{\cos(2\mathrm{Re}\omega)} = -a_3^- - a_4\cos(\delta) - \left[a_5\cos\left(\frac{\alpha_2}{2}\right) - a_6\cos\left(\frac{\alpha_2}{2}+\delta\right)\right]\tan(2\mathrm{Re}\omega)\,, \tag{B.5}$$

$$\frac{M_1U_{\tau1}^2 - M_2U_{\tau2}^2}{\cos(2\mathrm{Re}\omega)} = -a_7^- + a_4\cos(\delta) + \left[a_5\cos\left(\frac{\alpha_2}{2}\right) + a_8\cos\left(\frac{\alpha_2}{2}+\delta\right)\right]\tan(2\mathrm{Re}\omega)\,, \tag{B.6}$$

where a_1 to a_8 are positive real values given by the light neutrino masses and their mixing angles:

$$a_1^\pm = m_2c_{13}^2s_{12}^2 \pm m_3s_{13}^2\,, \tag{B.7}$$

$$a_2 = 2\sqrt{m_2m_3}c_{13}s_{12}s_{13}\xi\,, \tag{B.8}$$

$$a_3^\pm = \pm m_2(c_{12}^2c_{23}^2 + s_{12}^2s_{13}^2s_{23}^2) + m_3c_{13}^2s_{23}^2\,, \tag{B.9}$$

$$a_4 = 2m_2c_{12}c_{23}s_{12}s_{13}s_{23}\,, \tag{B.10}$$

$$a_5 = 2\sqrt{m_2m_3}c_{12}c_{13}c_{23}s_{23}\xi\,, \tag{B.11}$$

$$a_6 = 2\sqrt{m_2m_3}c_{13}s_{12}s_{13}s_{23}^2\xi\,, \tag{B.12}$$

$$a_7^\pm = \pm m_2(c_{23}^2s_{12}^2s_{13}^2 + c_{12}^2s_{23}^2) + m_3c_{13}^2c_{23}^2\,, \tag{B.13}$$

$$a_8 = 2\sqrt{m_2m_3}c_{13}c_{23}^2s_{12}s_{13}\xi\,. \tag{B.14}$$

In case of IO the different U_{ai}^2 are only sensitive to the difference of the Majorana phase $\tilde{\alpha} = \alpha_2 - \alpha_1$, such that

$$\frac{M_1U_{e1}^2 + M_2U_{e2}^2}{\cosh(2\mathrm{Im}\omega)} = b_1^+ + b_2\sin\left(\frac{\tilde{\alpha}}{2}\right)\tanh(2\mathrm{Im}\omega)\,, \tag{B.15}$$

$$\frac{M_1U_{\mu1}^2 + M_2U_{\mu2}^2}{\cosh(2\mathrm{Im}\omega)} = b_3^+ - b_4^+\cos(\delta) - \left[b_5\sin\left(\frac{\tilde{\alpha}}{2}\right) + b_6\sin\left(\frac{\tilde{\alpha}}{2}-\delta\right) - b_7\sin\left(\frac{\tilde{\alpha}}{2}+\delta\right)\right]\tanh(2\mathrm{Im}\omega)\,, \tag{B.16}$$

$$\frac{M_1U_{\tau1}^2 + M_2U_{\tau2}^2}{\cosh(2\mathrm{Im}\omega)} = b_8^+ + b_4^+\cos(\delta) - \left[b_9\sin\left(\frac{\tilde{\alpha}}{2}\right) - b_6\sin\left(\frac{\tilde{\alpha}}{2}-\delta\right) + b_7\sin\left(\frac{\tilde{\alpha}}{2}+\delta\right)\right]\tanh(2\mathrm{Im}\omega)\,, \tag{B.17}$$

and

$$\frac{M_1U_{e1}^2 - M_2U_{e2}^2}{\cos(2\mathrm{Re}\omega)} = b_1^- - b_2\cos\left(\frac{\tilde{\alpha}}{2}\right)\tan(2\mathrm{Re}\omega)\,, \tag{B.18}$$

$$\frac{M_1U_{\mu1}^2 - M_2U_{\mu2}^2}{\cos(2\mathrm{Re}\omega)} = -b_3^- - b_4^-\cos(\delta) + \left[b_5\cos\left(\frac{\tilde{\alpha}}{2}\right) + b_6\cos\left(\frac{\tilde{\alpha}}{2}-\delta\right) - b_7\cos\left(\frac{\tilde{\alpha}}{2}+\delta\right)\right]\tan(2\mathrm{Re}\omega)\,, \tag{B.19}$$

$$\frac{M_1U_{\tau1}^2 - M_2U_{\tau2}^2}{\cos(2\mathrm{Re}\omega)} = -b_8^- + b_4^-\cos(\delta) + \left[b_9\cos\left(\frac{\tilde{\alpha}}{2}\right) - b_6\cos\left(\frac{\tilde{\alpha}}{2}-\delta\right) + b_7\cos\left(\frac{\tilde{\alpha}}{2}+\delta\right)\right]\tan(2\mathrm{Re}\omega)\,, \tag{B.20}$$

where b_1 to b_9 are the positive real numbers given by the light neutrino masses and mixings:

$$b_1^{\pm} = m_1 c_{12}^2 c_{13}^2 \pm m_2 s_{12}^2 c_{13}^2 \,, \tag{B.21}$$
$$b_2 = 2\sqrt{m_1 m_2} c_{12} s_{12} \xi \,, \tag{B.22}$$
$$b_3^{\pm} = \pm m_1 (c_{23}^2 s_{12}^2 + c_{12}^2 s_{13}^2 s_{23}^2) + m_2 (c_{12}^2 c_{23}^2 + s_{12}^2 s_{13}^2 s_{23}^2) \,, \tag{B.23}$$
$$b_4^{\pm} = 2(\pm m_2 - m_1) c_{12} c_{23} s_{12} s_{13} s_{23} \,, \tag{B.24}$$
$$b_5 = 2\sqrt{m_1 m_2} (c_{12} c_{23}^2 s_{12} - c_{12} s_{12} s_{13}^2 s_{23}^2) \xi \,, \tag{B.25}$$
$$b_6 = 2\sqrt{m_1 m_2} c_{12}^2 c_{23} s_{13} s_{23} \xi \,, \tag{B.26}$$
$$b_7 = 2\sqrt{m_1 m_2} s_{12}^2 c_{23} s_{13} s_{23} \xi \,, \tag{B.27}$$
$$b_8^{\pm} = \pm m_1 (c_{12}^2 c_{23}^2 s_{13}^2 + s_{12}^2 s_{23}^2) + m_2 (c_{23}^2 s_{12}^2 s_{13}^2 + c_{12}^2 s_{23}^2) \,, \tag{B.28}$$
$$b_9 = 2\sqrt{m_1 m_2} c_{12} s_{12} (s_{23}^2 - c_{23}^2 s_{13}^2) \xi \,. \tag{B.29}$$

It is worth mentioning that the dependence on $\tilde{\alpha}$ implies that one can choose $\alpha_1 = 0$ and consider α_2 as the running parameter without loss of generality. This is also true or NO since α_1 does not appear at all in U_{ai}^2 if the lightest neutrino is massless. Note that these expression hold for the most general seesaw Lagrangian. Moreover, the total mixing is given by

$$U^2 \simeq \frac{M_2 - M_1}{2M_1 M_2} (m_2 - m_3) \cos(2\mathrm{Re}\omega) + \frac{M_1 + M_2}{2M_1 M_2} (m_2 + m_3) \cosh(2\mathrm{Im}\omega) \,, \tag{B.30}$$

for NO and

$$U^2 \simeq \frac{M_2 - M_1}{2M_1 M_2} (m_1 - m_2) \cos(2\mathrm{Re}\omega) + \frac{M_1 + M_2}{2M_1 M_2} (m_1 + m_2) \cosh(2\mathrm{Im}\omega) \,, \tag{B.31}$$

for IO. Note that the different U_{ai}^2 can be expressed in terms of the small SB parameters μ and ϵ from eqs. (2.59), cf. subsection 2.2.4 for a discussion of the symmetry protected scenario. Therefore, it is useful to denote the limits

$$\lim_{\mathrm{Im}\omega \to \infty} \tanh(2\mathrm{Im}\omega) = 1 \,, \tag{B.32}$$
$$\lim_{\mathrm{Im}\omega \to \infty} \cosh(2\mathrm{Im}\omega) = \lim_{\mathrm{Im}\omega \to \infty} \sinh(2\mathrm{Im}\omega) = \frac{1}{2} \exp(2\mathrm{Im}\omega) = \frac{1}{2\epsilon} \,, \tag{B.33}$$

which arise in the limit $\epsilon \to 0$. Further, for the sake of testing the seesaw and also leptogenesis in future experiments, a mass degeneracy turns out to be required, i.e. $M_1 \simeq M_2 \simeq \bar{M}$, such that $\Delta M \ll M$ and thus $\mu \simeq 0$. If this deviation is too small to be resolved in the experiment, i.e. $U_{a1}^2 \simeq U_{a2}^2$, only the sum $U_a^2 = \sum_i U_{ai}^2$ can be observed. In that case, the LH sides of eqs. (B.1)-(B.3) and (B.15)-(B.17) collapse to $\frac{1}{2}\bar{M} U_a^2 \exp(2\mathrm{Im}\omega) = \frac{1}{2}\bar{M} U_a^2/\epsilon$, while the LH sides of eqs. (B.4)-(B.6) and (B.18)-(B.20) approximately vanish. Note that in the mass degenerate case U_a^2 and U^2 feature no dependence on $\mathrm{Re}\omega$. Further, we find that the different U_a^2/U^2 do neither depend on $\bar{M}$ nor on $\mathrm{Im}\omega$ for $\epsilon \to 0$. To leading order in $\sqrt{m_\odot/m_{\mathrm{atm}}}$ and keeping terms of order $1/\epsilon$ the approximations (6.3)-(6.8) are recovered.

FLAVOUR ASYMMETRIES CONSISTENT WITH NEUTRINO OSCILLATION DATA: The limited sensitivity of experiments directly sets an lower bound on the mixings U_{ai}^2. In order to decide if the heavy neutrinos can explain the light neutrino masses or even if they can account for the baryon asymmetry, one needs to require are large mixing U_{ai}^2.

This comes along with large Yukawa couplings that increase the strength of the washout. A scenario that prevents the generated baryon charge to be washed out too quickly is given by requiring a strongly flavour asymmetric washout. See chapter 5 for a detailed discussion. The asymmetry in the flavours are driven by the combination of the Majorana phases $\alpha_{1,2}$ and the Dirac phase δ. In case of NO the maximally asymmetric washout is given when the electron has its minimal relative value that is allowed by the seesaw mechanism: $U_e^2/U^2 \simeq 0.006$. This can be realised when $\alpha_2 = -2\delta + \pi$. For IO the electron has to couple maximally, $U_e^2/U^2 \simeq 0.94$, which is given by $\alpha_2 - \alpha_1 = \pi$. See figure 6.1 for a graphical illustration for the region that is allowed by neutrino oscillation data.

SEESAW LINES: Particularly when plotting U_a^2 or U^2 over the average mass $\bar{M}$ the seesaw mechanism imposes a lower bound on the mixing. Basically for a given mass $\bar{M}$ the mixing has to be large enough in order to explain the light neutrino masses, cf. the seesaw equation. Note that due to the possibility of having an approximate $B - L$ symmetry there exists no upper bound on the mixings just by the seesaw constraints. It is the leptogenesis constraint that will impose an upper bound since the washout must not be too strong. We refer the $U^2 - \bar{M}$ or $U_a^2 - \bar{M}$ curve that is minimised for each $\bar{M}$ to as the seesaw line. In the approximate mass degenerate case, $\Delta M \ll \bar{M}$, the seesaw line for the total U^2 is trivially given by $\mathrm{Im}\omega = 0$. This can be seen when looking at eqs. (B.30) and (B.31), where the first terms approximately vanish, and is valid for any choice of the other seesaw parameters and for both neutrino mass orderings. This changes when minimising the different U_a^2. Setting $\xi = 1$ the minimal values for U_a^2 are given by a certain choice of phases (α_2, δ) for NO and $(\alpha_2 - \alpha_1, \delta)$ in case of IO, cf. eqs. (B.1)-(B.3) and (B.15)-(B.17), respectively. The $\mathrm{Im}\omega$ that minimises U_a^2 is obtained by semi-numerically solving that system for these phases. For NO one obtains

$$U_e^2 : (\alpha_2, \delta) = (\pi, 0) \qquad \to \mathrm{Im}\omega \simeq 0.769\,, \tag{B.34}$$
$$U_\mu^2 : (\alpha_2, \delta) = (\pi, \pi) \qquad \to \mathrm{Im}\omega \simeq 0.450\,, \tag{B.35}$$
$$U_\tau^2 : (\alpha_2, \delta) = (-\pi, 0) \qquad \to \mathrm{Im}\omega \simeq 0.368\,, \tag{B.36}$$

while for IO one has

$$U_e^2 : (\alpha_2, \delta) = (\pi, \forall\delta) \qquad \to \mathrm{Im}\omega \simeq 0.815\,, \tag{B.37}$$
$$U_\mu^2 : (\alpha_2, \delta) = (\pi, 0) \qquad \to \mathrm{Im}\omega \simeq 1.751\,, \tag{B.38}$$
$$U_\tau^2 : (\alpha_2, \delta) = (\pi, \pi) \qquad \to \mathrm{Im}\omega \simeq 1.297\,, \tag{B.39}$$

Here, $\forall\delta$ indicates that the seesaw line for U_e^2/U^2 is independent of the choice of δ.

PARAMETER DEGENERACY: The parameter space in the Casas-Ibarra parametrisation (2.52) inherits an unphysical parameter degeneracy, such that there are many choices of the internal parameters that lead to the same U_{ai}^2:

A shift $\mathrm{Re}\omega \to \mathrm{Re}\omega + \pi$ changes the sign of the Yukawa couplings Y_{ia} for all components. When looking at the Lagrangian such a shift can be compensated by redefining the fields according to $N_i \to -N_i$. In case of IO, Y_{ia} are invariant under swapping the sign of ξ while simultaneously adding 2π to α_2. For NO such a transformation changes the sign of Y_{ia}. Furthermore, a simultaneous sign flip of ξ, ΔM and $\mathrm{Im}\omega$ while transforming $\mathrm{Re}\omega \to \pi - \mathrm{Re}\omega$ changes the labels of the two states N_1 and N_2. These transformations

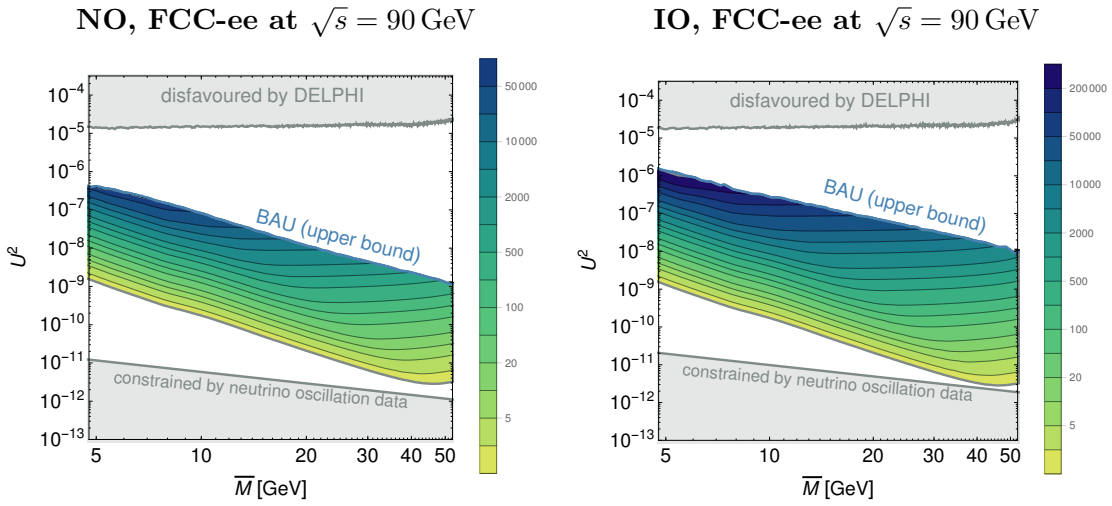

FIGURE B.1: This plot is taken from ref. [3] and gives the minimal number of events which are expected at the FCC-ee with a center of mass energy of $\sqrt{s} = 90\,\mathrm{GeV}$ for parameter points that are consistent with leptogenesis. The left and right panel describe NO and IO. The upper bound on the BAU is given by the blue line. For masses $\bar{M} \gtrsim 5\,\mathrm{Gev}$ the lower bound on the BAU is below the seesaw line. Therefore, the disfavoured region, that is shown in grey, is given by the seesaw line and the exclusion line from DELPHI.

leave the mixing U_{ai}^2 and the Lagrangian invariant. As a consequence, these are unphysical transformations.

In contrast, there is an invariance of U_{ai}^2 under the change $(\delta, \alpha_2, \mathrm{Re}\omega) \to (-\delta, 2\pi - \alpha_2, -\mathrm{Re}\omega)$. This is called a physical invariance as it is does not leave the Lagrangian invariant and consequently changes the physics. This invariance can be broken by independent measurements of ΔM and δ.

Note that U_a^2 is invariant under an additional transformation on the phases, which, however, has no analytic form since it requires solving the trigonometric functions (B.1)-(B.3) and (B.15)-(B.17). This degeneracy is physical and cannot be broken by a measurement of δ. This effect is particularly important when detecting heavy neutrinos in experiments that cannot resolve their mass splitting. As a consequence, any measurement of U_a^2 corresponds to at least two sets of fundamental parameters such as α, δ and $\mathrm{Re}\omega$. Thus, there are at least two possibilities for U_b^2 with $b \neq a$ for a given U_a^2.

B.2 TOTAL NUMBER OF EVENTS EXPECTED AT FCC-EE, ILC AND CEPC

The figures in this section provide detailed information about the number of events that are expected in the different experiments: Figure B.1 and B.2 correspond to the Z-pole run at the FCC-ee and ILC/CEPC, respectively. The run of CEPC and ILC at their maximal energy is presented in figure B.3.

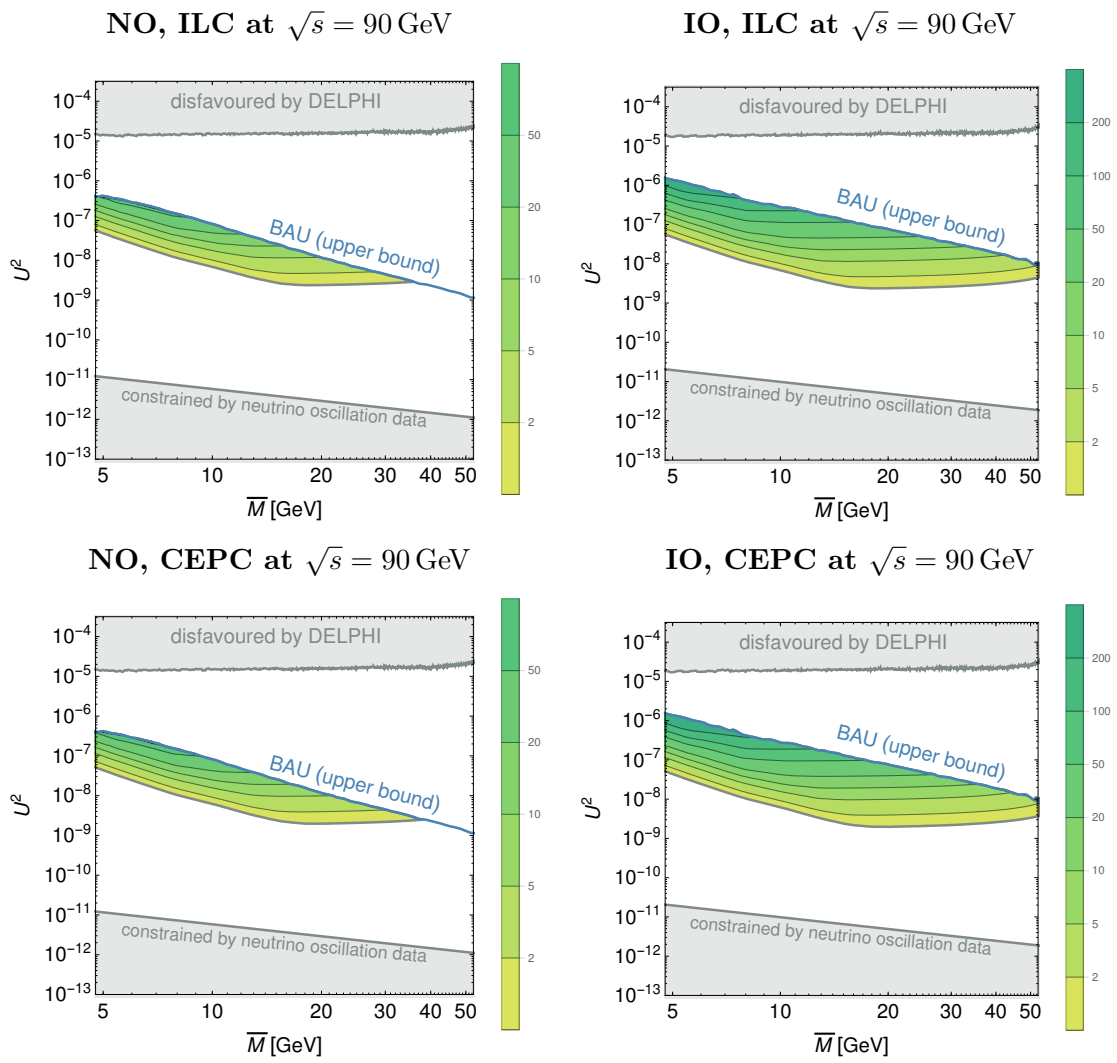

FIGURE B.2: This plot is taken from ref. [3] and gives the minimal number of events which are expected at the CEPC (top panel) and ILC (bottom panel) with a center of mass energy of $\sqrt{s} = 90\,\mathrm{GeV}$ for parameter points that are consistent with leptogenesis. The left and right panel describe NO and IO. The upper bound on the BAU is given by the blue line. For masses $\bar{M} \gtrsim 5\,\mathrm{Gev}$ the lower bound on the BAU is below the seesaw line. Therefore, the disfavoured region, that is shown in grey, is given by the seesaw line and the exclusion line from DELPHI.

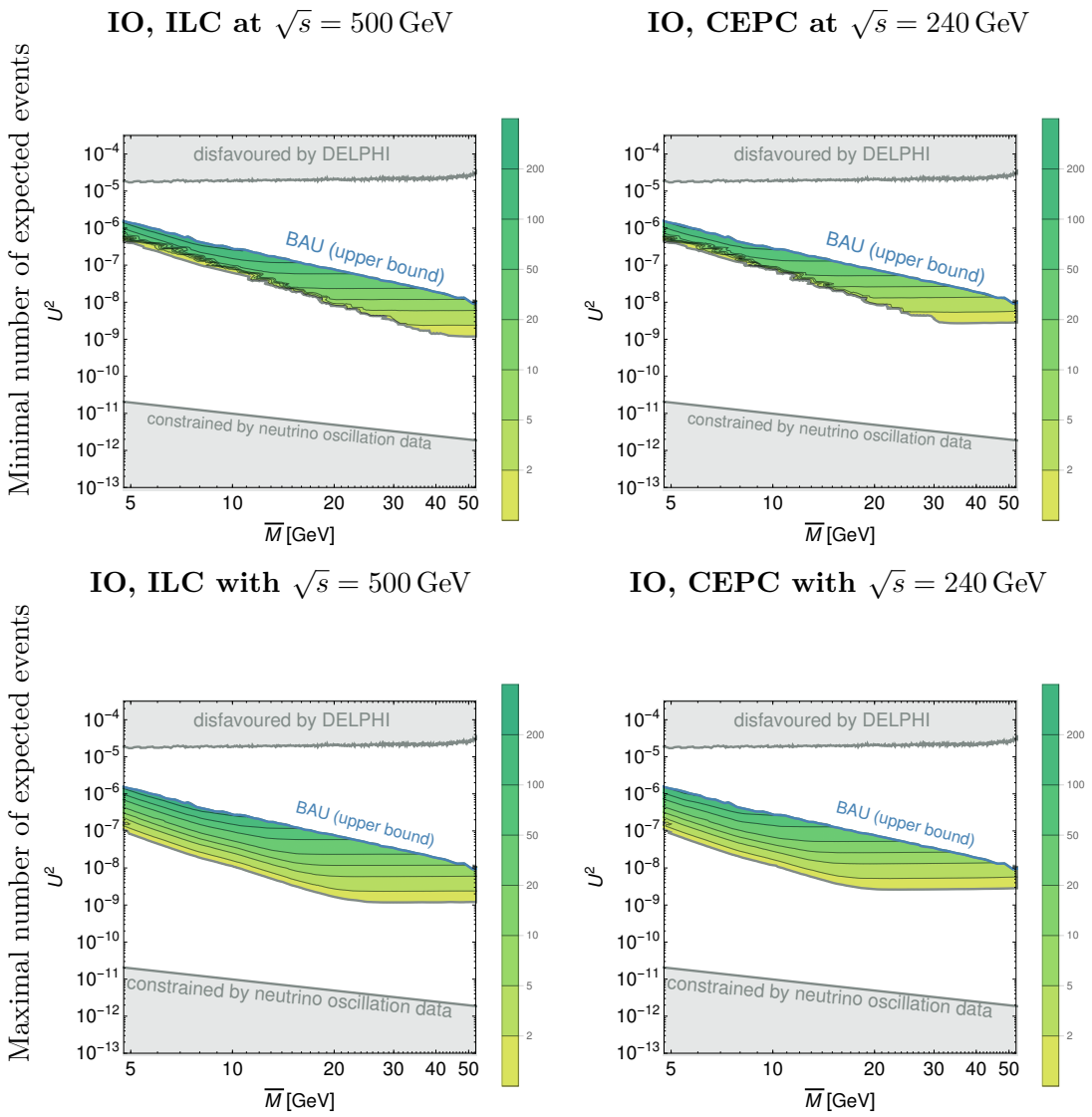

FIGURE B.3: This plot is taken from ref. [3] and gives the minimal (top row) and maximal (bottom panel) number of events which are expected at the ILC with a center of mass energy of $\sqrt{s} = 500\,\mathrm{GeV}$ (left column) and at the CEPC with $\sqrt{s} = 240\,\mathrm{GeV}$ (right column) for parameter points that are consistent with leptogenesis and for IO. The upper bound on the BAU is given by the blue line. For masses $\bar{M} \gtrsim 5\,\mathrm{Gev}$ the lower bound on the BAU is below the seesaw line. Therefore, the disfavoured region, that is shown in grey, is given by the seesaw line and the exclusion line from DELPHI.

BIBLIOGRAPHY

[1] M. Drewes, B. Garbrecht, D. Gueter, and J. Klaric, "Testing the low scale seesaw and leptogenesis," *JHEP* **08** (2017) 018, arXiv:1609.09069 [hep-ph].

[2] M. Drewes, B. Garbrecht, D. Gueter, and J. Klaric, "Leptogenesis from Oscillations of Heavy Neutrinos with Large Mixing Angles," *JHEP* **12** (2016) 150, arXiv:1606.06690 [hep-ph].

[3] S. Antusch, E. Cazzato, M. Drewes, O. Fischer, B. Garbrecht, D. Gueter, and J. Klaric, "Probing Leptogenesis at Future Colliders," arXiv:1710.03744 [hep-ph].

[4] S. Antusch, E. Cazzato, M. Drewes, O. Fischer, B. Garbrecht, D. Gueter, and J. Klaric, "Probing the Seesaw Mechanism and Leptogenesis with the International Linear Collider," in *International Workshop on Future Linear Collider (LCWS2017) Strasbourg, France, October 23-27, 2017*. 2018. arXiv:1801.06534 [hep-ph]. https://inspirehep.net/record/1649084/files/arXiv:1801.06534.pdf.

[5] M. Drewes, B. Garbrecht, J. Klarić, and D. Gueter, "Leptogenesis with GeV-Scale Right-Handed Neutrinos," *J. Phys. Conf. Ser.* **873** no. 1, (2017) 012027.

[6] M. Drewes, B. Garbrecht, D. Gueter, and J. Klaric, "Leptogenesis: Improving predictions for experimental searches," *PoS* **ICHEP2016** (2017) 514, arXiv:1611.08504 [hep-ph].

[7] M. Drewes, B. Garbrecht, D. Gueter, and J. Klaric, "On the relation between the CP phases in the PMNS matrix, CP-violation with sterile neutrinos and leptogenesis," in *18th International Workshop on Neutrino Factories and Future Neutrino Facilities Search (NuFact16) Quy Nhon, Vietnam, August 21-27, 2016*. 2016. arXiv:1611.04769 [hep-ph]. https://inspirehep.net/record/1498082/files/arXiv:1611.04769.pdf.

[8] B. Garbrecht and D. Gueter, "Diffusion constants during the electroweak phase transition: leading order results,".

[9] M. Drewes and D. Gueter, "Quasiparticles at finite temperature in the symmetric phase of the Standard Model,".

[10] **Particle Data Group** Collaboration, K. A. Olive *et al.*, "Review of Particle Physics," *Chin. Phys.* **C38** (2014) 090001.

[11] R. H. Cyburt, B. D. Fields, K. A. Olive, and T.-H. Yeh, "Big Bang Nucleosynthesis: 2015," *Rev. Mod. Phys.* **88** (2016) 015004, arXiv:1505.01076 [astro-ph.CO].

[12] **WMAP** Collaboration, G. Hinshaw *et al.*, "Nine-Year Wilkinson Microwave Anisotropy Probe (WMAP) Observations: Cosmological Parameter Results," *Astrophys. J. Suppl.* **208** (2013) 19, arXiv:1212.5226 [astro-ph.CO].

[13] **Planck** Collaboration, P. A. R. Ade *et al.*, "Planck 2015 results. XIII. Cosmological parameters," *Astron. Astrophys.* **594** (2016) A13, arXiv:1502.01589 [astro-ph.CO].

[14] A. Strumia and F. Vissani, "Neutrino masses and mixings and...," arXiv:hep-ph/0606054 [hep-ph].

[15] K. N. Abazajian *et al.*, "Light Sterile Neutrinos: A White Paper," arXiv:1204.5379 [hep-ph].

[16] M. Drewes, "The Phenomenology of Right Handed Neutrinos," *Int. J. Mod. Phys.* **E22** (2013) 1330019, arXiv:1303.6912 [hep-ph].

[17] M. Fukugita and T. Yanagida, "Baryogenesis Without Grand Unification," *Phys. Lett.* **B174** (1986) 45–47.

[18] P. Minkowski, "$\mu \to e\gamma$ at a Rate of One Out of 10^9 Muon Decays?," *Phys. Lett.* **67B** (1977) 421–428.

[19] M. Gell-Mann, P. Ramond, and R. Slansky, "Complex Spinors and Unified Theories," *Conf. Proc.* **C790927** (1979) 315–321, arXiv:1306.4669 [hep-th].

[20] R. N. Mohapatra and G. Senjanovic, "Neutrino Mass and Spontaneous Parity Violation," *Phys. Rev. Lett.* **44** (1980) 912.

[21] T. Yanagida, "Horizontal Symmetry and Masses of Neutrinos," *Prog. Theor. Phys.* **64** (1980) 1103.

[22] J. Schechter and J. W. F. Valle, "Neutrino Masses in SU(2) x U(1) Theories," *Phys. Rev.* **D22** (1980) 2227.

[23] J. Schechter and J. W. F. Valle, "Neutrino Decay and Spontaneous Violation of Lepton Number," *Phys. Rev.* **D25** (1982) 774.

[24] **Planck** Collaboration, P. A. R. Ade *et al.*, "Planck 2013 results. XVI. Cosmological parameters," *Astron. Astrophys.* **571** (2014) A16, arXiv:1303.5076 [astro-ph.CO].

[25] A. D. Sakharov, "Violation of CP Invariance, c Asymmetry, and Baryon Asymmetry of the Universe," *Pisma Zh. Eksp. Teor. Fiz.* **5** (1967) 32–35. [Usp. Fiz. Nauk161,61(1991)].

[26] G. 't Hooft, "Symmetry Breaking Through Bell-Jackiw Anomalies," *Phys. Rev. Lett.* **37** (1976) 8–11.

[27] G. 't Hooft, "Computation of the Quantum Effects Due to a Four-Dimensional Pseudoparticle," *Phys. Rev.* **D14** (1976) 3432–3450. [Erratum: Phys. Rev.D18,2199(1978)].

[28] V. A. Kuzmin, V. A. Rubakov, and M. E. Shaposhnikov, "On the Anomalous Electroweak Baryon Number Nonconservation in the Early Universe," *Phys. Lett.* **155B** (1985) 36.

[29] M. D'Onofrio, K. Rummukainen, and A. Tranberg, "Sphaleron Rate in the Minimal Standard Model," *Phys. Rev. Lett.* **113** no. 14, (2014) 141602, arXiv:1404.3565 [hep-ph].

[30] E. K. Akhmedov, V. A. Rubakov, and A. Yu. Smirnov, "Baryogenesis via neutrino oscillations," *Phys. Rev. Lett.* **81** (1998) 1359–1362, arXiv:hep-ph/9803255 [hep-ph].

[31] P. Di Bari, "An introduction to leptogenesis and neutrino properties," *Contemp. Phys.* **53** no. 4, (2012) 315–338, arXiv:1206.3168 [hep-ph].

[32] M. E. Shaposhnikov, "Possible Appearance of the Baryon Asymmetry of the Universe in an Electroweak Theory," *JETP Lett.* **44** (1986) 465–468. [Pisma Zh. Eksp. Teor. Fiz.44,364(1986)].

[33] M. E. Shaposhnikov, "Baryon Asymmetry of the Universe in Standard Electroweak Theory," *Nucl. Phys.* **B287** (1987) 757–775.

[34] D. E. Morrissey and M. J. Ramsey-Musolf, "Electroweak baryogenesis," *New J. Phys.* **14** (2012) 125003, arXiv:1206.2942 [hep-ph].

[35] T. Konstandin, "Quantum Transport and Electroweak Baryogenesis," *Phys. Usp.* **56** (2013) 747–771, arXiv:1302.6713 [hep-ph]. [Usp. Fiz. Nauk183,785(2013)].

[36] J. S. Schwinger, "Brownian motion of a quantum oscillator," *J. Math. Phys.* **2** (1961) 407–432.

[37] L. V. Keldysh, "Diagram technique for nonequilibrium processes," *Zh. Eksp. Teor. Fiz.* **47** (1964) 1515–1527. [Sov. Phys. JETP20,1018(1965)].

[38] K.-c. Chou, Z.-b. Su, B.-l. Hao, and L. Yu, "Equilibrium and Nonequilibrium Formalisms Made Unified," *Phys. Rept.* **118** (1985) 1.

[39] J. Berges, "Introduction to nonequilibrium quantum field theory," *AIP Conf. Proc.* **739** (2005) 3–62, arXiv:hep-ph/0409233 [hep-ph]. [,3(2004)].

[40] T. Prokopec, M. G. Schmidt, and S. Weinstock, "Transport equations for chiral fermions to order h bar and electroweak baryogenesis. Part 1," *Annals Phys.* **314** (2004) 208–265, arXiv:hep-ph/0312110 [hep-ph].

[41] T. Prokopec, M. G. Schmidt, and S. Weinstock, "Transport equations for chiral fermions to order h-bar and electroweak baryogenesis. Part II," *Annals Phys.* **314** (2004) 267–320, arXiv:hep-ph/0406140 [hep-ph].

[42] J. M. Cornwall, R. Jackiw, and E. Tomboulis, "Effective Action for Composite Operators," *Phys. Rev.* **D10** (1974) 2428–2445.

[43] F. Bezrukov, D. Gorbunov, and M. Shaposhnikov, "On initial conditions for the Hot Big Bang," *JCAP* **0906** (2009) 029, arXiv:0812.3622 [hep-ph].

[44] T. Asaka and M. Shaposhnikov, "The nuMSM, dark matter and baryon asymmetry of the universe," *Phys. Lett.* **B620** (2005) 17–26, arXiv:hep-ph/0505013 [hep-ph].

[45] T. Asaka, S. Blanchet, and M. Shaposhnikov, "The nuMSM, dark matter and neutrino masses," *Phys. Lett.* **B631** (2005) 151–156, arXiv:hep-ph/0503065 [hep-ph].

[46] M. Drewes *et al.*, "A White Paper on keV Sterile Neutrino Dark Matter," *JCAP* **1701** no. 01, (2017) 025, arXiv:1602.04816 [hep-ph].

[47] T. Endoh, T. Morozumi, and Z.-h. Xiong, "Primordial lepton family asymmetries in seesaw model," *Prog. Theor. Phys.* **111** (2004) 123–149, arXiv:hep-ph/0308276 [hep-ph].

[48] A. Pilaftsis and T. E. J. Underwood, "Electroweak-scale resonant leptogenesis," *Phys. Rev.* **D72** (2005) 113001, arXiv:hep-ph/0506107 [hep-ph].

[49] A. Abada, S. Davidson, F.-X. Josse-Michaux, M. Losada, and A. Riotto, "Flavor issues in leptogenesis," *JCAP* **0604** (2006) 004, arXiv:hep-ph/0601083 [hep-ph].

[50] E. Nardi, Y. Nir, E. Roulet, and J. Racker, "The Importance of flavor in leptogenesis," *JHEP* **01** (2006) 164, arXiv:hep-ph/0601084 [hep-ph].

[51] S. Blanchet and P. Di Bari, "Flavor effects on leptogenesis predictions," *JCAP* **0703** (2007) 018, arXiv:hep-ph/0607330 [hep-ph].

[52] W. Buchmuller, R. D. Peccei, and T. Yanagida, "Leptogenesis as the origin of matter," *Ann. Rev. Nucl. Part. Sci.* **55** (2005) 311–355, arXiv:hep-ph/0502169 [hep-ph].

[53] S. Davidson, E. Nardi, and Y. Nir, "Leptogenesis," *Phys. Rept.* **466** (2008) 105–177, arXiv:0802.2962 [hep-ph].

[54] S. Blanchet and P. Di Bari, "The minimal scenario of leptogenesis," *New J. Phys.* **14** (2012) 125012, arXiv:1211.0512 [hep-ph].

[55] S. Davidson and A. Ibarra, "A Lower bound on the right-handed neutrino mass from leptogenesis," *Phys. Lett.* **B535** (2002) 25–32, arXiv:hep-ph/0202239 [hep-ph].

[56] W. Buchmuller, P. Di Bari, and M. Plumacher, "Cosmic microwave background, matter - antimatter asymmetry and neutrino masses," *Nucl. Phys.* **B643** (2002) 367–390, arXiv:hep-ph/0205349 [hep-ph]. [Erratum: Nucl. Phys.B793,362(2008)].

[57] B. Garbrecht, F. Gautier, and J. Klaric, "Strong Washout Approximation to Resonant Leptogenesis," *JCAP* **1409** no. 09, (2014) 033, arXiv:1406.4190 [hep-ph].

[58] L. Covi, E. Roulet, and F. Vissani, "CP violating decays in leptogenesis scenarios," *Phys. Lett.* **B384** (1996) 169–174, arXiv:hep-ph/9605319 [hep-ph].

[59] M. Flanz, E. A. Paschos, U. Sarkar, and J. Weiss, "Baryogenesis through mixing of heavy Majorana neutrinos," *Phys. Lett.* **B389** (1996) 693–699, arXiv:hep-ph/9607310 [hep-ph].

[60] A. Pilaftsis, "Resonant CP violation induced by particle mixing in transition amplitudes," *Nucl. Phys.* **B504** (1997) 61–107, arXiv:hep-ph/9702393 [hep-ph].

[61] A. Pilaftsis, "CP violation and baryogenesis due to heavy Majorana neutrinos," *Phys. Rev.* **D56** (1997) 5431–5451, arXiv:hep-ph/9707235 [hep-ph].

[62] A. Pilaftsis and T. E. J. Underwood, "Resonant leptogenesis," *Nucl. Phys.* **B692** (2004) 303–345, arXiv:hep-ph/0309342 [hep-ph].

[63] S. Iso and K. Shimada, "Coherent Flavour Oscillation and CP Violating Parameter in Thermal Resonant Leptogenesis," *JHEP* **08** (2014) 043, arXiv:1404.4816 [hep-ph].

[64] R. E. Shrock, "General Theory of Weak Leptonic and Semileptonic Decays. 1. Leptonic Pseudoscalar Meson Decays, with Associated Tests For, and Bounds on, Neutrino Masses and Lepton Mixing," *Phys. Rev.* **D24** (1981) 1232.

[65] R. E. Shrock, "General Theory of Weak Processes Involving Neutrinos. 2. Pure Leptonic Decays," *Phys. Rev.* **D24** (1981) 1275.

[66] P. Langacker and D. London, "Mixing Between Ordinary and Exotic Fermions," *Phys. Rev.* **D38** (1988) 886.

[67] A. Abada, V. De Romeri, S. Monteil, J. Orloff, and A. M. Teixeira, "Indirect searches for sterile neutrinos at a high-luminosity Z-factory," *JHEP* **04** (2015) 051, arXiv:1412.6322 [hep-ph].

[68] **FCC-ee study Team** Collaboration, A. Blondel, E. Graverini, N. Serra, and M. Shaposhnikov, "Search for Heavy Right Handed Neutrinos at the FCC-ee," *Nucl. Part. Phys. Proc.* **273-275** (2016) 1883–1890, arXiv:1411.5230 [hep-ex].

[69] **SHiP** Collaboration, E. Graverini, N. Serra, and B. Storaci, "Search for New Physics in SHiP and at future colliders," *JINST* **10** no. 07, (2015) C07007, arXiv:1503.08624 [hep-ex].

[70] S. Antusch and O. Fischer, "Testing sterile neutrino extensions of the Standard Model at future lepton colliders," *JHEP* **05** (2015) 053, arXiv:1502.05915 [hep-ph].

[71] T. Asaka and T. Tsuyuki, "Seesaw mechanism at electron-electron colliders," *Phys. Rev.* **D92** no. 9, (2015) 094012, arXiv:1508.04937 [hep-ph].

[72] A. Abada, D. Bečirević, M. Lucente, and O. Sumensari, "Lepton flavor violating decays of vector quarkonia and of the Z boson," *Phys. Rev.* **D91** no. 11, (2015) 113013, arXiv:1503.04159 [hep-ph].

[73] S. Antusch, E. Cazzato, and O. Fischer, "Displaced vertex searches for sterile neutrinos at future lepton colliders," *JHEP* **12** (2016) 007, arXiv:1604.02420 [hep-ph].

[74] S. Antusch, E. Cazzato, and O. Fischer, "Sterile neutrino searches at future e^-e^+, pp, and e^-p colliders," *Int. J. Mod. Phys.* **A32** no. 14, (2017) 1750078, arXiv:1612.02728 [hep-ph].

[75] J. C. Helo, M. Hirsch, and S. Kovalenko, "Heavy neutrino searches at the LHC with displaced vertices," *Phys. Rev.* **D89** (2014) 073005, arXiv:1312.2900 [hep-ph]. [Erratum: Phys. Rev.D93,no.9,099902(2016)].

[76] E. Izaguirre and B. Shuve, "Multilepton and Lepton Jet Probes of Sub-Weak-Scale Right-Handed Neutrinos," *Phys. Rev.* **D91** no. 9, (2015) 093010, arXiv:1504.02470 [hep-ph].

[77] A. M. Gago, P. Hernández, J. Jones-Pérez, M. Losada, and A. Moreno Briceño, "Probing the Type I Seesaw Mechanism with Displaced Vertices at the LHC," *Eur. Phys. J.* **C75** no. 10, (2015) 470, arXiv:1505.05880 [hep-ph].

[78] C. O. Dib, C. S. Kim, K. Wang, and J. Zhang, "Distinguishing Dirac/Majorana Sterile Neutrinos at the LHC," *Phys. Rev.* **D94** no. 1, (2016) 013005, arXiv:1605.01123 [hep-ph].

[79] W.-Y. Keung and G. Senjanovic, "Majorana Neutrinos and the Production of the Right-handed Charged Gauge Boson," *Phys. Rev. Lett.* **50** (1983) 1427.

[80] A. Datta, M. Guchait, and D. P. Roy, "Prospect of heavy right-handed neutrino search at SSC / CERN LHC energies," *Phys. Rev.* **D47** (1993) 961–966, arXiv:hep-ph/9208228 [hep-ph].

[81] A. Datta, M. Guchait, and A. Pilaftsis, "Probing lepton number violation via majorana neutrinos at hadron supercolliders," *Phys. Rev.* **D50** (1994) 3195–3203, arXiv:hep-ph/9311257 [hep-ph].

[82] A. Kobach and S. Dobbs, "Heavy Neutrinos and the Kinematics of Tau Decays," *Phys. Rev.* **D91** no. 5, (2015) 053006, arXiv:1412.4785 [hep-ph].

[83] L. Canetti, M. Drewes, and B. Garbrecht, "Probing leptogenesis with GeV-scale sterile neutrinos at LHCb and Belle II," *Phys. Rev.* **D90** no. 12, (2014) 125005, arXiv:1404.7114 [hep-ph].

[84] B. Shuve and M. E. Peskin, "Revision of the LHCb Limit on Majorana Neutrinos," *Phys. Rev.* **D94** no. 11, (2016) 113007, arXiv:1607.04258 [hep-ph].

[85] D. Milanes, N. Quintero, and C. E. Vera, "Sensitivity to Majorana neutrinos in $\Delta L = 2$ decays of B_c meson at LHCb," *Phys. Rev.* **D93** no. 9, (2016) 094026, arXiv:1604.03177 [hep-ph].

[86] T. Asaka and H. Ishida, "Lepton number violation by heavy Majorana neutrino in B decays," *Phys. Lett.* **B763** (2016) 393–396, arXiv:1609.06113 [hep-ph].

[87] D. Gorbunov and M. Shaposhnikov, "How to find neutral leptons of the νMSM?," *JHEP* **10** (2007) 015, arXiv:0705.1729 [hep-ph]. [Erratum: JHEP11,101(2013)].

[88] T. Asaka, S. Eijima, and A. Watanabe, "Heavy neutrino search in accelerator-based experiments," *JHEP* **03** (2013) 125, arXiv:1212.1062 [hep-ph].

[89] M. Drewes, J. Hajer, J. Klaric, and G. Lanfranchi, "NA62 sensitivity to heavy neutral leptons in the low scale seesaw model," arXiv:1801.04207 [hep-ph].

[90] T. Spadaro, "Perspectives from the NA62 experiment, Talk given at the PBC Kickoff Meeting - CERN (September 2016),".

[91] **SHiP** Collaboration, M. Anelli *et al.*, "A facility to Search for Hidden Particles (SHiP) at the CERN SPS," arXiv:1504.04956 [physics.ins-det].

[92] S. Alekhin *et al.*, "A facility to Search for Hidden Particles at the CERN SPS: the SHiP physics case," *Rept. Prog. Phys.* **79** no. 12, (2016) 124201, arXiv:1504.04855 [hep-ph].

[93] **LBNE** Collaboration, T. Akiri *et al.*, "The 2010 Interim Report of the Long-Baseline Neutrino Experiment Collaboration Physics Working Groups," arXiv:1110.6249 [hep-ex].

[94] **LBNE** Collaboration, C. Adams *et al.*, "The Long-Baseline Neutrino Experiment: Exploring Fundamental Symmetries of the Universe," arXiv:1307.7335 [hep-ex].

[95] R. W. Rasmussen and W. Winter, "Perspectives for tests of neutrino mass generation at the GeV scale: Experimental reach versus theoretical predictions," *Phys. Rev.* **D94** no. 7, (2016) 073004, arXiv:1607.07880 [hep-ph].

[96] S. Antusch, E. Cazzato, and O. Fischer, "Higgs production from sterile neutrinos at future lepton colliders," *JHEP* **04** (2016) 189, arXiv:1512.06035 [hep-ph].

[97] A. Das and N. Okada, "Inverse seesaw neutrino signatures at the LHC and ILC," *Phys. Rev.* **D88** (2013) 113001, arXiv:1207.3734 [hep-ph].

[98] S. Banerjee, P. S. B. Dev, A. Ibarra, T. Mandal, and M. Mitra, "Prospects of Heavy Neutrino Searches at Future Lepton Colliders," *Phys. Rev.* **D92** (2015) 075002, arXiv:1503.05491 [hep-ph].

[99] P. Q. Hung, T. Le, V. Q. Tran, and T.-C. Yuan, "Lepton Flavor Violating Radiative Decays in EW-Scale ν_R Model: An Update," *JHEP* **12** (2015) 169, arXiv:1508.07016 [hep-ph].

[100] S. Antusch and O. Fischer, "Testing sterile neutrino extensions of the Standard Model at the Circular Electron Positron Collider," *Int. J. Mod. Phys.* **A30** no. 23, (2015) 1544004.

[101] **NOvA** Collaboration, D. S. Ayres *et al.*, "NOvA: Proposal to Build a 30 Kiloton Off-Axis Detector to Study $\nu_\mu \to \nu_e$ Oscillations in the NuMI Beamline," arXiv:hep-ex/0503053 [hep-ex].

[102] A. I. Bochkarev and M. E. Shaposhnikov, "Electroweak Production of Baryon Asymmetry and Upper Bounds on the Higgs and Top Masses," *Mod. Phys. Lett.* **A2** (1987) 417.

[103] K. Kajantie, M. Laine, K. Rummukainen, and M. E. Shaposhnikov, "The Electroweak phase transition: A Nonperturbative analysis," *Nucl. Phys.* **B466** (1996) 189–258, arXiv:hep-lat/9510020 [hep-lat].

[104] M. B. Gavela, P. Hernandez, J. Orloff, and O. Pene, "Standard model CP violation and baryon asymmetry," *Mod. Phys. Lett.* **A9** (1994) 795–810, arXiv:hep-ph/9312215 [hep-ph].

[105] P. Huet and E. Sather, "Electroweak baryogenesis and standard model CP violation," *Phys. Rev.* **D51** (1995) 379–394, arXiv:hep-ph/9404302 [hep-ph].

[106] M. B. Gavela, P. Hernandez, J. Orloff, O. Pene, and C. Quimbay, "Standard model CP violation and baryon asymmetry. Part 2: Finite temperature," *Nucl. Phys.* **B430** (1994) 382–426, arXiv:hep-ph/9406289 [hep-ph].

[107] P. Huet and A. E. Nelson, "Electroweak baryogenesis in supersymmetric models," *Phys. Rev.* **D53** (1996) 4578–4597, arXiv:hep-ph/9506477 [hep-ph].

[108] L. Fromme, S. J. Huber, and M. Seniuch, "Baryogenesis in the two-Higgs doublet model," *JHEP* **11** (2006) 038, arXiv:hep-ph/0605242 [hep-ph].

[109] D. J. H. Chung, B. Garbrecht, M. J. Ramsey-Musolf, and S. Tulin, "Yukawa Interactions and Supersymmetric Electroweak Baryogenesis," *Phys. Rev. Lett.* **102** (2009) 061301, arXiv:0808.1144 [hep-ph].

[110] D. J. H. Chung, B. Garbrecht, M. Ramsey-Musolf, and S. Tulin, "Supergauge interactions and electroweak baryogenesis," *JHEP* **12** (2009) 067, arXiv:0908.2187 [hep-ph].

[111] D. J. H. Chung, B. Garbrecht, M. J. Ramsey-Musolf, and S. Tulin, "Lepton-mediated electroweak baryogenesis," *Phys. Rev.* **D81** (2010) 063506, arXiv:0905.4509 [hep-ph].

[112] M. Shaposhnikov, "A Possible symmetry of the nuMSM," *Nucl. Phys.* **B763** (2007) 49–59, arXiv:hep-ph/0605047 [hep-ph].

[113] S. Weinberg, "Baryon and Lepton Nonconserving Processes," *Phys. Rev. Lett.* **43** (1979) 1566–1570.

[114] Z. Maki, M. Nakagawa, and S. Sakata, "Remarks on the unified model of elementary particles," *Prog. Theor. Phys.* **28** (1962) 870–880.

[115] B. Pontecorvo, "Neutrino Experiments and the Problem of Conservation of Leptonic Charge," *Sov. Phys. JETP* **26** (1968) 984–988. [Zh. Eksp. Teor. Fiz.53,1717(1967)].

[116] I. Esteban, M. C. Gonzalez-Garcia, M. Maltoni, I. Martinez-Soler, and T. Schwetz, "Updated fit to three neutrino mixing: exploring the accelerator-reactor complementarity," *JHEP* **01** (2017) 087, arXiv:1611.01514 [hep-ph].

[117] M. Lattanzi and M. Gerbino, "Status of neutrino properties and future prospects - Cosmological and astrophysical constraints," arXiv:1712.07109 [astro-ph.CO].

[118] A. Pilaftsis, "Radiatively induced neutrino masses and large Higgs neutrino couplings in the standard model with Majorana fields," *Z. Phys.* **C55** (1992) 275–282, arXiv:hep-ph/9901206 [hep-ph].

[119] J. Lopez-Pavon, E. Molinaro, and S. T. Petcov, "Radiative Corrections to Light Neutrino Masses in Low Scale Type I Seesaw Scenarios and Neutrinoless Double Beta Decay," *JHEP* **11** (2015) 030, arXiv:1506.05296 [hep-ph].

[120] J. A. Casas and A. Ibarra, "Oscillating neutrinos and muon —> e, gamma," *Nucl. Phys.* **B618** (2001) 171–204, arXiv:hep-ph/0103065 [hep-ph].

[121] M. Shaposhnikov, "The nuMSM, leptonic asymmetries, and properties of singlet fermions," *JHEP* **08** (2008) 008, arXiv:0804.4542 [hep-ph].

[122] E. Calzetta and B. L. Hu, "Nonequilibrium Quantum Fields: Closed Time Path Effective Action, Wigner Function and Boltzmann Equation," *Phys. Rev.* **D37** (1988) 2878.

[123] P. Millington and A. Pilaftsis, "Perturbative nonequilibrium thermal field theory," *Phys. Rev.* **D88** no. 8, (2013) 085009, arXiv:1211.3152 [hep-ph].

[124] M. Beneke, B. Garbrecht, C. Fidler, M. Herranen, and P. Schwaller, "Flavoured Leptogenesis in the CTP Formalism," *Nucl. Phys.* **B843** (2011) 177–212, arXiv:1007.4783 [hep-ph].

[125] B. Garbrecht, F. Glowna, and P. Schwaller, "Scattering Rates For Leptogenesis: Damping of Lepton Flavour Coherence and Production of Singlet Neutrinos," *Nucl. Phys.* **B877** (2013) 1–35, arXiv:1303.5498 [hep-ph].

[126] B. Garbrecht and T. Konstandin, "Separation of Equilibration Time-Scales in the Gradient Expansion," *Phys. Rev.* **D79** (2009) 085003, arXiv:0810.4016 [hep-ph].

[127] H. A. Weldon, "Dynamical Holes in the Quark - Gluon Plasma," *Phys. Rev.* **D40** (1989) 2410.

[128] H. A. Weldon, "Covariant Calculations at Finite Temperature: The Relativistic Plasma," *Phys. Rev.* **D26** (1982) 1394.

[129] B. Garbrecht and M. Garny, "Finite Width in out-of-Equilibrium Propagators and Kinetic Theory," *Annals Phys.* **327** (2012) 914–934, arXiv:1108.3688 [hep-ph].

[130] M. Beneke, B. Garbrecht, M. Herranen, and P. Schwaller, "Finite Number Density Corrections to Leptogenesis," *Nucl. Phys.* **B838** (2010) 1–27, arXiv:1002.1326 [hep-ph].

[131] M. L. Bellac, *Thermal Field Theory*. Cambridge University Press, 2011. http://www.cambridge.org/mw/academic/subjects/physics/theoretical-physics-and-mathematical-physics/thermal-field-theory?format=AR.

[132] P. B. Arnold, G. D. Moore, and L. G. Yaffe, "Transport coefficients in high temperature gauge theories. 1. Leading log results," *JHEP* **11** (2000) 001, arXiv:hep-ph/0010177 [hep-ph].

[133] P. B. Arnold, G. D. Moore, and L. G. Yaffe, "Transport coefficients in high temperature gauge theories. 2. Beyond leading log," *JHEP* **05** (2003) 051, arXiv:hep-ph/0302165 [hep-ph].

[134] J. M. Moreno, M. Quiros, and M. Seco, "Bubbles in the supersymmetric standard model," *Nucl. Phys.* **B526** (1998) 489–500, arXiv:hep-ph/9801272 [hep-ph].

[135] P. John and M. G. Schmidt, "Do stops slow down electroweak bubble walls?," *Nucl. Phys.* **B598** (2001) 291–305, arXiv:hep-ph/0002050 [hep-ph]. [Erratum: Nucl. Phys.B648,449(2003)].

[136] G. D. Moore, "Computing the strong sphaleron rate," *Phys. Lett.* **B412** (1997) 359–370, arXiv:hep-ph/9705248 [hep-ph].

[137] C. Lee, V. Cirigliano, and M. J. Ramsey-Musolf, "Resonant relaxation in electroweak baryogenesis," *Phys. Rev.* **D71** (2005) 075010, arXiv:hep-ph/0412354 [hep-ph].

[138] J. M. Cline, M. Joyce, and K. Kainulainen, "Supersymmetric electroweak baryogenesis," *JHEP* **07** (2000) 018, arXiv:hep-ph/0006119 [hep-ph].

[139] M. Joyce, T. Prokopec, and N. Turok, "Nonlocal electroweak baryogenesis. Part 1: Thin wall regime," *Phys. Rev.* **D53** (1996) 2930–2957, arXiv:hep-ph/9410281 [hep-ph].

[140] A. Anisimov, D. Besak, and D. Bodeker, "Thermal production of relativistic Majorana neutrinos: Strong enhancement by multiple soft scattering," *JCAP* **1103** (2011) 042, arXiv:1012.3784 [hep-ph].

[141] B. Garbrecht and M. Herranen, "Effective Theory of Resonant Leptogenesis in the Closed-Time-Path Approach," *Nucl. Phys.* **B861** (2012) 17–52, arXiv:1112.5954 [hep-ph].

[142] C. Fidler, M. Herranen, K. Kainulainen, and P. M. Rahkila, "Flavoured quantum Boltzmann equations from cQPA," *JHEP* **02** (2012) 065, arXiv:1108.2309 [hep-ph].

[143] G. Sigl and G. Raffelt, "General kinetic description of relativistic mixed neutrinos," *Nucl. Phys.* **B406** (1993) 423–451.

[144] L. Canetti, M. Drewes, T. Frossard, and M. Shaposhnikov, "Dark Matter, Baryogenesis and Neutrino Oscillations from Right Handed Neutrinos," *Phys. Rev.* **D87** (2013) 093006, arXiv:1208.4607 [hep-ph].

[145] J. Ghiglieri and M. Laine, "GeV-scale hot sterile neutrino oscillations: a numerical solution," *JHEP* **02** (2018) 078, arXiv:1711.08469 [hep-ph].

[146] B. Garbrecht, "More Viable Parameter Space for Leptogenesis," *Phys. Rev.* **D90** no. 6, (2014) 063522, arXiv:1401.3278 [hep-ph].

[147] D. Besak and D. Bodeker, "Thermal production of ultrarelativistic right-handed neutrinos: Complete leading-order results," *JCAP* **1203** (2012) 029, arXiv:1202.1288 [hep-ph].

[148] S. Blanchet, P. Di Bari, D. A. Jones, and L. Marzola, "Leptogenesis with heavy neutrino flavours: from density matrix to Boltzmann equations," *JCAP* **1301** (2013) 041, arXiv:1112.4528 [hep-ph].

[149] A. Abada, S. Davidson, A. Ibarra, F. X. Josse-Michaux, M. Losada, and A. Riotto, "Flavour Matters in Leptogenesis," *JHEP* **09** (2006) 010, arXiv:hep-ph/0605281 [hep-ph].

[150] R. Barbieri, P. Creminelli, A. Strumia, and N. Tetradis, "Baryogenesis through leptogenesis," *Nucl. Phys.* **B575** (2000) 61–77, arXiv:hep-ph/9911315 [hep-ph].

[151] W. Buchmuller and M. Plumacher, "Spectator processes and baryogenesis," *Phys. Lett.* **B511** (2001) 74–76, arXiv:hep-ph/0104189 [hep-ph].

[152] B. Garbrecht and P. Schwaller, "Spectator Effects during Leptogenesis in the Strong Washout Regime," *JCAP* **1410** no. 10, (2014) 012, arXiv:1404.2915 [hep-ph].

[153] J. A. Harvey and M. S. Turner, "Cosmological baryon and lepton number in the presence of electroweak fermion number violation," *Phys. Rev.* **D42** (1990) 3344–3349.

[154] S. Yu. Khlebnikov and M. E. Shaposhnikov, "Melting of the Higgs vacuum: Conserved numbers at high temperature," *Phys. Lett.* **B387** (1996) 817–822, arXiv:hep-ph/9607386 [hep-ph].

[155] M. Laine and M. E. Shaposhnikov, "A Remark on sphaleron erasure of baryon asymmetry," *Phys. Rev.* **D61** (2000) 117302, arXiv:hep-ph/9911473 [hep-ph].

[156] S. Eijima and M. Shaposhnikov, "Fermion number violating effects in low scale leptogenesis," *Phys. Lett.* **B771** (2017) 288–296, arXiv:1703.06085 [hep-ph].

[157] J. Ghiglieri and M. Laine, "GeV-scale hot sterile neutrino oscillations: a derivation of evolution equations," *JHEP* **05** (2017) 132, arXiv:1703.06087 [hep-ph].

[158] A. Atre, T. Han, S. Pascoli, and B. Zhang, "The Search for Heavy Majorana Neutrinos," *JHEP* **05** (2009) 030, arXiv:0901.3589 [hep-ph].

[159] O. Ruchayskiy and A. Ivashko, "Experimental bounds on sterile neutrino mixing angles," *JHEP* **06** (2012) 100, arXiv:1112.3319 [hep-ph].

[160] A. Kusenko, "Sterile neutrinos: The Dark side of the light fermions," *Phys. Rept.* **481** (2009) 1–28, arXiv:0906.2968 [hep-ph].

[161] A. Boyarsky, O. Ruchayskiy, and M. Shaposhnikov, "The Role of sterile neutrinos in cosmology and astrophysics," *Ann. Rev. Nucl. Part. Sci.* **59** (2009) 191–214, arXiv:0901.0011 [hep-ph].

[162] M. Drewes and B. Garbrecht, "Combining experimental and cosmological constraints on heavy neutrinos," *Nucl. Phys.* **B921** (2017) 250–315, arXiv:1502.00477 [hep-ph].

[163] F. F. Deppisch, P. S. Bhupal Dev, and A. Pilaftsis, "Neutrinos and Collider Physics," *New J. Phys.* **17** no. 7, (2015) 075019, arXiv:1502.06541 [hep-ph].

[164] T. Asaka, S. Eijima, and H. Ishida, "Mixing of Active and Sterile Neutrinos," *JHEP* **04** (2011) 011, arXiv:1101.1382 [hep-ph].

[165] **NA3** Collaboration, J. Badier *et al.*, "Direct Photon Production From Pions and Protons at 200-GeV/c," *Z. Phys.* **C31** (1986) 341.

[166] G. Bernardi *et al.*, "FURTHER LIMITS ON HEAVY NEUTRINO COUPLINGS," *Phys. Lett.* **B203** (1988) 332–334.

[167] **CHARM** Collaboration, F. Bergsma *et al.*, "A Search for Decays of Heavy Neutrinos in the Mass Range 0.5-GeV to 2.8-GeV," *Phys. Lett.* **166B** (1986) 473–478.

[168] J. Orloff, A. N. Rozanov, and C. Santoni, "Limits on the mixing of tau neutrino to heavy neutrinos," *Phys. Lett.* **B550** (2002) 8–15, arXiv:hep-ph/0208075 [hep-ph].

[169] **DELPHI** Collaboration, P. Abreu *et al.*, "Search for neutral heavy leptons produced in Z decays," *Z. Phys.* **C74** (1997) 57–71. [Erratum: Z. Phys.C75,580(1997)].

[170] **L3** Collaboration, O. Adriani *et al.*, "Search for isosinglet neutral heavy leptons in Z0 decays," *Phys. Lett.* **B295** (1992) 371–382.

[171] D. I. Britton *et al.*, "Improved search for massive neutrinos in pi+ —> e+ neutrino decay," *Phys. Rev.* **D46** (1992) R885–R887.

[172] **CHARM II** Collaboration, P. Vilain *et al.*, "Search for heavy isosinglet neutrinos," *Phys. Lett.* **B343** (1995) 453–458. [Phys. Lett.B351,387(1995)].

[173] **NuTeV, E815** Collaboration, A. Vaitaitis *et al.*, "Search for neutral heavy leptons in a high-energy neutrino beam," *Phys. Rev. Lett.* **83** (1999) 4943–4946, arXiv:hep-ex/9908011 [hep-ex].

[174] **LHCb** Collaboration, R. Aaij *et al.*, "Search for Majorana neutrinos in $B^- \to \pi^+\mu^-\mu^-$ decays," *Phys. Rev. Lett.* **112** no. 13, (2014) 131802, arXiv:1401.5361 [hep-ex].

[175] **ATLAS** Collaboration, G. Aad *et al.*, "Search for heavy Majorana neutrinos with the ATLAS detector in pp collisions at $\sqrt{s} = 8$ TeV," *JHEP* **07** (2015) 162, arXiv:1506.06020 [hep-ex].

[176] **CMS** Collaboration, V. Khachatryan *et al.*, "Search for heavy Majorana neutrinos in $\mu^\pm\mu^\pm$+ jets events in proton-proton collisions at $\sqrt{s} = 8$ TeV," *Phys. Lett.* **B748** (2015) 144–166, arXiv:1501.05566 [hep-ex].

[177] **Belle** Collaboration, D. Liventsev *et al.*, "Search for heavy neutrinos at Belle," *Phys. Rev.* **D87** no. 7, (2013) 071102, arXiv:1301.1105 [hep-ex]. [Erratum: Phys. Rev.D95,no.9,099903(2017)].

[178] **WA66** Collaboration, A. M. Cooper-Sarkar *et al.*, "Search for Heavy Neutrino Decays in the BEBC Beam Dump Experiment," *Phys. Lett.* **160B** (1985) 207–211.

[179] **FMMF** Collaboration, E. Gallas *et al.*, "Search for neutral weakly interacting massive particles in the Fermilab Tevatron wide band neutrino beam," *Phys. Rev.* **D52** (1995) 6–14.

[180] **E949** Collaboration, A. V. Artamonov *et al.*, "Search for heavy neutrinos in $K^+ \to \mu^+ \nu_H$ decays," *Phys. Rev.* **D91** no. 5, (2015) 052001, arXiv:1411.3963 [hep-ex]. [Erratum: Phys. Rev.D91,no.5,059903(2015)].

[181] **PIENU** Collaboration, M. Aoki *et al.*, "Search for Massive Neutrinos in the Decay $\pi \to e\nu$," *Phys. Rev.* **D84** (2011) 052002, arXiv:1106.4055 [hep-ex].

[182] **NOMAD** Collaboration, P. Astier *et al.*, "Search for heavy neutrinos mixing with tau neutrinos," *Phys. Lett.* **B506** (2001) 27–38, arXiv:hep-ex/0101041 [hep-ex].

[183] T. Yamazaki *et al.*, "Search for Heavy Neutrinos in Kaon Decay,". [Conf. Proc.C840719,262(1984)].

[184] R. S. Hayano *et al.*, "HEAVY NEUTRINO SEARCH USING K(mu2) DECAY," *Phys. Rev. Lett.* **49** (1982) 1305.

[185] M. Agostini *et al.*, "Background free search for neutrinoless double beta decay with GERDA Phase II," arXiv:1703.00570 [nucl-ex]. [Nature544,47(2017)].

[186] **KamLAND-Zen** Collaboration, A. Gando *et al.*, "Search for Majorana Neutrinos near the Inverted Mass Hierarchy Region with KamLAND-Zen," *Phys. Rev. Lett.* **117** no. 8, (2016) 082503, arXiv:1605.02889 [hep-ex]. [Addendum: Phys. Rev. Lett.117,no.10,109903(2016)].

[187] **Particle Data Group** Collaboration, J. Beringer *et al.*, "Review of Particle Physics (RPP)," *Phys. Rev.* **D86** (2012) 010001.

[188] **FlaviaNet Working Group on Kaon Decays** Collaboration, M. Antonelli *et al.*, "An Evaluation of $|V_{us}|$ and precise tests of the Standard Model from world data on leptonic and semileptonic kaon decays," *Eur. Phys. J.* **C69** (2010) 399–424, arXiv:1005.2323 [hep-ph].

[189] S. Aoki *et al.*, "Review of lattice results concerning low-energy particle physics," *Eur. Phys. J.* **C74** (2014) 2890, arXiv:1310.8555 [hep-lat].

[190] **HPQCD, UKQCD** Collaboration, E. Follana, C. T. H. Davies, G. P. Lepage, and J. Shigemitsu, "High Precision determination of the pi, K, D and D(s) decay constants from lattice QCD," *Phys. Rev. Lett.* **100** (2008) 062002, arXiv:0706.1726 [hep-lat].

[191] **Heavy Flavor Averaging Group** Collaboration, Y. Amhis *et al.*, "Averages of B-Hadron, C-Hadron, and tau-lepton properties as of early 2012," arXiv:1207.1158 [hep-ex].

[192] S. Antusch and O. Fischer, "Non-unitarity of the leptonic mixing matrix: Present bounds and future sensitivities," *JHEP* **10** (2014) 094, arXiv:1407.6607 [hep-ph].

[193] **MEG** Collaboration, J. Adam *et al.*, "New constraint on the existence of the $\mu^+ \to e^+\gamma$ decay," *Phys. Rev. Lett.* **110** (2013) 201801, arXiv:1303.0754 [hep-ex].

[194] G. Blankenburg, J. Ellis, and G. Isidori, "Flavour-Changing Decays of a 125 GeV Higgs-like Particle," *Phys. Lett.* **B712** (2012) 386–390, arXiv:1202.5704 [hep-ph].

[195] **NA62** Collaboration, C. Lazzeroni *et al.*, "Precision Measurement of the Ratio of the Charged Kaon Leptonic Decay Rates," *Phys. Lett.* **B719** (2013) 326–336, arXiv:1212.4012 [hep-ex].

[196] G. Czapek *et al.*, "Branching ratio for the rare pion decay into positron and neutrino," *Phys. Rev. Lett.* **70** (1993) 17–20.

[197] **Gfitter Group** Collaboration, M. Baak, J. Cúth, J. Haller, A. Hoecker, R. Kogler, K. Mönig, M. Schott, and J. Stelzer, "The global electroweak fit at NNLO and prospects for the LHC and ILC," *Eur. Phys. J.* **C74** (2014) 3046, arXiv:1407.3792 [hep-ph].

[198] **SLD Electroweak Group, DELPHI, ALEPH, SLD, SLD Heavy Flavour Group, OPAL, LEP Electroweak Working Group, L3** Collaboration, S. Schael *et al.*, "Precision electroweak measurements on the Z resonance," *Phys. Rept.* **427** (2006) 257–454, arXiv:hep-ex/0509008 [hep-ex].

[199] **CDF, D0** Collaboration, T. E. W. Group, "2012 Update of the Combination of CDF and D0 Results for the Mass of the W Boson," arXiv:1204.0042 [hep-ex].

[200] P. Hernandez, M. Kekic, and J. Lopez-Pavon, "Low-scale seesaw models versus N_{eff}," *Phys. Rev.* **D89** no. 7, (2014) 073009, arXiv:1311.2614 [hep-ph].

[201] O. Ruchayskiy and A. Ivashko, "Restrictions on the lifetime of sterile neutrinos from primordial nucleosynthesis," *JCAP* **1210** (2012) 014, arXiv:1202.2841 [hep-ph].

[202] **SHiP** Collaboration, E. Graverini, "SHiP sensitivity to Heavy Neutral Leptons," *CERN-SHiP-NOTE-2016-003* (Sep, 2016) , http://cds.cern.ch/record/2214085. http://cds.cern.ch/record/2214085.

[203] S. Antusch, E. Cazzato, and O. Fischer, "Sterile neutrino searches via displaced vertices at LHCb," *Phys. Lett.* **B774** (2017) 114–118, arXiv:1706.05990 [hep-ph].

[204] T. Hambye and D. Teresi, "Higgs doublet decay as the origin of the baryon asymmetry," *Phys. Rev. Lett.* **117** no. 9, (2016) 091801, arXiv:1606.00017 [hep-ph].

[205] T. Hambye and D. Teresi, "Baryogenesis from L-violating Higgs-doublet decay in the density-matrix formalism," *Phys. Rev.* **D96** no. 1, (2017) 015031, arXiv:1705.00016 [hep-ph].

[206] M. Gronau, C. N. Leung, and J. L. Rosner, "Extending Limits on Neutral Heavy Leptons," *Phys. Rev.* **D29** (1984) 2539.

[207] **DELPHI** Collaboration, P. Abreu *et al.*, "Searches for heavy neutrinos from Z decays," *Phys. Lett.* **B274** (1992) 230–238.

[208] P. Hernández, M. Kekic, J. López-Pavón, J. Racker, and J. Salvado, "Testable Baryogenesis in Seesaw Models," *JHEP* **08** (2016) 157, arXiv:1606.06719 [hep-ph].

[209] M. Drewes and S. Eijima, "Neutrinoless double β decay and low scale leptogenesis," *Phys. Lett.* **B763** (2016) 72–79, arXiv:1606.06221 [hep-ph].

[210] T. Asaka, S. Eijima, and H. Ishida, "On neutrinoless double beta decay in the νMSM," *Phys. Lett.* **B762** (2016) 371–375, arXiv:1606.06686 [hep-ph].

[211] B. Garbrecht, F. Glowna, and M. Herranen, "Right-Handed Neutrino Production at Finite Temperature: Radiative Corrections, Soft and Collinear Divergences," *JHEP* **04** (2013) 099, arXiv:1302.0743 [hep-ph].

[212] H. A. Weldon, "Structure of the gluon propagator at finite temperature," *Annals Phys.* **271** (1999) 141–156, arXiv:hep-ph/9701279 [hep-ph].